Synthesis and Characterization of Pyrrole Based Adhesion Promoter Systems on Oxide Substrates

Dissertation

zur Erlangung des akademischen Grades

Doctor rerum naturalium

(Dr. rer. nat.)

vorgelegt

der Fakultät Mathematik und Naturwissenschaften

der Technischer Universität Dresden

von

Diplomchemiker Xuediao Cai

geboren in V. R. China

Gutachter:	**Prof. Dr. rer. nat. Hans-Jürgen Adler**
	Prof. Dr. rer. nat. Brigitte Voit
	Prof. RNDr. Stanislav Nešpůrek, Dr. Sc.
Eingereicht am :	**01. 12. 2004**
Tag der Verteidigung:	**09. 02. 2005**

Synthesis and Characterization of Pyrrole Based Adhesion Promoter Systems on Oxide Substrates

Dissertation

for the award of the degree of

Doctor rerum naturalium

(Dr. rer. nat.)

In the

Faculty of Mathematics and Natural Sciences

Dresden University of Technology

By

Ms. Sci. Xuediao Cai

born in Henan, P. R. China

Referees:	**Prof. Dr. rer. nat. Hans-Jürgen Adler**
	Prof. Dr. rer. nat. Brigitte Voit
	Prof. RNDr. Stanislav Nešpůrek, Dr. Sc.
Date of submission:	**01. 12. 2004**
Date of defence:	**09. 02. 2005**

Contents

Chapter 1 Introduction

1.1 The Goal: Adhesive and Well-Ordered Conducting Polymer Films on Substrates

For the past several decades, polymers have increasingly been used as insulators in the electronic devices and integrated circuits. Some were known in their conductive forms, but not well characterized and with not much interest paid to their conductivity. The first conjugated polymer, polythiazyl $(SN)_x$, was discovered in 1975, which possessed metallic conductivity and becomes superconductor at 0.29 K [1]. However, the idea of using polymers for their electrical conducting properties actually emerged in 1977 with the findings of Shirakawa et al. [2] that iodine doped trans-polyacetylene, $(CH)_x$, exhibits conductivity of 10^3 S/cm. This opened an entire new field for the discovery and development of conducting polymers, and the Nobel Prize in Chemistry was award to Alan J. Heeger, Alan G. MacDiarmid and Hideki Shirakawa in 2000. Since then, an active interest in synthesizing other organic polymers possessing this property has been initiated. As a result, other conducting polymers having π-electron conjugated structures (conjugated polymers), such as polyaniline (PAni), polypyrrole (PPy), polythiophene (PT), poly(p-phenylene), and polycarbazole [3-5] have been synthesized for exploring them in devices. The conductivity of these polymers can be tuned from insulating regime to conducting regime by chemical modification or by the degree and nature of doping. Besides this, polymers offer the advantages such as light weight, flexibility, corrosion-resistance, high chemical inertness, electrical insulation, and the ease of processing etc. Technological opportunities for application of the conducting polymer materials in such diverse areas as rechargeable batteries, electromagnetic interference shielding, corrosion inhibition, polymer light-emitting diodes, photodetectors, flexible “plastic” transistors and electrodes, electroluminescent polymer displays, to name only a few, continue to be actively pursued.

Among conducting polymers, polypyrrole (PPy) is one of the extensively studied electronic materials. Thus this material has received much attention because of various technological applications [6-9]. PPy found applications as transparent electrode in organic light-emitting diodes substituting traditionally used oxides [10-11], in photoelectrochemical cells [12], in intrinsically conducting shielding adhesives [13], in humidity and gas sensors [14-18], in corrosion protections [19-21] and in rectifying double layer devices [22, 23].

Most of the applications require adhesive and well-defined films composed of molecules with tailor-made properties in unique spatial arrangements with respect to each other and to the substrate [24-26]. Our aim is to get such adhesive and well-defined PPy films on various substrates, such as silicon, ITO, or some metals.

1.2 The Problem: Poor Adhesion between PPy and Substrates by Electrochemical or Chemical Polymerization

Though PPy received considerable interest, processing it into an ultrathin film is still a challenging task because of its intractability, insolubility and infusibility in most of the common organic solvents. PPy is usually synthesized by electrochemical and chemical oxidative polymerization techniques. The coating of substrates with PPy film can be achieved by the following possible approaches.

- **Spin-coating**: Spreading the solution of soluble PPy on the surface of the substrate, followed by the evaporation of the solvent. Besides the difficulties concerned with the desired uniform coating of the substrate surface with the solution of PPy, the main problem is the insolubility in nearly all solvents of practical interest [27-32]. During the past years, some progress has been made in the chemical modification of the parent PPy structure to get more soluble polymer derivatives. However, the distortion of the molecular structure of PPy occurs upon such chemical modification, leading to a drastic decrease of the electric conductivity of the resulting polymers.
- **Electropolymerization of monomers at the electrodes**: Electropolymerization is usually a good technique to obtain PPy films on conducting electrode substrates. However, electropolymerization is strongly restricted by the use of conducting materials, such as metals or carbon materials, whereas no electropolymerized PPy layer can be obtained on insulating surfaces.
- **Chemical polymerization**, provided with relatively strong chemical oxidants like ammonium peroxydisulfate (APS), ferric ions, permanganate or hydrogen peroxide. Chemical polymerization occurs in the bulk of the solution, and the resulting polymers precipitate as insoluble solids. However, a part of polymers, formed by chemical polymerization, can be deposited spontaneously on the surface

of some substrates, immersed into the polymerization solution. The distribution of the resulting conducting polymers between the precipitated and deposited forms depends on many variables and varies within a broad range.

- **Surface chemical polymerization**: Chemical polymerization provided directly on the surface. In this case, the surface to be coated is enriched either with a monomer or an oxidizing agent and after that it is treated with a solution of either oxidizer or monomer, respectively. A major advantage of this process is that the polymerization starts at the surface, whereas no bulk polymerization in the solution takes place. The disadvantage of this process is that it is limited by materials than can be covered or enriched with a layer of either monomer or oxidizer in a separate stage, preceding the surface polymerization.

Though PPy film can be obtained by several methods like described above. However, in most cases, adhesion between the polymer and the substrate is poor because of weak physical interactions between them. Therefore, polypyrrole can be easily peeled-off as a free-standing film from the substrate [33-38]. Getting the adhesive polypyrrole films on the substrates is a big problem.

1.3 One Solution: Adhesion Promoter to Connect the Conducting Polymer and Substrate Surface

Molecular self-assembly is a strategy for nanofabrication that involves designing molecules and supramolecular entities so that shape complementarity causes them to aggregate into desired structures. “Self-Assembled Monolayers (SAMs)” represent one type of structure that is using molecular self-assembly to build structure and function on the nanometer scale. A fast growing area in this field is the study of organized mono- or multilayers of conducting polymers or oligomers having possible applications in many fields. The conducting polymers form a one-dimensional electron system with electrical and optical properties, which are strongly influenced by interchain interactions. In this context, self-assembly monolayers, which have desired control on the molecular level, should be considered as a potential technique for the construction of more highly ordered materials. Monolayers on substrates formed by self-assembly technique can be used as surface modification, which usually lead to the hydrophilic surface of the substrate to hydrophobic surface, e.g. sulphur group modified gold, organosilanes group modified silicon surface and carbonyl acid group modified oxide

surface. Once a second functional group was introduced to the monolayers, covalent grafting of different top layers is possible by reacting this functional group and other monomer or polymers. This also can be used to grafting of conducting polymers to the substrate. The molecules deposited as monolayer on the substrate are adhesion promoters, which connect the substrate and top layers by chemical bond. In the field of conducting polymers, most of the studies report the use of pyrrol-, thiophene- or phenyl-functionalized alkanethiol- or organosilane derivatives as adhesion promoter to increase the adhesion of the polymers to the substrate [39-49].

Such adhesion promoter has two functional group, anchoring group and polymerizable group, connected by an alkyl chain (Fig. 1.1). The anchoring group (e.g. silane, phosphonic acid, thiol) can react with the substrate surface by chemisorption, and the polymerizable group (e.g. pyrrole, thiophene) can be chemically or electrochemically induced to polymerize.

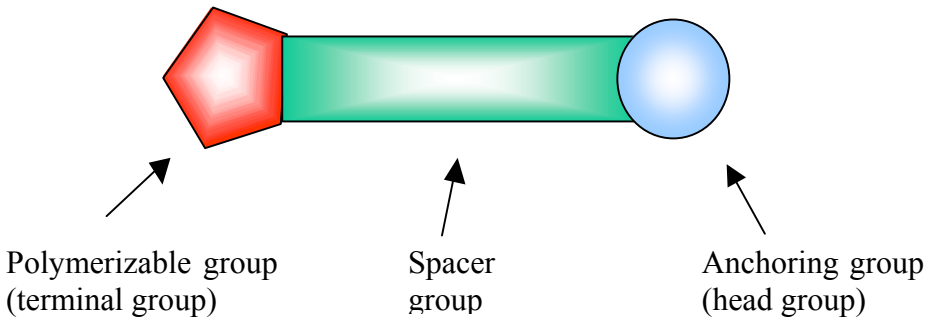

Fig. 1.1 Model of the synthesized compound

There are two steps to produce the adhesive polymer film on substrates. Firstly, the substrate is modified by the adhesion promoter. Therefore, the substrate is dipped in a solution containing adhesion promoter, until a highly organized and densely packed molecular layer is formed on the substrate. The formation of this self-assembly (SA) monolayer is driven by a strong interaction between the substrate and the anchoring group of the adhesion promoter, e.g. the interaction between sulphur and a gold substrate, trichlorosilane and a hydroxylated silicon surface, phosphonic acid and oxide metal surface. Secondly, the polymer film is grafted on the modified substrate. This modified substrate is polymerized with a monomer by chemical or electrochemical polymerization. Hence, adhesive polymer film was obtained.

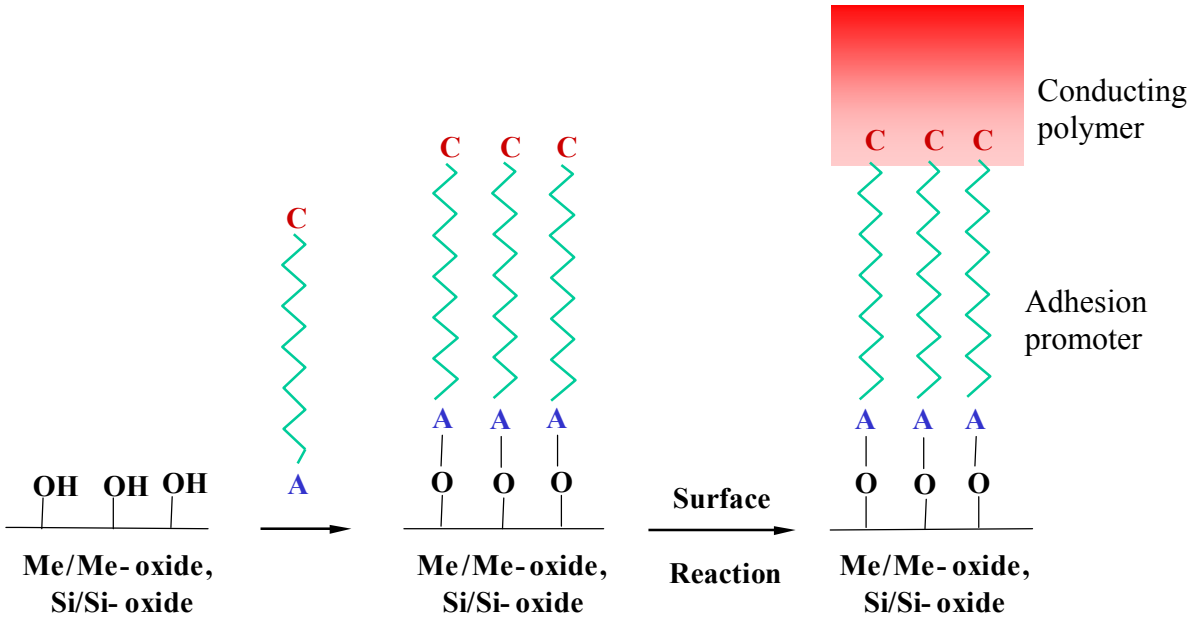

Fig. 1.2 Grafting conducting polymer film on substrate

1.4 Aim and Scope of This Work

The aim of this work is to modify substrate surfaces by grafting adhesive polypyrrole (PPy) films onto the oxide substrate surfaces such as Si/SiO_2, Ti/TiO_2, Ta/Ta_2O_5, and Al/Al_2O_3, and investigate the possible applications. Therefore, new adhesion promoters have to be designed and synthesized. Previous studies in our group were investigated with polythiophene. It included grafting of polythiophene on ω-(3-thienyl) alkyl phosphonic acids modified metal substrates by chemical and electrochemical polymerization and adhesive films were obtained. Also ω-functionalized thienyl trichlorosilanes were investigated on Si wafers. However, thiophene has some drawbacks, which makes its study a bit difficult. Firstly, the unsubstituted polythiophene is an infusible polymer and so its processability is a problem. And secondly, its oxidation potential is high (1.6 V/SCE) compared to pyrrole (0.8 V/SCE). Now our choice of the polymeric system is PPy, an inherently conducting polymer due to interchain hopping of electrons. Grafting of polypyrrole onto substrate surface can be achieved through chemical and electrochemical polymerization. Chemical polymerization provides a possibility to generate grafted polymers. To achieve this, pretreatment of the oxide substrate surfaces with an adhesion promoter was required, which would compatibilise the substrate surface with the polymerizable monomers.

Chapter 2 describes the various surface analytical methods and tools to characterize the modified surface. These techniques include contact angle measurement, grazing incident FTIR, surface plasmon resonance spectroscopy (SPR), ellipsometry, X-ray photoelectron spectroscopy (XPS) and scanning electron microscopy (SEM). Once it is ensured that the self-assembly monolayer is formed, further surface reactions that can be carried out. In-situ polymerization with pyrrole monomer produces conductive polymer films can be characterized by SEM, atomic force microscopy (AFM), ellipsometry, UV-VIS spectroscopy.

Chapter 3 describes the design of the adhesion promoter and the formation of the self-assembly monolayer. The 3-substituted pyrrole phosphonic acids or trimethoxysilanes and 1-substituted pyrrole organosilane monolayers are designed as adhesion promoters. This involved the synthesis of ω-(3-pyrrolyl alkyl) phosphonic acids, ω-(3-pyrrolyl alkyl) trimethoxysilanes and ω-(1-pyrrolyl alkyl) organosilanes.

Chapter 4 describes the synthesis of the adhesion promoters (1-substituted pyrrole and 3-substituted pyrrole derivatives) and characterization of the self-assembly layer. The most challenging part of the project was to synthesize 3-pyrrolyl alkyl phosphonic aicd and 3-pyrrolyl alkyl trimethoxysilanes. Until now these compounds have not been described in the literature. Various new procedures have been developed to achieve the 3-substituted pyrrole alkyl phosphonic acid and trimethoxysilanes.

Chapter 5 describes the formation and the properties of the polypyrrole films obtained by chemical and electrochemical polymerization. The formation of homogeneous, adhesive polypyrrole films with rang up thickness are described in this chapter.

Two of the possible applications of these polymer films, such as humidity sensors and FET were described in chapter 6.

Chapter 2 Analytical Tools and Techniques

In the study of monolayers and thin films on flat surfaces, both their surface and bulk properties are important. In this chapter, we introduce several analytical methods to characterize the main properties of our synthesized monolayers and thin films. Contact angles with water as liquid are measured to evaluate wetting properties, surface free energy, and to get information on surface order. Ellipsometry is used to measure the thickness and uniformity of freshly prepared films. Surface Plasmon Resonance Spectroscopy (SPR) is used to measure the kinetics of the monolayer formation process and to get the information of optimum adsorption time. "Grazing incident" FTIR spectroscopy is used to learn about molecular orientation, packing behavior and coverage. We also use X-ray Photoelectron Spectroscopy (XPS) to study surface composition, monolayer structure and binding states, and surface imaging techniques (SEM and AFM) to learn about the surface topography. Electrochemical methods such as Cyclic Voltammetry (CV) and Electrochemical Impedance Spectroscopy (EIS) are also used to study the electroactivity of the monolayers and polymers.

2.1 Contact Angle Measurements

To study the hydrophobicity and the uniformity of the modified substrates, the static contact angle of a water drop lying on the substrate (sessile drop) was measured.

The quality of a stable monolayer and thin film can be estimated from wetting measurements. This is due to the fact that the shape of a liquid drop on a plane, homogeneous surface (which is the result of the free energy of this drop) is affected by the free energy of this surface (Fig. 2.1). The force per unit length, as well as the free energy per unit area, acting on a surface or interface is equal to the interfacial tension γ (mNm^{-1} or dyn cm^{-1}), and the work done on a system when increasing the area by dA at constant γ is γdA. The work of adhesion between a solid and a liquid is defined as

$$\mathbf{W_{sl}} = \gamma_{sv} + \gamma_{lv} + \gamma_{sl} \qquad \text{Eq. 2.1}$$

Where **W** is the work,

γ_{sv}---- the surface interfacial tension between solid -vapor interface

γ_{lv}---- the surface interfacial tension between liquid-vapor interface

γ_{sl}---- the surface interfacial tension between solid-liquid interface

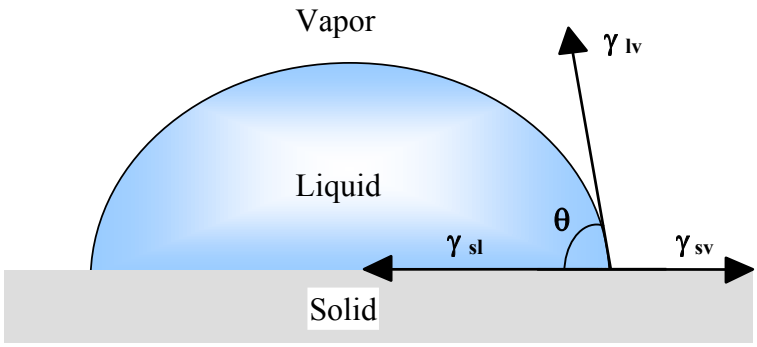

Fig. 2.1 Schematic of an axisymmetric sessile-drop contact angle system

When a liquid does not wet a surface completely, it forms an angle θ, the contact angle with the surface. In the past several decades, numerous techniques have been used to measure contact angles, which were inspire by the idea of using the equation first derived by Thomas Yong [50] in 1805. Yong's equation governs the equilibrium of the three interfacial tensions and the Yong contact angle θ of a liquid drop on a solid.

$$\gamma_{lv} \cos \theta = \gamma_{sv} - \gamma_{sl} \qquad \text{Eq. 2.2}$$

The Young's equation expresses that the contact angle of a liquid with known surface tension on a sample with an unknown surface tension does not only depend on the surface tension of the sample but also on the interfacial tension. In practice this means that the surface tension of the sample can not be determined by contact angle measurements with a single liquid.

Exact surface tension determination by contact angle measurements is difficult, but contact angle measurements, by a single liquid can be qualitatively used for examination of surfaces given different surface treatments.

The contact angle is not a property of the liquid or the substrate but the interaction between them. The angle of a drop on a solid surface is the result of the balance between the cohesive forces in the liquid and the adhesive forces between the solid and the liquid. If there is no interaction between the solid and the liquid, the contact angle will be 180°. As the interaction between the solid and liquid increases, the liquid spreads until θ= 0° and equation 2.2 becomes

$$\gamma_{lv} = \gamma_{sv} - \gamma_{sl} \qquad \text{Eq. 2.3}$$

A contact angle less than 90° indicates that the substrate is readily wetted by the test liquid (Fig. 2.2a), while an angle greater than 90° shows that the substrate will resist wetting (Fig. 2.2b).

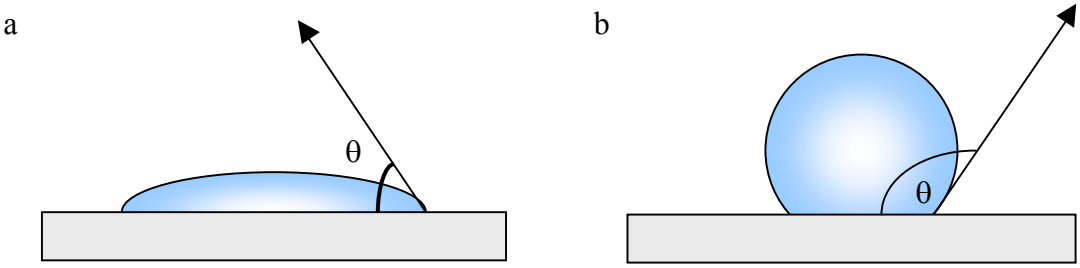

Fig. 2.2 (a). Hydrophilic (θ<90°) and (b). hydrophobic surface (θ>90°)

The derivation of Yong's equation assumes that the solid surface is smooth, homogeneous and rigid, it should also be chemically and physically inert with respect to the liquids to be employed. Ideally, according to Yong's equation, a unique contact angle is expected for a given system (e.g. liquid drop on a solid surface) [51]. Usually, two kinds of contact angle: static contact angle and dynamic contact angle were measured.

A liquid droplet placed on a solid, non-absorbent surface will reach an 'equilibrium' condition where no further spreading of the droplet occurs. The contact angle reading, which is determined at this condition is the 'static' contact angle. For high viscosity liquids (e.g. glycerin) it is necessary to wait until the spreading stops before a reading is determined.

On absorbent materials, where the liquid penetrates into the substrate, the contact angle will continuously change as a function of time. In certain applications (e.g. printing, gluing) the process time is sometimes critical for the process to work. To measure this 'dynamic contact angle' as well as 'rate of absorption' and spreading, it is necessary to capture a sequence of images during the interaction

In a real system, however, a range of contact angles is usually obtained instead. The upper limit of the range is the advancing contact angle, θ_a, which is the contact angle found at the advancing edge of a liquid drop. The lower limit is the contact angle, θ_r, which is the contact angle found at the receding edge. The different between the advancing and receding contact angles is known as the contact angle hysteresis, θ_{hyst}.

$$\theta_{hyst} = \theta_a - \theta_r \qquad \text{Eq. 2.4}$$

In more recent studies, contact angle hysteresis was found to be related to molecular mobility and packing of the surface, liquid penetration and surface swelling.

There are different methods stated for the measurement of the contact angle:

1). Sessile-Drop Method

This optical contact angle method is used to estimate wetting properties of a localized region on a solid surface. The angle between the baseline of the drop and the tangent at the drop boundary is measured. If an intentional effect is not made to measure advancing or receding angles when contact angles are measured by the sessile drop method, the measured angle will be between θ_a and θ_r, and often nearer to θ_a.

The sessile drop method usually is used to determine the static contact angle or dynamic contact angle. The measured static contact angle does not depend on the diameter of the drop. Depending on the liquid used the contact angle can change within seconds or minutes. The causes of the alteration are the dissolving capacity of the solid in the liquid, the alteration in the composition of the liquid or sedimentation effects.

KRÜSS DSA10 goniometer (drop shape analysis) was used for static contact angle measurements

2). Dynamic Wilhemy Plate Method

It is a method for calculating average advancing and receding contact angles on solids of uniform geometry. Wetting force on the solid is measured when it is immersed in or withdrawn from a liquid of known surface tension. The dynamic Wilhemy plate method can be used to determine the static contact angle, dynamic contact angle or cyclic contact angle.

A K12 processor tensiometer from Krüss GmbH was used to measure the contact angle in our experiment.

Our choice of method was the sessile drop method where water (the chosen liquid) was made to come in contact with the solid substrates. The measurements were done to estimate the change in surface properties after the adsorption.

2.2 Ellipsometry

Ellipsometry is an optical technique that uses polarized light to probe the dielectric properties of a sample. The most common application of ellipsometry is the analysis of very thin films.

Through the analysis of the state of polarization of the light that is reflected from the sample, ellipsometry can yield information about layers that are thinner than the wavelength of the light itself, down to a single atomic layer. Depending on what is already known about the sample, the technique can probe a range of properties including the layer thickness, morphology, or chemical composition.

For the purpose of our research, we are most interested in determining film thickness.

Basics

Transmission and Reflection

An illustration of the transmitted, reflected, and incident beams is shown in Fig. 2.3. A beam of light is incident on a sample at some arbitrary angle of incidence θ_i, the angle of incidence is defined as the angle between the input beam direction and the direction normal to the sample surface. At the boundary of the medium, one part of the light will be reflected at angle θ_r, while the other part will be transmitted through the sample at angle θ_t. Snell's law requires that all three beams are in the plane of incidence (shaded red in Fig. 2.3). The plane of incidence is defined as that plane which contains the input beam, the output beam, and the direction normal to the sample surface.

The transmission and reflection measurements acquire the intensity ratios, T and R respectively, over a given range of wavelengths. T and R are defined as the ratio of the light intensity being transmitted or reflected over the incident light intensity on the sample, as shown in Eq.(2.5) and Eq.(2.6)

$$T = I_t / I_i \qquad \text{Eq. 2.5}$$

$$R = I_r / I_I \qquad \text{Eq. 2.6}$$

Ellipsometry

Ellipsometry is the common optical technique for the determination of the thickness of thin homogeneous films when a plane-polarized light beam reaches the surface at different angles [52-55]. It is resolved into parallel and perpendicular components (p- and s-polarized, respectively). These components are reflected from the surface in a different way, i.e. the amplitude and phase of both components are changed. When the s- and p-polarized reflected light beams are combined, the result is elliptically polarized light (Fig. 2.4). Ellipsometry uses this phenomenon to estimate the thickness of a transition region between the surface and air

by measuring the ratio R between R_p and R_s, the reflection coefficients of the p-and s-polarized light, respectively.

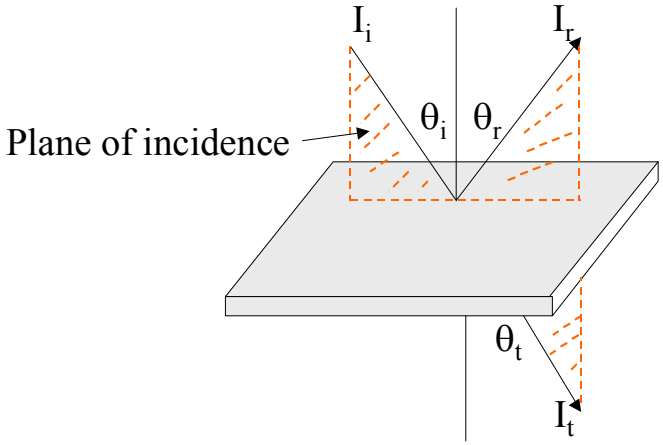

Fig. 2.3 Schematic showing the incident, reflected and transmitted light

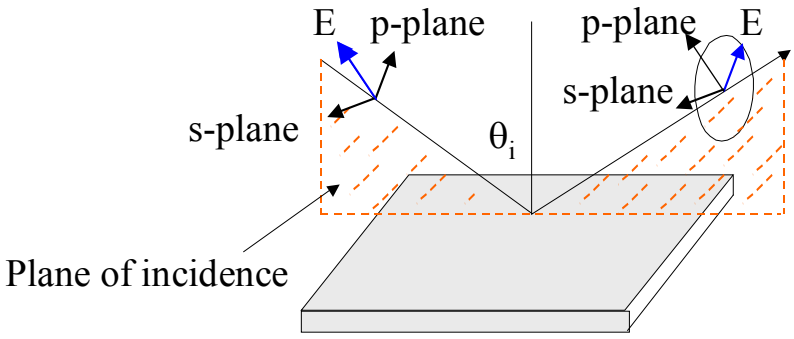

Fig. 2.4 Schematic of the geometry of an ellipsometry experiment

Ellipsometry measures the change in polarization state of light reflected from the surface of a sample. The measured values are expressed as ψ and Δ. These values are related to the ratio of Fresnel reflection coefficients, R_p and R_s for p and s-polarized light, respectively.

$$\tan(\psi)\, e^{i\Delta} = R_p/R_s \qquad \text{Eq. 2.7}$$

Because ellipsometry measures the ratio of two values, it can be highly accurate and very reproducible. From Eq. (2.7) the ratio is seen to be a complex number, thus it contains "phase" information contained in Δ, which makes the measurement very sensitive. In Fig. 2.4 a linearly polarized input beam is converted to an elliptically polarized reflected beam. For any angle of incidence greater than 0° and less than 90°, p-polarized light and s-polarized will be reflected differently.

The coordinate system used to describe the ellipse of polarization is the p-s coordinate system. The s-direction is taken to be perpendicular to the direction of propagation and parallel to the sample surface. The p-direction is taken to be perpendicular to the direction of propagation and contained in the plane of incidence.

We can measure the polarization of the reflected light with a quarter-wave plate followed by an analyzer; the orientations of the quarter-wave plate and the analyzer are varied until no light passes through the analyzer (Fig. 2.5). From these orientation and the direction of polarization of the incident light we can calculate the relative phase change $\cos(\Delta)$ and the relative amplitude change $\tan(\psi)$ introduced by reflection from the surface.

An ellipsometer measures the changes in the polarization state of light when it is reflected from a sample. If the sample undergoes a change, for example a thin film on the surface changes its thickness, then its reflection properties will also change. Measuring these changes in the reflection properties can allow us to deduce the actual change in the film thickness.

The most important application of ellipsometry is to study thin films. In the context of ellipsometry a thin film is one that ranges from essentially zero thickness to several thousand Angstroms, although this range can be extended in some cases. If a film is thin enough that it shows an interference color then it will probably be a good ellipsometric sample. The sensitivity of an ellipsometer is such that a change in film thickness of a few Angstroms is usually easy to detect.

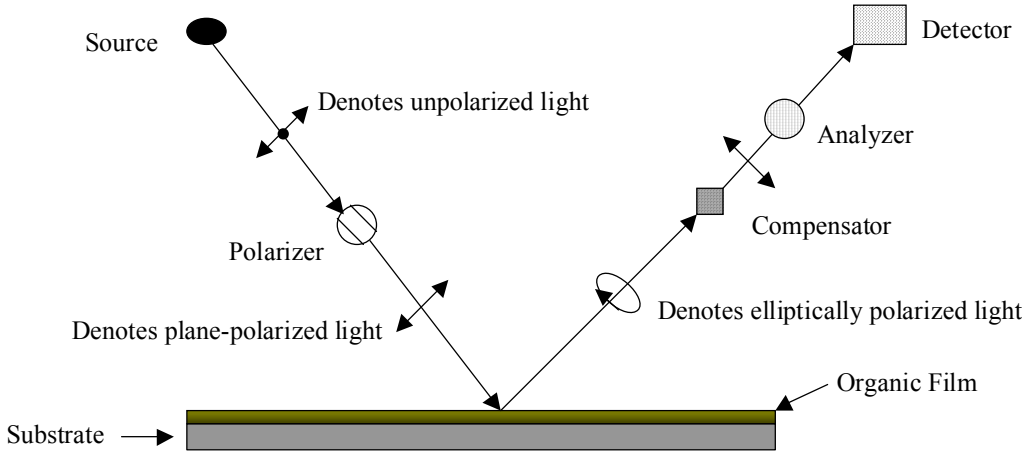

Fig. 2.5 A schematic description of an ellipsometer. (Adapted from Gaines [56])

For a clean surface, Δ and ψ are the output of an ellipsometry measurement and can be interpreted into layer thickness provided the right model for the surface. These two

parameters are directly related to the complex index of refraction (n) of the surface. In order to interpret the ellipsometry data into layer thickness it is necessary to know or assume values for the refractive index for each separate layer on the surface.

The complex refraction index is a representation of the optical constants of a material, it is represented by

$$\hat{n} = n\,(1\text{-}ik) \qquad \text{Eq. 2.8}$$

where n is the ordinary refraction index and k is the extinction coefficient.

The real part or index of refraction, n, defines the phase velocity of light in material:

$$\nu = c/n \qquad \text{Eq. 2.9}$$

where ν is the speed of light in the material and c is the speed of light in vacuum. The imginary part or extinction coefficient, k, determines how fast the amplitude of the wave decreases. The extinction coefficient is directly related to the absorption of a material and is related to the absorption coefficient by

$$\alpha = 4\pi k / \lambda \qquad \text{Eq. 2.10}$$

where α is the absorption coefficient and λ is the wavelength of light.

Once a film having a different index of refraction n_f is coated on the surface, Δ and ψ are related to the complex indices of both the film and the substrate, and to the film thickness. Typically, the compensator is set at an azimuth of 70° and the experimental data are expressed as

$$\delta\Delta = \Delta_0 - \Delta \qquad \text{Eq. 2.11}$$

$$\Delta\Psi = \Psi_0 - \Psi \qquad \text{Eq. 2.12}$$

Where Δ_0 and Ψ_0 are the ellipsometric angles characteristic of the clean substrate surface, and Δ and Ψ those measured for the substrate with the film. From n and k, we can calculate the thickness of the film.

In our experiment, ELX-02 Ellipsometer from DRE GmbH was used. The wavelength of laser is 623,8 nm and incident angle is 70°. An isotropic three-layer model (Si/SiO_2/monolayer/air) was used for determining the thickness of the oxide layers and monolayer or polymer film by using the literature data for optical constants (n = 3.865, k = 0.018 for Si; n = 1.465, k = 0 for

SiO_2; and n = 1.45, k = 0 for monolayer; n = 1.50 for polymer; n_0 =1 for air, where n and k are the real and imaginary part of the refractive index, respectively) [57, 58]

2.3 Surface Plasmon Resonance Spectroscopy (SPR)

Surface Plasmon Resonance (SPR) technique is used in development and characterization of ultra-thin films [59-62]. The SPR measurements are made using optical systems that control parameters to which SPR is sensitive, namely incident angle, wavelength of incident light, degree of polarization, and optical materials. In general, a typical SPR experiment requires a dielectric substrate, a prism in most cases, which has been coated with a suitable noble metal at a precise thickness. The combination of the substrate, noble metal, and sample in contact with the metal, allows for the generation and support of surface plasmon polaritons that are formed along the metal dielectric interface. These polaritons are highly damped charge density waves oscillating at optical frequencies, and may be excited if the materials and optical properties of an experimental system are chosen correctly.

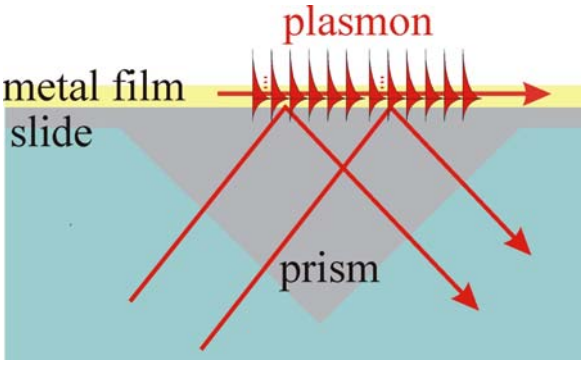

Fig. 2. 6 SPR excitation with a prism, then the observation of plasmon is possible: the metal film is thin enough to monitor the plasmons from the backside

In general, the SPR are not measured directly, but their presence is inferred by monitoring the light intensity reflected from the substrate/metal interface. The reflected light will contain a deep minimum in intensity, and this minimum occurs at what is termed the resonance for the surface polariton, or plasmon. The monitoring of the surface plasmon reflectivity curve, and in particular, the position of the resonance, yields what is generally known as surface plasmon resonance spectroscopy. The position of the reflectivity minimum is very sensitive to the interface properties between in the substrate face and the liquid. Changes in metal film thickness, surface adsorbed species, and liquid dielectric properties are all seen as changes in

the SPR curves (Fig. 2.6). SPR has been shown to be sensitive to very low levels of material adsorbed onto a surface.

The scan and kinetic SPR measurement modes are widely used to describe events occuring at the metal interface [63]. In the scan mode, reflectivity changes are monitored as a function of the angle of incidence of the incoming laser beam. For angles smaller than the critical angle, a steady rise in the reflectivity is observed, while for angles larger than the critical angle, a steady drop in reflectivity is observed until reaching a certain angle at which the reflectivity signal reaches a minimum. This angle is called the resonance angle. For values higher than the resonance angle, a steady increase in the reflectivity value is observed.

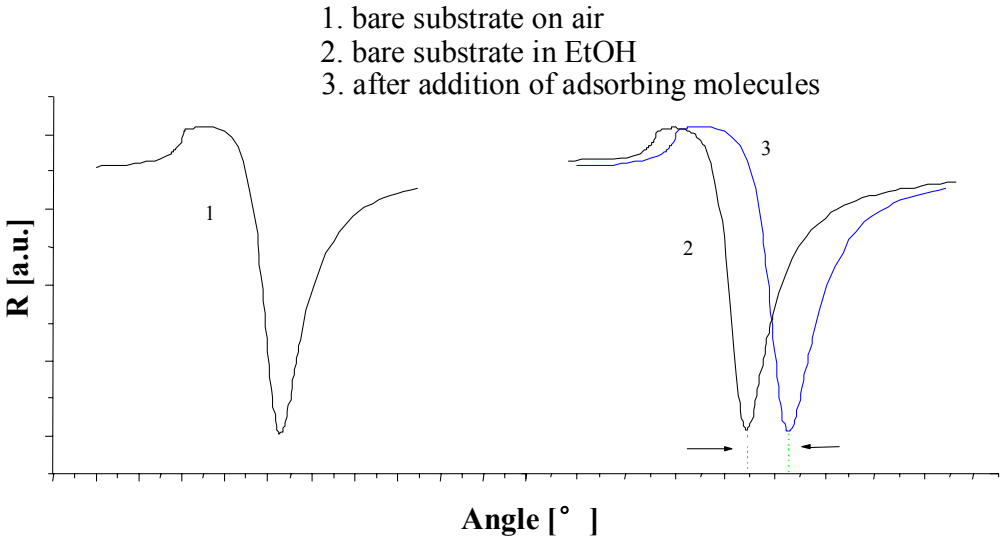

Fig. 2.7 SPR curve

The resonance angle is strongly dependent on the dielectric constant of the medium surrounding the metal interface, the laser wavelength, and the dielectric properties of the metal. Any changes in the dielectric properties of the medium will result in a shift in the resonance angle, which is usually the case when some material binds to or dissociates from the metal surface. These events can be monitored in real-time using the kinetic measurement mode. In this mode, reflectivity changes occuring at a specific incident angle are monitored as a function of time.

Assuming that the thickness of the dielectic film is much less than the wavelength of the probe laser, we can estimate the film thickness (d_f) from [64]

$$d_f = \frac{\varepsilon_s \lambda (\varepsilon_m)^{1/2} (\varepsilon_s - \varepsilon_m)}{2\pi} \frac{\varepsilon_f}{(\varepsilon_f - \varepsilon_s)(\varepsilon_f - \varepsilon_m)} \left(\frac{\varepsilon_m + \varepsilon_s}{\varepsilon_m \varepsilon_s} \right)^2 \qquad \text{Eq. 2.13}$$

In our experiment, special substrates were prepared: on LaSFN9 glass sheets, 50 nm gold were evaporated and then a 2.5 nm Al_2O_3 layer was deposited on it. Because we cannot determine the exact refraction index and thickness of Al_2O_3 layer. Due to unknown of the thickness and refraction index of Al_2O_3 layer, the thickness of the adsorbed layer is difficult to calculate. Kinetic SPR mode was used to study the adsorption of the adhesion promoter.

2.4 Grazing Incident FTIR

Grazing incident FTIR spectroscopy is a very useful technique that gives information about the direction of the transition dipoles in e.g. adsorbed an organic thin film.

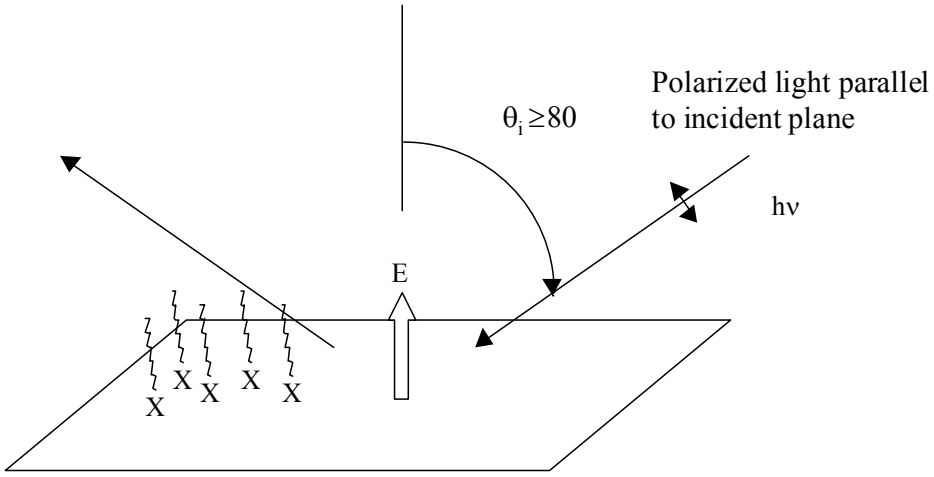

Fig. 2.9 A schematic diagram of the grazing incident FTIR

Theoretical consideration of the IR spectroscopy of the monolayers adsorbed on a metal surface showed that the reflection-adsorption spectrum is measured most efficiently at high angles of incidence, typically at 80-85 degree, and that only the component of incident light, which is parallel to the plane of incidence, gives measurable absorption [65]. Figure 2.9 presents a schematic description of a monomolecular film on a mirror, with an incident light and direction of the polarization.

For example, an alkyl phosphonic acid molecule is adsorbed on a metal surface (Fig. 2.10) while both the symmetric and asymmetric methylene vibrations (ν_s and ν_a, respectively of the alkyl chain) are parallel to the metal plane, the symmetric vibration and both asymmetric vibrations of the methyl group have components that are perpendicular to the surface, therefore, the methylene groups in a perpendicular, all-trans alkyl chain will not be picked up by the p-polarized light. Once the alkyl chain tilts from the normal to the plane, the symmetric

and asymmetric vibrations of the methylene groups no longer are parallel to the surface and thus will appear in the grazing incident spectra [66].

The intensity of the methylene vibrations in the spectra is a direct function of the tilt angle of the alkyl chain. This unique property of the grazing-incident experiment allows the calculation of the molecular orientation from FTIR spectra [59].

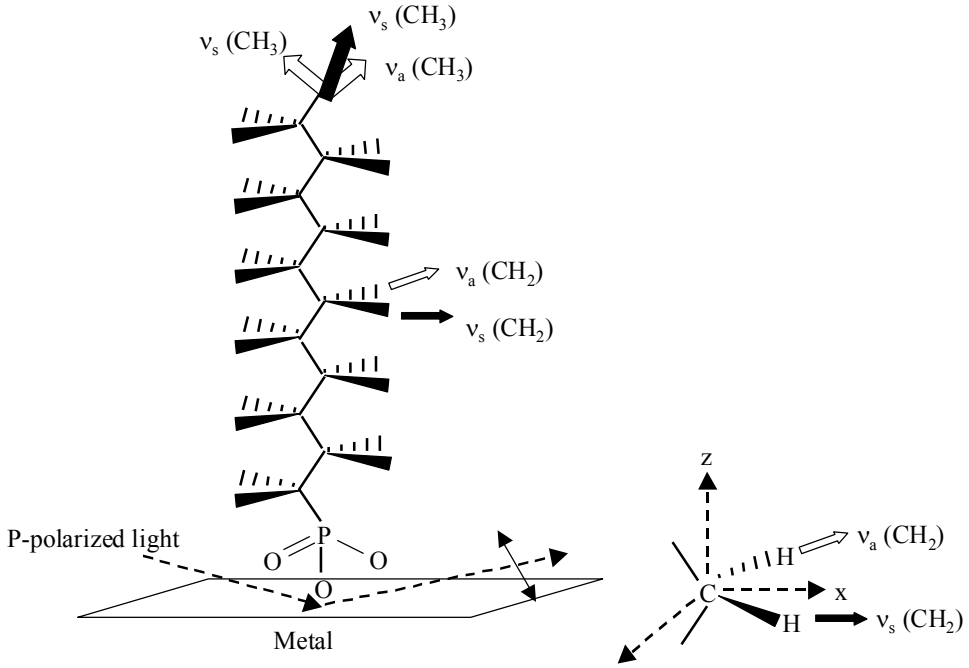

Fig. 2.10 An alkyl phosphonic acid on metal surface in a grazing-incident FTIR experiment (left), and an in-plane diagram of the CH_2 group and its transition dipoles (right)

In our experiment, grazing incident FTIR was measured using a MTC-detector and FT-80 unit from Spectra Tech Inc. All spectra consist of 500-1000 scans at 4 cm^{-1} resolution and were rationed to metal plates.

2.5 X-Ray Photoelectron Spectroscopy (XPS)

The metal substrates coated with the synthesized compounds were subjected to XPS in order to get information about the surface composition and orientation of the adsorbed molecules.

XPS probes the first ~ 5-10 nm of a surface and provides the following information:

- Identification of all elements (except) H and He) present at concentrations >0.1 atomic %.
- Molecular environment (oxidation states, bonding atoms).

- Laterial variations in surface composition.
- Non-destructive element depth profiles and surface heterogeneity (10nm).

XPS uses a soft X-ray source (Alkα and Mgkα) to ionize electrons from the surface of a solid sample. The binding energy of these electrons are measured and are characteristic of the elements and associated chemical bonds (chemical state) in the top few atomic layers of the material.

Samples can be tilted to affect the escape depth of the electrons and thus determine the depths of overlayers on the surface. For analysis beyond the top 1-5nm an inert gas ion gun (normally Argon) can be used to sputter off the surface layers before analysis. Alternating sputtering and XPS spectral acquisition permits chemical depth profiles to be obtained.

Photoelectron spectroscopy utilizes photo-ionization and energy-disperse analysis of the emitted photoelectrons to study the composition and electronic state of the surface region of a sample. Traditionally, when the technique has been used for studies it has been subdivided according to the source of exciting radiation into XPS & UPS.

X-ray Photoelectron Spectroscopy (XPS) –uses soft (200-2000 eV) X-ray excitation to examine core-levels.

The energy of a photon is given by the Einstein relation [67]:

Where $E = h\nu$ Eq. 2.14

h- Planck's constant (6.62×10^{-34} J s)

ν- frequency (Hz) of the radiation

In XPS, the photon is adsorbed by an atom in a molecule or solid, leading to photo-ejection of electrons from atoms near the surface.

The kinetic energy distribution of the emitted photoelectrons can be measured using any appropriate electron energy analyzer and a photoelectron spectrum can thus be recorded.

The process of photoionisation can be considered in several ways: one way is to look at the overall process as follows:

$$A + h\nu \rightarrow A^+ + e^- \quad \text{Eq. 2.15}$$

Conservation of energy than requires that:

$$E(A) + h\nu \rightarrow E(A^+) + E(e^-) \quad \text{Eq. 2.16}$$

Since the electron's energy is present solely as the kinetic energy (KE) this can be rearranged to give the following expression for KE of the photoelectron:

$$KE = h\nu + E(A^{+}) \qquad \text{Eq. 2.17}$$

The final terms in brackets, representing the difference in energy between the ionized and neutral atoms, is generally called the binding energy (BE) of the electron. This then leads to the following commonly quoted equation:

$$KE = h\nu - BE \qquad \text{Eq. 2.18}$$

For each and every element, there will be a characteristic binding energy associated with each core atomic orbital i.e. each element will give rise to a characteristic set of peaks in the photoelectron spectrum at kinetic energies determined by the photon energy and the respective binding energies. The presence of peaks at particular energies therefore indicates the presence of specific element in the sample under study. Furthermore, the intensity of the peak is related to the concentration of the element within the sampled region. Thus, the technique is capable yielding a quantitative analysis and is sometimes known by the alternative acronym, ESCA (Electron Spectroscopy for Chemical Analysis). Knowing the kinetics (KE) of the emitted electrons and the energy ($h\nu$) of the incoming photon, the binding energy (BE) is easily calculated:

$$BE = h\nu - KE \qquad \text{Eq. 2.19}$$

XPS instruments consist of an X-ray source, an energy analyzer for the photoelectrons, and an electron detector. The analysis and detection of photoelectrons requires that the sample is placed in a high-vacuum chamber, exposed to monochromatic X-radiation and the properties of inner-shell electrons are probed. Since the photoelectron energy depends on X-ray energy, the excitation must be monochromatic. The energy of the photoelectrons is analyzed by a multichannel detector such as a microchannel plate.

The most important physical parameters required for analysis are the inelastic electron mean free path and the photoionization cross section. The inelastic mean free path (IMFP), λ, which the distance covered by an electron between two inelastic shocks, is an important parameter determining the electron emission from solids excited by electrons or photons. Besides, the by far most important physical effect that must be taken care of is the fact that the XPS signal attenuates strongly with the depth on the nano-meter scale. It is this property that makes XPS interesting and powerful because it gives the technique its high surface sensitivity. However

this is also the source of the highest uncertainty in quantitative interpretation of XPS unless it is accounted for. Different methods have been suggested. One possibility is to measure the variation in peak intensity with the angle of emission and another is to analyze the energy distribution in an energy range around the peak energy.

Due to the penetrating nature of x-rays, special techniques is used that can emphasize the contribution from atoms in different depth positions in a film. For example, the use of X-rays at a grazing angle to the surface emphasizes the contribution from surface atoms, and a study of photoelectron spectroscopy as a function of the take-off angle offers an excellent way to study atom distribution in a film [68, 69].

Non-destructive profiling techniques of XPS are based on either the energy or the emission angle dependence of the mean escape depth (or inelastic mean free path, IMFP) of the emitted electrons. This technique can measure the thickness of the adsorbed layer on the substrate. For example, if one compares the intensities of two or more XPS peaks of the same element at low and high kinetic energies, the mean depth of origin of the element signals can be obtained and can be used to determine the thickness of a segregation layer, or of an adsorbed layer. For example, if we compare the relative intensities of low energy (I_b) and high energy (I_B) peaks of a substrate covered by an overlayer of adsorbate, A, of thickness, d, with those of the clean surface (I^0_b and I^0_B, respectively), it would follow that the thickness can be estimated from

$$d = [(\lambda^0_{b,A}\,\lambda^0_{B,A})/(\lambda^0_{B,A} - \lambda^0_{b,A})]\cos\varphi\,\ln[(I^0_b / I^0_B)/(I_b / I_B)] \qquad \text{Eq. 2.20}$$

where λ is the relevant IMFP of the substrate XPS signal through the overlayer A, and φ is the electron take-off angle measured from the sample normal.

Angle resolved XPS measurement is a method for non-destructive probing of thin surface layers (<10 nm) by an electrostatic analyzer. Increasing the photoelectron take-off angle by rotating the sample in the energy dispersive plane of the analyser reduces the sampling depth of the technique. The basis of the angle dependent profiling method can be seen in the $\cos\varphi$ dependence of the electron signal. For a given electron energy, varying the take-off angle changes the effective mean escape depth between its full value at $\varphi = 0^\circ$ and a minimum at glancing take-off angles. The total probing depth is limited to about three times the inelastic mean free path (tyically < 5 nm) while the depth resolution is generally limited by the experimental error in the intensity measurement. This method can determine the orientation of the monolayer. At low take-off angle, the main information is about the top layer. At high take-off angle, the main information is about deep layer. Comparing the ratio of the top atom

and deep atom to the take-off angle, the orientation of the monolayer on the substrate can be obtained. By comparing the relative intensities of peaks at the same kinetic energy over a number of different take-off angles it is possible to calculate layer thicknesses. Alternately, comparing relative intensities at low and high take off angles, indicate whether a species is enriched or depleted in the surface region. This is useful for the analysis of thin films on surfaces where it is possible to determine the molecular orientation to the surface.

In our experiment, XPS studies were carried out using a Physical Electronics PHI 5700 ESCA system using MgKα radiation (1253.6 eV). The pressure in the analysis chamber was maintained at 10^{-10} mbar. The samples were measured at room temperature using software StdPH1. The curve fitting procedure used Gaussian components. Angle-resolved XPS measurements were done at five different angles (5°, 20°, 45°, 70° and 85°) to investigate the orientation of the adsorbed molecules and the ordering of the film.

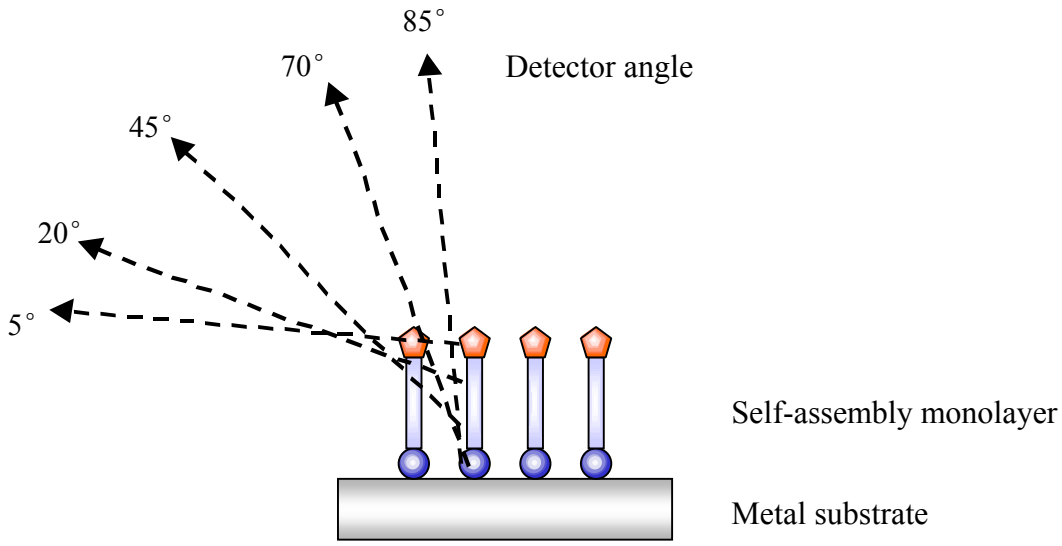

Fig. 2.11 Angle dependent XPS measurement

2.6 Atomic Force Microscopy (AFM)

The Atomic Force Microscopy (AFM) is being used to solve processing and materials problems in a wide range of technologies. The materials being investigated include thin and thick film coatings, synthetic and biological membranes, polymers, and semiconductors. By using AFM one can not only image the surface in atomic resolution but also measure the force at nano-newton scale and the thickness of the coatings.

The principle of atomic force microscopy is illustrated in Fig. 2.12. The tip is brought very close to the surface until a preset deflection of the tip is reached. The deflection of the tip is measured by a laser beam reflected on the cantilever just above the tip. A circular laser detector divided into four quadrant sections, detects the reflected laser beam. The deflection of the tip is measured by the difference in intensity between upper two and the lower two quadrants of the laser detector. While scanning in the X and Y direction a feedback system from the laser detector to the Z-direction piezo-transducer keeps the deflection of the tip on the present value. The X, Y and Z position of the piezo-transducer is recorded to form a topographic picture of the surface of the sample.

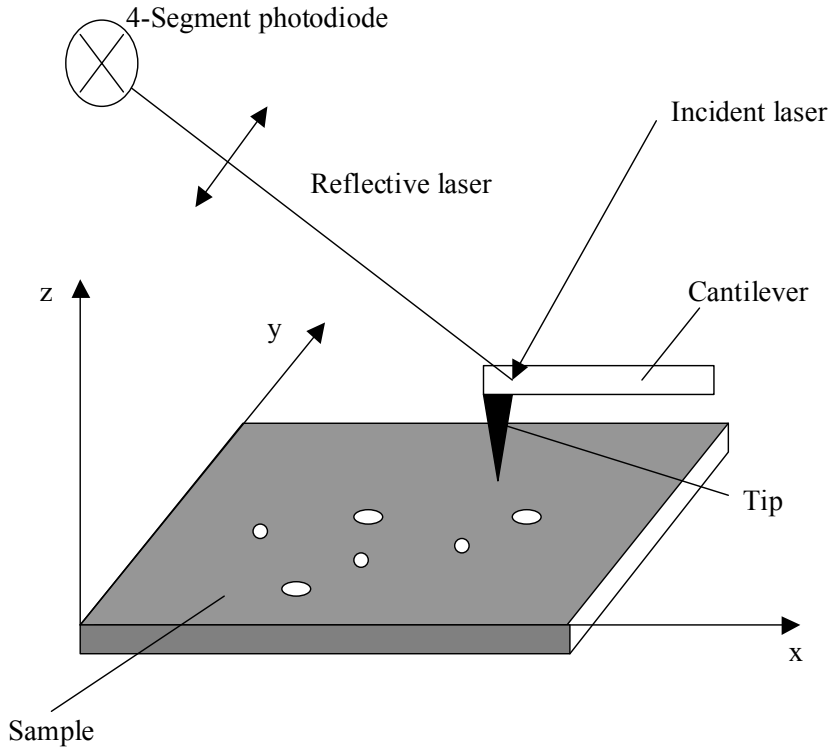

Fig. 2.12 Setup of the AFM

There are three different modes in atomic force microscopy: contact mode, tapping mode, and non-contact mode. In non-contact mode, the tip oscillates above the adsorbed fluid layer on the surface. It does not come in contact with the sample surface. The sample is not damaged during non-contact mode; however, the scan speed is much slower, there is lower lateral resolution, and it may be used only with very hydrophobic samples. Non-contact mode is not used very often because of these disadvantages.

Contact mode is the original way the first atomic force microscopes were operated. The tip is brought close to the surface that a preset value of deflection is reached. The deflection of the

cantilever depends on the force between the tip and the sample surface on the spring constant of the cantilever. The deflection of the cantilever can be adjusted during scanning adjusting the operational force between the tip and the surface. The operational force in contact mode AFM varies from one to several hundred nano-Newtons. The image formations can be done in two different ways in contact mode AFM. By recording the Z-position at constant deflection (force) resulting in a topographic picture of the surface. As mentioned before the photo detector is divided into four quadrants making it possible to detect the lateral deflection of the cantilever as it scans the surface. This can be utilized in analysis of apparently flat samples containing domains with different friction to the tip. This technique is referred to friction mode or lateral force microscopy. Contact mode is excellent for investigations of hard solid surfaces but the force between the tip and surface is often sufficiently high to disorder soft material on the surface during scanning by inelastic deformation.

To overcome the limitations of the contact mode in studying soft materials, modulation techniques have been developed. In these methods either the cantilever is vibrated at its resonance or the vertical sample position is modulated. The tip-sample force interaction causes a change in the amplitude, the phase and the resonance frequency of the vibrating cantilever. Tapping mode is a modulation mode, where the tip is vertically oscillated at its resonance frequency. When the sample approaches the vibrating tip, they come into intermittent contact, thereby lowering the vibration frequency as detected by the reflected laser beam at the photo detector. The amplitude drop is used as feedback to the Z-direction. By tapping instead of constant contact, the tip sample lateral force is greatly reduced and the short tip-sample contact time prevents inelastic surface modification. Topographic images of the surface are recorded at a preset amplitude drops value. Tapping mode also gives the possibility to image the phase shift between the driven and the actual oscillations of the cantilever as a function of the X, Y coordinates analogue to the topographic image. The phase shift is connected to the dissipation of energy through inelastic processes. The phase image can reveal differences in viscoelasticity, friction and adhesion between domains on the surface.

In our case, the AFM measurement used was Nanoscope Dimension 3100 from Veeco/USA working in tapping mode. It opened in air at constant deflection (i.e., vertical contact force) with triangular-shaped, Aluminum-coated Si_3N_4 microlevers. The tip of the microlevers had a standard aspect ratio (about 1:1), and the levers had a normal force constant of 0.03 N/m. The constant-force set point was about 0.1 nN, while the images acquired were 256x256-pixel

maps. All images are standard top-view topographic maps, where the brightness is proportional to the quota of the features over the sample surface; i.e., light means mountain, dark means valley. The images shown are generally representative of the samples, since the same images appear in four different regions of the analyzed samples, positioned at the vertices of a 4-mm-side square, centered at the specimen.

2.7 Electrochemical Impedance Spectroscopy (EIS)

Virtually every liquid and solid is able to pass current when a voltage is applied to it. When the voltage is constant (DC), the ratio of the applied voltage to the current (U/I) is known as the resistance of the material.

If variable voltage (AC) is applied to the material, the ratio U/I is known as the impedance. In many materials, especially those, which are not generally regarded as conductors of electricity, the impedance varies as the frequency of the applied voltage changes, due to the properties of the liquid or solid. This may be due to the physical structure of the material, to chemical processes within it, or to a combination of both. Thus, if a measurement of impedance over a suitable frequency range is made, and the results plotted on suitable axes, it is possible to relate the results to the physical and chemical properties of the material. This technique is known as Electrochemical Impedance Spectroscopy (EIS) and is used to investigate a huge variety of materials and chemical mechanisms.

EIS is a power tool for examining many chemical and physical processes in solutions as well as solids. For solution phase electrochemistry a complex sequence of coupled processes such as, electron transfer, mass transport and chemical reaction can all control or influence the output from an electrochemical measurement. The main advantage of EIS is that we can use purely electronic models to represent an electrochemical cell. An electrode interface undergoing an electrochemical reaction is typically analogous to an electronic circuit consisting of a specific combination of resistors and capacitors. For this reason, EIS can be used to study the property of the conducting polymer films and the adsorption process of the adhesion promoter on electrode.

The term resistance and impedance both denote an opposition to the flow of electrons or current. In direct current (DC), only resistors produce this effect. However, in alternating current (AC) circuits, two other elements, capacitors and inductors, impede the flow of

electrons, impedance can be expressed as a complex number, where the resistance is the real component and the combined capacitance and inductance is the imaginary component.

In AC theory, where the frequency is non-zero, the analogous E and I are defined as potential and current respectively and Z is defined as the impedance, the AC equivalent of resistance.

$$E = I\,Z \qquad \text{Eq. 2.21}$$

From equation 2.21 we can calculate the impedance vector as the quotient of the voltage and current vectors:

$$Z_{total} = (E' + E''j)/(I' + I''j) \qquad \text{Eq. 2.22}$$

Where the AC voltage vector, E; can also be expressed as a complex number:

$$E_{total} = E' + E''j \qquad \text{Eq. 2.23}$$

The resulting vector expression for the AC impedance,

$$Z_{total} = Z' + Z''j \qquad \text{Eq. 2.24}$$

The absolute magnitude of the impedance can be expressed as

$$|Z| = (Z' + Z'')^{1/2} \qquad \text{Eq. 2.25}$$

and the phase angle can be defined by

$$\tan\theta = Z''/Z' \qquad \text{Eq. 2.26}$$

In an electrochemical cell slow electrode kinetics, slow preceding chemical reactions and diffusion can all impede electron flow and can be considered analogous to the resistors, capacitors and inductors that impede the flow of electrons in an AC circuit.

In an EIS measurement, the specimen is subjected to an AC potential over a range of frequencies, and the phase (with respect to the applied potential) and amplitude of the current are measured at each frequency. In order to interpret the EIS results, an equivalent circuit approximates the impedance response of a specimen. The components of the circuit have a physical correspondence to components of the specimen. For metal electrodes against a saturated porous material composed of an insulating solid framework and a pore space filled with electrolyte, the impedance response can be approximated by an equivalent circuit composed of resistors R and capacitors C. However, for a polymer film grafted on the electrode, there is a more complex system. The circuit diagram is different with a combination of capacitors and resistors. To determine which equivalent circuit describes the behavior of an

electrochemical system, we measure impedance over a range of frequencies. The standard technique is to apply an AC voltage or current a wide range of frequencies and measure the current or voltage response of the electrochemical system.

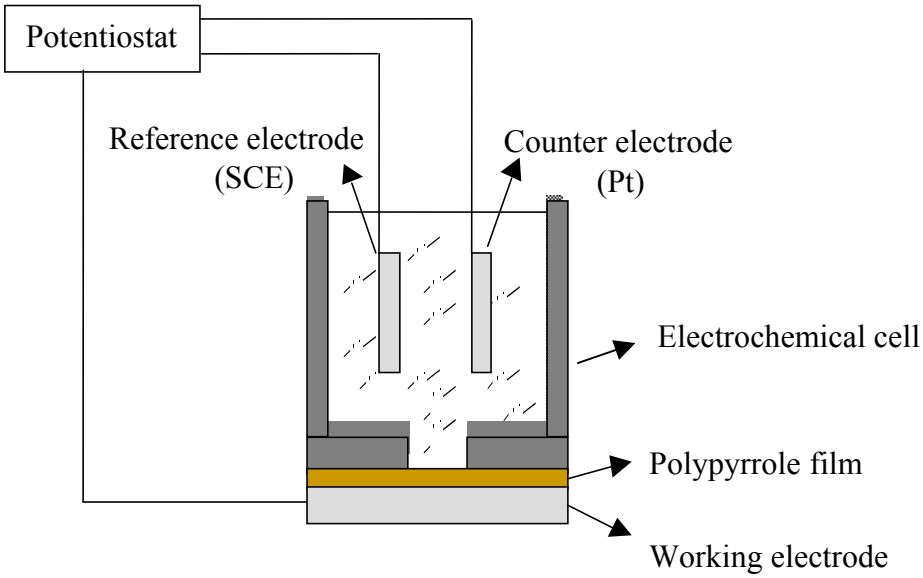

Fig. 2.13 Setup for EIS measurement

In our experiment, EIS measurements were carried out in a monomer free solution with Zahner electric IM5d impedance instrument. A Ti disc electrode (A= 0.125 cm^2) sealed in epoxy resin served as the working electrode and Pt plate as the counter electrode. Saturated calomel electrode (SCE) was used as the reference electrode. An AC amplitude of mV was applied in the frequency range of 100 KHz to 0.1 Hz using 10 points per decade. For each film, the impedance spectra were obtained between the potential range 0.4 V to –1.4 V in steps of 0.1 V. The films were allowed to equilibrate for 10 min at each potential being measured. Fig. 2.8 shows the setup for measuring EIS.

Chapter 3 Ultrathin Films

Ultrathin organic films are currently gaining interest in many areas such as integrated optics, biosensors, chemical sensors, friction reducing coating, surface orientation layers and molecular electronics. Most of the applications require well-defined and adhesive films composed of molecules with tailor-made properties in unique spatial arrangements with respect to each other and to the substrates.

An organized self-assembly monolayer (SAM) is a single layer of molecules on a substrate in which the molecules exhibit a high degree of orientation, molecular order and packing (Fig. 3.1). There are two common methods for depositing a monolayer, namely Langmuir-Blodgett and self-assembly technique. In this work, the self-assembly technique was used to get monolayer.

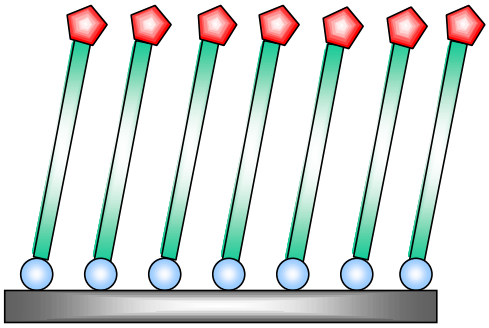

Fig. 3.1 Scheme of monolayer structure

3.1 Langmuir-Blodgett (LB) Technique

Typical LB films are prepared by transferring monolayers of amphiphilic molecules at the air-water interface onto solid substrates. The amphiphilic molecule is a molecule that is insoluble in water, with one end that is hydrophilic, and, therefore, is preferentially immersed in the water, and the other that is hydrophobic, and preferentially resides in the air (or in the nonpolar solvent). The amphiphilic molecules are first dissolved in an organic solvent that is immiscible with water, spread on the water surface, and compressed by decreasing the area in which the

molecules are confined, to form a monolayer at the air-water interface. Then the monolayer is transferred onto a solid substrate either by dipping the substrate through the interface or by touching it to the interface. The procedure can be used to obtain ultrathin films with the structure and thickness (monolayer or multilayer) controlled at molecular level. Three possible structures produced by LB technique are shown in Fig. 3.2.

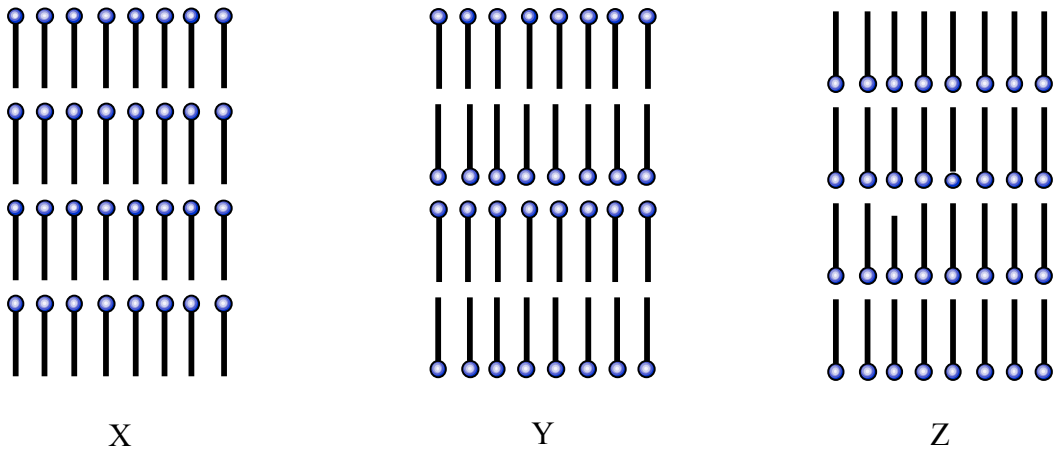

Fig. 3.2 X, Y and Z –mode in Langmuir-Blodgett film deposition

The first LB film of a conducting polymer was prepared by Iyoda et al. using an amphiphilic polypyrrole derivative mixed with octadecane [70-73]. This precursor LB film on subsequent electropolymerization gave a lateral conductivity of 0.1 S/cm and with the conductivity in the perpendicular direction being 10^{-11} S/cm. Several other methods were also demonstrated to fabricate PPy films [74]. Ultrathin films of 3-octadecyl pyrrole and 3-octadecanoyl pyrrole were also subsequently obtained by using LB technique. 3-Octadecanoyl pyrrole films were found to be highly anisotropic with conducting in the plane being two orders of magnitude higher that across the perpendicular direction. LB films of PANi, PPV, PT were also prepared and studied for possible application in molecular electronics devices [75-79].

3.2 Self-Assembly Technique

3.2.1 Definition of Self-Assembly Monolayer (SAM)

The drawbacks of using LB technique are that it is a time-consuming process and films tend to be fragile and mechanically instable. The self-assembly technique offers an alternative route to prepare monolayer thin films of highly ordered multifunctional compounds in a more effective and time saving manner. This technique is more advantageous than the LB technique

in the sense that each layer in self-assembly (SA) film can be covalently linked and no excessive deposition can take place as it is limited by the reactive sites on the layer surface [80]. In self-assembly technique, monomolecular films of a surfactant are spontaneously formed on a substrate upon exposure of surfactant solution. The principal driving force for the formation of such films is the specific interaction between the surfactant head group and the substrate surface. Depending on the structure of the surfactant, these films can be disordered (liquid-like) or well-packed, resembling the organization of crystals. The degree of order in a monolayer is the product of many factors, including geometric considerations, electrostatic and dipole-dipole interactions within the monolayer, affinity of the head group of the surfactant to the surface, etc. A successful self-assembly requires a relatively strong bond between the substrate and an atom or moiety in the surfactant, and an additional lateral interaction between molecules in the monolayer. The strength of the head group-substrate bonds and the lateral interactions lead to the monolayer resist removal by a solvent rinse. Unlike the popular LB monolayer, SAMs remained relatively obscure until the 1980s when several researchers discovers that long-chain thiols and disulfides spontaneously formed remarkably well-packed and stable monolayer on gold substrates [81, 82]. SAMs provide facile means of defining the chemical composition and structure of a surface, therefore, they have become the focus of intensive investigation. Potential technological applications can be found in areas such as wetting, lubrication, adhesion, corrosion, biocompatibility, catalyst, and chemical sensing and nanoscale lithography. When SAMs are used in areas of adhesion, such surfactants are called adhesion promoters.

3.2.2 Types of Self-Assembly Monolayers on Substrates

There are several types of SA methods that yield organic monolayers. The first is based on the reaction of trichloro-or trialkoxysilanes with a hydroxylated surface (SiO_2 on Si, Al_2O_3 on Al, glass, etc.) [83-85], and even gold without any surface oxide [86, 87]. The second, conveniently prepared by exposure of gold surface to a thiol or disulfide solution, relies on the strength of sulfur-gold interactions [81, 88]. Generation of alkane radicals near an oxide-free silicon surface results in the formation of a densely packed SAM in which a methene carbon is directly bonded to a silicon surface atom [89, 90]. Others include phosphate or a phosphonate group on oxide surface (Ta_2O_5, TiO_2) [91-94], alcohols and amines on platinum [95], and carboxylic acids on aluminum oxide [96], and silver [97].

3.2.3 Energy Interaction in a Self-Assembly Process

Self-assembled monolayers of long chain functionalized compounds (e. g. thiols, silanes, carboxylic acids, and phosphonic acids) form organic interfaces with properties largely controlled by the end groups of the molecules comprising the films. These monolayers provide a unique link between the science of organic surfaces and technologies that seek to exploit their adaptable characters.

From the energetic point of view, a self-assembly surfactant molecule (adhesion promoter) can be divided into three parts (Fig. 3.3). The first part is the head group that provides the most exothermic process, i.e., chemisorption on the substrate surface. The very strong molecular-substrate interaction results in an apparent bond with pining of the head group to a specific site in the surface through a chemical bond. This can be a covalent Si-O bond in the case of alkyltrichlorosilanes on hydroxylated surfaces; a covalent but slightly polar Au-S bond in the case of alkanethiols on gold, or an ionic $-COO^{-}Ag^{+}$ bond in the case of carboxylic acids on AgO/Ag. The energy associated with the chemisorption is of the order of tens of kcal/mol. As a result of the exothermic head group-substrate interactions, molecules try to occupy every available binding site on the surface, and in this process they bring the adsorbed molecules close enough together.

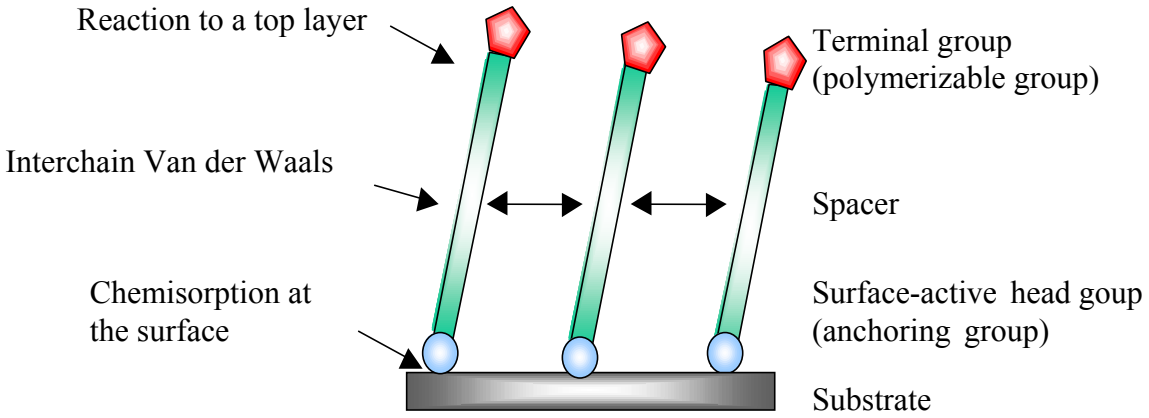

Fig. 3.3 Model of a adhesion promoter

The second molecular part is the spacer, which usually is the alkyl chain. Van der Waals interactions between the alkyl chain form the adsorbed molecules to an ordered and closely packed assembly. The energies associated with this interchain Van der Waals interactions are at the order of few (< 10) kcal/mol (exothermic).

The third molecular part is the terminal group. When this terminal group is functionalized with a polymerizable moiety, it can be chemically or electrochemically induced to polymerize. Successful self-assembly requires a relatively strong bond between the substrate and an atom or moiety in the molecule, and an additional lateral interaction between molecules in the monolayer. The strength of the head group-substrate bonds, the lateral interactions and the density of packing result in sufficient stability that the monolayer resists removal by a washing with a solvent.

3.3 Preparation of SAMs

3.3.1 Substrates/Head Groups

It is well known that pre-treatment of the substrate has reasonable influence on surface properties, which direct adsorption of SA molecule. Substrates have to be pre-treated and activated for a specific chemical interaction between the head group and the active center of the substrate. The surface of substrate can be either an oxide or unoxide one depending on the head group. To some extent, the choice of substrate is dictated by the application of the SAM. For the most highly oriented crystalline SAM, a single crystalline and atomically flat substrate is desired.

Gold is the most popular substrate for thiol SAMs. Owing to its noble character, gold substrates can be handled in air without the formation of an oxide surface layer, and can survive harsh chemical treatments to remove organic contaminants. Evaporated or sputtered gold films (typically 50-200 nm thick) on glass; silicon or cleaved mica substrates prepare the gold surface. The driving force for the interaction of alkyl sulphide is the formation of a covalent bond Au-S [98]. SAMs of alkane thiolates on gold are generally the most investigated systems as they form unique layers. Therefore, they became ideal model systems for studying the self-assembly process.

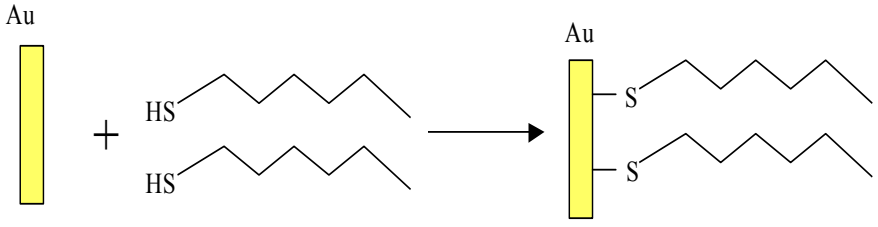

Scheme 3.1 Thiol SAMs

The other coinage metals, silver and copper, and platinum have also been used as substrates for thiols SAMs. For freshly evaporated silver or copper thin films, surface oxides exist prior to SAM deposition. The self-assembly process appears to remove the oxide layer from silver but not from copper, yielding lower quality SAMs on the latter substrate [99-101].

Modification of oxide surfaces such as SiO_2, Al_2O_3 and TiO_2 by organosilanes of the type Y-spacer-$SiX_1X_2X_3$ continues to be a promising field of research, due to the process responsible for the monolayer formation is relatively simple and leads to strongly bonded molecules to the substrates [102-107]. Substrates like Si/SiO_2 can react with trichlorosilanes resulting in a three dimensional network of reactive Si-OH groups and Si-O-Si bonds. According to Carim et al. [108] the treatment with pirañha solution yields substrates with the surface of Si-O group concentration of $5*10^4/Å^2$. This is essential for the surface condensation process. For metal substrates, the surface can be electropolished and then pre-treated with staining solution (acid-base) or ultrasonically with acetone [109].

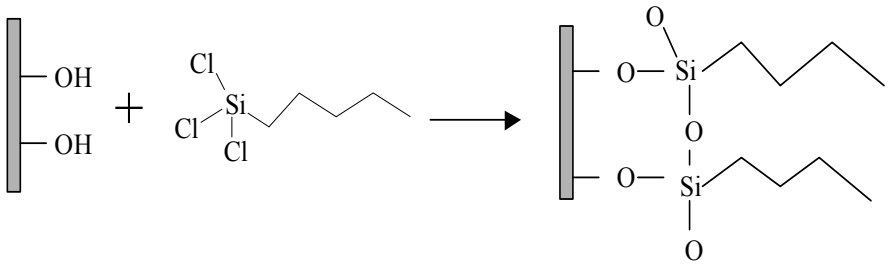

Scheme 3.4 SAMs of trichlorosilane on Si/SiO_2

Phosphonic acids can be adsorbed on TiO_2 and Ta_2O_5 surface to produce dense, highly ordered monolayers in a “tails-up “ configuration. It is reported that phosphonic acid possess strong chelation properties and hence, they are employed as corrosion inhibitors [110], for metal extraction [111], and in biochemical applications [112].

Titanium and titanium alloy substrates are mainly used in the aircraft industry and marine equipment due to their low density and high mechanical. They are also considered as the metallic biomaterials of choice, a field where it is necessary to engineer and control surface modification of the oxide layer [113] For example, titanium-nanoscaled interdigitated electrodes are presently investigated for miniature and sensitive biosensors [114].

Normally the incipient oxide film on the surface of titanium is 80 Å thick. Sputtering the oxide film with argon changes the composition of the oxide film. This is of significance with

respect to many applications like corrosion resistance or the adhesion strength of the adsorbed molecule. The nature of the oxide film becomes important in deciding the extent of modification [115].

Tantalum oxide has a high refractive index, which renders it ideal for application in a planar-waveguide based bioaffinity sensor [116].

3.3.2 Solution Adsorption

Immersion of the substrates into a homogeneous solution of a suitable self-assembly molecule at room temperature followed by rinsing is the most common approach for depositing the SAM. Usually any solvent capable of dissolving the molecule is suitable. Ethanol is the most popular solvent. But for organosilane SAMs, the solvent is usually an apolar hydrocarbon solvent.

For millimolar or higher concentrations of thiols, a disordered monolayer is deposited in a few seconds. There is a much slower transformation over a period of hours to days into a highly oriented and densely packed monolayer [117, 118].

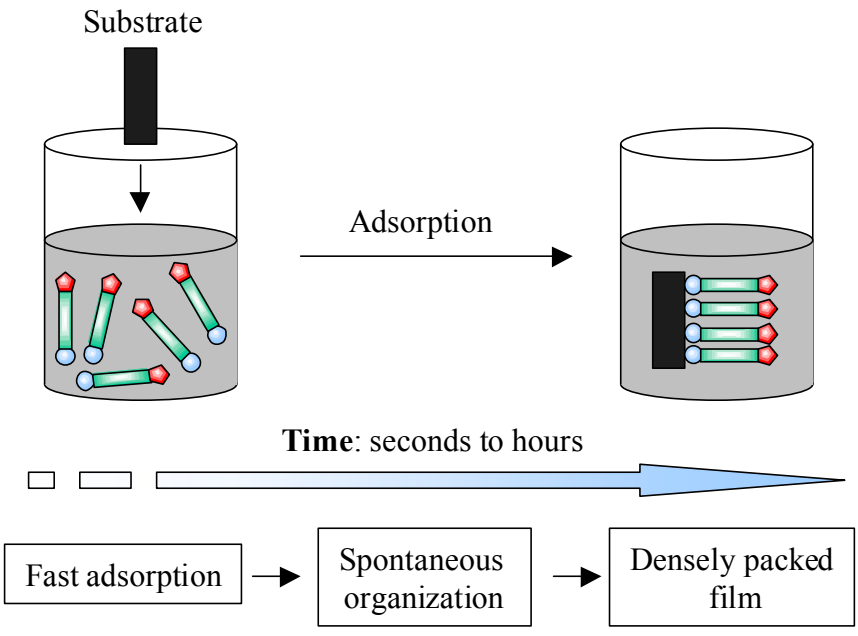

Fig. 3.5 **Immersion of a substrate to an adhesion promoter solution leads to formation of a SAM. The principle driving force for SAM formation is the affinity of adhesion promoter head groups for the surface of the support.**

Grafting of alkoxysilanes on oxide surfaces usually requires relatively concentrated solutions (10^{-2}-1 M) [119,120] to yield dense monolayers, and to control their oligomerization in solution [119]. Grafting of trichlorosilyl groups is an attractive alternative because low concentrations (~ 10^{-3} M) in apolar hydrocarbon solvents (toluene, bicyclohexyl, etc) and short reaction times are sufficient to form tightly packed monolayers [121, 122].

The rates of the monolayers formation showed strong dependence on the nature of the head group of the coupling agent. Helmy et al reported that on the basis of the kinetics measurements, the following range of reactivity on TiO_2 was established: $C_{18}H_{37}SiCl_3$ >> $C_{18}H_{37}PO(OH)_2$ > $C_{18}H_{37}Si(CH_3)_2Cl$; $C_{18}H_{37}Si(OCH_3)_3$ > $C_{18}H_{37}SiH_3$ [123]

3.4 Application of SAMs in Conducting Polymers

In the field of conducting polymers, most of the studies report the use of pyrrol-, thiophene- or phenyl-functionalized self -assembly monolayers to increase the adhesion of the polymer films to the substrate. Rubinstein reported that 4-Mercaptoaniline increases the uniformity of subsequently deposited polyaniline [124]. Kowalik used mercapto-substituted 2,5-(2-pyrrolyl) thiophene deposited on gold to enhance the adhesion of thick overlayers of polypyrrole [125]. Willicut and McCarley found that the monolayers formed from a series of short chain ω-(N-pyrrolyl) alkane thiol monomers can enhance the nucleation, growth, smoothness, and adhesion of PPy [126-129]. At the same time, Collard and Sayre synthesized 3-substituted pyrrole monomers with long alkyl chains, they also found that these monomers form well-ordered monolayers enhance the nucleation and adhesion of poly (3-ethyl pyrrole), as well as an increase in conductivity [130-132]. Nishizawa et al. found that dodecylsulfonate amplified the promotion of lateral growth of PPy on n-alkylsilane-treated surface. They attributed the promotion by alkylsilanes to adsorption of pyrrole monomers and oligomers at the hydrophobic surface [133]. Mekhalif et al. discovered that alkanethiols on platinum increased the conjugation length of electro-deposited polybithiophene films. When aromatic thiols were used, adhesion was improved relative to bare surfaces, the morphology was more rough and globular, the films were denser, and the conjugation length again increased [134]. Lo et al. used N-(3-amino propyl) pyrrole to passivate active spots on $YBa_2Cu_3O_{7-\delta}$, which dominate the polymer growth dynamics at early polymerization times, allowing PPy to grow uniform films quickly with good contact to the substrate and improved morphology [135]. Simon et al. [136] and Wu and Chen [137] for adhering polypyrrole on silicon substrate successfully used

N- (3- (trimethoxysilyl) propyl pyrrole. Guiseppi-Elie et al. [138] and Faveroll et al. [139] constructed other original pyrrole substituted organosilane monolayers for grafting polypyrrole on SiO_2 substrate. Huang et al. [140] used patterned n-octadecylsiloxane monolayers on SiO_2 substrates for selective and directed deposition of conducting polymers. These few examples emphasize that self-assembled monolayers, which have desired control on molecular level, should be considered as a potential technique for the construction of more highly ordered and adhesive materials. These researchers reported materials closely related to our subject.

3.5 Design of Adhesion Promoter

The aim of the project is to graft adhesive conducting polymers onto oxide substrates. For this purpose the adhesion promoter between an oxide surface and a polymeric matrix is required. Such kind of adhesion promoters was designed having a surface reactive group, an aliphatic or aromatic spacer, and a reactive group for top polymer layer.

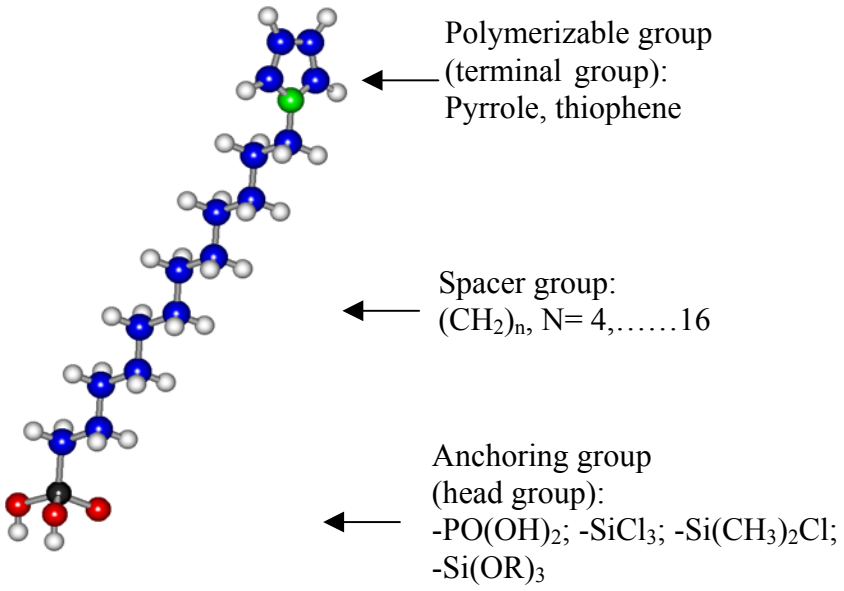

Fig. 3.6 Model of the synthesized compound

Head group: Among the various anchoring group chemistries available, the relatively robust nature of siloxane-anchored SAMs and phosphonate-SAMs and their convinient attachment to a wide range of hydroxyl-and/or oxide-bearing surface makes them particularly attractive for surface modification in a variety of applications.

Helmy and Fadeev reported that SAMs of $C_{18}H_{37}Si(CH_2)_2Cl$ and $C_{18}H_{37}PO(OH)_2$ show a uniform mechanism of the film growth, and SAMs of $C_{18}H_{37}SiX_3$ (X= H, Cl, OCH_3) have an island-like mechanism of the film growth [123].

Phosphonic acids forming strong bonds with several metal surfaces were chosen as surface-active groups (head group) on metal oxide substrates, whereas silane derivatives were used on silicon surface.

Spacer group: In order to investigate the effect of the alkyl chain length on the adsorption process and the surface reaction, the flexible alkyl chain functions were used as a distance holder between two functional groups. Finklea reported that in highly ordered SAMs, the orientation of the terminal group can depend on the number of methylenes separaring the terminal group from the anchoring group (the ‘ odd-even ‘ effect) [141].

Terminal group: The choice of the terminal group offers the extension to other polymer systems. Conducting polymers, which typically cocsist of conjugated double bonds, show strong inter-chain interaction and are difficult to process due to their non-fusibility and insolubility. For grafting conducting polymers on the substrates, the introduction of polymerizable groups like thiophene and pyrrole into the adhesion promoter which allows an in-situ surface polymerization with further monomers directly on the substrate are necessary. Therefore pyrrole was chose as terminal groups. As usually grown, polypyrrole films do not adhere well to substrates, are rough and irregular, and have conductivitie which are too small for most practical applications. For bulk polypyrrole, it has been shown that the conductivity can be improved when the material is grown in a more ordered, constrained geometry.

Chapter 4 Adhesion Promoters

For grafting adhesive conducting polymer films on substrates, there is a need to introduce an adhesion promoter that would act as a compatibiliser between the polymer and the substrate. Surface in-situ chemical polymerization or electropolymerization could be practiced such that the adhesion promoter can bring the polymer and the substrate in contact.

In this chapter, the synthesis of such adhesion promoters, namely functionalized N-pyrrolyl derivatives and 3-pyrrolyl derivatives that were able to adsorbed on oxide surface and to run various homo- and copolymerization process (chemically and electrochemically) is described. The adsorption behavior of these adhesion promoters on oxide substrates was also studied. The structure of the adhesion promoter is described below.

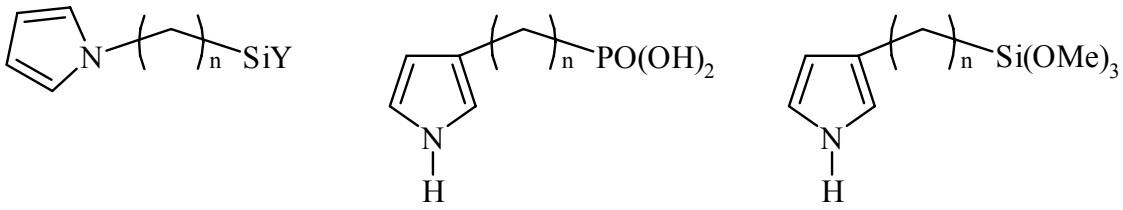

n= 6, 8, 11, 16 n= 4, 6, 8, 11 n= 11

Y= -Cl_3, -$ClMe_2$

Structure 4.1 Structure of adhesion promoters

4.1 Chemistry of Pyrrole

Pyrrole is a colorless liquid, b.p. 129.8°C at 760 torr, m. p. 23.4°C, density 0.970 g/ml at 20°C. It gradually turns brown in air and is slightly hygroscopic, taking up approximately 3% by weight of water at room temperature. It has low solubility in water but is miscible with most of the organic solvents. Polymers based on pyrrole ring system show considerable promising applications as semiconducting and conducting materials.

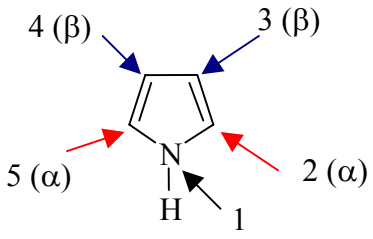

Structure 4.2 Pyrrole

Pyrrole is π-excessive (electron-rich) 5-membered heterocycle with six π-electrons delocalized over the ring. It undergoes electrophilic substitution normally at the 2- or 5- (α) position. Substitution at 1-, 3-, and 4- positions need drastic conditions. Nucleophillic substitution is virtually unknown in pyrrole. Valence bond representations of the structure of pyrrole include the four zwitterionic resonance forms shown in scheme 4.1, so the reactivity of pyrrole ring towards electrophiles at 2-position is due to Wheland intermediates having the same number of double bonds as the starting molecule.

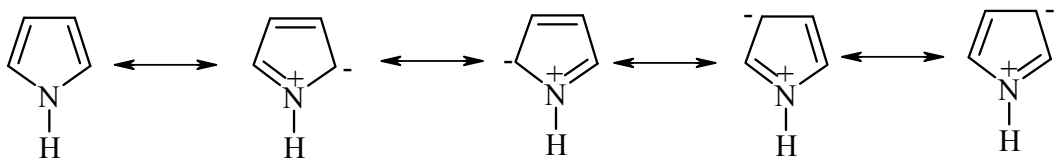

Scheme 4.1 Valence bonds

4. 2 N-Substituted Pyrrole Monomers as Adhesion Promoters

Electrophilic substitution at the nitrogen atom of pyrrole ring normally occurs under strongly basic conditions, except for proton exchanges, which normally readily occurs under both mildly acidic conditions or in the presence of aqueous base. The pKa of the pyrrole NH is 17.5, and so, although proton exchange occurs readily in aqueous base, alkylation (or acylation) can normally be effected by conversion into pyrrolyl Grignard or by use of strong bases as sodamide, liquid ammonia or potassium t-butoxide in t-butanol or DMSO. Alkylation on nitrogen can also be effected with aqueous base by the use of phase-transfer catalytic methods and if electron-withdrawing substituents are present in the pyrrole ring, the more readily formed N-anions can be alkylated under milder basic conditions.

N-alkylation of pyrrole bearing an acidic hydrogen attached to nitrogen is generally accomplished by the treatment of this compound with an appropriate base followed by the treatment of the resulting salt with an alkylating agent.

Since the pyrrolyl anions exhibit ambident behaviour as nucleophile, alkylation can occur at carbon as well as at nitrogen. The amount of N-alkylation relative to C-alkylation depends on a number of factors, including the base employed for the deprotonation of the heterocycle, the solvent, and the alkylating agent. Thus, for the salts derived from pyrrole, the base (and hence, the cation associated with the pyrrolyl anion) can influence the ratio of N to C alkylation. Although nitrogen alkylation generally predominates when the cation is a sodium

or potassium ion, carbon alkylation usually predominates with the harder cations like lithium or magnesium, which are tightly bound to nitrogen. Various new procedures have been developed in which the N-alkylation of pyrrole can be accomplished with little or no interference from the C-alkylation. Some procedures rely on the use of dipolar aprotic solvents [142-145], one in which thallium salt of pyrrole is employed [146] and several procedures which rely on phase-transfer catalysis by quaternary ammonium salts [147, 148].

The phase transfer procedures appear to be the most useful in terms of condition, yield, and convenience. Alkylation is effected by simply stirring a solution containing the alkylating agent, the heterocycle and a catalyst in the presence of a concentrated solution of sodium hydroxide. Exclusive N-alkylation is observed but inspire of these advantages there are several disadvantages, which decrease the applicability of this procedure. For example, when alkyl iodide is employed as alkylating agent, respectable yields of the product are obtained only when a stoichiometric amount of the catalyst is used. In addition, there are a number of solvents in which quaternary ammonium salts are insoluble. Also the functional group attached to pyrrole nucleus, which are labile to hydrolysis in the presence of hydroxide would not be able to survive the phase-transfer alkylation procedure catalysed by quaternary ammonium salts.

Another method that takes care of the above drawbacks uses 18-crown-6 as catalyst and potassium t-butoxide as base. The procedure is convenient and mild and generally gives rise to exclusive N-alkylation [149].

We chose a molecule containing two reactive functional groups, i. e. pyrrole and silane connected by an alkyl chain. Silane was taken as the other functional group as previous studies showed that silane produced oriented, well-ordered monolayers on a flat oxide surface and also resulted in stable and adhesive film.

4.2.1 Synthesis of (N-pyrrolyl) Alkyl Silanes

As discussed above various methods are available in literature for the synthesis of N-derivatives of pyrrole. A three-step route was adopted to synthesize the (N-pyrrolyl) alkyl silanes [150]. The first step was the conversion of pyrrole into its potassium salt which served as a precursor for the synthesis of (N-pyrrolyl) alkene [144, 145, 151]. This intermediate is known and has been synthesized [152]. The formation of the potassium salt of pyrrole requires inert atmosphere and complete anhydrous conditions for its synthesis. Alkylation is

then achieved without the isolation of the potassium salts by addition of an excess of the appropriate alkene halide at room temperature.

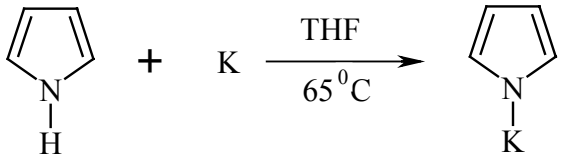

Scheme 4.2 Synthesis of pyrrole potassium salt

The reaction of alkali metal salt of pyrrole with alkene halide is complex but alkylation at nitrogen is usually predominant (see Scheme 4.3), this depends on the number of factors, the most important being the medium of reaction and the size of the alkali metal. Thus, the sodium and potassium salts (ionic radii of 0.98 Å for Na^+ and 1.33 Å for K^+) of pyrrole form predominantly nitrogen-alkylated products, whereas Li and Mg salts (each with an ionic radius of 0.78 Å) give predominantly carbon-alkylated products. For a given medium, both under heterogeneous conditions and in solution, the relative percentage of N-alkylation increases with the decreasing coodinating ability of the cation in the order $Li^+<Na^+<K^+<(CH_3)_3NC_6H_5^+$. Addition of tetra-butylammonium bromide to any reaction mixture increases the relative percentage of N-alkylation.

In non-polar organic solvents the alkali metal salts of pyrrole are highly dissociated through co-ordination of the nitrogen in the pyrrolyl ion. The use of DMSO as a dipolar aprotic solvent is well known and excellent results have been obtained. Due to DMSO, the salt is highly solvated and hence dissociated and relatively soluble. In general, the percentage of alkylation at the nitrogen atom (N-position) increases with the solvating power of the medium and decreases with the coordinating ability of the metal ion. These effects are explained on the basis of the dissociation of the pyrrolyl-metal ion pair.

On this basis, the reaction mechanism is postulated as given

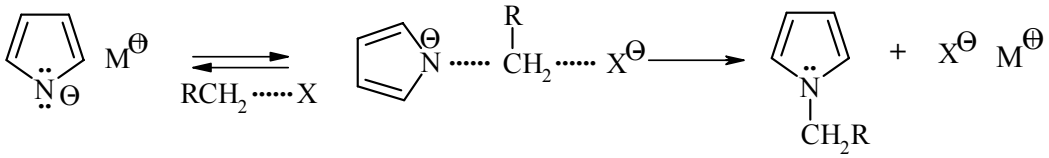

Scheme 4.3 Mechanism of N-alkylation

Two times excess of alkene halide in DMSO was added dropwise to the solution of potassium pyrrole salt in DMSO under the following conditions.

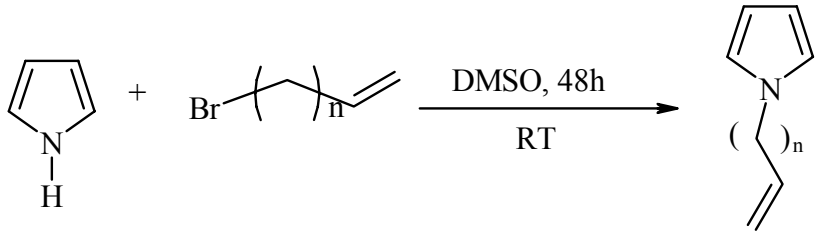

Scheme 4.4 Synthesis of ω-(pyrrol-1-yl) alkene

The N-pyrrole alkyl chlorosilane was obtained by hydrosilylation of N-pyrrole alkene according to Anti-Markovnikow mechanism [153-155].

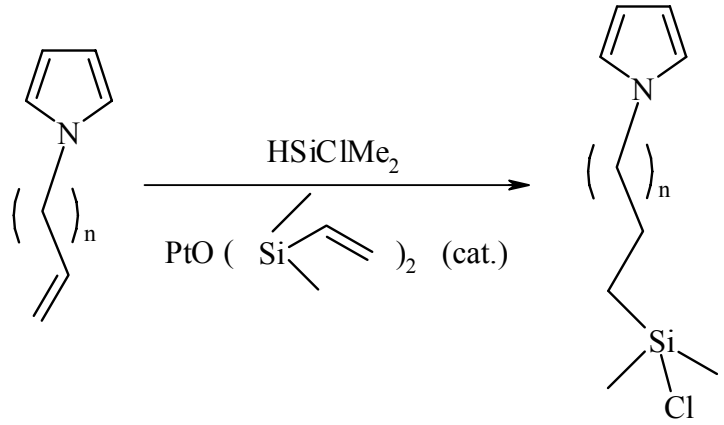

Scheme 4.5 Hydrosilylation

Hexachloroplatinic acid was usually used as hydrosilylated catalyst due to the mild reactive conditions. Compared to hexachloroplatinic acid, 1,3-divinyl-1,1,3,3-tetramethyldisiloxan platinum (0)-complex has more advantages. It is a homogeneous catalyst and has high selectivity for reaction [156].

In this work, homogeneous catalyst 1,3-1,1,3,3-tetramethyldisiloxan-platin (0)-complex was used.

4.2.1.1 Synthesis of ω-(pyrrol-1-yl) alkene

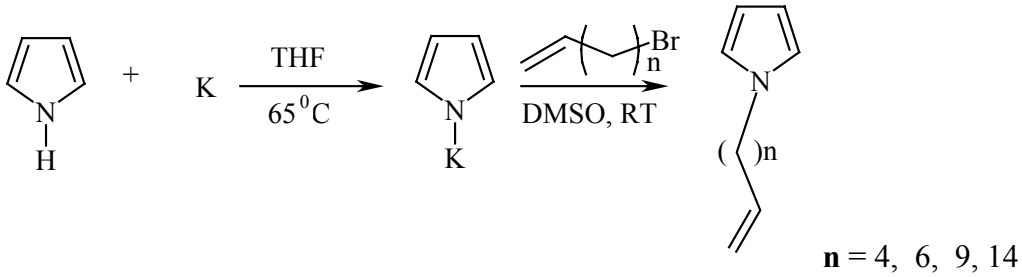

Scheme 4.6 Synthesis of ω-(pyrrol-1-yl) alkene

A total of 1.17 g (30 mmol) of potassium, freshly cut into small pieces under n-heptane, was added to a solution of 2.52 g (338 mmol) of pyrrole in 80 ml dry THF under dry argon atmosphere. The mixture was warmed until the potassium melted and was then stirred until all traces of potassium had disappeared. To this mixture, 20 ml DMSO was added, and then the solution of 60 mmol of alkene bromide in 100 ml of DMSO was added over a period of 1 hour. The mixture was stirred at room temperature for 2 days. Then the solution was poured into saturated sodium bicarbonate solution. The organic layer was separated and the aqueous layer extracted with 50 ml portions of ether (3 times). The combined ether extracts and organic phase were dried over $MgSO_4$ and then the solvent was removed under vacuum. The pure colorless compound was obtained by column chromatography (eluent: n-hexene:dichloromethane, 10:1).

Identification:

- ***6-(pyrrol-1-yl) hexene:***

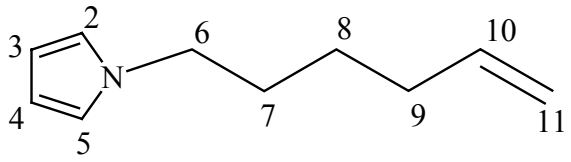

Structure 4.3 Structure of 6-(pyrrol-1-yl) hexene

Yield: 43.5**%**

^{1}H-NMR (500 MHz, chloroform, δ in ppm): 6.67 [2H, (H2, 5), m], 6.16 [2H, (H3, 4), m], 5.84-5.76 [1H, (H10), m], 5.05-4.98 [2H, (H11), m], 3.91-3.87 [2H, (H6), $J_{6,7}$ = 7.1Hz, t], 2.12-2.08 [2H, (H9), m], 1.84-1.80 [2H, (H7), m], 1.45-1.40 [2H, (H8), m].

IR (chloroform, ν_{max}/cm^{-1}): 3101-3078 (arom. C-H), 2933 (ν_{as} CH_2), 2861 (ν_s CH_2), 1641 (C=C), 1541-1501 (pyrrole ring), 1441-1371 (C-N).

Elemental analysis:

$C_{10}H_{15}N$: Calculated: C, 80.48; H, 10.13; N, 9.39.

Found: C, 80.62; H, 9.98; N, 9.50.

- ***8-(pyrrol-1-yl) octene:***

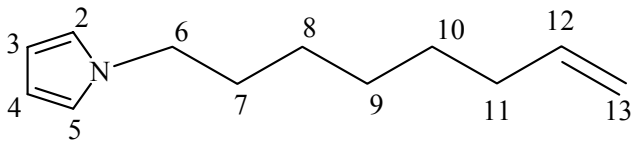

Structure 4.4 Structure of 8-(pyrrol-1-yl) octene

Yield: 65.7**%**

^{1}H-NMR (500 MHz, chloroform, δ in ppm): 6.67 [2H, (H2, 5), m], 6.16 [2H, (H3, 4), m], 5.86-5.78 [1H, (H12), m], 5.04-4.96 [2H, (H13), m], 3.90-3.87 [2H, (H6), $J_{6,7}$ =7.1Hz, t], 2.09-2.06 [2H, (H11), m], 1.83-1.78 [2H, (H7), m], 1.48-1.38 [6H, m].

IR (chloroform, ν_{max}/cm^{-1}): 3101-3075 (arom. C-H), 2928 (ν_{as} CH_2), 2856 (ν_s CH_2), 1640 (C=C), 1539-1500 (pyrrole ring), 1447-1360 (C-N).

Elemental analysis:

$C_{12}H_{19}N$: Calculated: C, 81.30; H, 10.80; N, 7.90.

Found: C, 81.73; H, 10.62; N, 8.27.

- ***11-(pyrrol-1-yl) undecene***:

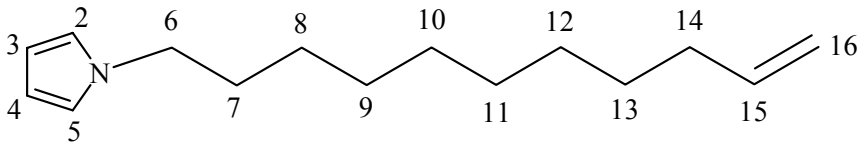

Structure 4.5 Structure of 11-(pyrrol-1-yl) undecene

Yield: 77.5%

^{1}H-NMR (500 MHz, chloroform, δ in ppm): 6.67-6.66 [2H, (H2, 5), m], 6.16-6.15 [2H, (H3, 4), m], 5.87-5.79 [1H, (H15), m], 5.04-4.94 [2H, (H16), m], 3.89-3.86 [2H, (H6), $J_{6,7}$ = 7.2Hz, t], 2.07-2.04 [2H, (H14), m], 1.81-1.76 [2H, (H7), m], 1.51-1.30 [12H, m].

IR (chloroform, ν_{max}/cm^{-1}): 3101-3076 (arom. C-H), 2926 (ν_{as} CH_2), 2854 (ν_s CH_2), 1640 (C=C), 1538-1500 (pyrrole ring), 1460-1365 (C-N).

Elemental analysis:

$C_{15}H_{25}N$: Calculated: C, 82.13; H, 11.49; N, 6.39.

Found: C, 82.61; H, 11.44; N, 6.74.

- ***16-(pyrrol-1-yl) hexdecene:***

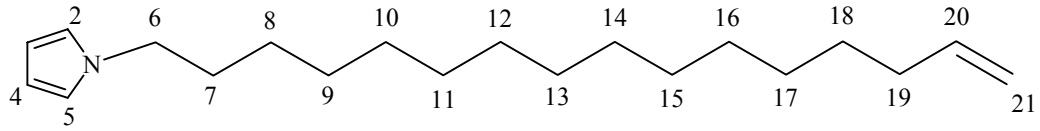

Structure 4.6 Structure of 16-(pyrrol-1-yl) hexdecene

Yield: 79.6%

^{1}H-NMR (500 MHz, chloroform, δ in ppm): 6.64 [2H, (H2, 5), m], 6.13 [2H, (H3, 4), m], 5.85-5.77 [1H, (H20), m], 5.01-4.92 [2H, (H21), m], 3.87-3.84 [2H, (H6), $J_{6,7}$ = 7.2Hz, t], 2.06-2.02 [2H, (H19), m], 1.78-1.74 [2H, (H7), m], 1.52-1.25 [22H, m].

IR (chloroform, ν_{max}/cm^{-1}): 3101-3076 (arom. C-H), 2924 (ν_{as} CH_2), 2653 (ν_s CH_2), 1640 (C=C), 1536 -1500 (pyrrole ring), 1462-1366 (C-N).

Elemental analysis:

$C_{20}H_{35}N$: Calculated: C, 82.98; H, 12.18; N, 4.84.

Found: C, 83.72; H, 12.23; N, 4.19.

4.2.1.2 Synthesis of ω-(pyrrol-1-yl) alkyl silanes

The same procedure was applied for the synthesis of 1-pyrrolyl-alkyl dimethylchlorosilane (PMCS) and 1-pyrrolyl-alkyl trichlorosilane (PUTS).

In a round flask was added 0.5 g ω-(pyrrol-1-yl) alkene, 5 ml dimethylchlorosilane and a catalytic amount of 1,3-divinyl-1,1,3,3,-tetramethylsiloxane platin complex at –5 ~ 0°C. The mixture was stirred at low temperature for 1 hour. Then the mixture was warmed to room temperature and stirred overnight. The excess dimethylchlorosilane was removed to get desired compound, respectively.

Identification:

- ***6-(pyrrol-1-yl hexyl) dimethylchlorosilane (PMCS-6):***

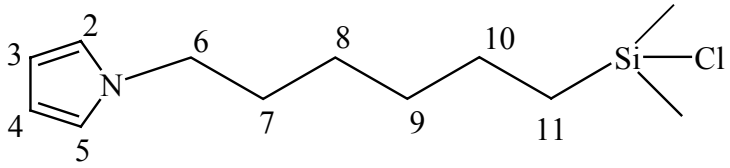

Structure 4.7 Structure of 6-(pyrrol-1-yl hexyl) dimethylchlorosilane

^{1}H-NMR (500 MHz, chloroform, δ in ppm): 6.65 [2H, (H2, 5), m], 6.14 [2H, (H3, 4), m], 3.87-3.84 [2H, (H6), $J_{6,7}$ = 7.2Hz, t], 1.80-1.76 [2H, (H7), m], 1.43-1.30 [6H, m], 0.82-0.79 [2H, (H11), $J_{10,11}$= 8.0Hz, t], 0.41 [6H, Si-CH_3, s]

^{13}C-NMR (500 MHz, chloroform, δ in ppm): 120, 108, 49, 31, 31, 26, 24, 22.

^{29}Si-NMR (500 MHz, chloroform, δ in ppm): -67.90

IR (chloroform, ν_{max}/cm^{-1}): 3103 (arom. C-H), 2925 (ν_{as} CH_2), 2856 (ν_s CH_2), 1500-1452 (pyrrole ring), 1407-1363 (C-N), 1252 (ν_{as} CH_3 def.), 841-795 (Si-CH_3 rocking vib.), 615 (Si-Cl).

Elemental analysis:

$C_{12}H_{22}ClNSi$: Calculated: C, 59.11; H, 9.09; N, 5.74.

Found: C, 60.03; H, 9.30; N, 5.24.

- ***8-(pyrrol-1-yl octcyl) dimethylchlorosilane (PMCS-8):***

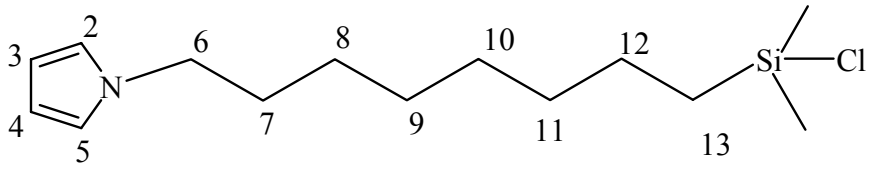

Structure 4.8 Structure of 8-(pyrrol-1-yl octyl) dimethylchlorosilane (PMCS-8)

^{1}H-NMR (500 MHz, chloroform, δ in ppm): 6.65 [2H, (H2, 5), m], 6.14 [2H, (H3, 4), m], 3.88-3.85 [2H, (H6), $J_{6,7}$ = 7.2Hz, t], 1.79-1.75 [2H, (H7), m], 1.42-1.30 [10H, m], 0.83-0.79 [2H, (H13), $J_{12,13}$= 8.0Hz, t], 0.41 [6H, Si-CH_3, s]

^{13}C-NMR (500 MHz, chloroform, δ in ppm): 120, 107, 49, 32, 31, 29, 26, 22, 18.

^{29}Si-NMR (500 MHz, chloroform, δ in ppm): -67.90

IR (chloroform, ν_{max}/cm^{-1}): 3101 (arom. C-H), 2924 (ν_{as} CH_2), 2854 (ν_s CH_2), 1500-1462 (pyrrole ring), 1406-1364 (C-N), 1253 (ν_{as} CH_3 def.), 841-796 (Si-CH_3 rocking vib.), 617 (Si-Cl).

Elemental analysis:

$C_{14}H_{26}ClNSi$: Calculated: C, 61.84; H, 9.64; N, 5.15.

Found: C, 62.88; H, 9.85; N.4.87.

- ***11-(pyrrol-1-yl undecyl) dimethylchlorosilane (PMCS-11)***

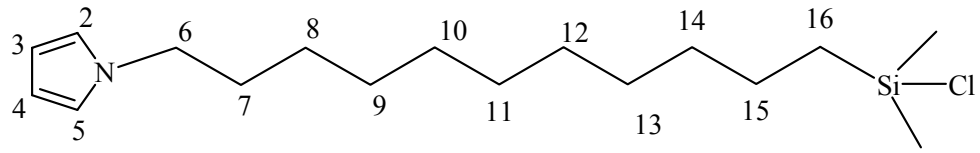

Structure 4.9 Structure of 11-(pyrrol-1-yl undecyl) dimethylchlorosilane (PMCS-11)

^{1}H-NMR (500 MHz, chloroform, δ in ppm): 6.64 [2H, (H2, 5), m], 6.13 [2H, (H3, 4), m], 3.87-3.84 [2H, (H6), $J_{6,7}$ = 7.2Hz, t], 1.78-1.73 [2H, (H7), m], 1.41-1.25 [16H, m], 0.82-0.79 [2H, (H16), $J_{15,16}$= 8.1Hz, t], 0.39 [6H, Si-CH_3, s]

^{13}C-NMR (500 MHz, chloroform, δ in ppm): 120, 107, 49, 32, 31, 29, 29, 26, 22, 18.

^{29}Si-NMR (500 MHz, chloroform, δ in ppm): -67.87

IR (chloroform, ν_{max}/cm^{-1}): 3101 (arom. C-H), 2926 (ν_{as} CH_2), 2854 (ν_s CH_2), 1500-1460 (pyrrole ring), 1407-1363 (C-N), 1254 (ν_{as} CH_3 def.), 841-795 (Si-CH_3 rocking vib.), 616 (Si-Cl).

Elemental analysis:

$C_{17}H_{32}ClNSi$: Calculated: C, 65.03; H, 10.27; N, 4.46.

Found: C, 65.56; H, 9.98; N, 4.31.

- ***16-(pyrrol-1-yl hexadecyl) dimethylchlorosilane (PMCS-16):***

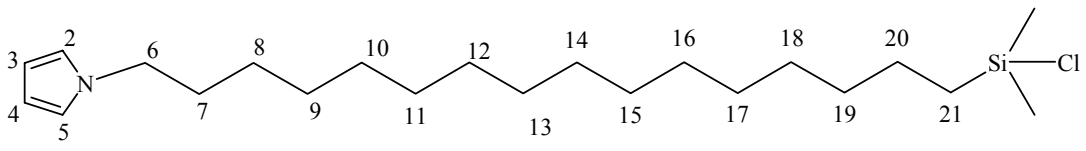

Structure 4.10 Structure of 16-(pyrrol-1-yl hexadecyl) dimethylchlorosilane (PMCS-16)

^{1}H-NMR (500 MHz, chloroform, δ in ppm): 6.64 [2H, (H2, 5), m], 6.13 [2H, (H3, 4), m], 3.86-3.82 [2H, (H6), $J_{6,7}$ = 7.2Hz, t], 1.77-1.73 [2H, (H7), m], 1.40-1.20 [26H, m], 0.80-0.78 [2H, (H21), $J_{20,21}$= 8.1Hz, t], 0.39 [6H, Si-CH_3, s]

^{13}C-NMR (500 MHz, chloroform, δ in ppm): 120, 107, 49, 32, 31, 29, 29, 26, 22, 18.

^{29}Si-NMR (500 MHz, chloroform, δ in ppm): -67.85

IR (chloroform, ν_{max}/cm^{-1}): 3101 (arom. C-H), 2926 (ν_{as} CH_2), 2854 (ν_s CH_2), 1500-1460 (pyrrole ring), 1407-1363 (C-N), 1252 (ν_{as} CH_3 def.), 841-795 (Si-CH_3 rocking vib.), 616 (Si-Cl).

Elemental analysis:

$C_{22}H_{42}ClNSi$: Calculated: C, 68.79; H, 11.02; N, 3.65.

Found: C, 70.59; H, 11.62; N, 3.18.

- ***6-(pyrrol-1-yl hexyl) trichlorosilane (PUTS-6):***

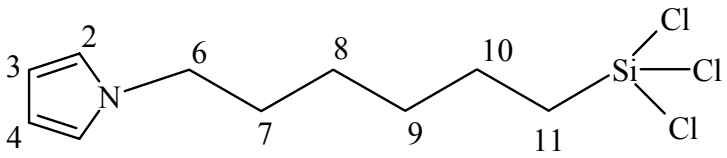

Structure 4.11 Structure of 6-(pyrrol-1-yl hexyl) trichlorosilane (PUTS-6)

^{1}H-NMR (500 MHz, chloroform, δ in ppm): 6.64 [2H, (H2, 5), m], 6.15 [2H, (H3, 4), m], 3.87-3.84 [2H, (H6), $J_{6,7}$ = 7.2Hz, t], 1.79-1.75 [2H, (H7), m], 1.43-1.30 [6H, m], 0.82-0.79 [2H, (H11), $J_{10,11}$= 8.0Hz, t].

^{13}C-NMR (500 MHz, chloroform, δ in ppm): 120, 108, 49, 31, 31, 26, 24, 22.

IR (chloroform, ν_{max}/cm^{-1}): 3103 (arom. C-H), 2925 (ν_{as} CH_2), 2856 (ν_s CH_2), 1500-1452 (pyrrole ring), 1407-1363 (C-N), 615 (ν_{as} Si-Cl).

Elementalal analysis:

$C_{10}H_{16}Cl_3NSi$: Calculated: C, 42.13; H, 5.62; N, 4.92.

Found: C, 41.25; H, 5.78; N, 4.53.

- ***11-(pyrrol-1-yl undecyl) trichlorosilane (PUTS-11):***

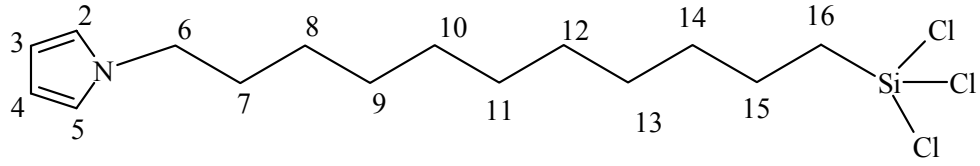

Structure 4.12 Structure of 11-(pyrrol-1-yl undecyl) trichlorosilane (PUTS-11)

^{1}H-NMR (500 MHz, chloroform, δ in ppm): 6.65 [2H, (H2, 5), m], 6.12 [2H, (H3, 4), m], 3.86-3.84 [2H, (H6), J $_{6, 7}$ = 7.2Hz, t], 1.78-1.71 [2H, (H7), m], 1.41-1.25 [16H, m], 0.82-0.79 [2H, (H16), J $_{15, 16}$= 8.1Hz, t].

^{13}C-NMR (500 MHz, chloroform, δ in ppm): 120, 107, 49, 32, 31, 29, 29, 26, 22, 18.

IR (chloroform, ν_{max}/cm^{-1}): 3101 (arom. C-H), 2926 (ν_{as} CH_2), 2854 (ν_s CH_2), 1500-1460 (pyrrole ring), 1407-1363 (C-N), 616 (ν_{as} Si-Cl).

Elemental analysis:

$C_{15}H_{26}Cl_3NSi$: Calculated: C, 50.73; H, 7.33; N, 3.95.

Found: C, 51.07; H, 7.82; N, 3.14.

4.3 Monolayer Formation and Characterization

Self-assembly technique was used to get adsorbed layer on different substrates. Prior to monolayer formation the surface must be pretreated because the organic compounds from the air contaminate the surface. This contamination hinders the chemisorption of the compound onto the surface. Specific surface treatments are needed for metal/metal oxide substrate.

The silicon wafer was first treated with pirañha solution. The surface was treated with 3:1 (v/v) of concentrated H_2SO_4 and 30% H_2O_2 at 90°C for 30 min to clean the surface and produce more surface hydroxyl groups [157]. The acid-treated substrates were then washed with copious amounts of water and blown dry with argon.

The thickness of the silicon oxide overlayer on the silicon substrates before and after piranha solution treatment was calculated using ellipsometric parameters and Daf IBM software with the following settings (single layer mode): air, $n_0 = 1$, silicon oxide layer, $n_2 = 1.458$, silicon substrate, $n_s = 3.8600$, $k_s = 0{,}018$ (imaginary part of the refractive index). The thickness of silicon oxide for untreated samples was 3.9 ± 0.05 nm (average of three samples), and it is increased slightly (4.1 ± 0.05 nm) after the acid treatment.

TiO_2 substrates were cleaned in a sonication bath first with chloroform (5 min), then with acetone (5min), and finally ethanol (5 min). The substrates were then immersed in a mixture of H_2O/30% H_2O_2 / NH_3 (2:1:1 v/v) for 5s at 80°C. The substrates were rinsed with copious amounts of distilled water and dried under an argon flow [158].

The monolayers were formed by immersion of the substrates in a suitable concentrated solution of the organosilanes in bicyclohexyl from 5 min to 48 hours. The samples were then cleaned from the physisorbed silanes by sonication in three consecutive steps (10 min each) in fresh chloroform. They were dried in an argon flow and stored under argon atmosphere before characterization. The strategy for deposition of PMCS on oxide substrates is shown in scheme 4.7.

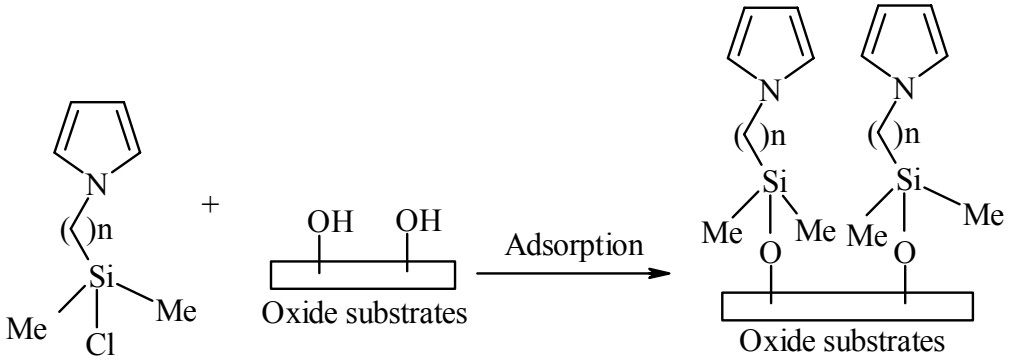

Scheme 4.7 Adsorption of PMCS on oxide substrates

The adsorbed layer was characterized by several techniques such as contact angle measurements, grazing incident FTIR, UV-VIS spectroscopy, SPR, XPS etc to identify the presence, order and orientation of the compound on the surface.

4.3.1 Contact Angle Measurement

The synthesized compounds were studied for their adsorption behavior on the oxidized surfaces. The contact angle was measured to investigate the presence of the compound on the surface and the wettability of the surfaces. Therefore, the adsorption was studied by varying solvent and adsorption time with PMCS-11 and PUTS-11 as model compounds.

The static contact angles of PMCS-11 in different solvents are presented in Fig. 4.1. The contact angle data showed that apolar hydrocarbon solvents (bicyclohexyl) and long reaction times lead to high hydrophobicity of the corresponding adsorbed layer [159].

These results indicated that the reactions of dimethylchlorosilanes at the solution-solid interface were very slow in the later stages of the reaction, and long reaction times (tens of hours /several days) are necessary.

Figure 4.2 presented the contact angle data for the PUTS-11 and PUTS-6 at different adsorption time. The contact angle data showed that the adsorption takes place very fast in several minutes, and the contact angles increases with chain length. This is because water penetrates the layer and interacts with silanols on the surface of the monolayers with short alkyl groups but does not penetrate the layer with longer alkyl groups [160].

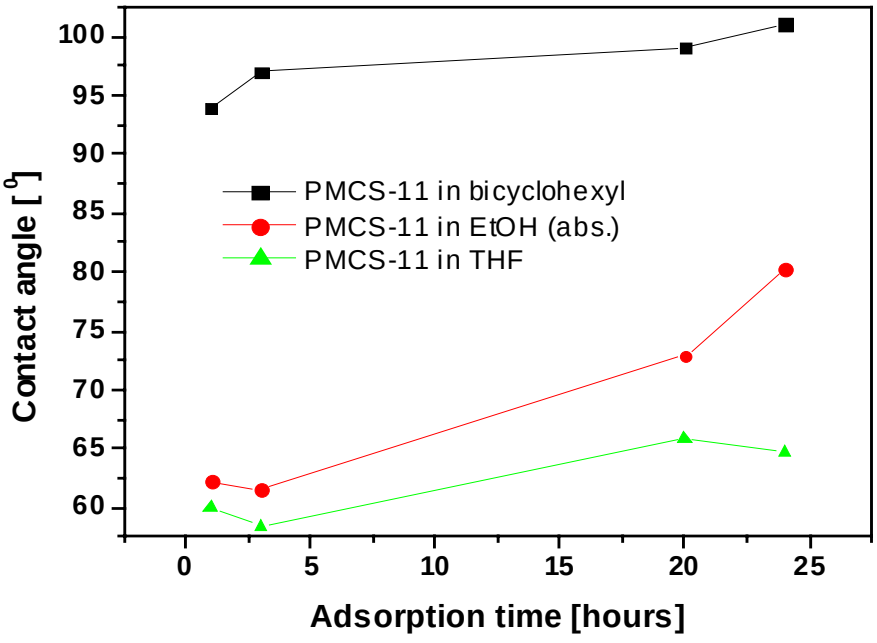

Fig. 4.1 Contact angle of PMCS-11 in different solvent

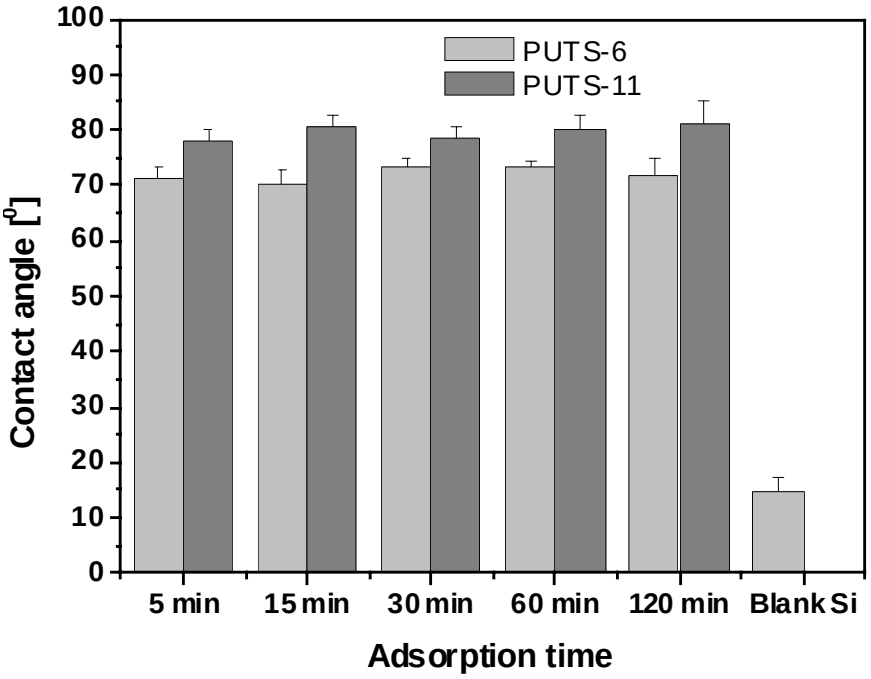

Fig. 4.2 Contact angle of PUTS-11 and PUTS-6 on Si wafer in different adsorption times

The contact angles of PUTS-11 and PMCS-11 in different concentrations were also measured (Fig. 4.3). From this figure, we can see that loose packed monolayer is formed for PUTS-11at concentrations lower than 0.033% (v/v) (≅ 1 mmol) leading to hydrophilic surfaces. For further investigations, 0.033% (v/v) solution was used.

Dimethylchlorosilanes contain only one hydrolysable group in the molecule. It is attractive in terms of the reproducibility of surface structures because only one type of grafting is possible in the system, i.e. covalent attachment to the surface by chemical bonds (Si-O-Si). Therefore, to yield a dense monolayer relatively high concentrated solutions are possible compared with that of trichlorosilanes (Fig. 4.3).

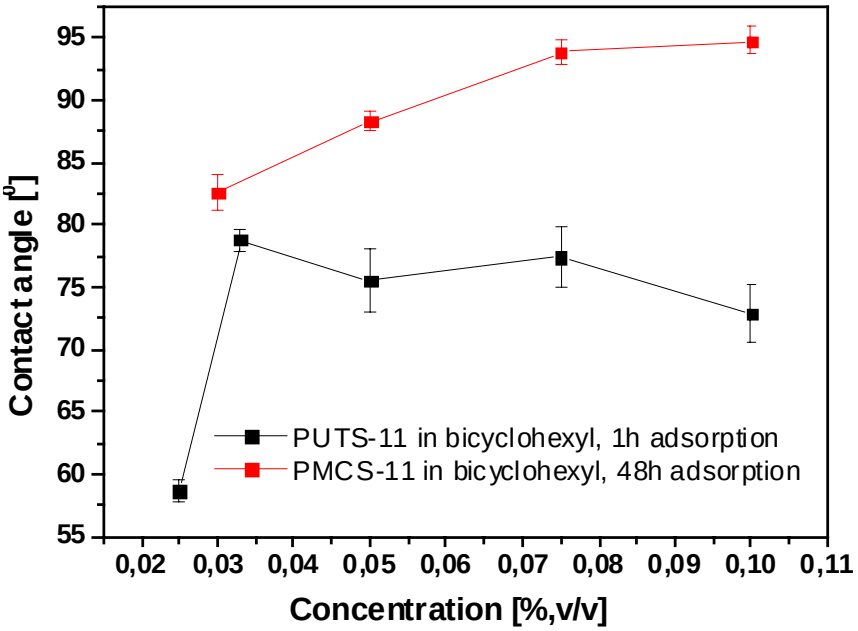

Fig. 4.3 Contact angle of PUTS-11 and PMCS-11 in different concentrations

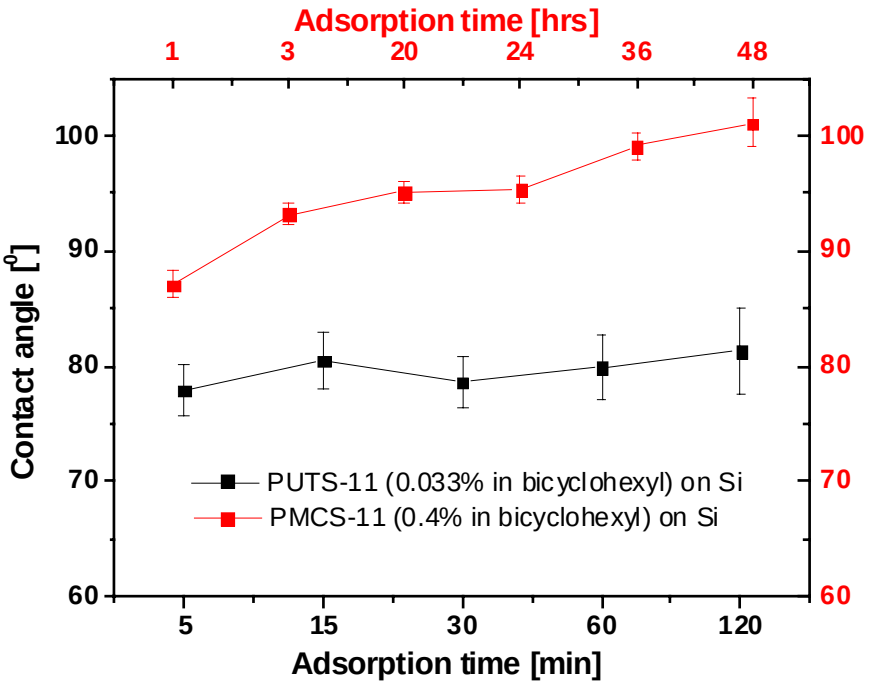

Fig. 4.4 Contact angle of PUTS-11 and PMCS-11

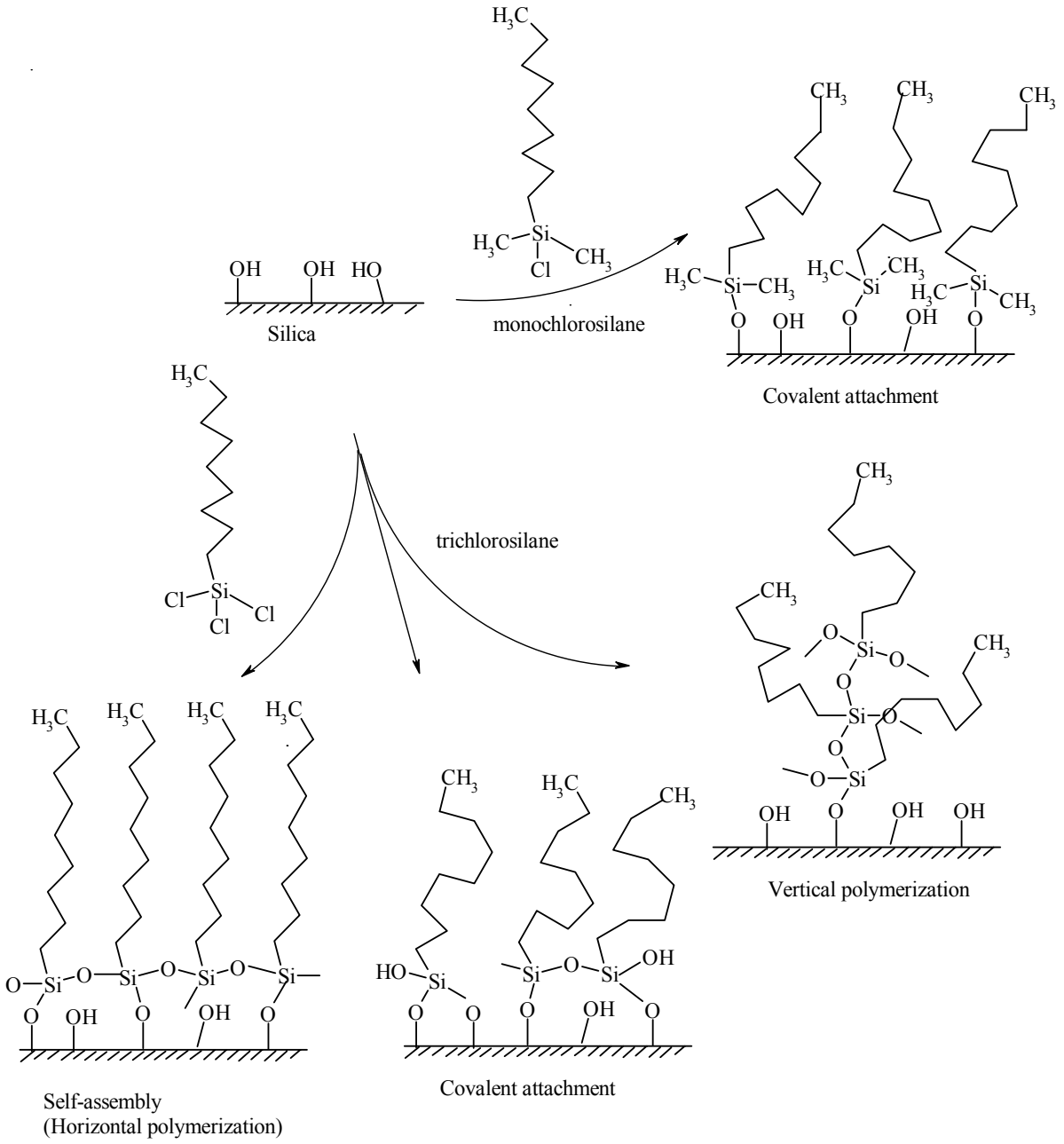

Scheme 4.8 Possible products of the reaction of alkylchlorosilane with silicon dioxide surface (adapted from A. Y. Fadeev et al.) [160]

Trichlorosilane, compared to monochlorosilane analogues, is more reactive and is capable of polymerizing in the presence of the additional of moisture, which gives rise to a number of possible surface structures (Scheme 4.8) [160]. Therefore, in high concentration vertical polymerization is favoured leading to a low contact angle.

There are some important conclusions from these contact angle results: (a). The time required to reach maximum non-wettability (high contact angle) increases with decreasing concentration of PMCS. (b). It takes much higher concentration to produce a good monolayer

on substrate for PMCS. (c). It is necessary to work with low concentrations in apolar hydrocarbon solvents and short adsorption time to form good monolayer.

Table 4.1 Contact angles and thickness of monolayers

Compounds	PMCS-6	PMCS-8	PMCS-11	PMCS-16	PUTS-11
Contact angle[°]	97.2±1.4	96.5±1.7	98.8±0.8	99.0±1.4	70.9±1.6
Layer thickness [nm]	0.10±0.3	1.2±0.1	1.5±0.4	2.6±0.1	1.6±0.5
Calculated length [nm]	1.4	1.5	2.1	2.7	2.1
Tilt angle [°]	48.2	37.9	44.2	15.8	38.7

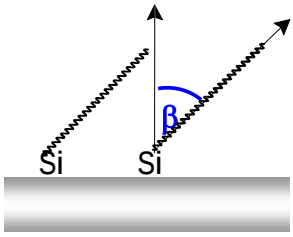

$$\cos\beta = \frac{\text{Layer thickness}}{\text{Molecule length}}$$

Fig. 4.5 Definition of tilt angle of adsorbed monolayer

The thickness of the layers and corresponding contact angles of different chain length PMCS and PUTS were determined by ellipsometry and are presented in table 4.1.

The static contact angles showed that the longer alkyl chain of PMCS lead to high hydrophobicity of surface. The thickness of the absorbed layers is in the order of the single molecule size; thus the layers are monomolecular, and the thickness increases gradually with alkyl chain length. This result indicated that PMCS with longer alkyl chains formed more compact monolayers on the substrates. It was also found that the thickness of PMCS and PUTS-11 on silicon wafers is not proportional to the chain length of the alkyl group and all are smaller than the size of PMCS and PUTS-11 calculated from molecular models. The thickness of these monolayers is consistently less than the length of PMCS and PUTS calculated from molecular models, which agrees with the literature reported for alkyltrichlorosilanes [160]. Theoretical and experimental research found that the molecule absorbed on the surface of the substrate is not perpendicular to the surface but are tilted on the surface [161]. Because the head-group of the adhesion promoter absorbed on the surface has more volume than the alkyl group. Especially the terminal-group is pyrrole ring. Given the cross-section area of the pyrrole ring, a configuration consisting of alkyl chains perpendicular to the surface would leave much free volume in the assembly. However, van der Waals

interactions to form the molecule are only effective when the alkyl chains have a minimum length of 10 C and when the alkyl chains close together. By tilting the molecules from the normal, the chains need less space and van der Waals interactions have more effective (Fig. 4.6). Therefore, to achieve close packing, the monolayer usually has tilt angle. The tilt angle of the PUTS-11 monolayer on silicon wafer was smaller than that of the PMCS-11 monolayer because of high bonding density. This is consistent with the fact that the two methyl groups of PMCS at the silicon atom need more space. Monochlorosilane cannot form closely packed structures on the surface.

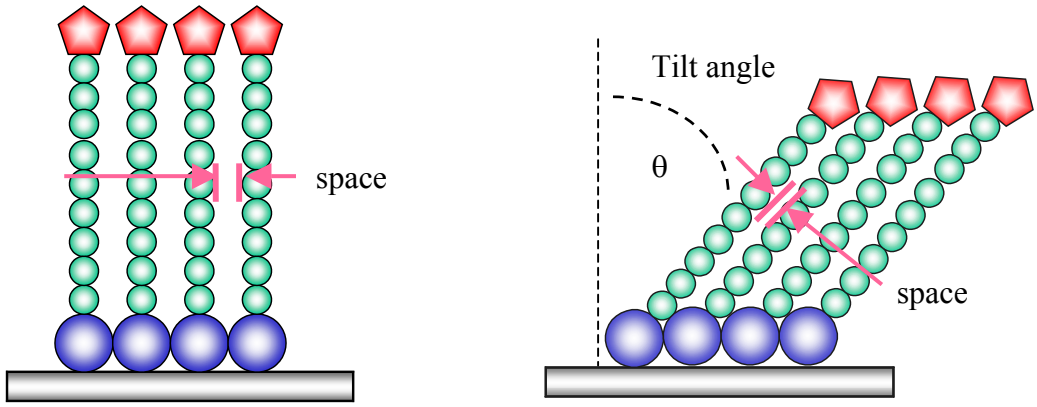

Fig. 4.6 Formation of close-packing monolayer

4.3.2 UV-VIS Spectroscopy

UV-VIS spectroscopy was used to establish the presence and to estimate the surface coverage of the monolayers on substrate. In order to compare with the monolayer, transmission spectra of the three monomers, pyrrole and N-methyl pyrrole (0,5 mM respectively) in ethanol are shown in Fig. 4.7. Up to approximately 240 nm, the spectra for all compounds were featureless, at higher energies there was a strong adsorption peak. The absorbance for PMCS as well as N-methyl pyrrole began at a lower energy due to a bathochromic shift from the substituent at 1-position [162, 163] and the same large adsorption peak due to the pyrrole moiety.

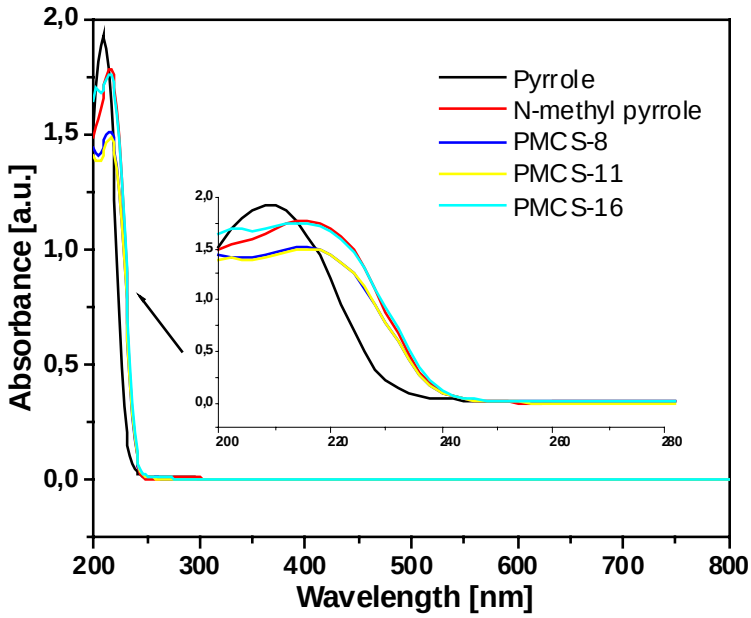

Fig. 4.7 UV-VIS spectra of monomers in ethanol

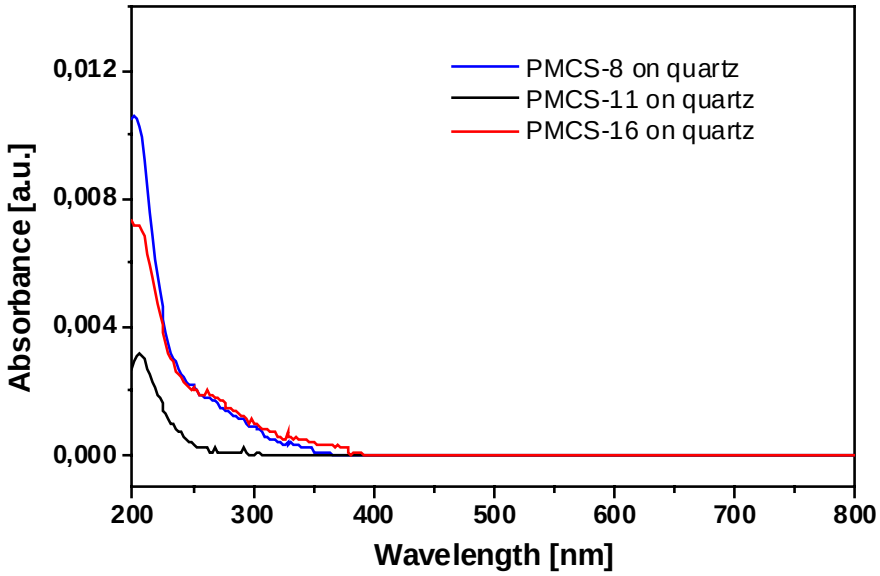

Fig. 4.8 UV-VIS spectra of PMCS monolayers on quartz

The adsorption of PMCS monolayers deposited on quartz from bicyclohexyl for 48 hours were shown in Fig. 4.8. Like the free monomers, the PMCS monolayers showed a strong increase in adsorption below 240 nm, beginning at 250 nm. The absorbance below 240 nm is due to the pyrrole moiety of the PMCS, not the alkyl chains [164]. For a comparison, we examined an undecyl dimethylchlorosilane monolayer prepared in the same way, and it did

not absorb between 300 nm and 200 nm due to no conjugated system in the molecule. The spectra, therefore, established that there were PMCS monolayers on the substrate.

A rough calculation of the amount of material on the surface can be made using the molar extinction coefficient of the monomers. Absorbance (A= - log (transmission)) was converted to molar extinction coefficient, ε, using Lambert Beer's law. The concentration of the monomers in ethanol was 0.5 mmol. The solutions were measured in quartz cuvettes with 0.5 cm depth. The maximum ε for all five monomers was ca. 7000 L/(mol cm). In the Lambert-Beer law, the absorbance A is unitless and the extinction coefficient ε has units of L/(mol cm), which is equivalent to 1000 cm^2/mol. If we assume an isotropic orientation of the monolayer, and that the monolayer and an equivalent amount of material in solution absorb the same amount of light, then we can use A/ε to obtain the surface concentration. Table 4.2 gave the average absorption of PMCS on substrates. This figure was not corrected for surface roughness. Although the measured absorbance was the result of subtracting two large numbers, and is there fore prone to error, the calculated surface concentration is surprisingly close to the 4 x 10^{-10} – 9 x 10^{-10} mol/cm^2 usually reported for surface coverage of self-assembled monolayers (SAMs) of alkyldimethylchlorosilane [165-169].

Table 4.2 Calculated surface concentration of PMCS on quartz

Compounds	**Absorbance (A1)** (in solution)	ε (L/mol cm) (ε = A1/C1*l)	Absorbance (A2) (on quartz)	Adsorption (mol/cm^2) (A2/ε*l)	Cross-sectional area (Å^2/molecule)
PMCS-8	1.53	6120	0.0026	$3.9x10^{-10}$	42.6
PMCS-11	1.52	6080	0.0031	$5.1x10^{-10}$	32.6
PMCS-16	1.76	7500	0.0072	$9x10^{-10}$	20

4.3.3 Surface Plasmon Resonance Spectroscopy (SPR)

The rates of surfactant like adhesion promoter adsorption onto a solid were determined by the transport of surfactant from the bulk solution to the surface and the intrinsic kinetics of adsorption and desorption. The adsorbed film formation due to the interactions between the surface and the surfactant. Surface plasmon resonance spectroscopy was used to study the kinetics of adsorption and desorption processes and the rate of the PMCS monolayer

formation. Therefore, special substrates were prepared: on LaSFN9 glass sheets, 50 nm gold were evaporated and then a 2.5 nm Al_2O_3 layer was deposited on which the adsorption of the adhesion promoter took place. In our SPR experiments with the stable cell, the reflected light is proportional to the quantity of material adsorbed and the time change in reflectance is related to the adsorption/desorption kinetics.

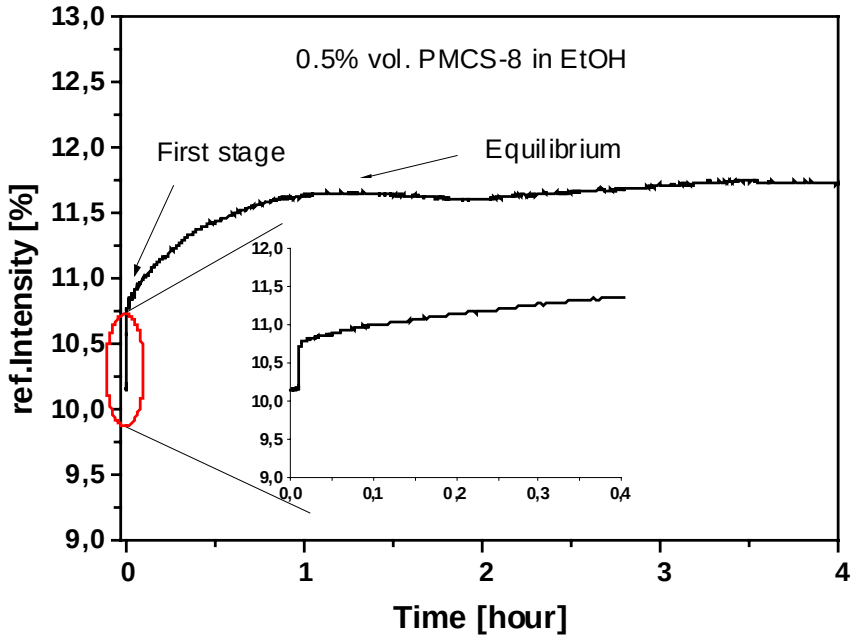

Fig. 4.9 SPR spectra of PMCS measured in kinetic mode

In Fig. 4.9, the change in reflectivity is depicted as a function of time. Two factors influenced the reflectivity, such as refractive index and thickness. From SPR spectrum, we are not sure which factor effected the reflective intensity. But we can see the reflective intensity changed with the adsorption time. This indicated that surface properties are changed due to adsorption.

4.3.4 Grazing Incident FTIR

Grazing incident FTIR was measured to study the presence and the order of the monolayer on the substrates. The IR spectra are shown in Fig. 4.10. A prominent feature of this spectrum is the presence of symmetric and asymmetric CH_2-stretching vibrations (at 2850 and 2918 cm^{-1} respectively), revealing the presence of methylene groups in the molecule. The presence of the band of Si-O-Si vibration (1130 –1140 cm^{-1}) in the spectrum of PMCS-8 on Ti revealed that the formation of the monolayer on Ti. The order in the PMCS-8 layers can be assessed from the position of the CH_2-stretching vibration. As shown in previous studies [170, 173],

the frequency of the CH_2-stretching vibration is characteristic for long-chain SAM's indicating close packed structures. For completely disordered structures, the frequency of the CH_2-stretching is close to that of a liquid alkane (ν_{as}~ 2924 cm^{-1}). For well-ordered SAMs, the frequency is shifted to lower wavenumbers, and it is close to that of a crystalline alkane (ν_{as} ~ 2915-2918 cm^{-1}) [174]. Fig. 4.10 shows that CH_2-stretching of PMCS-8 is 2918 cm^{-1}. This indicates SAMs with a high degree of order.

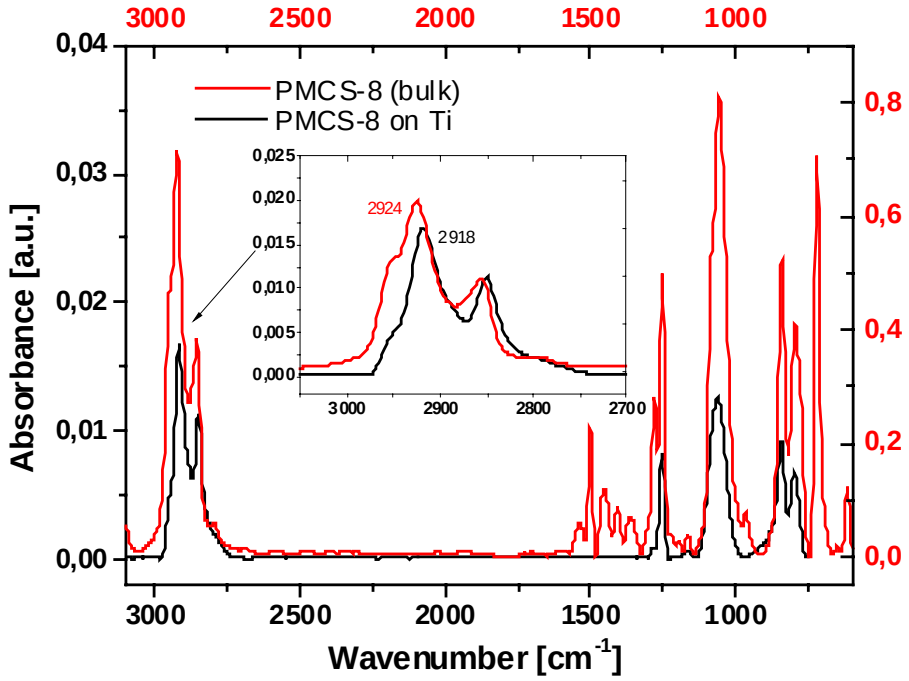

Fig. 4.10 Grazing incident FTIR spectrum of PMCS-8 on Ti

We found that ν_{as} CH_2 is decreasing with the increasing concentration of solution or adsorption time (see Fig. 4.11). During the adsorption, the early stages of the reactions can be pictured as isolated grafted molecules randomly distributed on the substrate. As the surface coverage increases, the order in the monolayer gradually increase (ν_{as} CH_2 decrease), approaching the final highly ordered or the closely packed state.

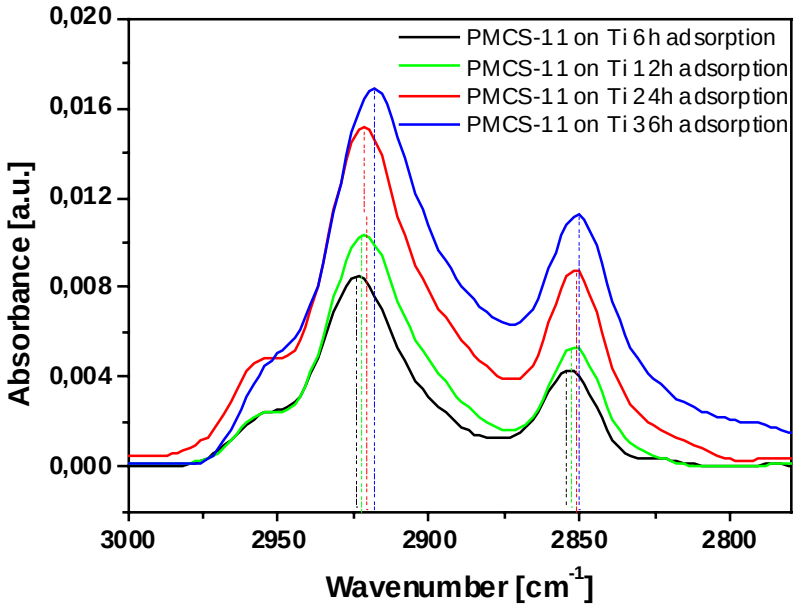

Fig. 4.11 Grazing incident IR spectra of PMCS-11 on Ti at different adsorption time

4.3.5 X-Ray Photoelectron Spectroscopy (XPS)

XPS spectroscopy was used to get information about the surface composition and orientation of the adsorbed molecules on substrates.

XPS characterized the orientation of the PMCS and PUTS on oxidized substrates. Figure 4.12 showed the survey spectrum of PUTS-11 on Si substrate. Table 4.3 presented the element concentration of PMCS and PUTS on Si substrates at different take off angles.

Figure 4.12 showed the survey spectrum of adsorbed PUTS on Si. The peaks of N and C belonging to the adsorbed molecule are clearly visible. The finding of N and C indicated that the adsorption of the molecules took place on the Si/SiO_2. Cl2p peak was observed in PUTS-11 survey spectrum, indicating the incomplete hydrolysis of Si-Cl bonds to yield Si-O-Si bond between molecules. In order to check the stoichiometry of the grafted layers formed from PUTS-11, PMCS-11 and PMCS-8, Table 4.3 also provided the C/N and Si/N ratios at different take-off angles. The derived C/N ratio for PUTS-11 at 45° take-off angle was close to the theoretical value 15/1, indicated that there was no contaminant on the surface. In the case of PMCS-11, the derived C/N ratio at 45° take-off angle was higher than the theoretical value 17/1, indicated some contaminant on the surface. Fig. 4.13 showed the carbon concentration dependent on the take-off angle. From this figure we can see, that the carbon concentration decreases with the increase of the take-off angle. The sharp dependence of the

carbon concentration on take-off angle supports the ellipsometry and contact angle data indicating that these layers are densely packed with pyrrole group on top of the monolayers [160].

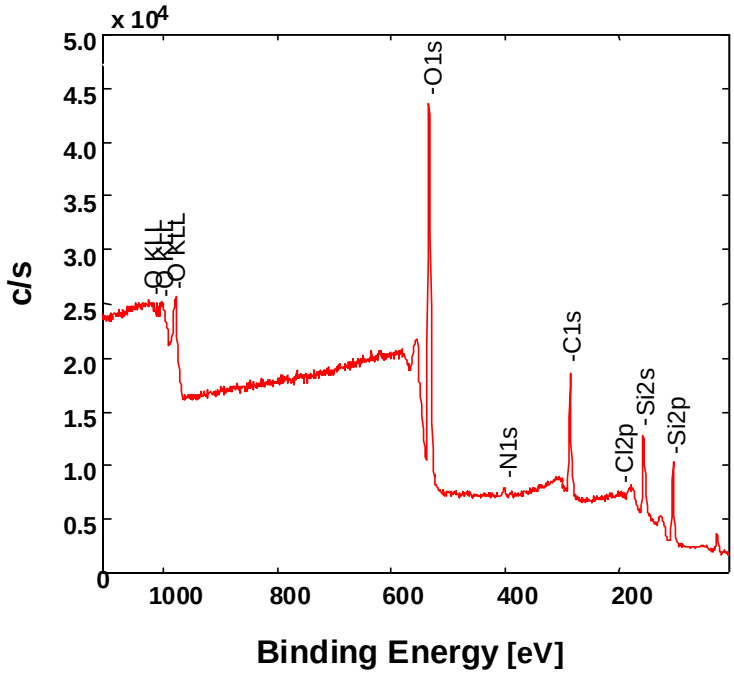

Fig. 4.12 Survey spectrum of PUTS-11 on silicon

Table 4.3 Angle dependence of the relative atomic concentration (%) for Si wafer after modification by PMCS and PUTS

(a). PUTS-11

Take-off angle [^{0}]	C1s (%)	N1s (%)	Si2p (%)	C/N	Si/N
20	76.37	3.86	19.77	19.7	5.1
45	62.62	2.74	34.64	22,8	12.6
70	53.02	2.97	44.01	17.8	14.8
85	50.09	1.99	47.92	25.1	24.1

(b). PMCS-11

Take-off angle [^{0}]	C1s (%)	O1s (%)	N1s (%)	Si2p (%)	C/N	Si/N
15	77.68	9.06	4.47	7.95	17.3	1.7
45	63.00	19.98	2.91	13.37	21.6	4.6
75	57.29	23.99	3.41	14.33	16.8	4.2

(c). PMCS-8

Take-off angle [^{0}]	C1s (%)	O1s (%)	N1s (%)	Si2p (%)	C/N	Si/N
15	76.93	7.76	6.03	7.56	12.7	1.2
45	60.76	16.37	5.81	15.43	10.5	2.6
75	47.65	29.77	4.00	17.32	11.9	4.33

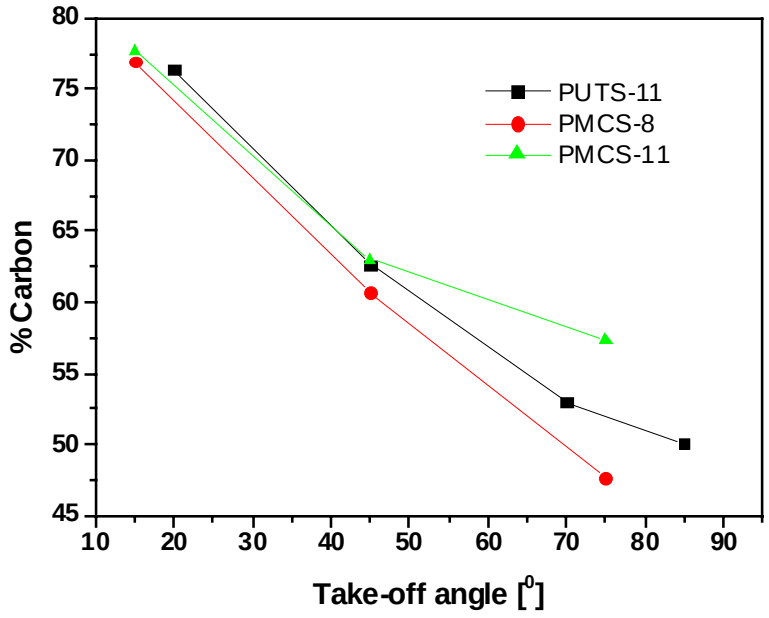

Fig. 4.13 Carbon content for silicon-supported layers of PMCS and PUTS at different detection angles

Angle-resolved XPS measurements were also done to study the orientation of the adsorbed PMCS on Ti oxide substrate. The measurements were done at 15°, 45°, and 75° angles. By varying the take off angle we get information from different depths of the adsorbed layer. Therefore, special marker atoms were used: N from the pyrrole group and Si from the silane group. We calculated I_{Si}/I_N to get an indication how the molecule is oriented on the surface relative to the detection angle. At a low take-off angle more N atoms were observed and at high take-off angle more Si atoms. An increase in the Si/N ratio with increasing take-off angle indicated that the molecules are oriented with the pyrrole group on top and the silane group attached to the surface (Fig. 4.14).

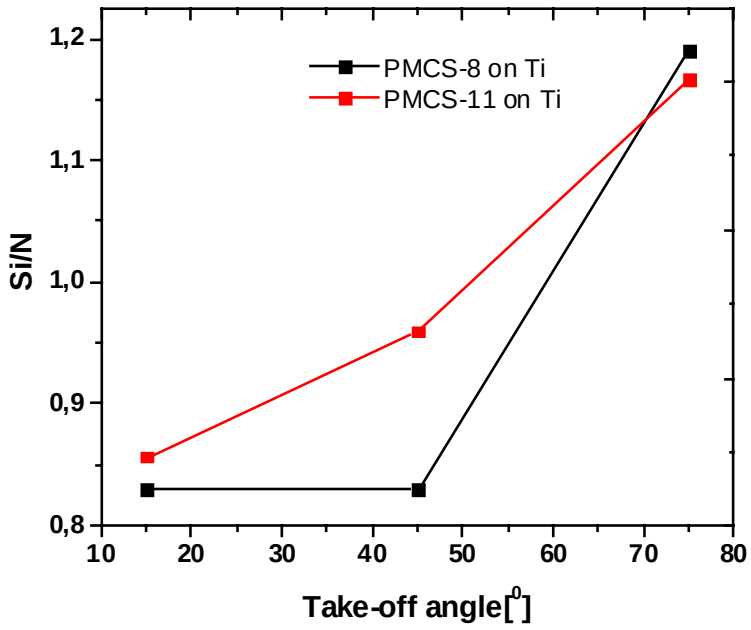

Fig. 4.14 AR-XPS measurements of adsorbed ω-(pyrrol-1-yl alkyl) silanes: Si/N ratios

From above the characterization of adsorbed layer, we can conclude that ω-(pyrrol-1-yl alkyl) silane layers formed monolayers with pyrrole group on top and silane group attached to the surface. The calculation of the tilt angles (showed in Table 4.2) of the adsorbed molecules revealed that the long chain derivatives formed more compact and well-ordered SAMs on Si substrate.

4.4 3-Substituted Pyrrole Phosphonic Acids as Adhesion Promoters

4.4.1 Synthesis of 3-Substituted Pyrrole Derivatives

The synthesis of 3-substituted pyrrole is more difficult than the synthesis of N-substituted pyrrole. In general, the high reactivity of the α-protons compared to the β-protons of the pyrrole ring guides an electrophilic substitution into the α-position. There are several successful processes to provide substitution to β-position.

A removable deactivating group (usually acyl) was introduced to pyrrole followed by the entry of an electrophilic substituent to the β-position [175]. This method is historically the first and the most intensively studied of the synthetic routes to 3-substituted pyrroles [176]. It is quite broad in scope but removal of the directing substituent is frequently not inconsequential.

a. The remarkable general acid induced isomerization of the readily preparable α-isomers [177]. This method occurs under mild conditions, but an apparent equilibrium mixture of the α- and β-isomer leads to a difficult separation.

b. A bulkyl group on nitrogen, such as a t-butyl or a trityl moiety is used to obstruct electrophilic attack at the α-position. Although substitutive selectivity for C-3 is indeed observed in this case, the process is of limited value because removal of the nitrogen substituent is difficult or the conditions required to effect N-dealkylation (e.g. $Na/MeOH/NH_3$) are incompatible with the survival of many functional groups [178, 179].

c. Protection of the pyrrole ring nitrogen with a phenylsulfonyl group [180-182] or the bulky triisopropylsilyl group [183, 184] can lead to substitution at the β-position. This method is useful to synthesize 3-substituted pyrrole due to the easily removable and stable N-protecting group. Especially, the Friedel-Crafts acylation of 1-(phenylsulfonyl) pyrrole and subsequent removal of the nitrogen substituent under alkaline conditions is an excellent route to 3-acyl pyrroles. 1-(phenylsulfonyl) pyrrole is easily synthesized either via the pyrrole-sodium salt [185] or by using KOH (solid or aqueous) [186] in the presence of a phase-transfer catalyst. Furthermore, this protecting group is easily removed under simple basic hydrolysis [187].

Reaction of 1-(phenylsulfonyl) pyrrole and ω-bromo acyl chlorides in the presence of $AlCl_3$ at 25°C in dichloromethane solution gives essentially quantitative yields of the corresponding 3-acylated product. $AlCl_3$ used as catalyst express high regioselective, compared with other Lewis acids such as $SnCl_4$, $TiCl_4$, $ZnCl_2$ and $FeCl_3$. 2-acyl pyrrole was the major isomer in the presence of $SnCl_4$ or $ZnCl_2$, while 3-acyl pyrrole was the predominant isomer in the presence of $TiCl_4$ or $FeCl_3$.

4.4.2 Reduction of carbonyl Group of 3-Acyl Pyrrole

Many reducing reagents are available for the conversion of carbonyl group to methylene group. For 1-(phenylsulfonyl) pyrrole, Clemmensen reduction is an available choice because the products are readily purified and obtained in good yields. Again, basic hydrolysis provides the desired 3-alkyl-1H-pyrrole. But for 3-acyl-1H-pyrrole, reduction of carbonyl group under acidic conditions results in polymerization of the pyrrole derivatives. Several reducing agents

were reported to reduce carbonyl group of pyrrole, such as BF_3 OEt_2 / $NaBH_4$ [188], p-$TsNHNH_2$ / $NaBH_3CN$ [189], and $NaBH_4$ / i-propanol [190]. The most effective system was $NaBH_4$ / i-propanol, which worked for a wide range of acyl pyrrole and gave pure products after a single work-up.

4.4.3 Synthesis of ω-(Pyrrol-3-yl) alkyl Phosphonic Acids

The synthesis of 3-substituted pyrrole alkyl phosphonic acid derivatives is described in detail for the very first time. These compounds were synthesized via a six-step procedure, which is outlined in scheme 4.9.

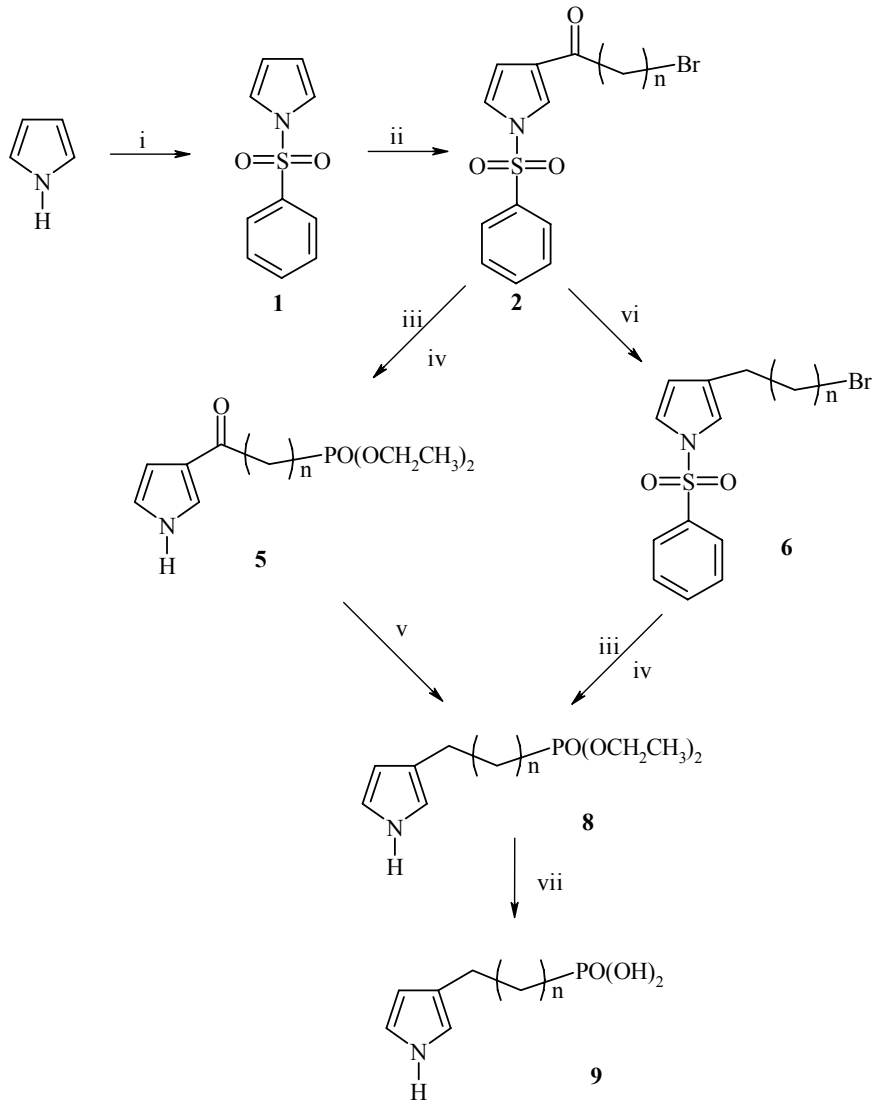

Scheme 4.9 General synthetic route to 3-substituted pyrrole phosphonic acids.

[Reagents and conditions: (i) K, THF, benzene sulphonylchloride, RT, 14-18 hours; (ii) Br (CH_2)nCOCl, $AlCl_3$, CH_2Cl_2, RT, then H_2O; (iii) triethyl phosphite, 180°C, 4 hours; (iv) 1,4-dioxane, 5N NaOH, RT; or 5N NaOH/ MeOH, refluxing (v) $NaBH_4$, i-propanol, reflux 36-50 hours; (vi) Clemmensen reduction, Zn(Hg)Cl, HCl, toluene, 18-20 hours; (vii) Me_3SiBr, CH_3CN, RT, 1hour, then MeOH/H_2O, RT, 2 hours.]

The procedure includes following main steps:

1. Introduction of phenylsulfonyl group at 1-position of pyrrole ring. The synthetic pathway rely on the protection of the pyrrole ring nitrogen with phenylsulfonyl group effects the substitution at 3-position.
2. Friedel-Crafts acylation of 1-phenylsulfonyl pyrrole with ω-bromoalkyl acylchlorides in the presence of $AlCl_3$. The protecting group guides the acylation reaction into the desired 3-position. As intermediate a terminal brominated oxoalkyl derivative is formed.
3. Reaction of terminal bromide with an appropriate phosphite derivative to get the phosphonic acid ester derivative.
4. Deprotection of pyrrole ring.
5. Reduction of oxo group under mild conditions.
6. Hydrolysis of phosphonic acid derivative to free acid.

The first two steps were carried out with quantitative yields of the corresponding 3-acylated product **2**. Because the chain length has a big influence on the product, the further reaction of **2** is possible in two ways either removal of protective group followed by phosphorization (Route **A**) or first introducing of phosphonic acid ester and then deprotection (Route **B**)(see scheme 4.10). As it can be seen in Table 4.4 for the yields of compounds **5**, route **B** is more appropriate than route **A** because of minimizing the formation of hydrolysis products. Another advantage is that the products of phosphorization of compound **4** can be directly hydrolyzed without further purification. But both routes **A** and **B** were not successful for short chain derivatives. Usually mild basic hydrolysis gives 3-acyl-1H-pyrole, in the case of **2a** and **2b**, the desired compounds **3a** and **3b** were not obtained due to bromo-group cleavage. Very low yields were obtained due to incomplete removal of protecting group. We have also tried to hydrolyze compound **4b** under vigorous conditions (NaOH/MeOH, refluxing) resulting in a cleavage of C-P bond.

Because both routes **A** and **B** were not suitable for short chain derivatives, another approach was adopted to synthesize 3-substituted pyrrole phosphonic acid, which is shown in scheme 4.11.

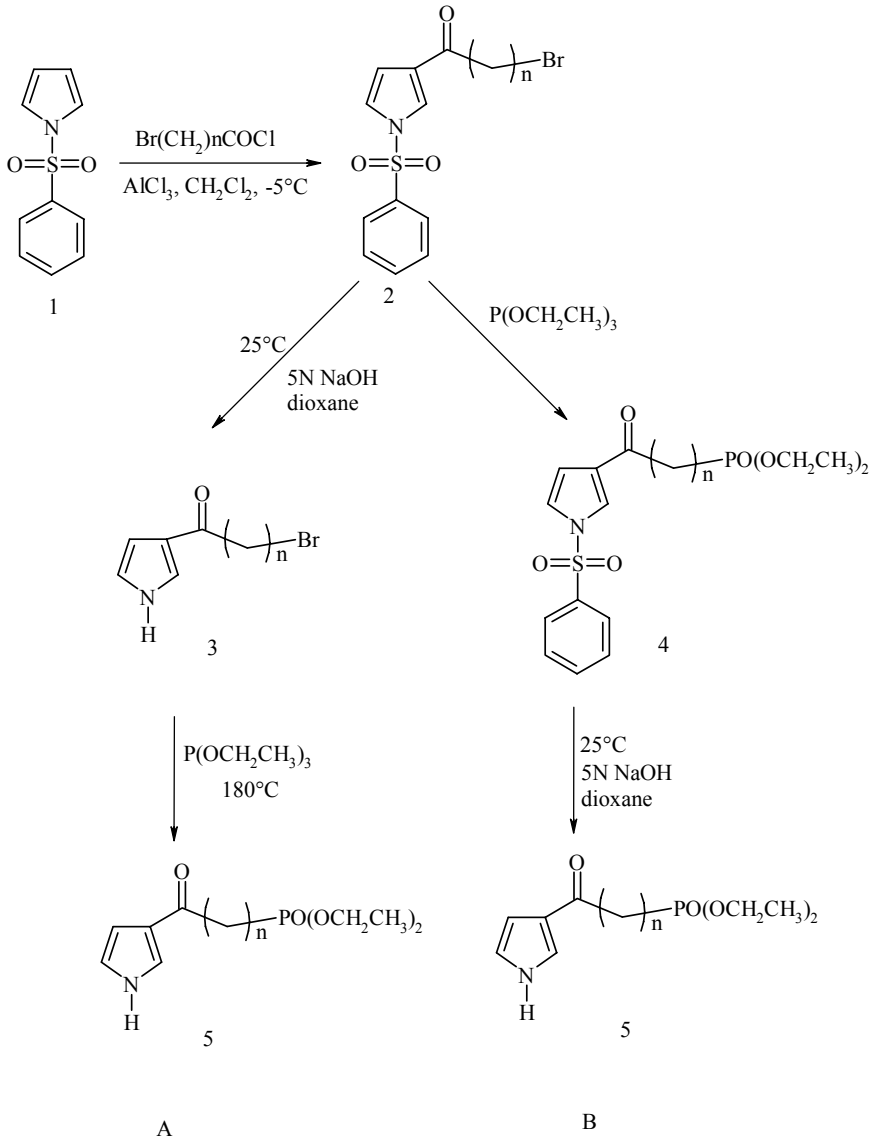

Scheme 4.10 Synthetic pathway to ω-(pyrrol-3-yl)-1-oxo-alkyl phosphonic acid ester

Table 4.4 Results of compounds 2 and 5

Entry	n	Compound 2		Compounds 5 [yield %]	
		Mp. [^{0}C]	Yield [%]	Route A	Route B
a	1	64-65	49	-	5
b	3	62-63	55	-	6
c	5	52-54	55	70	75
d	7	56-58	57	81	85
e	10	55-57	62	80	87

Clemmensen reduction of **2** gave appreciable yield of **6**. The product **6** reacted with triethyl phosphite to get 3-substituted pyrrole phosphonic acid ester **7**, followed by removing the protective group under refluxing condition. This method is also available to synthesize long alkyl chain derivatives (scheme 4.11).

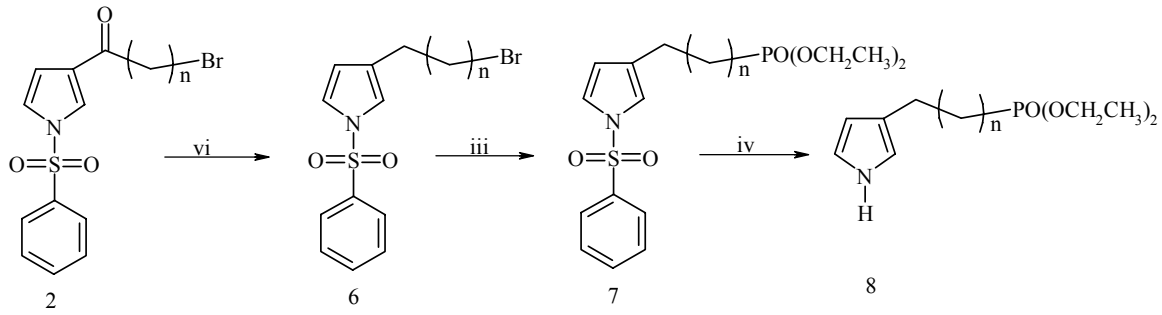

Scheme 4.11 Synthetic pathway to ω-(pyrrol-3-yl) butyl diethyl phosphonic acid ester

[Reagents and conditions: (vi) Clemmensen reduction, Zn(Hg)Cl, HCl, toluene, reflux 16-18h; (iii) triethyl phosphite, 180°C, 4h; (iv) 5N NaOH, MeOH, reflux 3h.]

Phosphonic acids are conveniently synthesized via dealkylation of phosphonic acid alkyl esters by acid-catalyzed hydrolysis, which can be carried out by heating with concentrated hydrochloric or hydrobromic acids for several hours [191]. However, in the case of 3-alkyl-1H-pyrrole, the pyrrole group is too delicate to survive the harsh reaction conditions. N. Gauvry [192] reported the usefulness of boron tribromide for the conversion of dialkyl phosphonates into the corresponding phosphonic acids via methanolysis. Rabinowitz [193], McKenna [194, 195] and others [196-199] reported the conversion of dialkyl phosphonates with chloro- or bromo- trimethylsilanes into the silyl esters, thus making the corresponding phosphonic acids readily available via hydrolysis with water. After investigating the methods, bromo trimethylsilane was chosen to react with compound **8** in organic solvent at 0°C, and the desired phosphonic acids **9** was obtained by hydrolysis of the silyl esters.

Compound **9** was obtained in low yield by hydrolysis of the corresponding silyl esters. The low yield is due to sensitivity of 3-alkyl pyrrole phosphonic acid towards oxygen, light and high temperature. To prevent polymerization of the intermediates, it was important to avoid the use of acids during work up. 3-alkyl pyrrole phosphonic acids were difficult to purify because these compounds decomposed during drying at room temperature and oxidized readily. C- alkyl pyrroles are known to be less stable than 1-alkyl pyrroles toward oxygen. From the IR spectrum, the instability of these compounds can also be confirmed (Fig. 4.15).

3-alkyl pyrrole phosphonic acids are highly oxidized even at low temperature. By converting the free acid into its ammonium salt the stability can be improved.

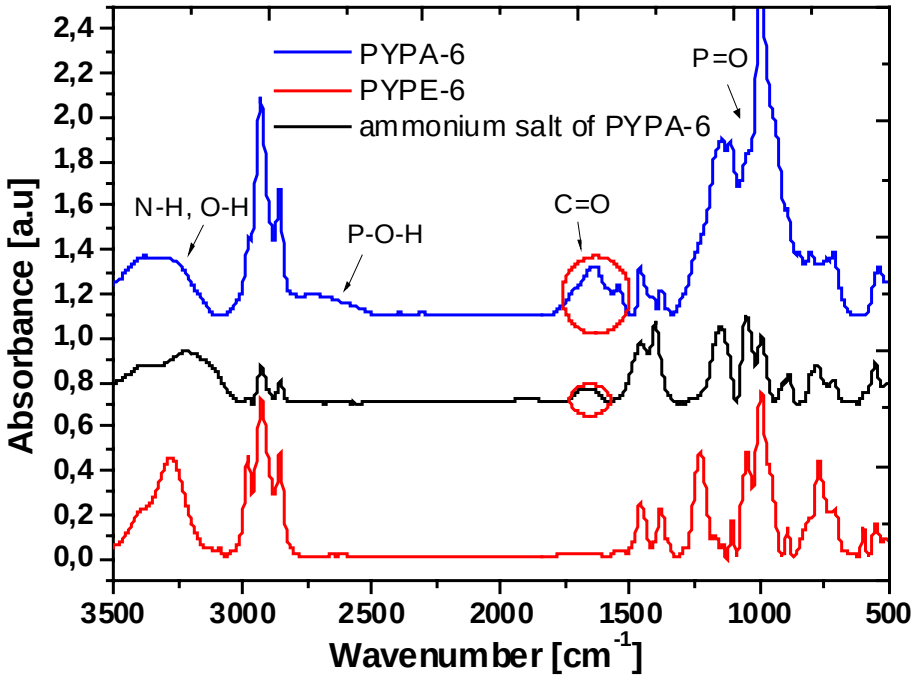

Fig. 4.15 FTIR spectra of PYPE-6, PYPA-6 and ammonium salt of PYPA-6

Figure 4.15 showed the FTIR spectra of the intermediate compounds 6-(3-pyrrolyl) hexyl diethyl phosphonic acid ester (**8c, PYPA-6**), 6-(3-pyrrolyl) hexyl phosphonic acid (**9c, PYPA-6**) and 6-(3-pyrrolyl) hexyl phosphonic acid ammonium salt (**10c, ammonium salt of PYPA-6)**. At 1710 cm^{-1}, **9c** has a carbonyl peak and at 1690 cm^{-1} a shoulder due to hydrogen bonded carbonyl. These bands indicated that some of the pyrrole moieties were oxidized [200]. The instability of this type compound toward oxygen is apparent. When it is converted into ammonium salt, the intensity at near 1700 cm^{-1} is decreased, indicating that the ammonium salt is more stable than the free acid.

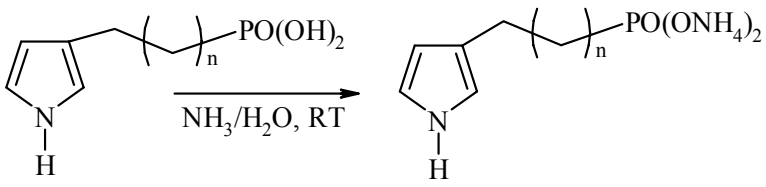

Scheme 4.12 Synthetic pathway to ω-(pyrrol-3-yl) alkyl phosphonic acid ammonium salt.

4.4.3.1 Synthesis of 1-Phenylsulfonyl–3-(ω-bromoacyl) pyrrole (2)

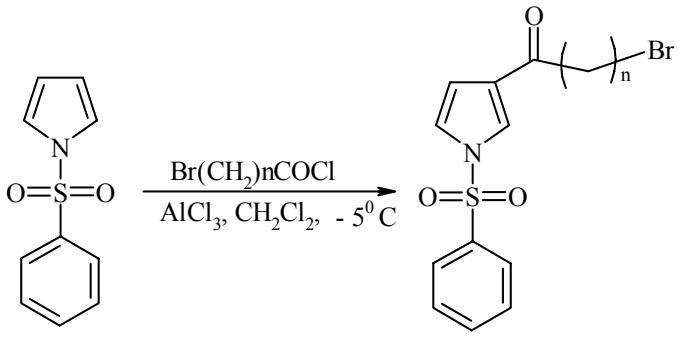

Scheme 4.13 Synthesis of 1-phenylsulfonyl–3-(ω-bromoacyl) pyrrole

6-bromohexanoyl chloride (6.0 g, 30 mmol) in 60 ml dichloromethane was added dropwise to a suspension of anhydrous aluminum chloride (4.3 g, 33 mmol) in 80 ml dry dichloromethane at 25°C under nitrogen atmosphere. After stirring at 25°C for 30 min., the solution was cooled down to 0°C and 1-(phenyl sulfonyl) pyrrole in 60-ml dichloromethane was slowly added dropwise. The mixture was stirred at room temperature for 20 hours. The reaction mixture was carefully hydrolyzed with water and the aqueous layer was extracted with dichloromethane. The combined organic layers were washed with brine and dried over anhydrous magnesium sulfate. The solvent was removed under reduced pressure to give dark-brown oil, which crystallized on cooling. The crude product **2c** was recrystallized from n-hexane - ethyl acetate (10:1) to obtain white needle crystals 55% yield, Mp. 52-54°C (53-54.5°C reported in literature [201].

- ***1-Phenylsulfonyl –3-(6-bromohexanoyl) pyrrole (2c)***

^{1}H-NMR ($CDCl_3$, 500 MHz, δ in ppm): 7.91-7.90 [2H, (H2', 6'), d, $J_{2',3'=6',5'}$ = 6.4 Hz], 7.72-7.71 [1H, (H2), m], 7.67-7.63 [1H, (H4'), m], 7.56-7.53 [2H, (H3', 5'), m], 7.14-7.13 [1H, (H5), m], 6.7-6.6 [1H, (H4), m], 3.41-3.38 [2H, (H11), t, $J_{11,10}$ = 6.6 Hz], 2.75-2.72 [2H, (H7), t, $J_{7,8}$= 7.3 Hz], 1.90-1.84 [2H, (H10), m], 1.72-1.66 [2H, (H8), m], 1.50-1.40 [2H, (H9), m].

IR (KBr, ν_{max}/cm^{-1}): 3138-3105 (arom. C-H), 1673 (C=O), 1544 (pyrrole ring).

Elemental analysis:

$C_{16}H_{18}BrNO_3S$: Calculated: C, 50.01; H, 4.72; N, 3.64; S, 8.34.

Found: C, 50.06; H, 4.75; N, 3.85; S, 8.29.

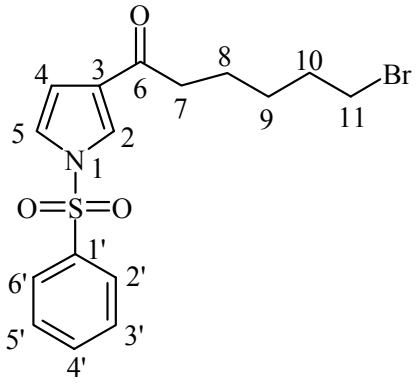

Structure 4.13 Structure of 1-Phenylsulfonyl-3-(11-bromoundecanoyl) pyrrole

To avoid complications, we have used an internally consistent numbering system to describe the positions obtained from NMR spectroscopy on these materials as above. For the precursors to these materials the numbering used on the individual components is used; i.e. the alkyl chain is numbered 6-11 or more, the arylsulfonate ring 1'-6', etc.

- ***1-phenylsulfonyl–3-(2-bromoethanoyl) pyrrole (2a)***

Yield: 49%, **Mp.:** 64-65°C

^{1}H-NMR (CDCl3, 500 MHz, δ in ppm): 7.90 [2H, (H2', 6'), d, J $_{2',3'=6',5'}$ = 7.6 Hz], 7.80 [1H, (H2), m], 7.60 [1H, (H4'), m], 7.55-7.53 [2H, (H3', 5'), m], 7.14 [1H, (H5), m], 6.7-6.6 [1H, (H4), m], 4.10 [2H, (H7), s].

IR (KBr, ν_{max}/cm^{-1}): 3135-3073 (arom. C-H), 1683 (C=O), 1582 (pyrrole ring).

Elemental analysis:

$C_{14}H_{14}BrNO_3S$: Calculated: C, 43.92; H, 3.07; N, 4.27; S, 9.77.

Found: C, 44.04; H, 3.11; N, 4.18; S, 9.80.

- ***1-phenylsulfonyl–3-(4-bromobutanoyl) pyrrole (2b)***

Yield: 55%, **Mp.:** 62-63°C

^{1}H-NMR ($CDCl_3$, 500 MHz, δ in ppm): 7.92-7.90 [2H, (H2', 6'), d, J $_{2',3'=6',5'}$ = 7.7Hz], 7.77-7.76 [1H, (H2), m], 7.67-7.63 [1H, (H4'), m], 7.56-7.53 [2H, (H3', 5'), m], 7.15-7.14 [1H, (H5), m], 6.7-6.6 [1H, (H4), m], 3.49-3.46 [2H, (H9), t, J $_{8,9}$ = 6.2 Hz], 2.94-2.91 [2H, (H7), t, J $_{7,8}$ = 6.9 Hz], 2.25-2.19 [2H, (H8), m]

IR (KBr, ν_{max}/cm^{-1}): 3133-3065 (arom. C-H), 1680 (C=O), 1547 (pyrrole ring).

Elemental analysis:

$C_{14}H_{14}BrNO_3S$: Calculated: C, 47.20; H, 3.96; N, 3.93; S, 9.00.

Found: C, 47.63; H, 3.99; N, 4.02; S, 8.96.

- ***1-phenylsulfonyl–3-(8-bromoctanoyl) pyrrole (2d)***

Yield: 57%, **Mp.:** 56-58°C.

^{1}H-NMR ($CDCl_3$, 500 MHz, δ in ppm): 7.91-7.89 [2H, (H2', 6'), d, $J_{2',3'=6',5'}$ =6.4 Hz], 7.72-7.71 [1H, (H2), m], 7.66-7.63 [1H, (H4'), m], 7.56-7.52 [2H, (H3', 5'), m], 7.13-7.12 [1H, (H5), m], 6.7-6.6 [1H, (H4), m], 3.39-3.37 [2H, (H13), t, $J_{12, 13}$ =6.8 Hz], 2.72-2.69 [2H, (H7), t, $J_{7, 8}$ = 7.3Hz], 1.85-1.62 [2H, (H12), m], 1,44-1,2 [6H, m].

IR (KBr, ν_{max}/cm^{-1}): 3152-3107 (arom. C-H), 1675 (C=O), 1543 (pyrrole ring).

Elemental analysis:

$C_{18}H_{22}BrNO_3S$: Calculated: C, 52.43; H, 5.38; N, 3.40; S, 7.78.

Found: C, 52.71; H, 5.51; N, 3.48; S, 7.60.

- ***1-phenylsulfonyl-3-(11-bromoundecanoyl) pyrrole (2e)***

Yield: 62%, **Mp.:** 55-57°C.

^{1}H-NMR ($CDCl_3$, 500 MHz, δ in ppm): 7.90 [2H, (H2', 6'), d, $J_{2',3'=6',5'}$ = 5.4 Hz], 7.72-7.71 [1H, (H2), m], 7.66-7.63 [1H, (H4'), m], 7.56-7.52 [2H, (H3', 5'), m], 7.13-7.12 [1H, (H5), m], 6.68-6.67 [1H, (H4), m], 3.4-3.37 [2H, (H16), t, $J_{15, 16}$ = 6.8 Hz], 2.70 [2H, (H7), t, $J_{7, 8}$ =7.5 Hz], 1.86-1.80 [2H, (H15), m], 1.70-1.60 [2H, (H8), m], 1.41-1.24 [12H, m].

IR (KBr, ν_{max}/cm^{-1}): 3146-3114 (arom. C-H), 1677 (C=O), 1546 (pyrrole ring).

Elemantal analysis:

$C_{21}H_{28}BrNO_3S$: Calculated: C, 55.51, H, 6.21; N, 3.08; S, 7.06.

Found: C, 56.87; H, 6.56; N, 3.06; S, 6.63.

4.4.3.2 Synthesis of 3-(ω-bromoacyl) pyrrole (3)

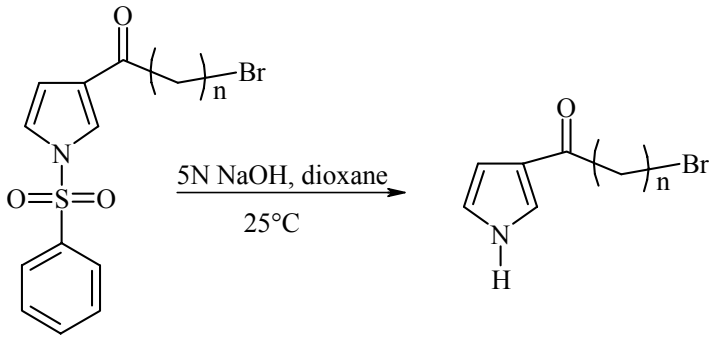

Scheme 4.14 Synthesis of 3-(ω-bromoacyl) pyrrole

2.4 g (6.2 mmol) 1-phenylsulfonyl-3-(6-bromohexanoyl) pyrrole (**2c**) was added to a mixture of 1,4-dioxane (60 ml) and NaOH solution (5 N, 60 ml in water), and stirred at room temperature for 50 hours. TLC (n-hexane- ethyl acetate 3:1) indicated one major and one minor product. The organic layer was collected, and the aqueous layer was thoroughly extracted with ethyl acetate. The combined extracts were washed with saturated NaCl solution, dried over $MgSO_4$, and concentrated under reduced pressure to give a white solid. Recrystallization from toluene-hexane (1:4) resulted in white crystals (**3c**) in 70% yield, Mp.73 -74°C

- ***3-(6-bromohexanoyl) pyrrole (3c)***

^{1}H-NMR ($CDCl_3$, 500 MHz, δ in ppmδ in ppm 8.7-8.5 [1H, (H1), br s], 7.4 [1H, (H2), overlapping ddd, $J_{2,1}$= 3.3 Hz and $J_{2,4=2,5}$ = 1.8 Hz], 6.8 [1H, (H5), m], 6.66-6.65 [1H, (H4), m], 3.42-3.39 [2H, (H11), t, $J_{10,11}$= 6.8 Hz], 2.78-2.75 [2H, (H7), t, $J_{7,8}$ = 7.4 Hz], 1.9 [2H, (H10), m], 1.8-1.7 [2H, (H8), m], 1.5-1.4 [2H, (H9), m].

IR (KBr, ν_{max}/cm^{-1}): 3400-3200 (N-H), 3115-3040 (arom. C-H), 1629 (C=O), 1545-1504 (pyrrole ring).

Elemental analysis:

$C_{10}H_{14}BrNO$: Calculated: C, 49.20, H, 5.78; N, 5.74; Br, 32.73.

Found: C, 49.42; H, 5.97; N, 5.67; Br, 32.45.

- ***3-(8-bromoctanoyl) pyrrole (3d)***

Yield: 82%, **Mp.:** 57-59°C

^{1}H-NMR ($CDCl_3$, 500 MHz, δ in ppm): 8.7-8.6 [1H, (H1), br s], 7.4 [1H, (H2), $J_{2,1}$ = 3.1 Hz and $J_{2,4=2,5}$ = 1.7 Hz], 6.78-6.76 [1H, (H5), m], 6.65 [1H, (H4), m], 3.40-3.38 [2H, (H13), t, $J_{12,13}$ = 6.9 Hz], 2.75-2.72 [2H, (H7), t, $J_{7,8}$ = 7.4 Hz], 1.8 [2H, (H12), m], 1.7 [2H, (H8), m], 1.5-1.3 [6H, (H9, H10, H11), m].

IR (KBr, ν_{max}/cm^{-1}): 3400-3100 (N-H), 3084-3044 (arom. C-H), 1632 (C=O), 1547-1505 (pyrrole ring).

Elemental analysis:

$C_{12}H_{18}BrNO$: Calculated: C, 52.95; H, 6.67; N, 5.15; Br, 29.36.

Found. C, 52.49; H, 6.85; N, 5.03; Br, 29.41.

- ***3-(11-bromoundecanoyl) pyrrole (3e)***

Yield: 80%. **Mp.:** 69-71°C

^{1}H-NMR ($CDCl_3$, 500 MHz, δ in ppm): 8.7-8.5 [1H, (H1), br s], 7.4 [1H, (H2), $J_{1,2}$ = 3.1 Hz and $J_{2,4=2,5}$ = 1.7 Hz, m], 6.77-6.76 [1H, (H5), m], 6.65 [1H, (H4), m], 3.39-3.37 [2H, (H16), t, $J_{15,16}$ = 6.9 Hz], 2.74-2.71 [2H, (H7), t, $J_{7,8}$ = 7.5 Hz], 1.86-1.80 [2H, (H15), m], 1.7 [2H, (H8), m], 1.4-1.2 [12H, m].

IR (KBr, ν_{max}/cm^{-1}): 3400-3200 (N-H), 3051 (arom. C-H), 1629 (C=O), 1507 (pyrrole ring).

Element analysis:

$C_{15}H_{24}BrNO$: Calculated: C, 57.33; H, 7.70; N, 4.46; Br, 25.43.

Found: C, 57.42; H, 8.16; N, 4.37; Br, 25.59.

4.4.3.3 Synthesis of ω-(pyrrol-3-yl acyl) diethyl phosphonic acid ester (5)

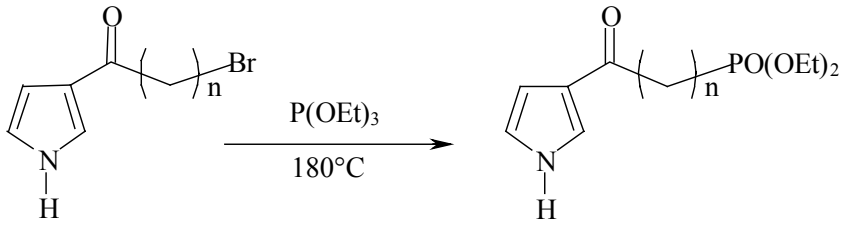

Scheme 4.15 Synthesis of ω-(pyrrol-3-yl acyl) diethyl phosphonic acid ester

1.2 g (3.1 mmol) N-phenylsulfonyl–3-(6-bromohexanoyl) pyrrole (**2c**) and 1.0 g (6 mmol) triethyl phosphite were heated for 3 hours at 170~180^{0}C with continuous distillation of ethyl bromide. After the reaction mixture was cooled to room temperature, and was added to the solution of 30 ml of 5 N NaOH and 30 ml of dioxane, and then left 72 hours at room temperature under stirring. The organic layer was collected, and the aqueous layer was extracted with ethyl acetate. The combined organic solution was washed with brine, dried over anhydrous magnesium sulfate, and evaporated under reduced pressure to obtain a yellow oily liquid. Column chromatography (silica gel, eluting with ethyl acetate) gave a yellow oil (**5c**) in 75% yield.

- ***6-(pyrrol-3-yl hexanoyl) diethyl phosphonic acid ester (5c)***

^{1}H-NMR ($CDCl_3$, 500 MHz, δ in ppm): 9.4-9.2 [1H, (H1), br s], 7.4 [1H, (H2), $J_{1,2}$ = 3.2 Hz and $J_{2,4=2,5}$ = 1.7 Hz, m], 6.76-6.74 [1H, (H5), m], 6.63-6.62 [1H, (H4), m], 4.20-4.00 [4H, ($-OCH_2CH_3$), m], 2.74-2.71 [2H, (H7), t, $J_{7,8}$ = 7.3 Hz], 1.75-1.71 [4H, (H11, 8), m], 1.70 [2H, (H10), m], 1.46-1.40 [2H, (H9), m], 1.34-1.22 [6H, ($-OCH_2CH_3$), t].

^{31}P-NMR ($CDCl_3$, 500 MHz): 32.5 ppm

IR (chloroform, ν_{max}/cm^{-1}): 3400-3200 (N-H), 3082 (arom. C-H), 1654 (C=O), 1226 (P=O), 1055 (ν_{as} P-O-C), 1029 (ν_s P-O-C).

Elemental analysis:

$C_{14}H_{24}NO_4P$: Calculated: C, 55.81; H, 8.03; N, 4.65.

Found: C, 55.49; H, 8.45; N, 4.42.

- ***2-(pyrrol-3-yl ethanoyl) diethyl phosphonic acid ester (5a)***

Yield: 5%,

^{1}H-NMR ($CDCl_3$, 500 MHz, δ in ppm): 9.9-9.8 [1H, (H1), br s], 7.40 [1H, (H2), $J_{1,2}$ = 3.0 Hz, $J_{2,4=2,5}$ = 1.4 Hz, m], 6.7[1H, (H5), m], 6.6 [1H, (H4), m], 4.00 [4H, ($-OCH_2CH_3$), m], 3.4-3.3 [2H, (H7), s], 1.21-1.8 [6H, m].

^{31}P-NMR ($CDCl_3$, 500 MHz): 33.8 ppm

IR (chloroform, ν_{max}/cm^{-1}: 3407-3200 (N-H), 3080 (arom. C-H), 1654 (C=O), 1220 (P=O), 1055 (ν_{as} P-O-C), 1028 (ν_s P-O-C).

Elemental analysis:

$C_{10}H_{16}NO_4P$: Calculated: C, 48.98; H, 6.58; N, 5.71.

Found: C, 48.42; H, 6.73; N, 5.54.

- ***4-(pyrrol-3-yl butanoyl) diethyl phosphonic acid ester (5b)***

Yield: 6%,

^{1}H-NMR ($CDCl_3$, 500 MHz, δ in ppm): 9.4-9.3 [1H, (H1), br s], 7.39-7.38 [1H, (H2), J1, 2 = 2.8 Hz, $J_{2,4=2,5}$ = 1.4 Hz, m], 6.8 [1H, (H5), m], 6.7-6.6 [1H, (H4), m], 4.1-4.00 [4H, (-OCH_2CH_3), m], 2.8 [2H, (H7), t, $J_{7,8}$ = 7.2 Hz], 2.0-1.9 [2H, (H9), t] , 1.8-1.7 [2H, (H8), m], 1.36-1.21 [6H, m].

^{31}P-NMR (CDCl3, 500 MHz): 32.6 ppm

IR (chloroform, ν_{max}/cm^{-1}): 3407-3200 (N-H), 3090 (arom. C-H), 1653 (C=O), 1226 (P=O), 1053 (ν_{as} P-O-C), 1028 (ν_s P-O-C).

Elemental analysis:

$C_{16}H_{28}NO_4P$: Calculated: C, 52.74; H, 7.38; N, 5.13.

Found. C, 52.56; H, 7.58; N, 4.98.

- ***8-(pyrrol-3-yl octanoyl) diethyl phosphonic acid ester (5d)***

Yield: 85%,

^{1}H-NMR ($CDCl_3$, 500 MHz, δ in ppm): 9.6 [1H, (H1), br s], 7.39-7.38 [1H, (H2), J1, 2 = 3.0 Hz, $J_{2,4=2,5}$ = 1.4 Hz, m], 6.73 [1H, (H5), m], 6.61 [1H, (H4), m], 4.11-4.00 [4H, (-OCH_2CH_3), m], 2.7 [2H, (H7), t, $J_{7,8}$ = 7.4 Hz], 1.70-1.55 [4H, (H13, 8), m], 1.36-1.21 [14H, m].

^{31}P-NMR (CDCl3, 500 MHz): 32.6 ppm

IR (chloroform, ν_{max}/cm^{-1}): 3407-3200 (N-H), 3080 (arom. C-H), 1654 (C=O), 1216 P=O), 1052 (ν_{as} P-O-C), 1028 (ν_s P-O-C).

Elemental analysis:

$C_{16}H_{28}NO_4P$: Calculated: C, 58.35; H, 8.57; N, 4.25.

Found: C, 58.26; H, 9.06; N, 4.04.

- ***11-(pyrrol-3-yl undecanoyl) diethyl phosphonic acid ester (5e)***

Yield: 87%,

^{1}H-NMR ($CDCl_3$, 500 MHz, δ in ppm): 9.4-9.1 [1H, (H1), br s], 7.40 [1H, (H2), $J_{1,2}$ = 3.1 Hz and $J_{2,4=2,5}$ = 1.6 Hz], 6.76-6.75 [1H, (H5), m], 6.6 [1H, (H4), m], 4.10-4.0 [4H, (-OCH_2CH_3), t], 2.80-2.70 [2H, (H7), t, $J_{7,8}$ = 7.4 Hz], 1.70 [4H, (H16, 8), m], 1.60-1.50 [2H, (H15), m], 1.4-1.20[18H, m].

^{31}P-NMR ($CDCl_3$, 500 MHz): 32.7 ppm

IR (chloroform, ν_{max}/cm^{-1}): 3443-3200 (N-H), 3109 (arom. C-H), 1654 (C=O), 1219 (P=O), 1056 (ν_{as} P-O-C), 1029 (ν_s P-O-C).

Elemental analysis:

$C_{19}H_{34}NO_4P$: Calculated: C, 61.44; H, 9.23; N, 3.77.

Found: C, 59.65; H, 9.45; N, 3.31.

4.4.3.4 Synthesis of 1-Phenylsulfonyl-3-(ω-bromoalkyl) pyrrole (6)

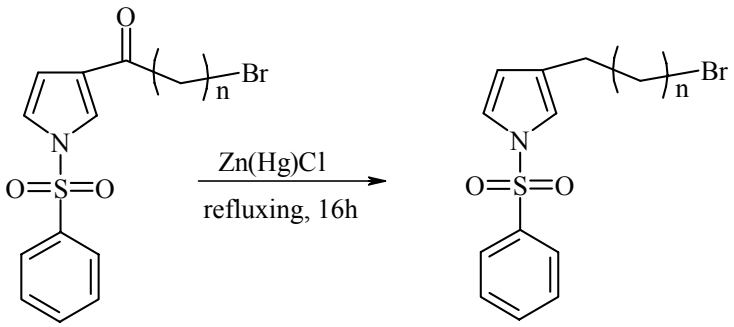

Scheme 4.16 Clemmensen reduction

The mixture of zinc metal (16 g) and mercuric chloride (2.64 g) in 20 ml of water and 1ml of 12 N HCl was stirred at 25^0C for 30 min. followed by decantation. To the solid was added 9.3 ml of water, 22 ml of 12 N HCl, 120 ml of toluene, and 3.3 g N-phenylsulfonyl-3-(6-bromohexanoyl) pyrrole. The mixture was refluxed for 16 hours and checked by TLC. The organic fraction was collected. The aqueous layer was extracted with toluene. The combined organic fraction was washed with water, dried over anhydrous magnesium sulfate, and concentrated in vacuo to give yellow liquid. The crude product was purified by column chromatography (silica gel, eluting with 10:4 n-hexane-ethyl acetate) to give colorless oil in 87% yield.

- ***1-phenylsulfonyl-3-(6-bromohexyl) pyrrole (6c)***

^{1}H-NMR ($CDCl_3$, 500 MHz, δ in ppm): 7.8 [2H, (H2', 6'), d, $J_{2',3'=6',5'}$ = 7.7 Hz], 7.6-7.4 [3H, (H3', 4', 5'), m], 7.1-7.0 [1H, (H5), m], 6.9-6.8 [1H, (H2), m], 6.1 [1H, (H4), m], 3.4-3.3 [2H, (H11), t, $J_{10, 11}$= 6.6 Hz], 2.4-2.3 [2H, (H6), t], 1.8 [2H, (H10), m], 1.5-1.2 [6H, m].

IR (chloroform, ν_{max}/cm^{-1}): 3135-3058 (arom. C-H), 1473 (pyrrole ring),

Elemental analysis:

$C_{15}H_{24}BrNO$: Calculated: C, 51.90; H, 5.44; N, 3.78; Br, 21.58.

Found: C, 52.08; H, 5.67; N, 3.71; Br, 21.36.

- ***1-phenylsulfonyl-3-(4-bromobutyl) pyrrole (6b)***

Yield: 78%,

^{1}H-NMR ($CDCl_3$, 500 MHz, δ in ppm): 7.82-7.81 [2H, (H2', 6'), d, $J_{2',3=6',5'}$ = 7.8 Hz], 7.59-7.57 [1H, (H4'), m], 7.56-7.50 [2H, (H3', 5'), m], 7.07-7.06 [1H, (H5), m], 6.90 [1H, (H2), m], 6.14-6.13 [1H, (H4), m], 3.37-3.35 [2H, (H9), t, $J_{8, 9}$ = 6.7 Hz], 2.41-2.38 [2H, (H6), t, $J_{7, 6}$ = 7.6 Hz], 1.84-1.80 [2H, (H8), m], 1.68-1.62 [2H (H7), m].

IR (chloroform, ν_{max}/cm^{-1}): 3136-3065 (arom. C-H), 1475 (pyrrole ring).

Elemental analysis:

$C_{14}H_{16}BrNSO_2$: Calculated: C, 49.13; H, 4.71; N, 4.09; S, 9.37; Br, 23.34.

Found: C, 49.56; H, 5.35; N, 4.02; S, 8.38; Br, 23.27.

4.4.3.5 Synthesis of ω-(pyrrol-3-yl alkyl) diethyl phosphonic acid ester (8) (PYPE)

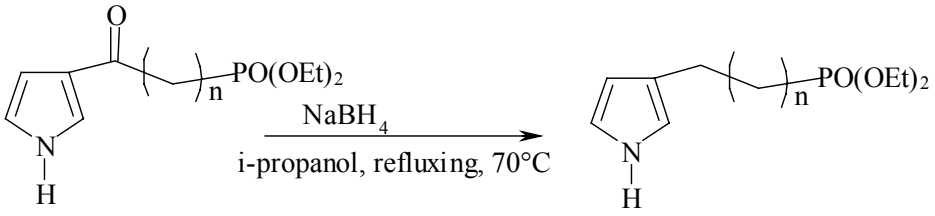

Scheme 4.17 Reduction of carbonyl group

The 6-(pyrrol-3-yl hexanoyl) diethyl phosphonic acid ester (5c) (2.0 g, 7 mmol) and $NaBH_4$ (2.7 g, 70 mmol) were added to i-propanol (70 ml) and refluxed for 50 hours. The reaction was carefully hydrolyzed with ice water, and then the reaction mixture was extracted with

ethyl acetate. The organic phase was dried over anhydrous magnesium sulfate and evaporated to give yellow oil. Column chromatography (silica gel, eluting with 5:1 ethyl acetate - hexane) gave a colorless oil in 50% yield (1.0 g).

- ***6-(pyrrol-3-yl hexyl) diethyl phosphonic acid ester (8c, PYPE-6)***

^{1}H-NMR (500 MHz, $CDCl_3$, δ in ppm): 8.4-8.2 [1H, (H1), br s], 6.8-6.7 [1H, (H5), m], 6.6-6.5 [1H, (H2), m], 6.10-6.00 [1H, (H4), m], 4.20-4.0 [4H, ($-OCH_2CH_3$), m], 2.51 [1H, (H6), t, $J_{6,7}$ = 7.7 Hz], 1.6-1.2 [16H, m].

^{31}P-NMR (500 MHz, $CDCl_3$): 31.6 ppm

IR (chloroform, ν_{max}/cm^{-1}): 3500-3091 (N-H), 1225 (P=O), 1142-1046 (ν_{as} P-O-C), 994 (ν_s P-O-C).

Elemental analysis:

$C_{14}H_{26}NO_3P$: Calculated: C, 58.52; H, 9.12; N, 4.87.

Found: C, 59.37; H, 10.26; N, 4.55.

- ***8-(pyrrol-3-yl octyl) diethyl phosphonic acid ester (8d, PYPE-8)***

Yield: 70%.

^{1}H-NMR (500 MHz, $CDCl_3$, δ in ppm): 8.2-8.0 [1H, (H1), br s], 6.71-6.70 [1H, (H5), m], 6.55 [1H, (H2), m], 6.06 [1H, (H4), m], 4.08-4.02 [4H, ($-OCH_2CH_3$), m], 2.47-2.44 [2H, (H6), t, $J_{6,7}$ = 7.6 Hz], 1.71-1.52 [6H, m], 1.36-1.23 [18H, m].

^{31}P-NMR (500 MHz, $CDCl_3$): 31.5 ppm

IR (chloroform, ν_{max}/cm^{-1}): 3500-3090 (N-H), 1227 (P=O), 1142-1047 (ν_{as} P-O-C), 994 (ν_s P-O-C).

Elemental analysis:

$C_{16}H_{30}NO_3P$: Calculated: C, 60.93; H, 9.59; N, 4.44.

Found: C, 61.18; H, 10.50; N, 4.38.

- ***11-(pyrrol-3-yl undecyl) diethyl phosphonic acid ester (8e, PYPE-11)***

Yield: 50%.

^{1}H-NMR (500 MHz, $CDCl_3$, δ in ppm): 8.2-8.1 [1H, (H1), br s], 6.80-6.79 [1H, (H5), m], 6.70-6.55 [1H, (H2), m], 6.10-6.03 [1H, (H4), m], 4.11-4.00 [4H, (-OCH2CH3), m], 2.47-2.44 [2H, (H6), t, $J_{6,7}$ = 7.6 Hz], 1.9-1.2 [30H, m].

^{31}P-NMR (500MHz, $CDCl_3$): 31.7 ppm

IR (chloroform, ν_{max}/cm^{-1}): 3500-3100 (N-H), 3092 (arom. C-H), 1225 (P=O), 1142-1047 (ν_{as} P-O-C), 994 (ν_s P-O-C).

Elemental analysis:

$C_{19}H_{36}NO_3P$: Calculated: C, 63.84; H, 10.15; N, 3.92.

Found: C, 63.88; H, 11.01; N, 3.34.

4.4.3.6 Synthesis of 4-(pyrrol-3-yl butyl) diethyl phosphonic acid ester (8b, PYPE-4)

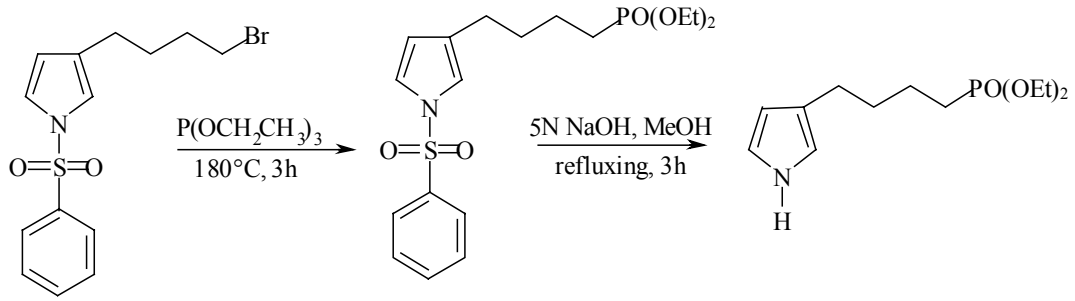

Scheme 4.18 Synthesis of 4-(pyrrol-3-yl butyl) diethyl phosphonic acid ester

1.2 g (3.3 mmol) 1-phenylsulfonyl–3-(4-bromobutyl) pyrrole (**6b**) and 1.0 g (6 mmol) triethyl phosphite were heated for 3 hours at 170~180^{0}C with continuous distillation of ethyl bromide. After the reaction mixture was cooled to room temperature, it was added to the solution of 30 ml of 5 N NaOH and 60 ml of methanol, and refluxed 3 hours. Reaction mixture was concentrated in vacuo. The aqueous solution was extracted with ethyl acetate. The combined organic solution was washed with brine, dried over anhydrous magnesium sulfate, and evaporated under reduced pressure to obtain a yellow oily liquid. Column chromatography (silica gel, eluting with ethyl acetate) gave a yellow oil (8b) in 35% yield.

^{1}H-NMR (500MHz,$CDCl_3$, δ in ppm): 8.2-8.0 [1H, (H1), br s], 6.71-6.69 [1H, (H5), m], 6.56-6.55 [1H, (H2), m], 6.06 [1H, (H4), m], 4.08-4.02 [4H, (-OCH2CH3), m], 2.50-2.48 [2H, (H6), t, $J_{6,7}$ = 6.9 Hz], 1.76-1.61 [6H, m], 1.32-1.23[6H, m]

^{31}P-NMR ($CDCl_3$, 500 MHz): 32.6 ppm

IR (chloroform, ν_{max}/cm^{-1}): 3500-3100 (N-H), 3084 (arom. H),1223 (P=O), 1095-1059 (ν_{as} P-O-C), 961 (ν_s P-O-C).

Elemental analysis:

$C_{16}H_{30}NO_3P$: Calculated: C, 55.59; H, 8.55; N, 5.40.

Found: C, 55.13; H, 9.24; N, 5.38.

4.4.3.7 Synthesis ω-(pyrrol-3-yl alkyl) phosphonic acid (9) (PYPA)

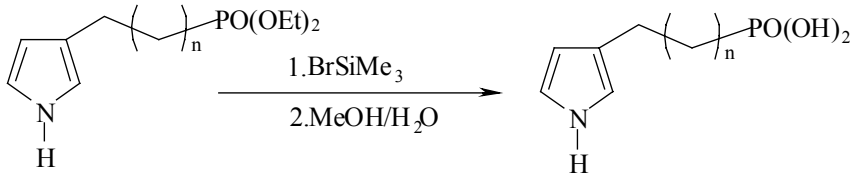

Scheme 4.19 Synthesis of ω-(pyrrol-3-yl alkyl) phosphonic acid

1.2 g (5 mmol) Trimethylsilyl bromide was added to 0.27 g (1mmol) of 6-(pyrrol-3-yl hexyl) diethyl phosphonic acid ester (**8c**) in dry acetonitrile (5 ml) at 0°C. After 1h the reaction mixture was stirred at room temperature for 2h. The solvent and excess of trimethylsilyl bromide were removed by rotary evaporation. 10 ml methanol/ water (2:1 volume ratios) was added to the residue under argon atmosphere, and stirred at room temperature for 2h. The solvent of the solution was removed by freeze-drying. The white solid was obtained in a yield of 33.4% (0.077 g)

- ***6-(pyrrol-3-yl hexyl) phosphonic acid (9c, PYPA-6)***

Yield: 33.4%,

^{1}H-NMR (500 MHz, methanol, δ in ppm): 10.54-10.29 [1H, (H1), br s], 6.83-6.82 [1H, (H5), m], 6.69-6.67 [1H, (H2), m], 6.11-6.06 [1H, (H4), m], 2.43-2.40 [2H, (H6), t, $J_{6,7}$ = 8.2 Hz], 1.65-1.29 [10H, m].

^{31}P-NMR (500 MHz, methanol): 31.2 ppm

IR (KBr, ν_{max}/cm^{-1}): 3600-3100 (N-H), 2800-2600 (P-O-H), 1143 (P=O), 1112-996 (P-O).

Elemental analysis:

$C_{10}H_{18}NO_3P$: Calculated: C, 51.94; H, 7.85; N, 6.06.

Found: C, 50.84; H, 8.17; N, 5.04.

- ***4-(pyrrol-3-yl butyl) phosphonic acid (9b, PYPA-4)***

Yield: 28%,

^{1}H-NMR (500 MHz, methanol, δ in ppm): 10.30-10.20 [1H, (H1), br s], 6.80 [1H, (H5), m], 6.6 [1H, (H2), m], 6.11-6.08 [1H, (H4), m], 2.50-2.48 [2H, (H6), t, $J_{6,7}$ = 7.5 Hz], 1.81-1.36 [6H, m].

^{31}P-NMR (500 MHz, methanol): 30.4 ppm

IR (KBr, ν_{max}/cm^{-1}): 3500-3100 (N-H), 2800-2500 (br. P-O-H), 1141 (P=O), 976-938 (P-O).

Elemental analysis:

$C_{15}H_{28}NO_3P$: Calculated: C, 47.29; H, 6.94; N, 6.89.

Found: C, 48.06; H, 7.83; N, 5.62.

- ***8-(pyrrol-3-yl octyl) phosphonic acid (9d, PYPA-8)***

Yield: 35%,

^{1}H-NMR (500 MHz, methanol, δ in ppm): 10.20-10.10 [1H, (H1), br s], 6.80 [1H, (H5), m], 6.65 [1H, (H2), m], 6.11-6.08 [1H, (H4), m], 2.51-2.48 [2H, (H6), t, $J_{6,7}$ = 7.4 Hz], 1.79-1.30 [14H, m].

^{31}P-NMR (500 MHz, methanol): 30.9 ppm

IR (KBr, ν_{max}/cm^{-1}): 3500-3100 (N-H), 2800-2500 (P-O-H), 1175 (P=O), 1000-996 (P-O).

Elemental analysis:

$C_{12}H_{22}NO_3P$: Calculated: C, 55.59; H, 8.55; N, 5.40.

Found: C, 55.33; H, 9.05; N, 4.80.

- ***11-(pyrrol-3-yl undecyl) phosphonic acid (9e, PYPA-11)***

Yield: 38%,

^{1}H-NMR (500 MHz, methanol, δ in ppm): 10.30-10.20 [1H, (H1), br s], 6.83-6.82 [1H, (H5), m], 6.67 [1H, (H2), m], 6.11-6.08 [1H, (H4), m], 2.51-2.48 [2H, (H6), t, $J_{6,7}$ = 7.5 Hz], 1.79-1.36 [20H, m].

^{31}P-NMR (500 MHz, methanol): 30.84 ppm

IR (KBr, ν_{max}/cm^{-1}): 3500-3100 (N-H), 2800-2500 (br. P-O-H), 1157 (P=O), 998 (P-O).

Elemental analysis:

$C_{15}H2_8NO_3P$: Calculated: C, 59.78; H, 9.36; N, 4.65.

Found: C, 59.01; H, 8.56; N, 3.76.

4.4.3.8 6-(Pyrrol-3-yl hexyl) phosphonic ammonium salt (10c)

Trimethylsilyl bromide (1.0 g) was added dropwise to 6-(pyrrol-3-yl hexyl) phosphonic acid ester (0.2 g, 0.73 mmol) in acetonitrile (3 ml) at 0°C for 1 h, then the reaction mixture was stirred for 2 h at room temperature. The solvent and excess of trimethylsilyl bromide were removed by rotary evaporation. The residue was added to 10 ml methanol / water (2:1 in volume ratios) at room temperature. After 30 min, 8 ml (25%) ammonium solution was added and stirred for 2h. Excess of ammonia and solvent were removed, and then the compound was dried under freeze drying to get a pink solid 0.12 g in yield 66.7%, Mp. 65-67°C

^{1}H-NMR (500 MHz, methanol, δ in ppm): 6.67 [1H, (H5), m], 6.54 [1H, (H2), m], 5.98 [1H, (H4), m], 2.52 [2H, (H6), d], 1.65-1.20 [18H, m].

^{31}P-NMR: (methanol, 500 MHz): 25.95 ppm

IR (KBr, ν_{max}/cm^{-1}): 3500-3100 (N-H), 1225 (P=O), 1142 (P-O).

Elemental analysis:

$C_{10}H_{24}N_3O_3P$: Calculated: C, 45.28; H, 9.06; N, 15.85.

Found: C, 43.77; H, 8.90; N, 14.26.

Same procedure was used to convert the free acid into its ammonium salt.

4.5 Monolayer Formation and Characterization

Metal substrates such as Ti/TiO_2, Ta/Ta_2O_5, Al/Al_2O_3 were used to adsorb ω-(pyrrol-3-yl alkyl) phosphonic acids (PYPA). These metal substrates were prepared by chemical vapor deposition on Si wafers.

Ti metal substrate (Ti/TiO_2): n-doped Si wafer/ 300 nm Ti

Ta metal substrate (Ta/Ta_2O_5): n-doped Si wafer/ 300 nm Ta

Al metal substrate (Al/Al_2O_3): n-doped Si wafer/ 300 nm Al

There are several methods to clean and activate the surface:

Normal cleaning: Rinsing with organic solvent or ultrasonic treatment to degrease.

Etching: Cleaning in the standard QCA SC1 (H_2O/NH_3 25%/H_2O_2 30%, v/v 2:1:1, 80°C, 5s) or pirañha solution to remove organic material and increase OH-group on surface.

Plasma cleaning: An air plasma generated by plasma cleaner/sterilizer.

Table 4.5 Contact angle data after substrate pretreatment by different methods

Metals	Methods	Contact angle [^{0}]
Ta	Rinsing	84.1 ± 1.92
Ta	Treatment with organic solvent (chloroform, acetone, ethanol, 5 min, respectively) by ultrasonication	67.9 ± 1.78
Ta	H_2O/NH_3 25%/H_2O_2 30% (2:1:1, v/v) , 80°C, 5s	45.6 ± 1.88
Ta	Piranha solution	27.0 ± 3.38

From the contact angle data, we can see that the pretreatments by H_2O/NH_3 25%/H_2O_2 30% (2:1:1, v/v) solution and piranha solution gave hydrophilic surfaces. But AFM measurements showed that these two methods of pretreatment increase the roughness of the surface. After the adsorption of the compound, the contact angle has no big difference [202]. Pretreatment by ultrasonic cleaning is adopted for further investigation.

The pretreated metal substrates were immersed in the solution of 1 mM ω-(pyrrol-3-yl alkyl) phosphonic acids in methanol for different time intervals (1 hr, 2 hrs, 6 hrs, and 24 hrs) followed by rinsing with methanol and drying under argon atmosphere. The adsorbed samples were characterized by various surface analytical techniques like contact angle measurement, SPR, UV-VIS spectroscopy, grazing incident FTIR, XPS etc.

ω-(Pyrrol-3-yl alkyl) phosphonic acids were studied for their adsorption behavior on the reactive metal surfaces. The compounds contain two reactive functional groups, N-H group from pyrrolyl and phosphonic acid groups. There are two possibilities for adsorption, with the

acidic phosphonic acid group or N-H group of the pyrrolyl ring. A first indication of adsorption taking place can be obtained from the contact angle measurements. When the phosphonic acid group reacts with the surface hydroxyls of the metal substrate, the terminal pyrrolyl group should cause a more hydrophobic surface (i. e. high contact angles). Whereas in the opposite case, the surface should be more hydrophilic. The reaction of the phosphonic acid group and N-H group of pyrrole ring with the substrate can be considered as base-acid interaction.

Table 4.6 Water contact angle data on different metal substrates

Monomers	Adsorption time [hours]	Metals		
		Ti	Ta	Al
PYPA-4	1	54.3 ± 1.54	60.9 ± 3.24	58.2 ± 2.65
	24	56.1 ± 1.92	58.4 ± 2.46	60.7 ± 3.16
PYPA-6	1	58.5 ± 3.42	71.7 ± 2.24	65.4 ± 4.33
	24	56.5 ± 3.97	66.9 ± 3.55	58.4 ± 3.44
PYPA-8	1	72.1 ± 2.05	71.5 ± 1.19	65.5 ± 2.56
	24	60.5 ± 2.03	64.1 ± 3.17	63.7 ± 1.92
PYPA-11	1	90.5 ± 2.79	88.6 ± 2.22	86.7 ± 2.84
	24	86.0 ± 2.49	80.9 ± 2.97	78.8 ± 5.03
Uncoated		48.6 ± 1.84	45.6 ± 1.78	45.8 ± 1.67

The comparison of the different contact angles (adsorption time, chain length) shows that the contact angles on modified substrates are higher than that of on unmodified substrate. This indicated that the adsorption has taken place. The contact angle of the shorter chain length molecule (PYPA-4) has no order on different metal substrates due to limited van der Waals interaction between the molecules. During the formation of the self-assembly monolayer, van der Waals interactions are the main forces to form the order and a closely packed assembly monolayer. Usually, the contact angle increases with the increasing of the adsorption time at the beginning of the adsorption process, then reach a plateau [66], e.g. alkanethiols on gold [203]. But in our results, the contact angle of 1-hour adsorption time for three chain derivatives (PYPA-6, PYPA-8 and PYPA-11) is slightly higher than that of 24 hours

adsorption time. The phosphonic acid group reacted with OH group on the surface to form acid-base interaction instead of the stable covalent bond. During the adsorption process, the desorption process also exists. This alternating of adsorption and desorption processes resulted in small difference between 1 hour and 24 hours adsorption time. Another possibility: is that N-H group from pyrrole ring attached to the surface resulted in the decrease of contact angle of the long adsorption time. This is just a hypothesis. It should be confirmed by other technique such as XPS.

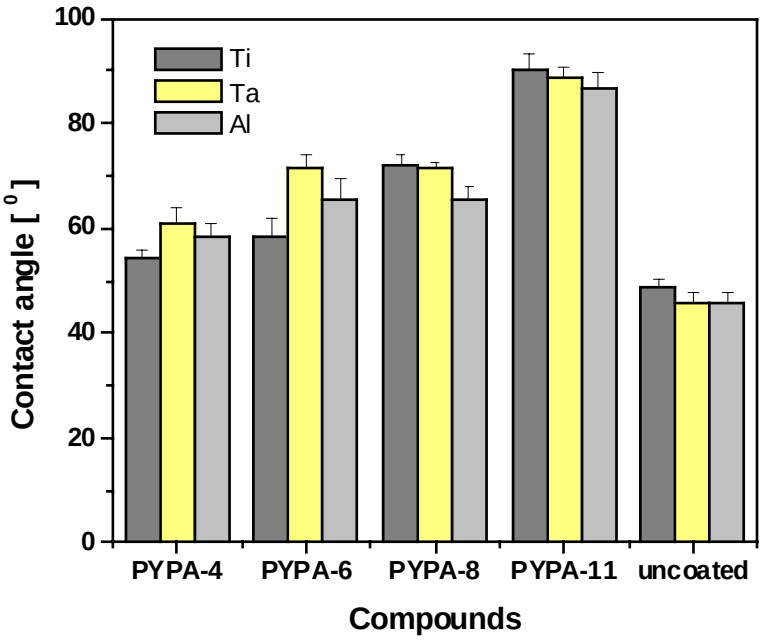

Fig. 4.16 Contact angle of PYPA on different metals adsorbed 1 hour

From the water contact angle data, we also can see that the contact angles increase with chain length (Fig. 4.16). The contact angle data showed that the longer alkyl chain of ω-(pyrrol-3yl alkyl) phosphonic acid (PYPA) leads to high hydrophobicity of the corresponding adsorbed surface. These results indicated that ω-(pyrrol-3yl alkyl) phosphonic acid (PYPA) with longer alkyl chains formed more compact adsorbed layers on the metal surface.

Grazing incident FTIR and UV-VIS spectra were taken to determine the presence of PYPA on the surface.

Figure 4.17 showed the grazing incident FTIR of PYPA-6 on Ta. There are three important features. The broad peak near 3250 cm^{-1} due to N-H vibration, it also could have contributions from O-H group. The aromatic C-H stretching (at 3000-3100 cm^{-1}) signal was observed. CH_2 stretching peaks at 2852 and 2923 cm^{-1} can also be seen clearly. The characteristic vibrations of the free phosphonic acids at 2900 cm^{-1} are not present in the surface spectrum. The P-O

stretching vibrations are shifted to higher wavenumbers. The absence of the P=O stretching vibrations at 1225 cm^{-1} and the mentioned P-OH bands were interpreted as evidence for a tridentate bonding mode [204]. These peaks were present on the adsorbed layers indicating that PYPA-6 is present on the surface.

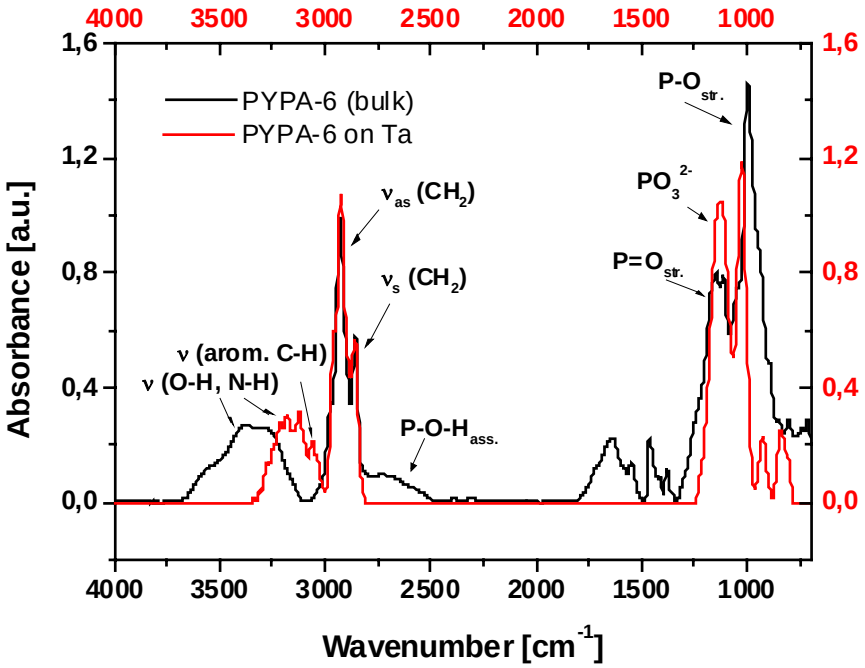

Fig. 4.17 Grazing incident FTIR of PYPA-6 on Ta

In the UV-VIS spectra, like the free monomers, the adsorbed layer also showed a strong absorbance above 250 nm. This absorbance is due to the pyrrole moiety of the PYPA.

FTIR and UV-VIS spectra therefore establish that PYPA compound presented on the surface.

SPR was also measured to study the kinetics of adsorption and desorption of PYPA on the substrates. The kinetic curves were measured at a fixed angle (56°) and compounds were dissolved in MeOH (1mM). Fig. 4.18 the SPR spectrum of PYPA-6 is shown as example. In the first stage the adsorption fast increases within a few seconds. The further ordering process takes more time. After 18 hrs the curve changed. When the process is disturbed the system is able to equalisise because the adsorption of phosphonates can be understood as dynamic process. Schwartz [205] observed that during the formation of octadecylphosphonic acid monolayers on mica dynamic adsorption/desorption processes also take place. Due to the unknown thickness and refraction index of Al_2O_3 on the gold layer, the thickness of the adsorbed layer cannot be calculated. SPR curves also show that the adsorbed layer is stable

after some time. But we are not sure if such layer is dense and ordered. This is due to the weak van der Waals interaction between the shorter chain adsorbate molecules on the substrate leading to a less-ordered adsorption layer.

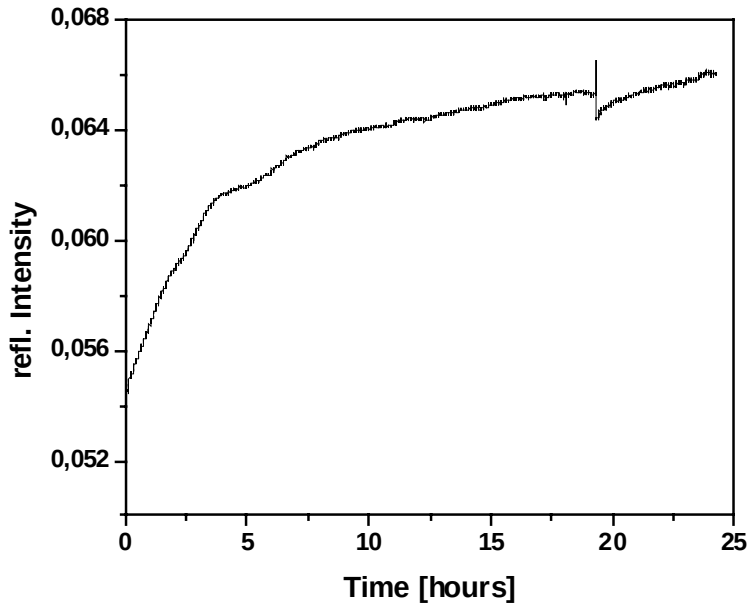

Fig. 4.18 SPR spectrum of PYPA-6

XPS was measured to study the atomic composition and binding state. Angle resolved XPS was used to study the orientation. We have mentioned before that PYPA has two functional groups. Contact angle data, grazing incident FTIR and UV-VIS spectra have confirmed that PYPA is on the surface.

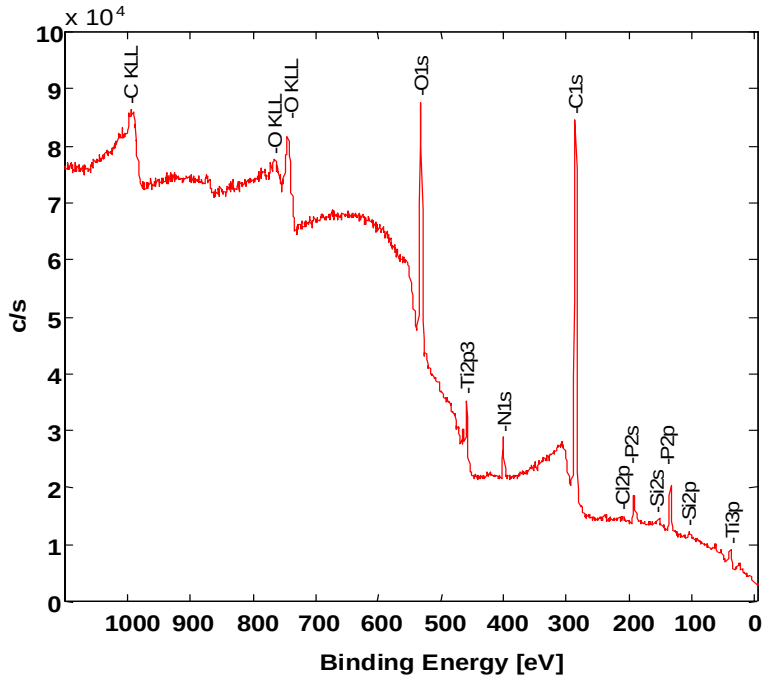

Fig. 4.19 Survey spectrum of PYPA-6 on Ti

The metal substrates coated with PYPA were subjected to XPS in order to get the information about surface composition. Fig. 4.19 showed the survey of the XPS spectrum of PYPA-6 on Ti.

Table 4.7 Immersion time dependence of the relative atomic concentration (%) for different metals after modification by PYPA-6 (take off angle 45)

(a). PYPA-6 on Ti

Adsorption time [hours]	C1s	N1s	P2p	O1s	Ti2p
1	66.47	4.50	4.97	21.80	2.25
2	47.38	4.24	3.08	36.56	8.74
6	60.87	3.43	3.39	26.87	5.45

(b). PYPA-6 on Ta

Adsorption times [hours]	C1s	N1s	P2p	O1s	Ta4f
1	70.40	4.56	5.29	18.95	0.74
2	41.17	3.78	3.08	39.80	12.17
6	42.95	4.35	3.64	37.82	11.24

(c). PYPA-6 on Al

Adsorption time [hours]	C1s	N1s	P2p	O1s	Al2p
1	66.71	4.43	5.13	20.53	3.57
2	63.24	5.08	5.85	22.27	3.57
6	52.85	3.46	4.79	26.24	12.65

The grafting behavior of PYPA-6 on Al, Ta and Ti substrates was evaluated as a function of the reaction of the adsorption time by XPS atomic relative concentration (Table 4.7). In order to check the stoichiometry of the grafted layers formed from PYPA-6, Table 4.8 provided the C/P and P/N ratios.

Table 4.8 Adsorption time dependence of the C/P and P/N ratios for Ti substrates after modification of PYPA-6

Metals	Adsorption time (hour)	C/P (10:1)	P/N (1:1)
Al	1	13.0	1.1
	2	10.8	1.1
	6	11.0	1.4
Ta	1	13.3	1.2
	2	13.4	0.8
	6	11.8	0.9
Ti	1	13.4	1.1
	2	15.3	0.7
	6	17.9	1.0

From the intensities of atomic composition, the atomic ratios C/P and P/N were calculated (see table 4.8). As we can see that the optimum adsorption time is different for the used substrates. On Al substrates the adsorption of PYPA-6 is optimal after 2 hours, because the C/P and P/N ratios are close to the theoretical values. In case of Ta substrates the optimal adsorption time is 6 hours, whereas on Ti substrates the adsorption is completed within 1 hour. This indicated that the formation of uniform, ordered and oriented adsorbed layer is

dependent on the density of the hydroxyl group on the surface. It is reported that there is 11-12 (–OH groups) per nm^2 on Ti and Al surface and 6 –OH groups per nm^2 on Ta [206].

The orientation of the molecule i.e. phosphonic acid and pyrrole group, which group is on top and which group is attached to the surface is studied by XPS. Angle-resolved XPS measurement were done at four different take-off angles (20°, 45°, 70° and 85°) to investigate the orientation of the adsorbed molecule on the surfaces. From the P/N ratios of PYPA-6 on different substrates at one adsorption time (Fig. 4.20), PYPA-6 showed an increase in P/N ratios with increasing take off angle on adsorbed substrates except on Ta substrate, thereby suggested the presence of packed pyrrolyl group on top and phosphonic acid group attached to the surface. The adsorption of the compound on Ta showed a decrease in P/N ratio with increasing of take off angle after 45°. It may arise from the presence of defects, such as pinholes and collapse sites in the adsorbed layer, as density of hydroxyl group on Ta surface is less than that of on Ti and Al substrates [206].

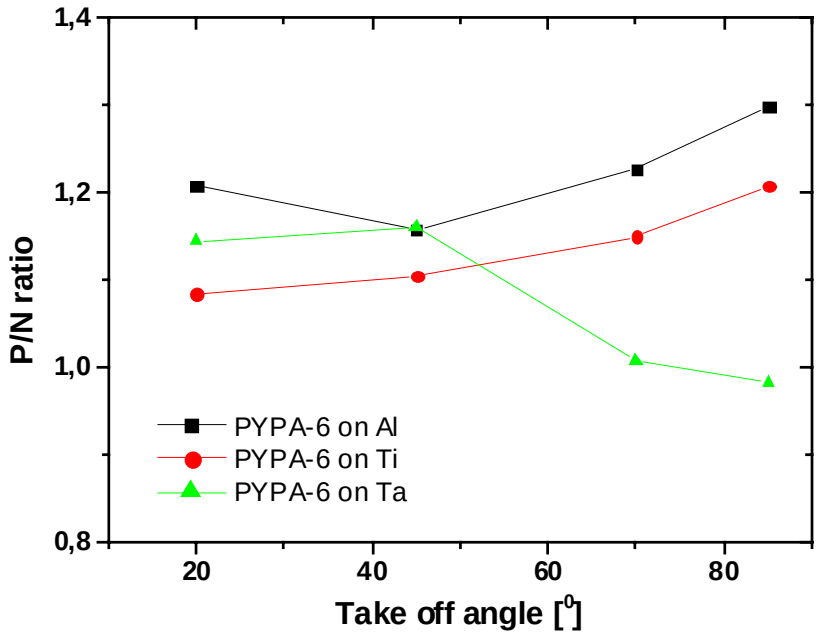

Fig. 4.20 AR-XPS measurements: P/N ratios of PYPA-6 on Ti, Al and Ta (I hour adsorption time)

Figure 4.21 compares the C1s and O1s peaks for Ti and Ti modified with PYPA-6. The C1s peak for Ti substrates can be resolved in three components: one at 284.89 eV corresponding to carbon in an aliphatic environment (CHx) and two others characteristic of C-O-C and (C=O)-O-C (from 286.1 and 287.0 eV) and (C=O)-O-C (288.9 eV) [207]. After reaction of Ti substrate with PYPA-6 molecules, the oxidized carbon components have practically

disappeared and C1s peak is mostly of the aliphatic type (Fig. 4.21a). Remarkable changes can be observed for O1s peak. The O1s peak for Ti substrates is at 530.33 eV. After reaction with PYPA-6, the spectrum shows the presence of additional components, which are characteristic for oxygen bound to phosphorus, P-O-Ti (532.03 eV) and P-OH (533.25 eV). The shift in the binding energy to higher values after adsorption and presence of additional O1s peaks suggested phosphonic acid group is attached to the surface.

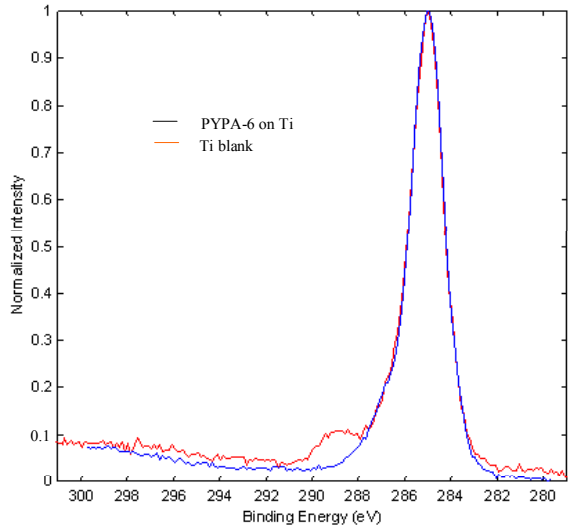

Fig. 4.21a C1s peaks of Ti and Ti modified with PYPA-6 (blue line: PYPA-6 on Ti; red line: Ti blank)

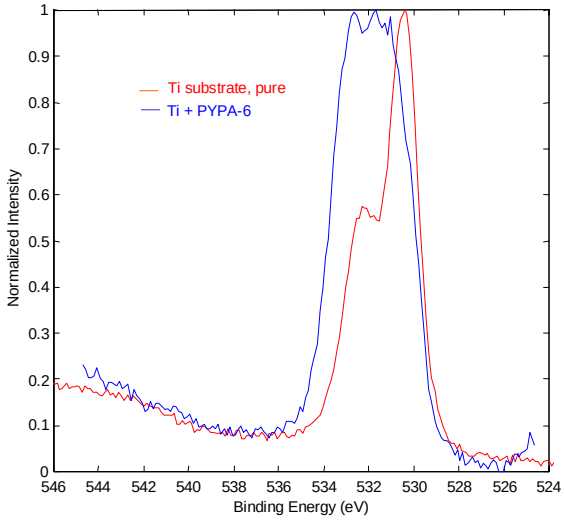

Fig. 4.21b O1s peaks of Ti and Ti modified with PYPA-6 (blue line: PYPA-6 on Ti; red line: Ti blank)

4.6 3-Substituted Pyrrole Trimethoxysilane as Adhesion Promoter

For comparison with 1-substituted pyrrole alkyl dimethylchlorosilane, we also tried to synthesize 3-substituted pyrrole alkyl dimethylchlorosilane. Unfortunately, this kind of compound is very sensitive to environment and tend to self-polymerization during the adsorption process compared to the 1-substituted ones. Therefore, 3-substituted pyrrole alkyl trimethoxysilane was chose as adhesion promoter.

We have discussed that there are several possibilities to synthesize 3-substituted pyrroles. The most effective pathway to 3-substituted pyrroles requires the introduction an electron-withdrawing group or a blocking group on the pyrrole nitrogen, which drives subsequent electrophilic substitution predominantly or exclusively at the 3-position. Here, we chose triisopropylsilyl group as blocking group to introduce substitution at the 3-position.

The preparation of 11-(pyrrol-3-yl) undecyl trimethoxysilane was carried out in four steps (scheme 4.20).

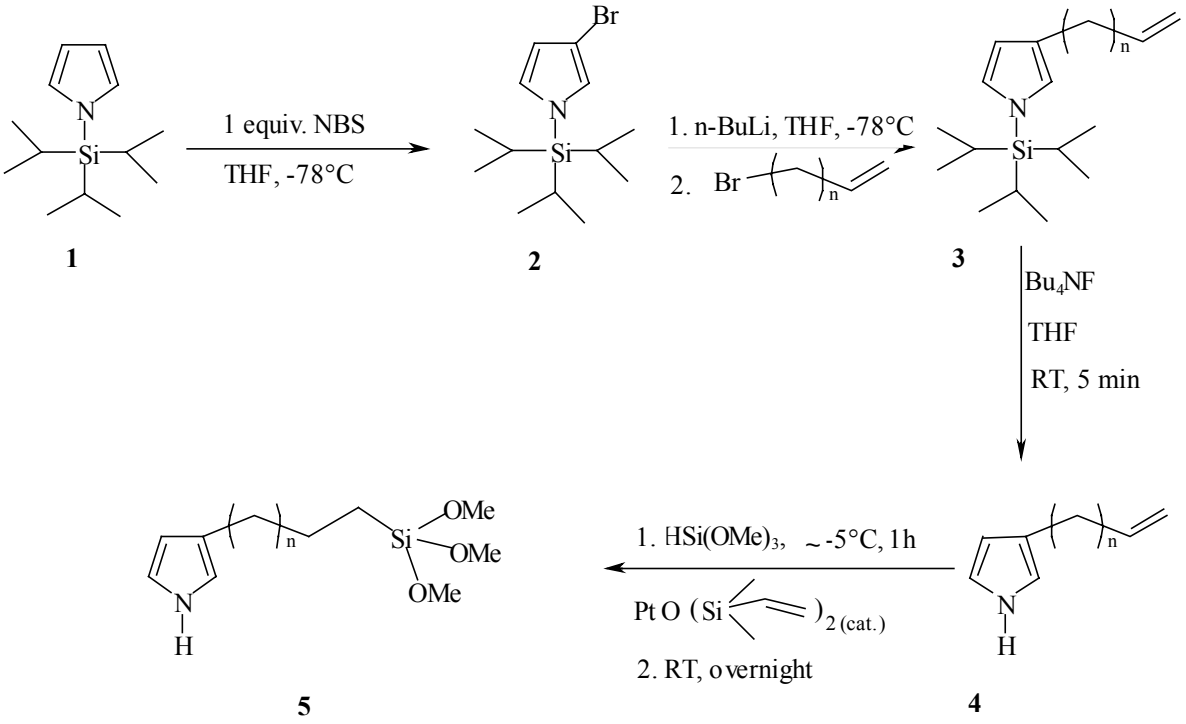

1 **2** **3** **4** **5**

Scheme 4.20 Synthetic procedure for 11-(pyrrol-3-yl) undecyl trimethoxysilane

In the first step, the reaction of 1-triisopropylsilyl pyrrole (TIPS-pyrrole) with 1 equivalent of N-bromosuccinimide (NBS) occurred rapidly at –78°C and gave a mixture of monobrominated pyrroles [208]. Column chromatography allows the isolation of **2** from the reaction mixture. Bray [208] reported that the amount of α-isomer increased with increasing of the reaction temperature. When the reaction temperature was maintained at –78°C the β:α isomer ratio was 25:1, and the main product was 3-bromo-1-TIPS-pyrrole. At room temperature the β:α isomer ratio decreased to 2:1. The ratio of TIPS-pyrrole to NBS also influenced the product. Bromination of TIPS-pyrrole with 1 equiv NBS at –78°C gave a 5.7:1 mixture of β:α isomer ratio. Bromination of TIPS-pyrrole with 2 equiv NBS at –78°C gave a 19:1 mixture of the 3,4-dibromo and 2,3,4-tribromocompounds. 2,3,4, tribromo compound increased with the increasing of NBS. In the second step, the lithiation of **2** was easily accomplished by bromine-lithium exchange with 1 equiv of n-butyllithium in THF at –78°C (15 min), and then a mixture of **3** and TIPS-pyrrole was obtained on reaction of 11-bromo-1-undecene with 3-(lithio-triisopropylsilyl) pyrrole [209]. This mixture was conveniently separated by silica gel chromatography after desilylation. The removal of silyl group was

easily accomplished with tetra-n-butylammonium fluoride to give **4** in good yield. Finally, platin complex catalyzed hydrosilylation of **4** by trimethoxysilane gave the desired compound **5** in good yield. This compound is a colorless liquid, when freshly synthesized, but becomes darker on standing. FTIR spectroscopy (Fig. 4.22) of this compound showed characteristic absorbances for methylene stretching (2929-2855 cm^{-1}), pyrrole C-H stretch (3093 cm^{-1}), N-H band (3300 cm^{-1}), aromatic C-C stretching of the pyrrole (1500 cm^{-1}), and Si-OMe band (1107, 1079 cm^{-1}).

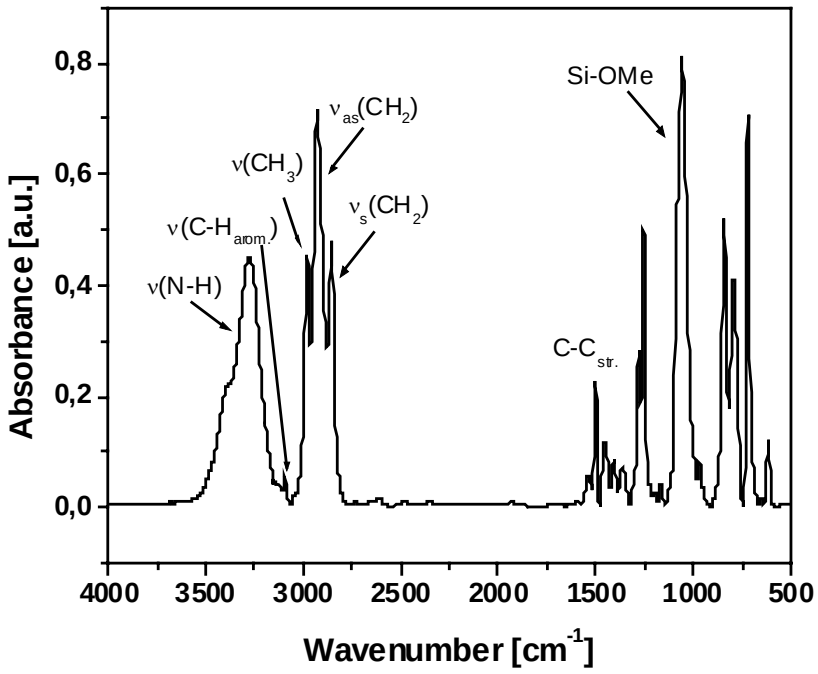

Fig. 4.22 IR spectrum of 3-PyTMS

4.6.1 Synthesis of 3-Bromo-1-(triisopropylsilyl) pyrrole

4.0 g (18 mmol) NBS was added to a stirred solution of 3.2 g (18 mmol) N-(triisopropylsilyl) pyrrole in anhydrous THF (80 ml) at –78°C. The reaction mixture was kept at –78°C for 2 hours and then left to reach room temperature (ca. 1 hour). THF was evaporated and 50 ml hexane was added, the resulting suspension was filtered, and the filtrate was evaporated in vacuum. Column chromatography (eluent: n-pentane) gave a pure compound in 79% yield (4.2 g).

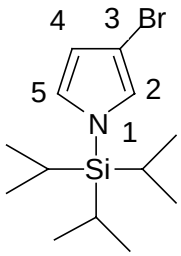

Structure 4.14 Structure of 3-bromo-1-(triisopropylsilyl) pyrrole

^{1}H-NMR (ppm, in $CDCl_3$, 500 MHz): 6.72 [1H, (H5) $J_{4,5}$= 1.41Hz, $J_{2,5}$= 2.25Hz, dd], 6.67 [1H, (H2), dd], 6.28 [1H, (H4), $J_{2,4}$= 1.41Hz, $J_{4,5}$= 2.83, dd], 1.43 [sept. 3H, (CH), J= 7.50Hz], 1.09 [18H, Me, J= 7.50Hz,d].

IR (in chloroform, ν_{max}/cm^{-1}): 2900 (CH_3), 1470 (pyrrole ring), 1200 (Si-C).

Elemental analysis:

$C_{13}H_{24}BrNSi$: Calculated: C, 51.65; H, 8.00; N, 4,63;

Found: C, 51.52; H, 8.17; N, 4.72

4.6.2 Synthesis of 3-(undece-1-ne)-1-triisopropylsilyl pyrrole

A solution of 1.5 M n-butyllithium in hexane (13.2 ml, 20 mmol) was added to a solution of 3-bromo-1-(triisopropylsilyl) pyrrole (6.04 g, 20 mmol) in anhydrous THF (80 ml) at –78°C. After 15 min at –78°C, 11-bromo-1-undecene (9.32 g, 40 mmol) was added and 15 min after the reaction was removed from the cooling bath and left to room temperature. The reaction mixture was quenched with 50 ml water and extracted with diethyl ether (3 x 40 ml). The extract was dried over $MgSO_4$ and evaporated in vacuum. The residue was then purified by column chromatography on silica gel using n-pentane to give 4.9 g of a mixture of desired compound and 1-(triisopropylsily) pyrrole in65% yield.

4.6.3 Synthesis of 3-(undece-1-ne) -1H-pyrrole

Tetra-n-butylammonium fluoride (2.5 g in silica gel, 2.7 mmol) was added to a stirred solution of 3-(undece-1-ne) -1-triisopropylsilyl pyrrole (1.0 g, 2.7 mmol) in 50 ml THF. After 5 min at room temperature, the reaction mixture was filtered, the filtrate was diluted with ether, and the organic phase was washed with water and dried over $MgSO_4$. Removal of the

solvent in vacuum gave a mixture, then column chromatography in eluting (hexane-ethyl acetate: 3:1) gave the pure compound in a yield of 65% (0.3 g).

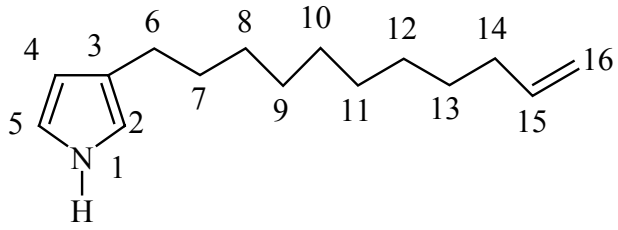

Structure 4.15 Structure of 3-(undece-1-ne) -1H-pyrrole

^{1}H-NMR (ppm, in $CDCl_3$, 500 MHz): δ 8.03 [1H, (H1), br. s], 6.73-6.71 [1H, (H5), J = 2.5Hz, m], 6.58 [1H, (H2), m], 6.11 [1H, (H4), m], 5.89-5.80 [1H, (H15), m], 5.04-4.94 [2H, (H16), m], 2.54-2.50 [2H, (H6), J = 4.9Hz, m], 2.13-2.06 [2H, (H14), m], 1,68-1.62 [m, 2H, (H13), m], 1.49-1.44 [2H, (H7), m], 1,29-1.08 [10H, m].

IR (in chloroform, cm^{-1}): 3390 (N-H), 3077 (arom. C-H), 2926 (ν_{as} CH_2), 2856 (ν_s CH_2), 1640 (C=C), 1463 (pyrrole ring).

4.6.4 Synthesis of 11-(pyrrol-3-yl) undecyl trimethoxysilane (3-PyTMS)

In a round flask were added 0.5 g ω-(pyrrol-3-yl) undecene, 5 ml trimethoxysilane and a catalytic amount of 1,3-divinyl-1,1,3,3,-tetramethylsiloxane platin complex at –5 ~ 0°C. The mixture was stirred at that low temperature for 1 hour. Then the mixture was warmed to room temperature and stirred overnight. The excess of trimethoxysilane was removed to get the desired product.

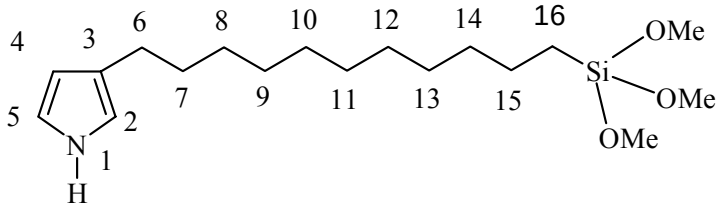

Structure 4.16 Structure of 11-(pyrrol-3-yl) undecyl trimethoxysilane

^{1}H-NMR (ppm, in $CDCl_3$, 500 MHz): δ 8.00[1H, (H1), br s], 6.71-6.70 [1H, (H5), J = 2.5Hz, m], 6.56 [1H, (H2), m], 6.08 [1H, (H4), m], 3.56-3.54 [9H, (OCH_3), s], 2.48-2.45 [2H, (H6), J = 7.7Hz, m], 1.57-1.52 [2H, (H7), m], 1,38-1.08 [18H, m].

^{29}Si-NMR (ppm, in $CDCl_3$, 500 MHz): -40.08

IR (in chloroform, ν_{max}/cm^{-1}): 3396 (N-H), 3090 (arom. C-H), 2925 (ν_{as} CH_2), 2851 (ν_s CH_2), 1462 (pyrrole ring), 1191 (Si-O-CH_3), 880-816 (ν_s Si-O-C)

4.7 Monolayer Formation and Characterization

The pretreatment of oxide substrates and the adsorbed layer formation on the oxide substrates were done as described in chapter 4.3.

The adsorption behavior of 11-(pyrrol-3-yl) undecyl trimethoxysilane (3-PyTMS) on oxide substrates was studied by contact angle measurement, UV-VIS spectroscopy, and XPS.

The static contact angles of 3-PyTMS adsorbed from different solvents are presented in table 4.9. The water contact angle data showed that in apolar hydrocarbon solvents (bicyclohexyl), the adsorbed surfaces have a high hydrophobicity.

Table 4.9 Contact angle data of 3-PyTMS adsorbed from different solvents (48 hours)

Solvents	MeOH	EtOH	bicyclohexyl
Contact angle [°]	78.7 ± 1.48	76.7 ± 2.29	102.7 ± 1.56

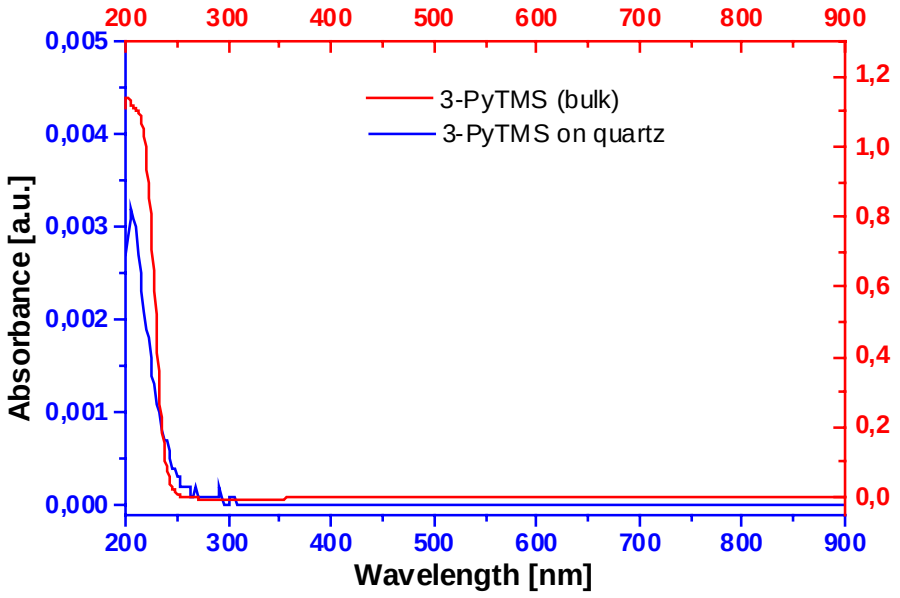

Fig. 4.23 UV-VIS of 3-PyTMS on quartz

UV-VIS spectra of 3-PyTMS adsorbed layers deposited on quartz from bicyclohexyl for 24 hours adsorption time were shown in Fig. 4.23 (axis on left, blue) together with the 3-PyTMS

monomer diluted in ethanol (axis on right, red). Like the free monomers, the 3-PyTMS adsorbed layers showed a strong increase in adsorption below 240 nm, beginning at 250 nm. The absorbance below 240 nm is due to the pyrrole moiety of the 3-PyTMS. The spectra establish that 3-PyTMS was adsorbed on the substrate.

3-PyTMS has two functional groups. Contact angle data, grazing incident FTIR and UV-VIS spectra have confirmed that 3-PyTMS is on the surface. Angle-resolved XPS was measured to study the orientation of the 3-PyTMS on the substrates.

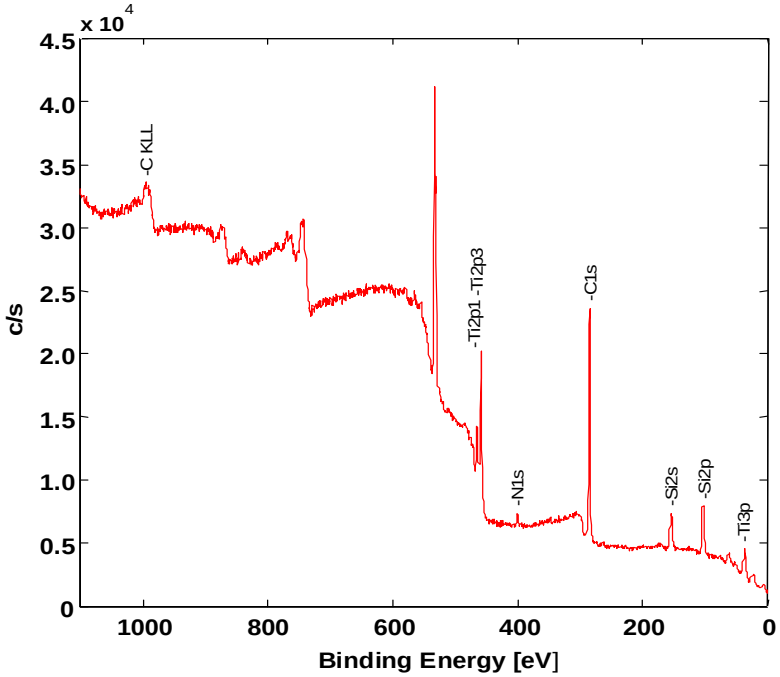

Fig. 4.24 Survey spectrum of 3-PyTMS on Ti

Fig. 4.24 showed the survey spectrum of adsorbed 3-PyTMS on Ti. The peaks of N, C and Si belonging to the adsorbed molecule are clearly visible. The finding of N, C and Si peaks indicated that the adsorption of the molecules took place on the Ti substrate. Fig. 4.25 showed the O1s peak for Ti substrate measured by XPS. The O1s peak for Ti_{pol} substrates was composed of three peaks corresponding to TiO_2 (529.9-530.3 eV), TiOH (531.6-531.8 eV) and adsorbed H_2O (532.5-533.2 eV). The reaction of Ti_{pol} substrates with 3-PyTMS shows a shoulder on the high-energy side of the O1s spectrum. This shoulder has been resolved in Si-O-Si and Si-O-Ti components, resulting from the grafting of silanes on the Ti surface and cross-linking of neighbouring Si-O-H groups. This indicated that the 3-PyTMS really adsorbed on the substrate and Si attached to the surface.

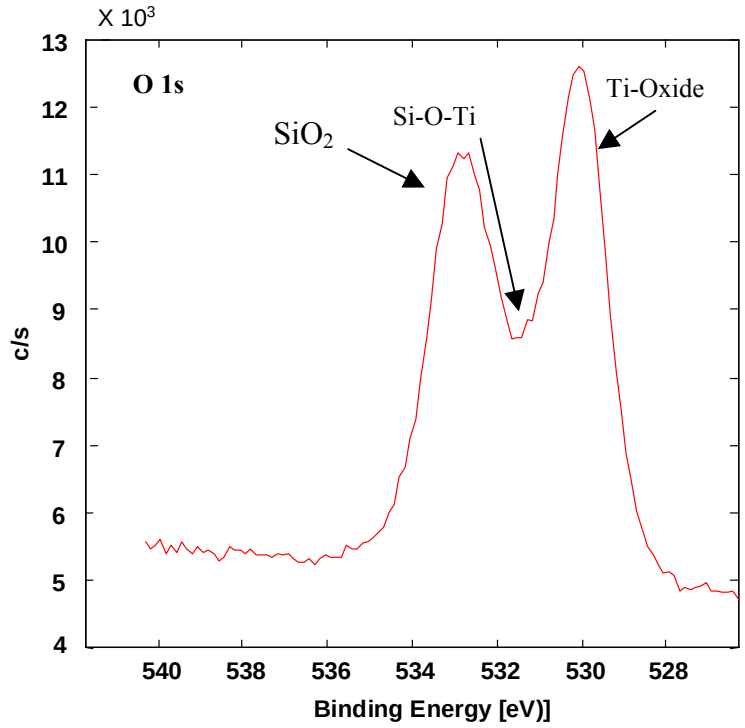

Fig. 4.25 O1s peaks of Ti modified with 3-PyTMS

Table 4.10 Angle dependence of the relative atomic concentration (%) for Ti substrate after modification by 3-PyTMS

Take-off angle [°]	C1s [0.314]	N1s [0.499]	O1s [0.733]	Si2p [0.368]	Ti2p [2.077]	Si/N	C/Si
20	44.6	2.4	36.7	8.1	8.2	3.37	5.5
30	42.5	2.5	38.3	7.5	9.2	3.0	5.7
45	41.8	2.5	38.4	7.0	10.2	2.80	6.0
60	40.0	2.4	39.7	6.9	11.0	2.90	5.8
80	37.5	2.2	40.9	7.1	12.3	3.23	5.3

The derived C/Si and Si/N ratios (table 4.10) for every take-off angle are far from the theoretical values, i.e. 14 and 1, respectively. It showed that at low take-off angle (≤ 45°), Si/N ratio decreases with the increasing of the take–off angle, and at high take-off angle, Si/N ratio increases with the increasing of the take-off angle. These may be due to the presence of defects, e.g. pinholes and collapse sites in the adsorbed layer (see scheme 4.21).

The thickness of the adsorbed layer on Ti was measured by XPS. It was found that the thickness (3.12 nm) was bigger than the size of the calculated 3-PyTMS molecular model (2.26 nm). The same result was found for the adsorbed layer on Si substrate (3.41 ± 0.32 nm) measured by ellipsometry. This confirmed that the adsorbed layer is not a monolayer but a multilayer [160].

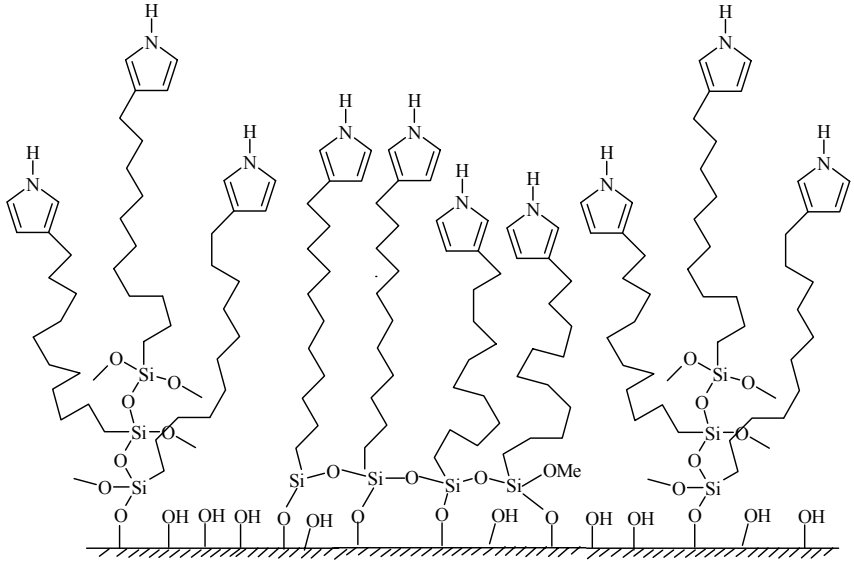

Scheme 4.21 Formation of adsorbed layer of 3-PyTMS

Chapter 5 Grafting Polypyrrole on the Modified Substrates

In this chapter, the synthesis and characterization of soluble polypyrrole derivatives are described. In-situ deposition of conducting polypyrrole thin films on adhesion promoter-modified oxide substrates has been achieved by chemical and electrochemical polymerization. Optimal reaction conditions were investigated. The thickness and morphology of the resulting films were controlled by the preparation conditions, such as choice of solvent, deposition time, pyrrole to oxidant ratio, and monomer concentration.

5.1 Conducting Polymers

5.1.1 Type of Conducting Polymers

The search for conducting polymers began at the end of the 1970s when an increase in conductivity of 12 orders of magnitude was observed in polyacetylene upon charge transfer doping [210]. This was closely followed by the fabrication of a free standing polypyrrole film by the oxidative electropolymerization of pyrrole [211]. Since then, an active interest has been initiated in synthesizing other organic polymers with this property. Electrochemical polymerization has been rapidly extended to other aromatic and heterocyclic compounds such as thiophene [212], furane, indole [213], carbazole, azulene, pyrene [214], and benzene [215]. A slightly different conducting polymer, polyaniline, also received a great deal of attention [216, 217] at the same time. It has become apparent from this large body of work that extensive delocalization of electrons along the polymer backbone is necessary for a polymer to behave as an electrical conductor. This delocalization of electrons may occur through the interaction of π-electrons in a highly conjugated chain or by a similar interaction of π-electrons with non-bonded electrons of heteroatoms such as sulphur and nitrogen in the backbone.

Table 5.1 Conducting polymers and conductivity [218-220].

Polymers	Structure	Conductivity (doping) [S· cm^{-1}]
Polyacetylene	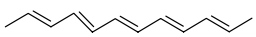	10^3-10^5
Polypyrrole	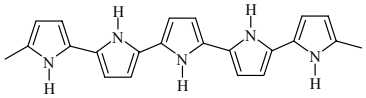	10-10^3
Polythiophene	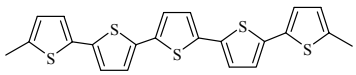	10-10^2
Polyaniline	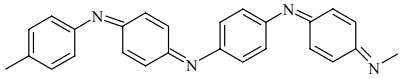	3-10^3
Polyphenylensulfide	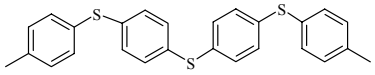	1-10^2

5.1.2 Mechanism of Conductivity

In inorganic semiconductors like silicium or germanium, the strong coupling between the constituting atoms and the long-range order lead to the delocalization of the electronic states and the formation of allowed valence and conduction bands, separated by a forbidden energy gap. By thermal activation or photo excitation, free electrons are generated in the conduction band, leaving positively charged holes in the valence band. The transport of these free charge carriers is desribed by quantum mechanism.

As we know, most polymers are insulator because their electrons are localized, that is, each of the electrons is attached to its own nucleus. In organic solids, intramolecular interactions are mainly covalent, but intermolecular interactions are due to much weaker Van der Waals and London forces. However, the conducting or semiconducting polymers have the conjugated double bonds. The double bond consists of a σ-bond and a π-bond. The electrons in the σ-bonds form the backbone of the chain, dominating the mechanical properties of the polymers. Due to the π-orbital overlap of neighboring molecules of the conjugated structure, the π-electrons delocalize along the entire chain, which provides their semiconduting and conducting properties. The σ-bonds form completely filled, low-lying energy bands have a much larger ionization potential than π-electrons (and a much large bandgap) and thus do not contribute in a major way to the electrical and optical properties. The π-bands, however, form

an energy band in which each carbon atom contributes one electron, and thus the band should be half-filled because of the spin degeneracy. In metals and conventional semiconductors, charge transport occurs in delocalized states. Such a model is no longer valid in low conductivity organic semiconductors, where a simple estimate shows that the mean free path of carriers whould become lower than the mean atomic distance. In these materials, the π-electrons are delocalized within a molecule and the carrier transport occurs through hopping of charges from one molecule to another.

Since the π-conjugated system in conducting polymers extends over the whole polymer chain, the conducting polymers can be regarded as one-dimensional polymer semiconductors. In these materials, in addition to direct electron and hole excitions across the semiconductor band gap, the one-dimensional system may support a host of exotic carrier types like solitons (topological defects without charge, with spin ½), polarons (electrons and holes, self-trapped by carrier-lattice interactions) soliton-polarons (charged topological defects without spin, self-trapped by carrier-lattice interactions), bipolarons (two carriers with charge of the same sign, bound by lattice distortion), and polaron-excitons (two carriers with charge of opposite sign, bound by lattice distortion) [221].

5.2 Polypyrrole

Pyrrole was known to form a conductive „pyrrole black“ [222] via spontaneous polymerization, and its history can be dated back in 1916 [223]. In 1968 [224], it was noted that pyrrole could be electrochemically polymerized using a variety of oxidation agents to give a black conducting powder. It can be synthesized both aqueous and non-aqueous solution during electrochemical polymerization. Polypyrrole has a relatively high conductivity and environmental stability in the conducting state. It is stable in a wild range of potential range, during thousands of charge-discharge cycles, and under properly selected conditions its response is fast. In contrast to polyaniline it can operate both in acidic and neutral solutions, which makes the polypyrrole electrode attractive for use as sensors material in the bioelectroanalytical chemistry. Polypyrrole is a relatively air stable organic conducting polymer, which suffers from poor processability. The use of new tailor made reactive statistical copolymers for the synthesis of sterically stabilized polypyrrole colloids is decribed [225]. Moreover, compared to other heterocycles its oxidation potential is low (table. 5.2). For all of these reasons polypyrrole has been an interesting material to study.

Pyrrole belongs to the well-known aromatic heterocyclic ring monomers. Its real structure is not well known, mainly due to its great complexity. Polypyrrole's macromolecular structure is generally known to consist of α-α' linkages, consecutively rotated 180°, and which are believed to create a one-dimensional polymer structure, though there are probably a number of α-β' linkages, which lead to a two-dimensional polymer structure [226](Fig. 5.1).

a

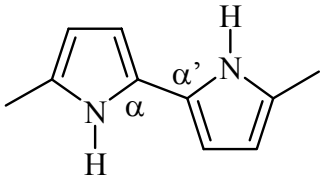

b

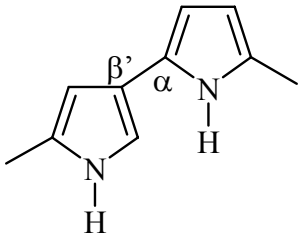

Fig. 5.1 Proposed chemical structures for the growth of polypyrrole. (a. α-α' linkages; b. α-β' linkages)

In an undoped state, polypyrrole is generally considered to have a so-called benzoid structure and is usually called the neutral state of polypyrrole. Usually conducting polymers in the neutral structure has low (in high crystallinity, 10^{-9}-10^{-6} S cm^{-1}) or no conductivity. Photo-exitation or thermal-excitation can only increase very less charge carriers. Removal or addition of electrons from the chain of the polymers to increase the charge carrier can be done by „doping". This „doping" is really a redox process slightly different from doping in conventional semiconductors which accomplished through the introduction of impurities. That means „p-doping" or oxidation with an anion accepting the removed electrons from the conducting polymer chain, and „n-doping" with reduction or donation of electrons to the conducting polymer chain. The redox process can be done by chemical electron donators or acceptors, or electrochemical processess.

As doping of the neutral polymer proceeds, the formation of structural and electronic defects will take place. At low concentrations, the first predominant kind of defect will be polarons, which give rise to the formation of two localized states within the bandgap, one split off from the top of the valence band (the HOMO level is pushed up in energy), and the other split from the bottom of the conduction band (the LUMO level is pushed down in energy). Further charge transfer from the polymer chain (i.e., higher doping levels) may then proceed either by formation of another polaron or by removal of the single electron in the lower polaron level. In most cases it is found to be favorable to form a doubly charged species-bipolarons.

Figure 5.2 shows the neutral, the polaron and bipolaron structures of polypyrrole, with the corresponding schematic band structures as well as the possible electric transition for each of them.

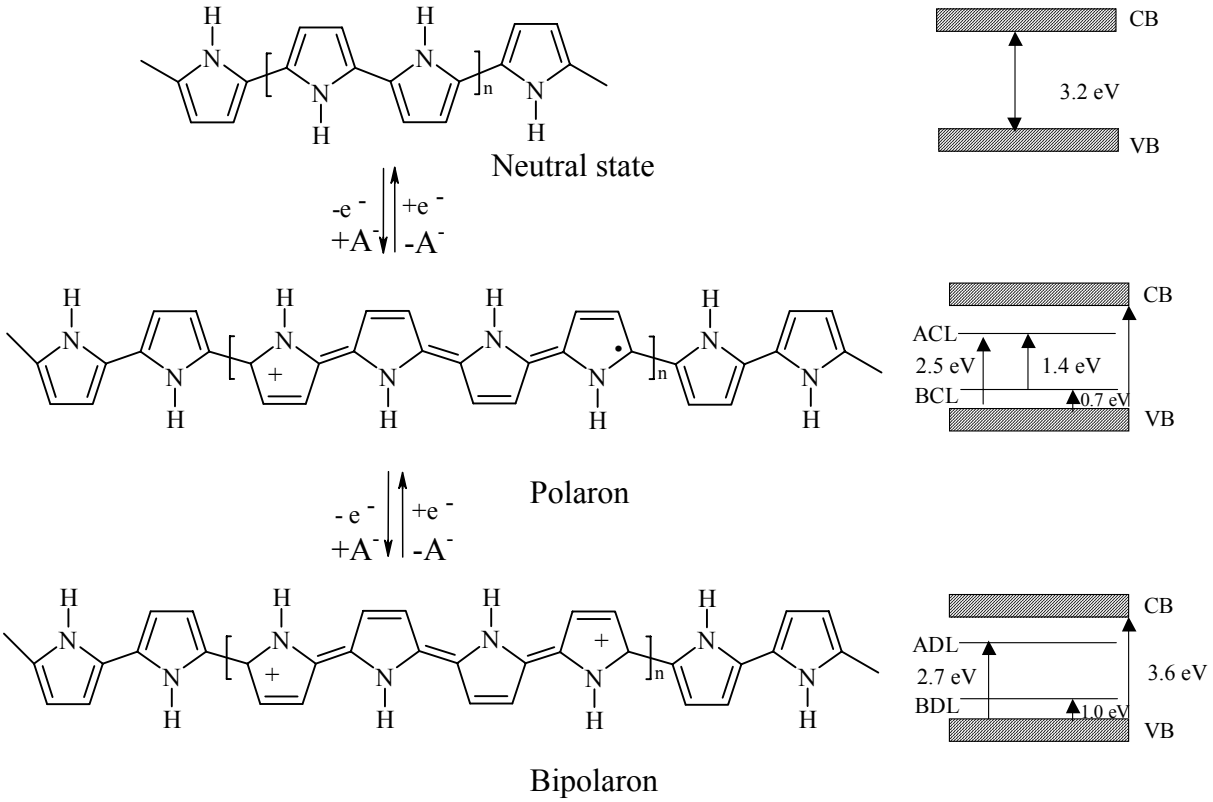

Fig. 5.2 Neutral state, polaron and bipolaron structures for lightly and heavily doped PPy, respectively, with their corresponding schematic band structures and the allowed electronic transitions

For polypyrrole, positively charged polarons and bipolarons have already been illustrated. Negatively charged polarons and bipolarons but in practice they do not exist, as polypyrrole cannot be n-doped stable. In an actual conducting polymer structure, the entire CP chain would first have to become nearly saturated with polarons before bipolaron formation commence. This is also supported by spectroelectrochemical studies, at low doping levels, spectra corresponding to polarons are first seen, before bipolaron spectra occur. In UV-VIS-NIR spectrum of polypyrrole, the single prominent valence-conduction (π-π^*) band transition in the pristine polymer (at ca. 388 nm) is accompanied by three additional polaron based transitions at low doping level (ca. 590 nm, 885 nm, 1771 nm), which finally evolve into two biparon based bands (ca. 459 nm, 1240 nm) at higher doping level.

In bipolaron structure, the two charges are not isolated on specific monomer units, but rather, are delocalized over several (generally 6 to 8) monomer units, but not the entire CP lattice.

Therefore, at high dopant concentrations the bipolarons, which are spinless, can become mobile under the application of an electrical field, thus giving rise to the high conductivity observed in conducting polymers. The gap between two bipolaron bands never goes to zero, thus polypyrrole cannot really reach the metallic state [227].

5.2.1 Synthesis of Polypyrrole

Polypyrrole can be prepared in various forms, depending on the method used and on the preparation conditions. A general difficulty of the reproducible polypyrrole preparation arises from its complexity. The structure and hence the properties of the resulting polypyrrole are strongly influenced by a number of variable (e.g., the oxidation potential, the monomer concentration, the preparation temperature) that are not perfectly controlled. Therefore, the results on polypyrrole vary widely. Two basic methods are used for the preparation of polypyrrole: chemical and electrochemical synthesis [228, 229]. The chemical synthesis of polypyrrole produces easily arbitrary amounts of polypyrrole in various forms, but its producibility is poor. The electrochemical synthesis of polypyrrole can be conveniently carried out. An advantage of the electrochemical methods is that the preparation process can be simply controlled through the current or the applied potential and the charge consumed. A disadvantage is that polypyrrole can be prepared only in the form of a relatively thin film deposited on the surface of a conducting material.

5.2.1.1 Chemical Polymerization of Polypyrrole

The chemical synthesis of polypyrrole is based on the chemical oxidation of the pyrrole monomer. Oxidation can take place in a gas phase (oxidation by I_2 vapor) or in an aqueous or nonaqueous solution, generally with oxidants involving $(NH_4)_2S_2O_8$, H_2O_2, and many kinds of salts containing transition metal ions (e.g. Fe^{3+}).

The mechanism consists, as a first step, of the oxidation of the monomer to form a radical cation. After the initial oxidation step, there is a coupling reaction, followed by a deprotonation and a one-electron oxidation in order to regenerate the aromatic system. From a mechanistic point of view, there are two unique stages to the coupling reaction (Fig. 5.3). There is the initial coupling reaction, which involve the coupling of pyrrole monomers to produce the dimeric intermediates, and there is the steady-state coupling reaction, which involves the reaction between the pyrrole monomer and the oligomeric and polymeric

intermediates. Considering the coupling reaction in the initial stages of the reaction, the originally formed radical cation could undergo a radical coupling reaction with another radical to form a dimer, or it could react like an electrophile and add to a neutral monomer. Chandrasekhar [230] reports that in a typical chemical polymerization, after initial radical ion generation, rather than a radical-radical coupling as in the generic electrochemical mechanism above, coupling occurs between radical and monomer. This is due to the fact that in the bulk of the reaction environment, where the radical initiators are generated, the concentration of the monomer is in excess, thus radical-monomer combination (generating another radical) is more likely to be the next propagation step after radical generation [230].

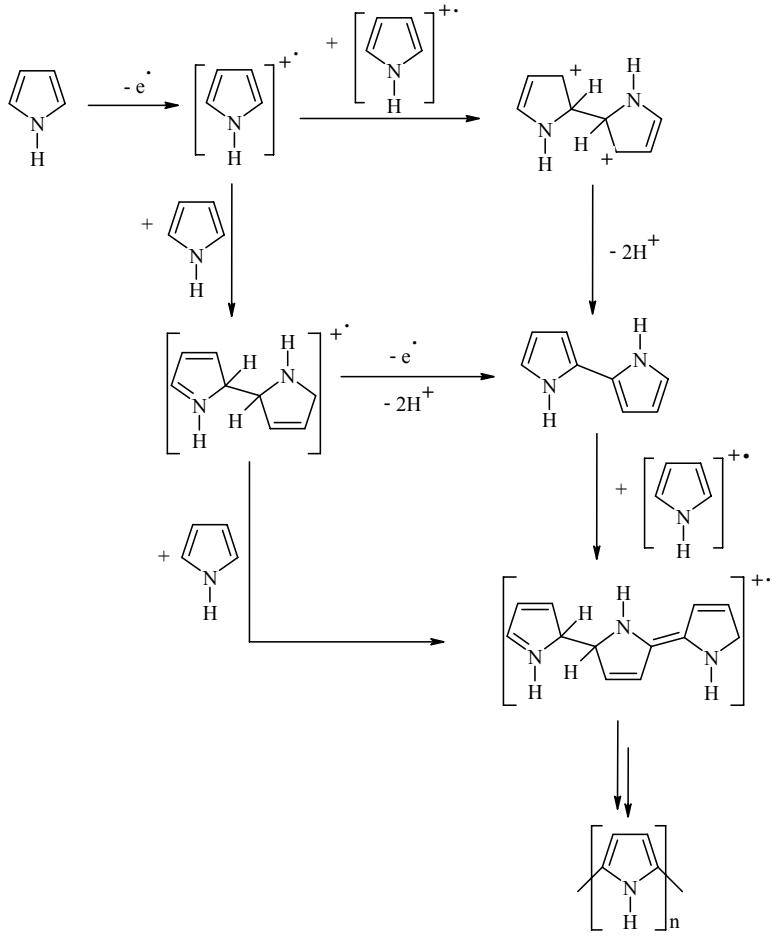

Fig. 5.3 Mechanism of chemical polymerization of polypyrrole [230]

For chemical polymerization, the effect of solvent and of the redox potential of the polymerizaton medium on polymer quality and morphology can be very strong. For example, Miyata and coworkers investigated typical chemical synthesis of polypyrrole using anhydrous $FeCl_3$ as oxidant/dopant in various solvents. They found that while methanol appeared to be the best solvent for optimal conductivity and morphology, the equilibrium redox potential of

the solution, controllable via the relative concentrations of the monomer and oxidant and via addition of $FeCl_3$, was a more important determinant of polymer quality. The polymer produced in this way also showed a more ordered, fibrillar morphology, and stretched films [231, 232].

For polypyrrole, control of morphology, conductivity, doping, and related factors is a little more difficult in chemical polymerizations. Because slight changes in temperature, concentration and other factors will yield substantial differences in polymer properties, and even identical synthetic procedures never yielding exactly the same polymer each time.

Chemical polymerization is a better method for the preparation of a large quantity of polypyrrole because it is free from the restriction of the electrode shape. Except for large amounts of powdery polypyrrole, the deposition of conducting polypyrrole films on conducting, and non-conducting materials, and porous glass is possible by this method. The anions present in the solution are simultaneously incorporated as the polypyrrole dopant during the chemical synthesis.

5.2.1.2 Electrochemical Polymerization of Polypyrrole

Many mechanisms for the electropolymerization of pyrrole have been made, but the most widely accepted one is that of Diaz et al. [233]. The electrochemical synthesis of polypyrrole is based on the anodic oxidation of the pyrrole monomer on the working electrode. During the polymerization, the resulting polymeric film is simultaneously oxidized and doped with the anions present in the background electrolyte. The electropolymerization can take place in either aqueous or non-aqueous solutions.

Like chemical polymerization, the initial step is the generation of the radical cation, but in the next step, the mechanism of the electrochemical polymerization is different from the chemical polymerization, according to most studies [211, 234-236]. The general mechanism consists as a first step of the oxidation of the monomer to form a radical cation. The second step involves monomer dimerization by radical-radical coupling, in which two protons are eliminated from the doubly charged dihydromer and a neutral species is formed. As the dimer is more easily oxidized than the monomer because of the increased stability of the formed radical cation, it is reoxidized to the cation and undergoes a further coupling with the monomeric radical cation. Fig 5.4 gives the pathway of electrochemical polymerization of pyrrole [230]. This pathway shows the following common features:

1. The initiation step is pyrrole radical generation via electrochemical oxidation;
2. Prapagation is via a). radical-radical coupling; b). elimination two protons from the radical-radical intermediate species, then generating the dimer; c). electrochemical oxidation of the dimer, generating another oligomeric radical; d). combination of this or similar oligomeric radicals with monomer radicals and repeat of steps 2b and 2c, polymer was built up;
3. Termination is via exhaustion of reactive radical species in the working electrode and accompany oxidative or other chain termination processes.

Initiation:

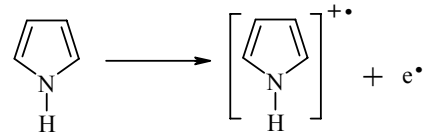

Prepagation:

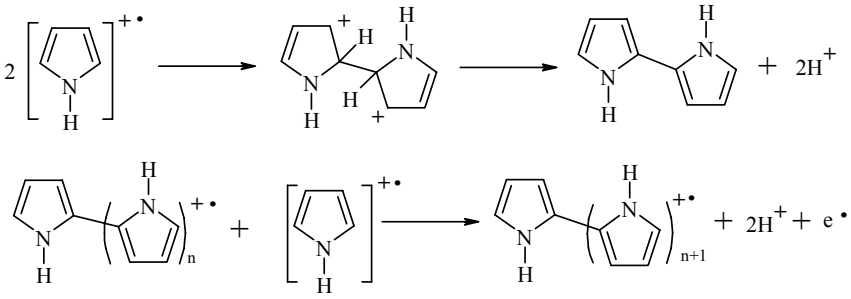

Termination:

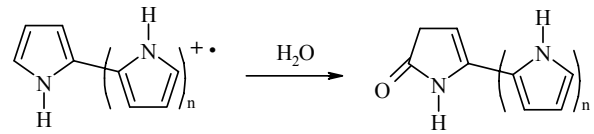

Fig. 5.4 Mechanism of electrochemical polymerization [Lit. 230]

The termination step in polymerization is not clear and different hypothesis have been proposed. Most researches believe that the reaction with water could be one of the reactions that quenches the polymerization.

The final polymer chain bears a charge of unity for every three or four pyrrole rings; this charge is counterbanced by the anion of the electrolyte salt. The elimination of the α protons indicated by this mechanism is consistent with the decrease in the pH value of the electrolyte solution during film growth.

There are a huge number of publications dealing with parameters influencing the final properties of polypyrrole samples during electrochemical polymerization. Only several important parameters are briefly discussed.

The solvent of electropolymerization is an important factor, which influence not only the quality of the polymer film obtained but also its conductivity, morphology, and subsequent electrochemical and chemical behavior. The nucleophilicity of the solvent is important for the electropolymerizaiton since the nucleophilic solvent is likely to attack the free radical intermediates. If the nucleophilic character of the solvent is enhanced, film formation is minimized. Films are not produced in the nucleophilic aprotic solvents such as DMF, DMSO unless the nucleophilicity of the solution is reduced by the addition of the protic acid [237]. Acetonitrile is one of the most useful polymerization solvents due to good nucleophilicity, facilitating proton removal in the polymerization, poorer solubility or insolubility of polymer as well as of oligomers, relative dryness, with sufficient water content for effective polymerization without early termination. Table 5.2 showed some solvents and electrolytes used for polypyrrole polymerization.

Table 5.2 Solvents and electrolytes used for polypyrrole polymerization [230].

Solvent/electrolyte	Polymerization
Acetonitrile/tetraethylammonium tetrafluoroborate	good
Acetonitrile/toluenesulfonic acid	good
Acetonitrile/tetraethylammonium tetrafluoroborate plus 1.0 M pyridine	none
Acetonitrile/lithium perchlorate	good
Methylene chloride/ tetrabutylammonium tetrafluorobonate	good
Butanone/tetrabutylammonium tetrafluorobarate	good
Propylene carbonate/tetrabutylammonium tetrafluoroborate	good
Dimethylformamide/tetrabutylammonium tetrafluorobonate	none
Dimethylformamide/toluenesulfonic acid	good

With regard to the electrolyte salt, the main considerations of the solvent are the solubility, degree of dissociation, and the nucleophilicity. For this reason most of the salts are tetra-alkyl ammonium salts since they are soluble in aprotic solvents. Good films are typically not produced when the anion is halide because halides are fairly nucleophilic and easy to oxidize. The highly nucleophilic anions such as OH^-, CN^-, CH_3COO^-, $C_6H_5COO^-$ do not produce good quality films either and instead produce soluble products, which colour the reaction solution.

The nature of the working electrode also plays an important role in the synthesis of polypyrrole. It is important that the working electrode does not oxide with the monomer. For this reason, polypyrrole was synthesized using an inert platinum or gold electrode. Polypyrrole has been synthesized on various substrates for specific applications. Pt wire is preferred for purely electrochemical characterization. For preparation of free standing films, graphite, special materials (e.g. basal-plane or pyrolytic graphite, or glaassy carbon) may be preferred. Iron [238, 239], stainless steel [240], and aluminum [241] electrodes have been used for corrosion studies, and n-Si is also successful for semiconductor application [242].

5.2.1.3 Factors Influencing Polymerization Reaction

No matter chemical or electropolymerization, the mechanism of polymerization of pyrrole is first the formation of the radical cation. While an organic monomer can undergo electropolymerizaiton or not, the keys lie in a combination of factors of stability of the radical cations generated in the first step and the oxidation potentials for generation of these. In nearly all cases, where successful electropolymerization is observed, the radical cation are found to be highly stabilized via mechanisms such as charge delocalization, and the electrochemical oxidation was reasonably facile. Because of the low oxidation potential it is possible to produce their radical cations more easily by oxidation. For example, carbazole, furane and indole produce poorly formed polymers with low conductivity on electropolymerization compared with polypyrrole due to all molecules whose radical cations are less well-stabilized than that of pyrrole [243]; and the oxidation potentials of indole and furan are all high comparable to that of pyrrole (in acetonitrile 0.9 V (indole), 1.85 V (furan), 0.8 V (pyrrole) vs. SCE) [244, 245]. Table 5.3 briefly summaries the oxidation potential of pyrrole and substituted pyrrole.

Table 5.3 Structures and oxidation potentials (Ep. Vs. $Ag/AgNO_3$) of substituted pyrrole [246]

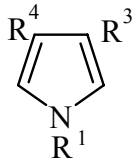

Monmers			Ep, V
R^1	R^3	R^4	
H	H	H	0.92 (0.80, E vs SCE) [230]
H	Me	H	0.78
H	Me	CO_2H	1.06
H	Me	CO_2Et	1.02
H	Me	CO_2Bz	1.02
Me	H	H	0.80 (E vs SCE)[230]

5.2.2 Substituted Pyrroles

Polypyrrole synthesized by conventional chemical and electrochemical methods is insoluble in common organic solvents. Its poor processibility has been explained by the presence of strong interchain interactions. For many years, much research has been focused on improving the processibility of the polymer in organic solvents. One useful method is using substituted pyrrole as monomers.

In pyrrole the electrophilic substitution occurs at 2-position under ambient conditions. Substitution at the 3-or 4- positions requires the use of a N-protected pyrrole derivatives like N-phenylsulfonyl pyrrole, and substitution at N-position needs the synthesis of alkali salt of pyrrole. In general, the percentage of alkylation at the N-atom increases with the solvating power of the medium and decreases with the coordinating ability of the metal ions.

A number of N- or 3-substituted pyrroles have beeen prepared [247-249]. Such substituted polypyrrole really increased its solubility in certain types of organic solvents [250, 251]. But

long alkyl substitution in N-position decrease the electrical conductivity presumably due to steric effects distorting the conjugated π system from coplanarity and/or reduction in interchain conductivity [252]. Several methods were used to improve the conductivity. By preparing copolymer films or controlling nucleation process, films of intermediate conductivity can be obtained. Pyrroles substituted in the 3- or 4-positions are usually preferred. When the substituents are not electron-withdrawing and /or too bulky, these monomers are easily oxidized and yield polymers with good conductivity [253].

Some functional groups will have dramatic effect on the polymerization process since they will provide self-doping eliminating or minimising the need for a supporting electrolyte [254, 255]. For example, monomers (I) and (II) shown below with $–SO_3H$ and –COOH groups provide the charge required to dope the polymer during oxidation and polymerization.

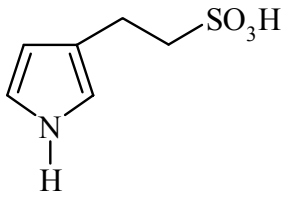

(I)

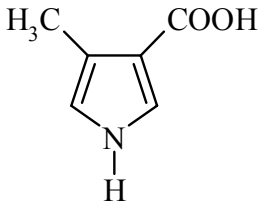

(II)

The electronic nature and bulkiness of the substituent governs the oxidation potential of the substituted pyrroles. As the bulkiness increases the oxidation potential also increases [256].

5.2.3 Properties of Polypyrrole

5.2.3.1 Transport Mechanism of Conducting Polymers

In conducting polymers upon the introduction of an electron or hole, a defect in the polymer chain has been created (i.e., polaron and bipolaron) as already mentioned. These charged defects are the real charge carriers in non-degenerated conducting polymers. Charge transport in conducting polymers consists generally of two components: intrachain and interchain transport. Intrachain charge transport occurs along the polymer backbone and requires less energy than interchain charge transport, which involves the hopping of the charge to neighboring chains. The dopant compounds play a very importment role in the hopping process during interchain charge transport. Since 1990, there are several models being developed to rationalize the hopping transport [230].

The conductivity σ of a conducting polymer is related to the mobility of charge carriers μ. σ can be described as follows

$$\sigma = n \cdot e \cdot \mu \qquad \text{Eq. 5.1}$$

where e is the electronic charge and n the number of charge carriers per unit volume.

The carrier mobility μ in the semiconducting polymer can be estimated by considering that the transition probability of the hopping process is related to diffusicity D, which in turn is related to the mobility through the Einstein‘ relation. One gets the following expression for the mobility [227]:

$$\mu = \frac{eR^2_{hop}}{kT} \nu_{ph} \exp\left[-2\alpha R_{hop} - \frac{W_{hop}}{kT}\right] \qquad \text{Eq. 5.2}$$

where R_{hop} is the average hopping distance, ν_{ph} is the hopping frequency (i.e., an optical photon frequency, ~ 3.61 x $10^{13} s^{-1}$) and W_{hop} is the activation energy. The expression exp ($2\alpha R_{hop}$) describe the overlap of the wave function between adjacent hopping states. With Eq. 5.2 it is possible to evaluate the mobility of the semiconducting polymer in the whole temperature range.

Table. 5.4 Conductivity of various derivatives of polypyrrole [258]

Polymer	Conductivity S cm^{-1}
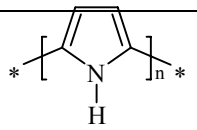	40
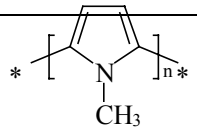	10^{-3}
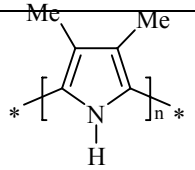	10
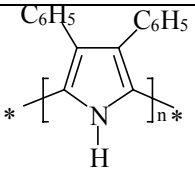	10^{-3}

The concentration of charge carriers in conjugated polymers may be altered by changing the extent of doping; e.g., electrochemically reduced PPy contains only a few charge carriers and is practically insulating. The carrier mobility may be thought of as a measure of the ease with which the charge carriers move through the material, and it is sensitive to the level of structural order present in the polymer. Thus, structural defects decrease the conductivity by lowering the mobility.

An additional functional groups introduced to the monomer influences the electrical properties of the resultant polymer. With increasing side chain length, μ clearly decreases: the more packing required for the longer chain would hinder hopping between chains for conduction [257].

5.2.3.2 Switching Properties

Charge can be reversibly inserted or removed from a conducting polymer by cycling the material from the oxidized to the reduced state, accompanied by a decrease in the conductivity. The process is usually described rather simplistically as indicated in equation 5.3:

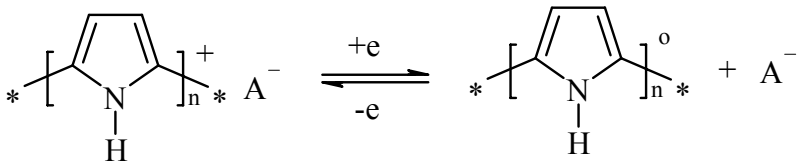

Eq. 5.3

The switch involves the mass and charge transfer in the film and charge transfer at the point of electrical contact (usually as inert electrode substrate). Recently, it was observed that the conductance of the polymer films reasonably changes in time after polymerization [259]. If the potential applied is too positive, over oxidation of the polymer occurs [260] and this polymeric material has inferior electrical properties. If the potential applied is too negative, hydrogen evolution and subsequent deterioration of the polymer occur.

5.2.4 Factors Influencing Electrical Behavior

The morphology and thickness of the polypyrrole films can strongly influence the electrical behavior [261]. It has been found that the thickness increases (above 300nm), the charge

transport tends to be space charge limited. But for very thinner films, the charge transport is limited by thermoionic emission. Thinner films can sometimes give inadequate response or wrong results, and thicker films frequently start showing much slower switching, unwanted diffusion effects [230]. Yuan et al [262] investigated the morphology of electrochemicallly deposited PPy films, demonstrating that the PPy films can form well-ordered neutral networks under some determined electropolymerization conductions. The improvement in structural order affords an increase in the charge carrier mobility. Schmeißer et.al [263] concluded that, when a polymerization current density above 3 $mA.cm^{-2}$ is used, the PPy film chains present 2-D sructures similar to the neutral networks observed by Yuan et al. These 2-D structures would facilitate the grain formation commonly observed in PPy films, being the carrier conduction made by interganular tunneling or by intergranular hopping at high temperature. For smoother PPy films, the average grain size is smaller and the grains are closer to each other, the energy barrier between them decrease improveing intergrain conduction.

5.3 Chemical Polymerization of 3-Substituted Pyrrole Derivatives

The use of conducting polymers as materials for chemical and gas sensors has been widely reported in the literature. In pratical, humidity and gas sensors using polypyrrole (PPy) as a sensing material have been described. However, polypyrrole synthesized by chemical and electrochemical methods is insoluble in common organic solvents. For increaseing the solubility of polypyrrole, polymerization of 3-substituted pyrrole monomers was involved.

5.3.1 Chemical Polymerization of 3-Substituted Polypyrrole

5.3.1.1 Common Procedure of Chemical Polymerization of 3-substituted Polypyrroles

A solution of NaS_2O_8 (0.5 mmol) in H_2O (4 ml) was added dropwise to a solution of the monomer ω-(pyrrol-3-yl alkyl) phosphonic acid (1.0 mmol) in methanol (20 ml) (or mixture of ω-(pyrrol-3-yl alkyl) phosphonic acid and pyrrole), and the resulting mixture was stirred at room temperature for 24 hours under argon. After 24h, the solvent was removed by rotary evaporation. The residue was added to methanol and the precipitated polymer was collected by filtration. The oxidant was removed by soxhlet extraction using water as solvent and the polymers were dried for analysis. The soluble polymer dissolved in methanol was collected and was removed the solvent by evaporation. The residue was dissolved in methanol again

and filtered. This process was done several times till NaS_2O_8 cannot be seen on filter paper. The obtained black powder (homopolymers or copolymers) was dried and then characterized by thermal studies. The molecular weight of the soluble poly (3-substituted pyrrrole) was analysized using MALDI-TOF-MS. The molecular weight of copolymer (coPYPA4/Py 1:3) was about 1540 g/mol.

5.3.1.2 Chemical Polymerization of Polypyrrole

1.0g pyrrole was taken in a single-necked round bottom flask provided with a magnetic stirrer. 20 ml of 2.0 M solution of $FeCl_3$ in water was added to the flask and the contents were stirred at room temperature. After 18h, $FeCl_3$ was removed by Soxhlet extraction using methanol as solvent. A black powder was obtained, which was dried and characterized by thermal studies.

5.3.2 Characterization of Polypyrrole Derivatives

The synthesized monomers were checked for their ability to polymerize. Homopolymerization of ω-(pyrrol-3-yl alkyl) phosphonic acids was carried out by chemical polymerization. $Na_2S_2O_8$ was used as oxidizing agent in methanol and in every case blackish powders could be obtained. The copolymerization of pyrrole and 3-substituted pyrrole alkyl phosphonic acids in different ratio with pyrrole were attempted. IR spectrum of homopolymers and copolymers were investigated (see Fig.5.5).

In the IR spectra, the N-H, C-H and CH_2 stretches between 3500 cm^{-1}and2850 cm^{-1}, usually not present in PPy, are clearly visible in the homopolymer and copolymer spectra. Especially, prominent features of these spectra are the presence of symmetric and asymmetric CH_2 stretching vibration at 2848 and 2919 cm^{-1}, revealing the presence of alkyl groups in the homopolymer and copolymer. The part of spectra of homopolymer and copolymer below 2000cm^{-1} are quite similar. The band at 1730cm^{-1} wavenumbers indicates that some of the pyrrole moieties were oxidized. Usually highly oxidized material shows a strong IR absorption at 4000-1600cm^{-1}; the broad featureless band has been attributed to a free charge carrier absorption. But from IR spectra, we can see that in the material synthesized as described here, the peak is not so broad indicated that the materials are low oxidized. And from IR spectra, we are not sure that the copolymers are real copolymers or a mixture of two homopolymers. It will be confirmed from thermo- analysis (see Fig. 5.7).

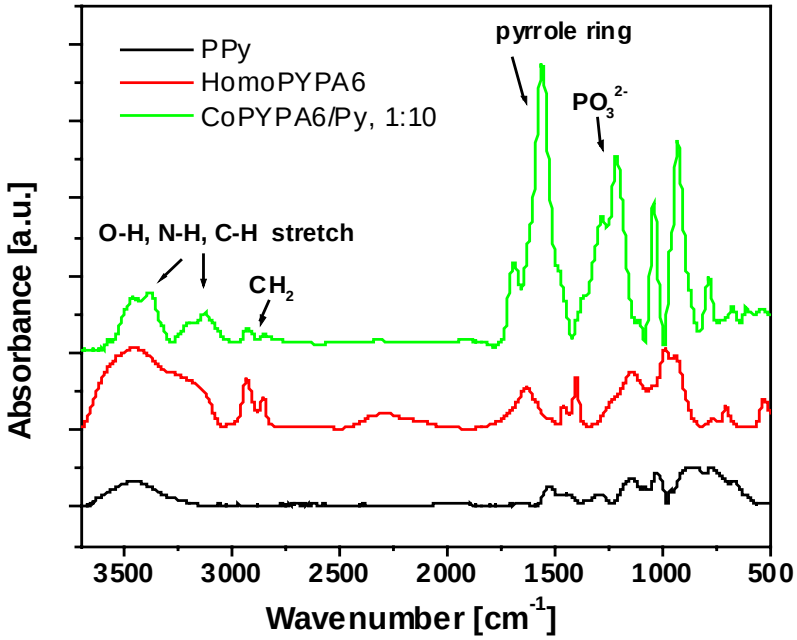

Fig. 5.5 IR spectrum of homopolymers and copolymers

Figure 5.6 showed the UV spectra of synthesized polymers. These synthesized polymers had nearly similar UV-VIS spectra with an absorption band at 235 nm. From these data it appears that the alkyl chain length does not affect the UV-VIS spectra of the 3-substituted polypyrroles. UV spectra showed a broad absorbance in the range of 200~800nm with a peak at about 500nm-550nm and a plateau at and beyond 800nm. An additional peak at 235nm might be attributed to unreacted monomers that are left in the product, whereas the optical spectra of the obtained material clearly indicate that polymer is formed. The absorption at about 350-390nm with a shoulder is indicative of a HOMO-LUMO "band" gap. They also show that the material is not highly oxidized because the absorption between 460-590nm is attributed to polaron/bipolaron based transitions at low a doping level. These results are in agreement with the IR spectra. When the polymer formed was kept in air for several hours, a decrease of the polymer yield and smaller molecular weights were measured [264]. This also agrees with the behavior of polypyrroles synthesized by conventional means, where only highly oxidized material is stable under ambient conditions.

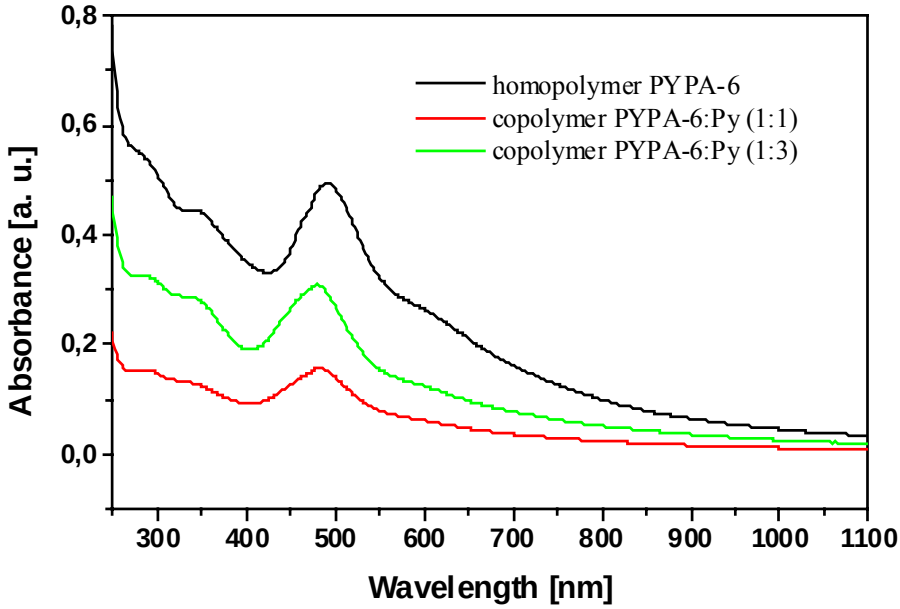

Fig. 5.6 UV-VIS spectra of homopolymers and copolymers

The thermal stability of homopolymers and copolymers obtained by chemical polymerization were assessed using thermogravimetric analysis from room temperature to 800°C under nitrogen (Fig. 5.7a,b).

The thermograms have roughly similar shapes at high temperature for homopolymers of PYPA-6, PYPA-8 and PYPA-11, showing a plateau value of weight fraction vs. temperature (Fig. 5.7a). Homopolymers of PYPA-6, PYPA-8 and PYPA-11 were all decomposed about 450°C compared to polypyrrole. The TGA indicated that the stability of 3-substituted homopoly (pyrrole)s was generally lower than that of polypyrrole and correlation of the stability of 3-alkyl derivatives polypyrrole with the chain length. The lower stability with increased chain length is due to the relative lack of cross-linking in the substituted polypyrrole when compared to polypyrrole. The same result was reported that the dodecyl and hexyl derivatives homopolypyrrole exhibited lower stability than polypyrrole [265].

The shapes of TGA curves for different copolymers changed with the content of pyrrole and the TGA curves of the copolymers with a higher content of pyrrole have the similar shape (except 1:1 ratio copolymer) like PPy indicating that the copolymers are real copolymers. Each sample was stable to temperature below 300°C (Fig. 5.7b)

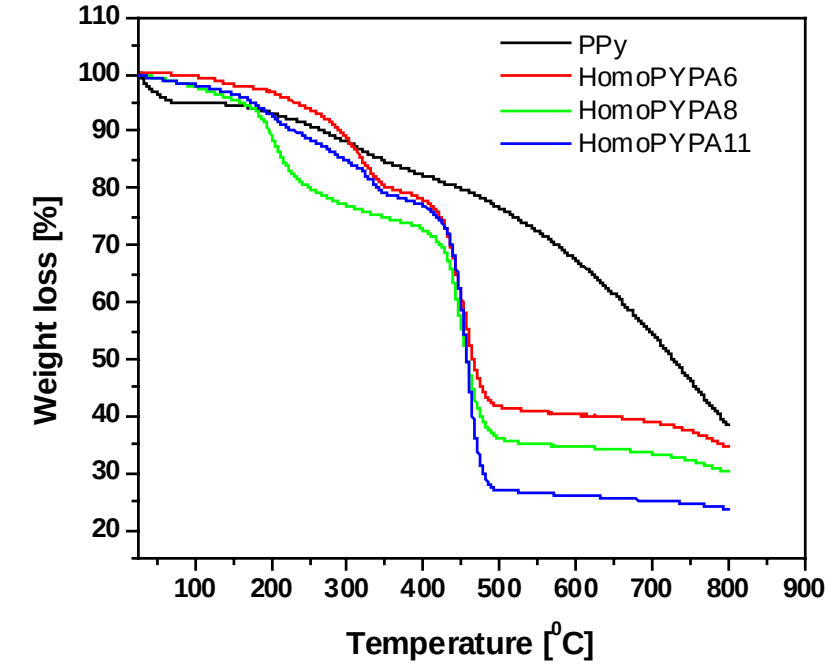

a

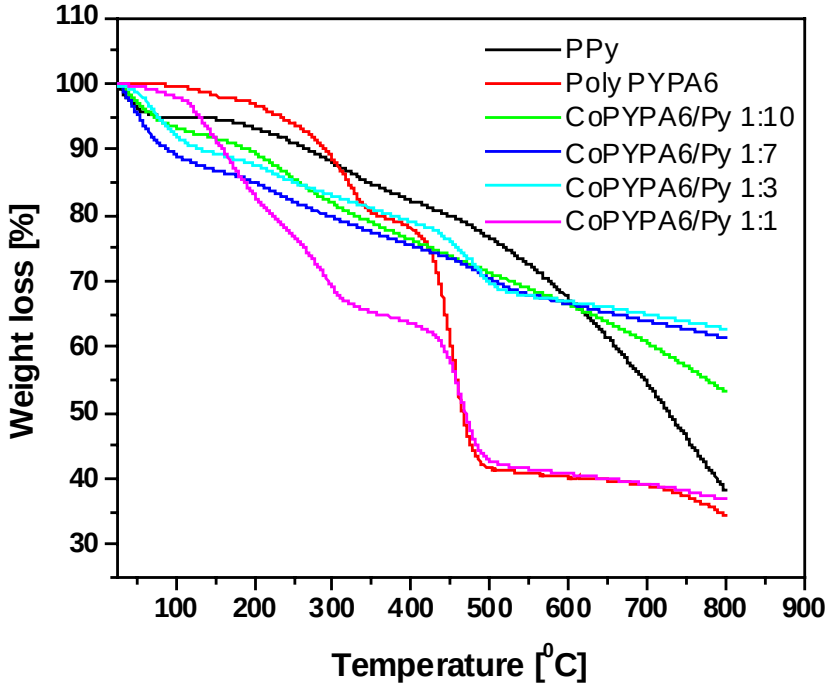

b

Fig. 5.7 TGA of homopolymers (a) and copolymers (b)

Table 5.5 Thermal stability of homopolymers and copolymers of pyrrole and ω-(pyrrol-3-yl alkyl) phosphonic acids (n=4,6,8,11)

Polymers	Decomposition temperature [°C]	Solubility (in methanol)
Polypyrrole, PPy	-	insoluble
HomopolyPYPA-6	280, 450	soluble
HomopolyPYPA-8	220, 450	soluble
HomopolyPYPA-11	200, 450	soluble
Copoly(PYPA4:Py)1:3	300, 465	soluble
Copoly(PYPA6:Py)1:1	280, 465	soluble
Copoly(PYPA6:Py)1:3	260, 470	soluble
Copoly(PYPA6:Py)1:5	-	insoluble
Copoly(PYPA6:Py)1:7	270, 470	insoluble
Copoly(PYPA6:Py)1:10	250	insoluble
Copoly(PYPA8:Py)1:3	265, 465	soluble
Copoly(PYPA11:Py)1:10	250	insoluble

5.4 Surface Polymerization of Modified Polypyrrole Films

It has been demonstrated with a variety of systems that surface-modified monomers of conductive polymers can serve as nucleation sites for chemical or electrochemical growth of conducting polymer films. The involvement of such surface-modified monomers units in the polymers results in a strongly adhered, conductive polymer layer compared to what is achieved by spin-coating or electropolymerization from bulk solution onto an unmodified surface. The functionalized adsorbed layer can also template the growth of conductive polymers, because the surface-modified monomers on substrates can change the interfacial environment. The resulting films will exhibit different morphologies and properties depending on the reaction condition.

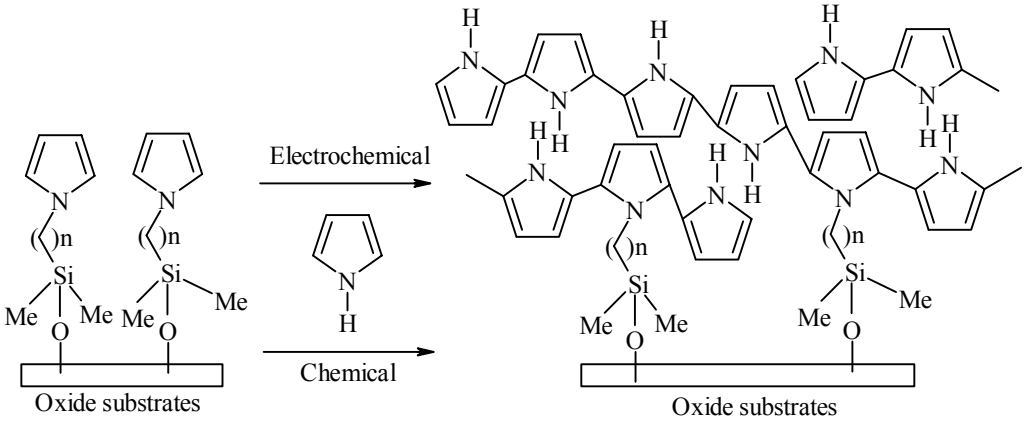

Scheme 5.1 Polymerisation of pyrrole via template modified surface

5.4.1 Chemical Deposition of Polypyrrole Films on Silane- or Phosphonic acid-modified Substrates

In a typical reaction, the substrate modified with the appropriate adhesion promoter was dipped in 1.7 M oxidant-H_2O solution, and a two times volume of 0.1 M pyrrole-MeOH solution was added. The mixture was stirred at room temperature for 24 h, and then the substrate was removed from solution. The sample was washed by sonication in three consecutive steps (10 min each) in methanol and water to remove the loose polymer attached on the film surface, and blown dry with argon. Other parameters for deposition of polypyrrole films were as follows: Pyrrole concentration = 0.01-0.15 M; oxidant: $Na_2S_2O_8$, $FeClO_4$, $FeCl_3$, $Mo(PO_4)_{12}$; Pyrrole to oxidant ratios 0.10-0.25; solvents: MeOH-H_2O, H_2O, CH_3CN; deposition time: 0.5h-24h; reaction atmosphere: air or nitrogen; reaction temperature: 0°C and room temperature.

5.4.2 Characterization of Polypyrrole Films Prepared by Surface Chemical Polymerization

The formation of polypyrrole films was identified by UV-VIS and Raman data, both spectra showed the characteristic absorption patterns of polypyrrole.

The UV-VIS absorption spectra (see Fig. 5.8) of the polypyrrole film exhibit a broad absorption maximum at about 900 nm, This intense low-energy band is associated with the conducting polymer in a low doping level [266]. In UV-VIS spectra, all polymers showed a

broad tailing absorption in the range of 300 nm to 500 nm. The tailing absorption is assumed to be due to a π-π* transition of a conjugated polymer main chain [267].

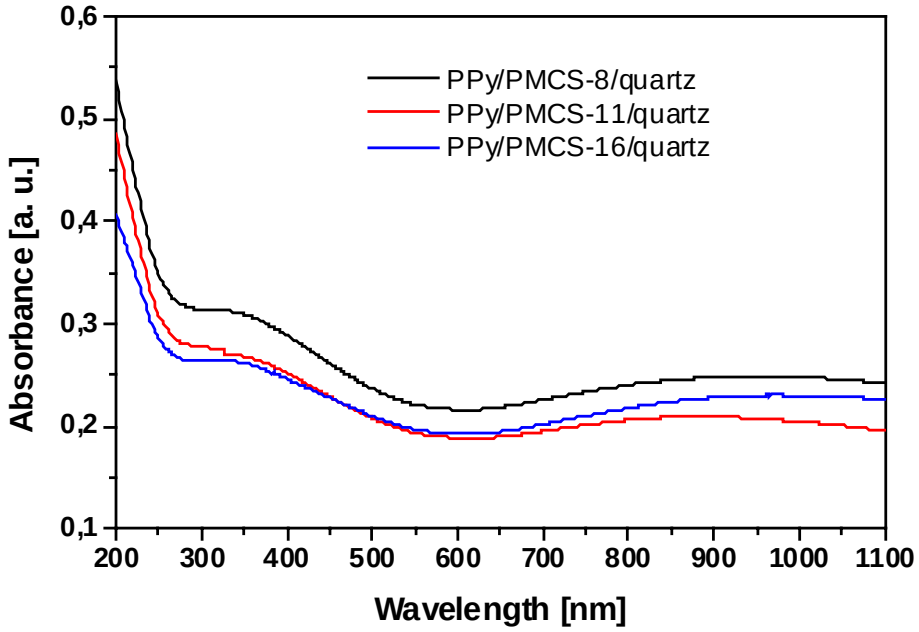

Fig. 5.8 UV of polypyrrole film

Acccording to Furukawa [268], it is possible to correlate to optical transitions, which makes Raman spectroscopy a valuable tool not only for the analysis of the deposition films but also for the characterization of the doping state and structural distortions of the conductive polymer skeleton. The Raman spectrum (see Fig. 5.9) was measured in 632.8 nm excitation wavelength. All peaks are broadened, and several additional broad peaks are visible in the 1600 to 1100 cm^{-1} region. These peaks are attributable to C=C stretch, C-C stretch, C-N stretch, and C-H bend vibrations, or due to the normal mode associated with a charged soliton, according to two different interpretations. The transition between the polaron (radical cation) and bipolaron (dication) states is also visible, for instance, the peak at ca. 986 cm^{-1} is assigned to the polaron state while that at 1369 cm^{-1} is associated to the bipolaron state.

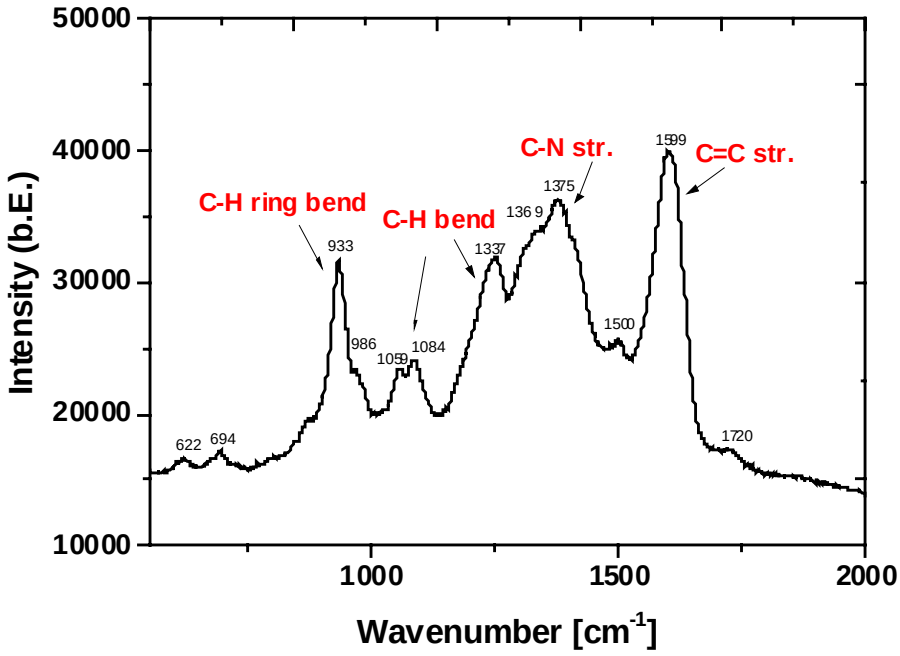

Fig. 5.9 Raman spectra of polypyrrole film

UV-VIS spectra and Raman spectra showed that the polypyrrole films on modified substrates have the typical characteristics of polypyrrole. These polypyrrole films have low doping level.

5.4.3 Surface Characterization of Polypyrrole Films

For the use of these polymer films in possible applications it is necessary to investigate the surface properties of the polymer films. The film roughness was determined using AFM measurements and the morphology of the deposition films were observed by SEM and AFM. Figure 5.10 showed the roughness of PPy/PYPA-6/Ta was 7.456 nm. The film thickness of this sample was 100 nm (measured by AFM).

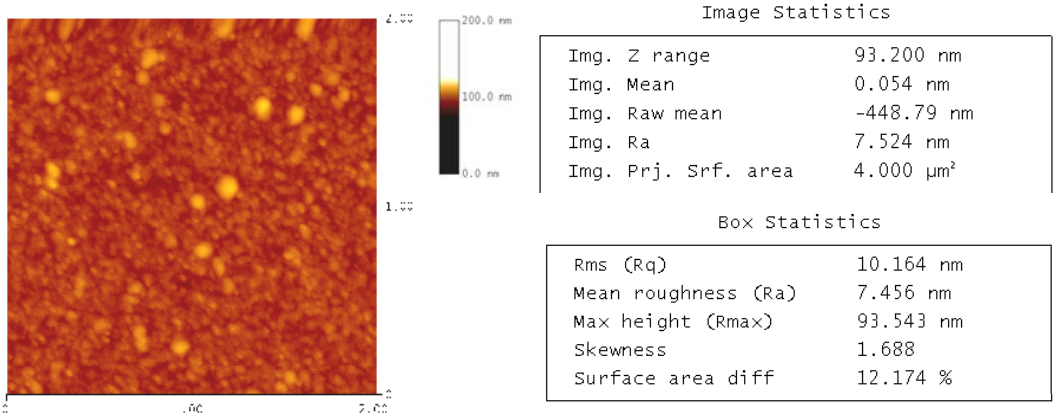

Fig. 5.10 Roughness measurement of PPy/PYPA-6/Ta

To investigate the influence of the chain length of adhesion promoter on the morphology of the deposited polypyrrole films, SEM and AFM measurements were used. Fig. 5.11 shows the AFM images of polypyrrole deposited on different chain length of ω-(pyrrol-1-yl) alkyl dimethylchlorosilane modified silicon substrates, and Fig. 5.12 shows the SEM of polypyrrole deposited on different chain length of ω-(pyrrol-3-yl) alkyl phosphonic acid modified tantalum substrate.

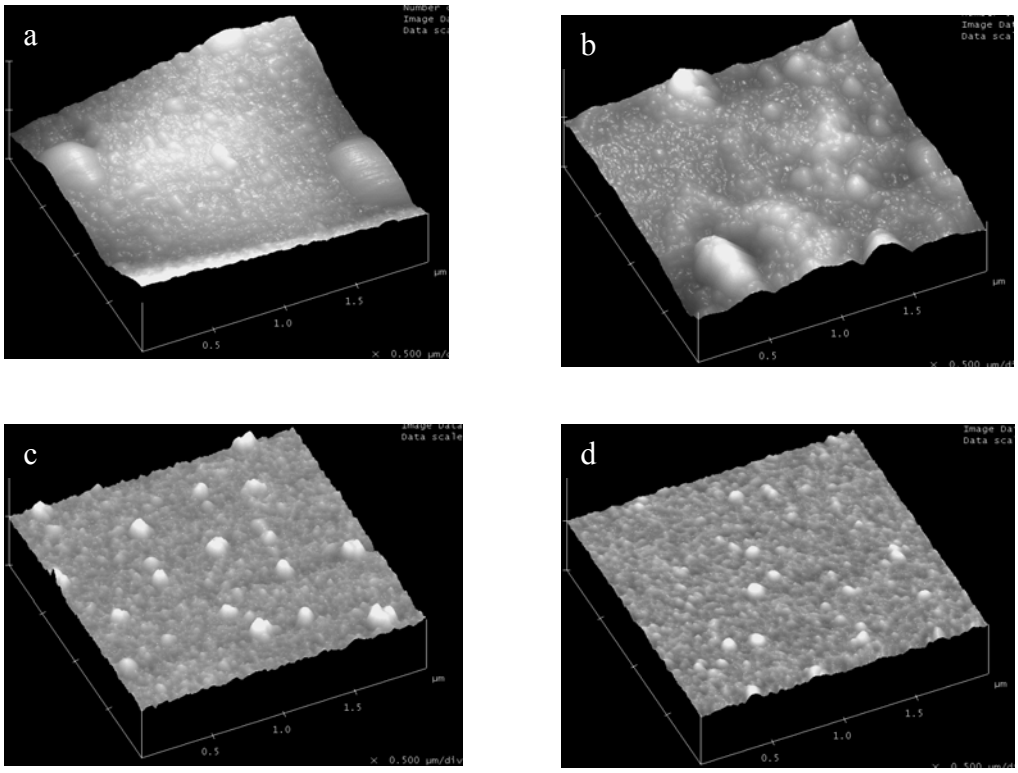

Fig. 5.11 AFM of polypyrrole films on PMCS modified substrates (a. PPy/PMCS-6/Si, R_f= 40 nm, thickness= 100 nm; b. PPy/PMCS-8/Si, R_f= 10 nm, thickness= 60 nm; c. PPy/PMCS-11/Si, R_f= 5 nm, thickness= 50 nm; d. PPy/PMCS-16/Si, R_f= 2.5 nm, thickness= 50 nm)

One can see that polypyrrole deposited on the adhesion promoter, which was either N-substituent or 3-substituent pyrrole with longer alkyl chains, have a smoother morphology than that of films deposited on adhesion promoter with shorter alkyl chains. Contact angle and ellipsometry data of the absorbed layer at chapter 4 have shown that adhesion promoters with longer alkyl chains formed more compact and ordered self-assembly absorbed layer on the oxide substrates. The consistent behavior of the absorbed layer and polymer films deposited on them suggested that the adhesion promoter on the surface provided nucleation sites for polymer chains to grow. Although we do not have any evidence to show that the polypyrrole chains are tethered on the pyrrole molecules of the absorbed layer, the existence of the pyrrole molecules on the surface affects the deposition and growth of the polypyrrole chains and the

resulting surface morphology of the polymer films. This phenomenon could be rationalized as the self-assembly absorbed layer creates an organic environment for organic polymer to deposit and grow.

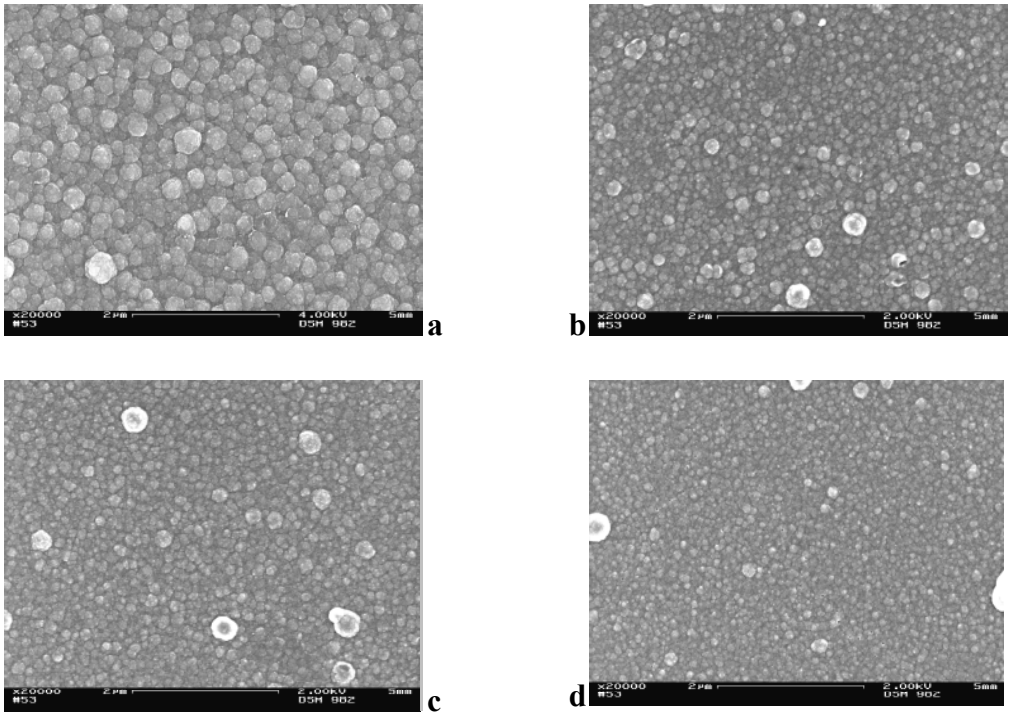

Fig. 5.12 SEM of polypyrrole films on PYPA modified substrates (a. PPy/PYPA-4/Ta; b. PPy/PYPA-6/Ta; c. PPy/PYPA-8/Ta; d. PPy/PYPA-11/Ta)

The solvent used in the polymerization procedure also affected the morphology of the resulting polymer films. We found that deposited polypyrrole films obtained from hydroxy containing solvents (such as methanol/H_2O) have smoother morphology (Fig. 5.13). Wu et al. reported that the quality of polymer films have the relationship with the relative permittivity of the solvent [269]. Solvents with higher relative permittivity will stabilize the radical cation during the polymerization, favouring the growth of polymer chains, and resulting in better quality films. Even though water has high relative permittivity ($\varepsilon = 78.54$) and is a relatively reactive molecule, polypyrrole films prepared from aqueous solution, while showing good adhesion, had a higher number of structural defect and very small thickness. Methanol ($\varepsilon = 32.63$) and water mixture (2:1 v/v) as solvent can solve this problem. Acetonitrile ($\varepsilon = 37.5$) is a good solvent for electropolymerization, however, in chemical polymerization, polypyrrole films prepared from acetonitile had higher surface roughness. These results are agreement with the literature reported [269, 270].

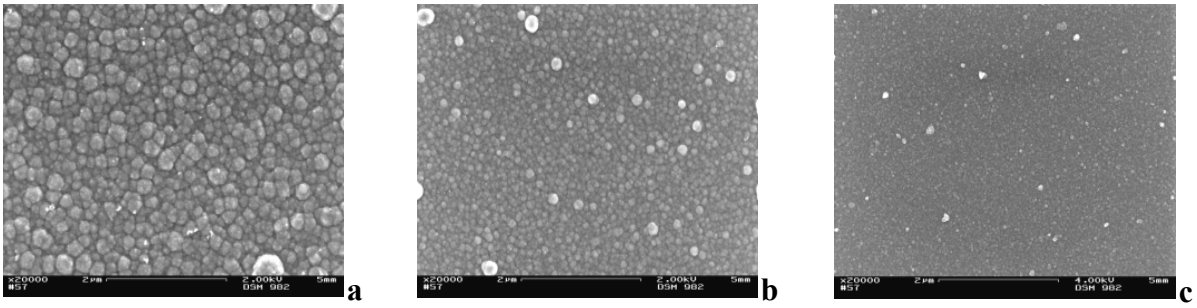

Fig. 5.13 SEM of polypyrrole films prepared in different solvent (a. acetonitrile; b. MeOH/H_2O; c. H_2O)

The kind of oxidant used in the polymerization also affected the quality of the resulting polymer films. With a low power catalytic oxidant the rate of the polymeriaztion is relatively slow, and the polymer film is relatively smooth. Using a more powerful oxidant such as $(NH_4)_2S_2O_8$ gave faster rates of polymeriaztion but always resulted in low dense and rough polymer films [271].

The morphology of the polypyrrole films deposited on modified substrates were influenced by the chain length of the adhesion promoters, the solvent and the kind of the oxidant. In general, the longer chain derivatives of adhesion promoter, higher relative permittivity solvent and lower powerful oxidant, the smaller the surface roughness of the resulting films.

The thickness of the polypyrrole films on Si wafer was determined by ellipsometry. The method was described in chapter 2. The thickness of the polypyrrole on metal substrates, such as Ta, Ti, was determined by AFM (Fig. 5.14).

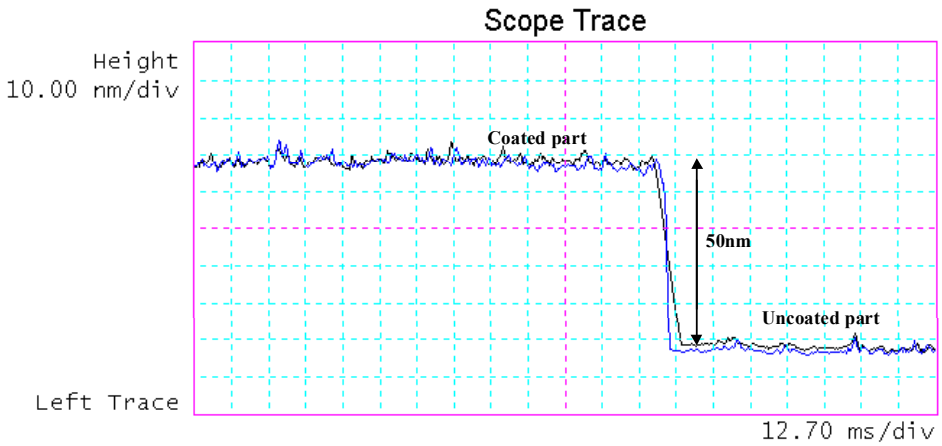

Fig. 5.14 Thickness measurement by AFM (PPy/PYPA-6/Ti by surface chemical polymerization)

The kind of oxidant and monomer to oxidant ratio were found to affect the quality of polypyrrole films. When $FeCl_3$ is used as oxidant, the resulted polypyrrole film is smooth but too thin compared with $FeClO_4$ or $Na_2S_2O_8$. The dependence of thickness on monomer/oxidant ratio at constant monomer concentration is shown in Fig. 5.15.

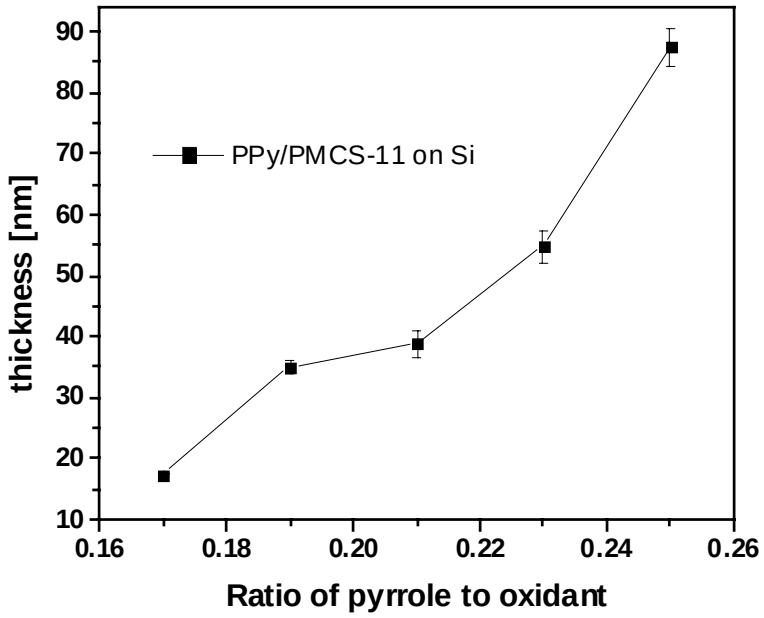

Fig. 5. 15 Effect of monomer to oxidant ratio on the thickness of polypyrrole films (deposition time 1h; pyrrole concentration 0.03M; oxidant $Na_2S_2O_8$; solvent MeOH/H_2O 2:1 v/v; RT, in air)

For a constant monomer to oxidant ratio, the effect of the monomer concentration on the thickness of polypyrrole film is shown in Fig. 5.16. It was found that polymer films prepared at a monomer concentration of 0.1 M have the highest thickness and smallest surface roughness when $Na_2S_2O_8$ was used as oxidant. At low monomer concentrations, pyrrole in solution has less chance to get covalently bonded to the adhesion promoter on the surface. The polypyrrole chains also have less chance to graft on the surface, while at higher concentrations, the reaction rate is too fast to allow growth of a dense film on the substrate; both circumstances are unfavourable for film growth. However, due to the limited solubility of $Na_2S_2O_8$ in water, the concentration of $Na_2S_2O_8$ can not be higher than 0.1 M. Wu reported that polypyrrole films prepared at monomer concentration of 1.5 M have the bigger thickness and smallest surface roughness when $FeCl_3$ was used as oxidant [269].

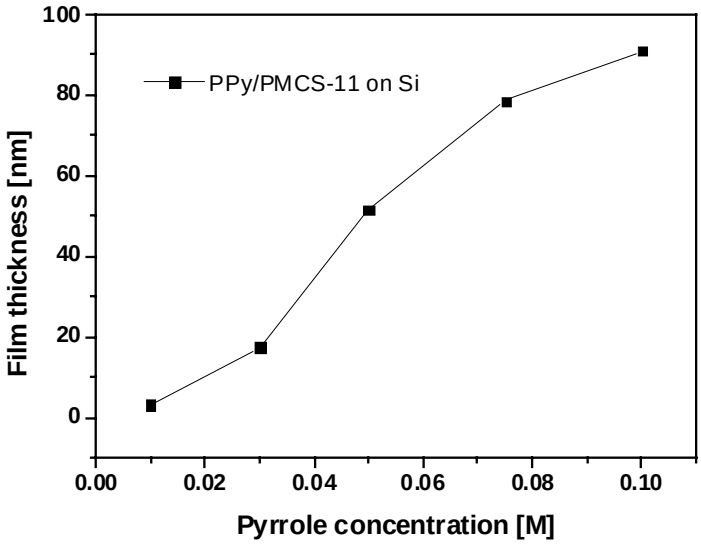

Fig. 5.16 Effect of monomer concentration on the thickness of the polypyrrole films (deposition time pyrrole to oxidant ratio 0.17; oxidant $Na_2S_2O_8$; solvent MeOH/H_2O 2:1 v/v; RT, in air)

Effect of deposition time on the thickness of the polypyrrole films is shown in Fig. 5.17. The thickness of the polypyrrole film increased as the deposition time during the first 4 hours and then reached a plateau due to complicated equilibrium processes between polypyrrole chains deposited on and removed from the substrate. It was also found that all pyrrole molecules were polymerized to polypyrrole after 20 hours. This was confirmed by the similar amount of polypyrrole powder recovered from the reaction vessel for deposition times more than 20 hours. The optimal deposition time is that when all monomers in solution are consumed.

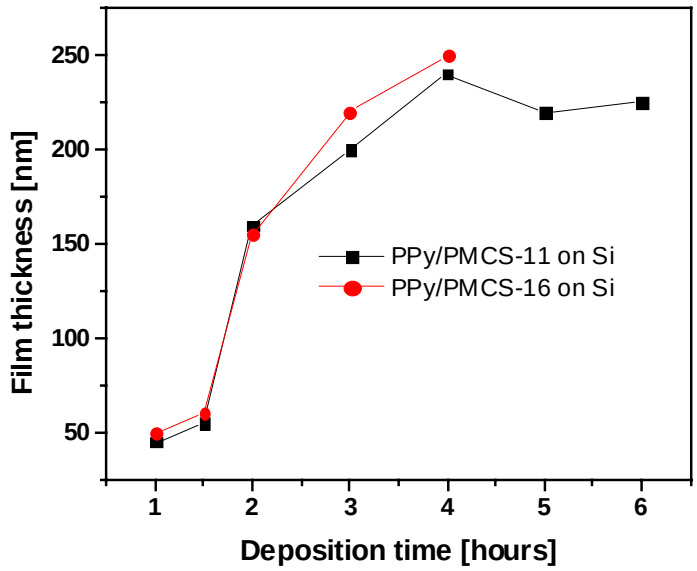

Fig. 5.17 Effect of deposition time on the thickness of the polypyrrole films (pyrrole to oxidant ratio0.23; oxidant $Na_2S_2O_8$; Pyrrole concentration 0.03M; solvent MeOH/H_2O 2:1 v/v; RT, in air)

The reaction atmosphere and temperature did not have any obvious effects on the properties of the polypyrrole films.

5.4.4 Effect of the Adhesion Promoter on the Deposition of the Polypyrrole Films

Polypyrrole films deposited on synthesized adhesion promoters modified substrates showed much better adhesion compared to those an unmodified substrates. In Fig. 5.18, polypyrrole film on a silane-modified substrate part clearly showed a smooth, continual and compact film, and on unmodified substrate part no polypyrrole film can be observed. When unmodified substrates were used, only loosely attached particles were found on the surface, which could be washed off easily with solvent. During the polymerization most of the polypyrrole chains are probably not directly bounded to the pyrrole molecules on the surface. However, for the adhesion promoter modified substrates, the formation of pyrrole molecules on the surface of the inorganic substrate increase the interaction between the organic polymer and the substrate, and therefore, increases the adhesion between them. At our reaction condition, adhesive films up to 450 nm in thickness can be obtanied on modified substrate.

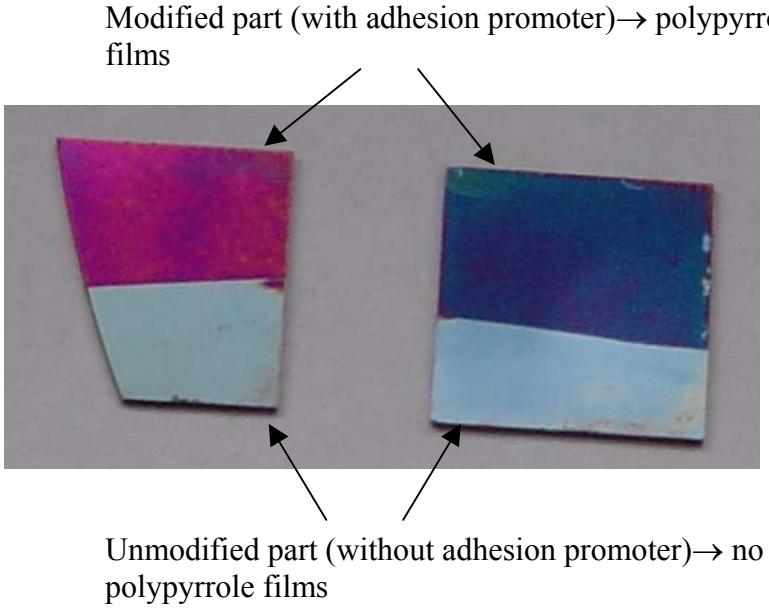

Fig. 5.18 Effect of the adhesion promoter on the deposition of the polypyrrole films (the thickness of red color polypyrrole film (left) 250 nm; the thickness of blue color polypyrrole film (right) 150 nm)

5.4.5 Electrical Conductivity of the Polypyrrole Films

The electrical conductivity of the polypyrrole films was measured in Prof. S. Nešpůrek group (Insitute of Macromolecular Chemistry, Academy of Sciences of the Czech Republic, Prague).

The j-V measurement was done in the way of recording current value with linearly or logarithmically increasing or decreasing the voltage at a designed time interval and voltage step by electrometer Keithely 6517A (Fig. 5.19). The measurement was automatically controlled by PC and could be done in air or in vacuum by changing the temperature range from –60 °C to 120 °C. The polypyrrole films were prepared by chemical polymerization of polypyrrole on PMCS-modified substrates like described above. Metal strips (Al or Au) were evaporated onto the polypyrrole layer. The thickness of the metal strips (Al or Au) is about 100 nm. The distance between strips is 300 μm. Electrical contacts was made on metal strip with silver paste. The measurement was done in vacuum (0.01 Pa).

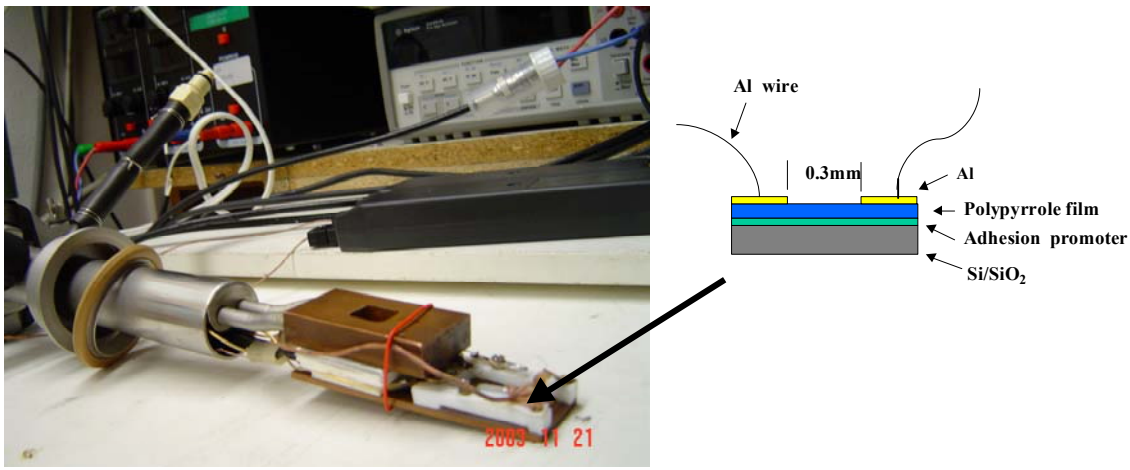

Fig. 5.19 Equipment of j-V measurement

The j-V characteristics of PPy films based on PMCS-n (n = 8, 11, 16) are shown in Fig. 5.20. The results illustrate that the value of the electrical current does not monotonically depend on the length of the spacer of the adhesion promoter monolayer; the changes in the current with the space length one can take as a scattering of the experimental values. This is due to our sample is coplanar sample. The measurement was taken place in the two-point geometry. Thus, PPy films based on PMCS-16 due to the best film quality, stability and reproducibility, were used for the further detail studies.

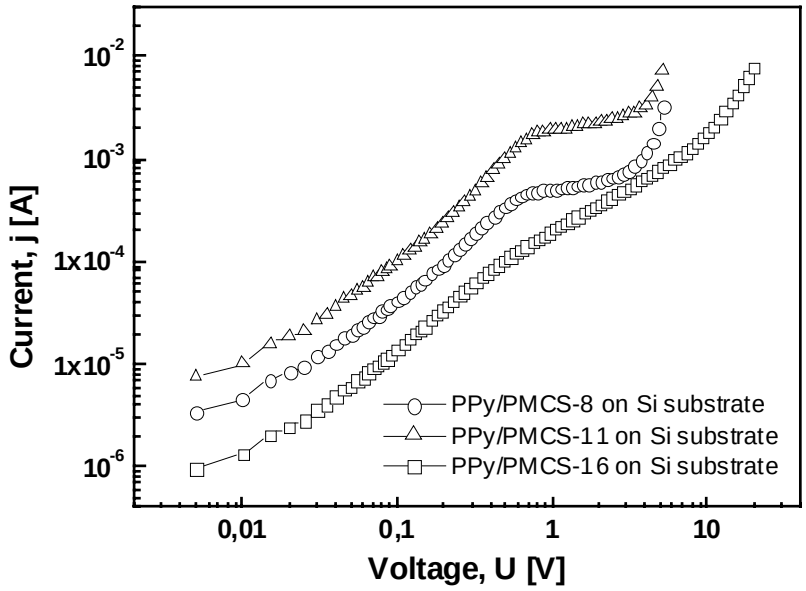

Fig. 5.20 The j-V characteristics for Si/SiO_2//PMCS-n/PPy/Al samples (n = 8, 11, 16).

Temperature dependences of j-V characteristics of Si/SiO_2/PMCS-16/PPy/Al sample are shown in Fig. 5.21. At room temperature and high temperatures, PPy film shows ohmic behaviour in all the voltage ranges where the material is conductive and it does not show irreversible changes. At low temperature, the range of voltage for which the resistance can be measured increases and it is easier to detect non-ohmic behavior. At low temperature, polypyrrole has ohmic behavior only at low voltage. With the increase of the voltage, the non-ohmic behavior can be observed. From this figure, we can see that at the constant voltage, the current increase with the temperature (see Fig. 5.22). The electrical current increases with temperature, the film shows a typical semiconductor behavior. In polypyrrole, and most of the organic conducting polymers, charges reside in granular islands or domains of delocalization. This is a consequence of the chemical constitution of the material; in the conducting oxidation state the neutral covalent-bonded backbone are protonated (p-doped) with a counterion sitting interstitially. Band structure calculations have shown that at low temperature the charges on the backbone form polaronic and even bipolaronic states. The remaining carrier are a result of the ionization of defects, which are near the middle of the gap and which can be ionized at high temperatures [272].

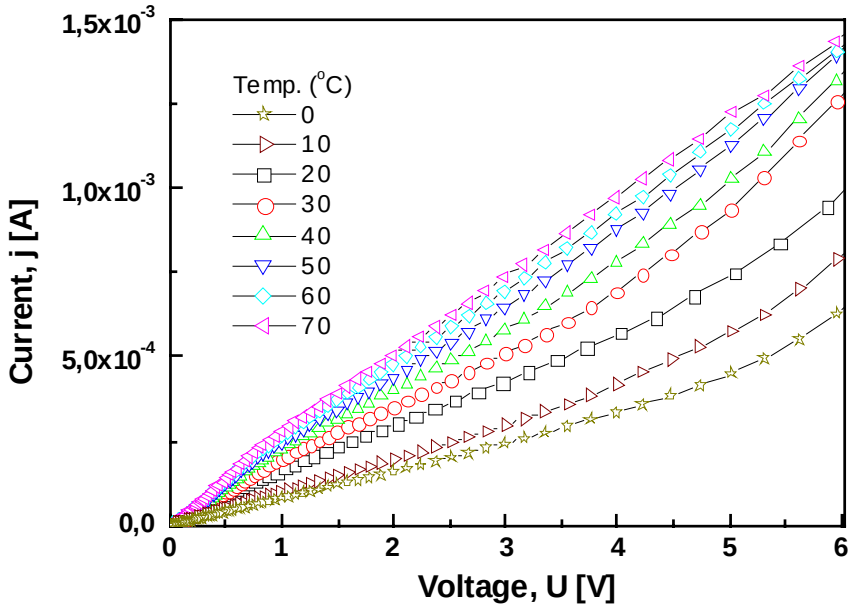

Fig. 5.21 The j-V characteristics for Si/SiO_2/PPy/PMCS-16/Al sample (thickness = 87 nm) at different temperatures.

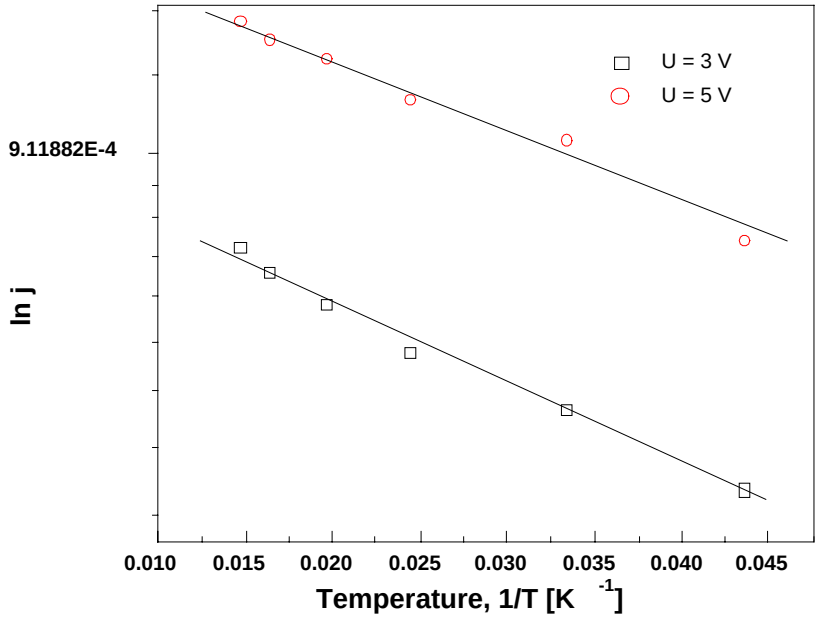

Fig. 5.22 The ln j vs T^{-1} plot for Si/SiO_2/PPy/PMCS-16/Al sample at constant voltage 3 V and 5 V

Figure 5.23 shows the replotted j-V characteristics in the form of ln (J/U) vs. $U^{1/2}$ (J is the current intensity, it is calculated by j divided the interceptive area of PPy layer). The linear behavior indicated by the straight line is coherent with the predictions of the model derived by Simmons [273] for charge carrier transport limited by thermionic injection into low mobility materials, which predicts a current density given by

$$j = qN_e\mu F \exp\left(-\frac{E}{kT}\right)\exp\left(\frac{\beta F^{1/2}}{kT}\right) \qquad \text{Eq. 5.4}$$

where q is the elementary charge, N_e is the effective density of states in the semiconductor, μ is the charge carrier mobility, F is the electric field strength, E is the energy barrier at the interface, k is the Boltzmann constant, T is the absolute temperature and β is a constant.

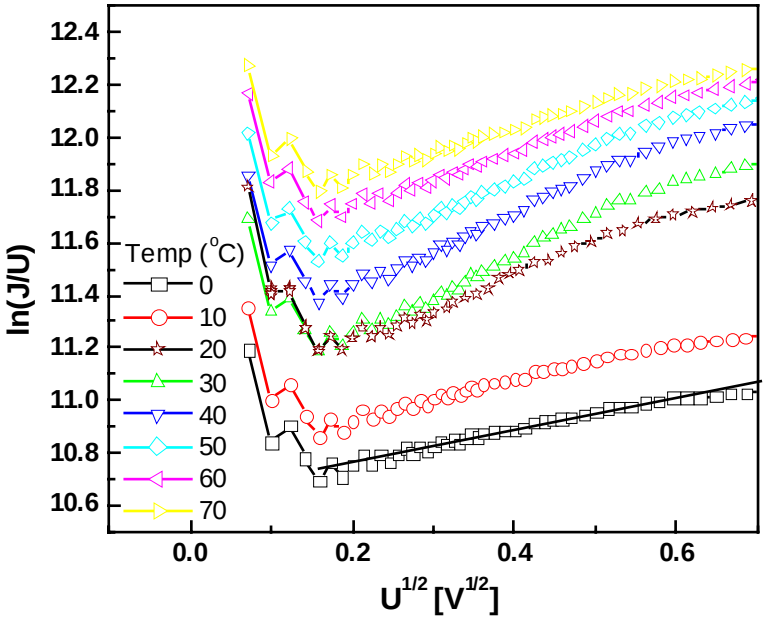

Fig. 5.23 The ln(J/U) vs. $U^{1/2}$ plot for Si/SiO_2/PPy/Al sample (thickness = 87 nm). The straight line indicates the linear fit.

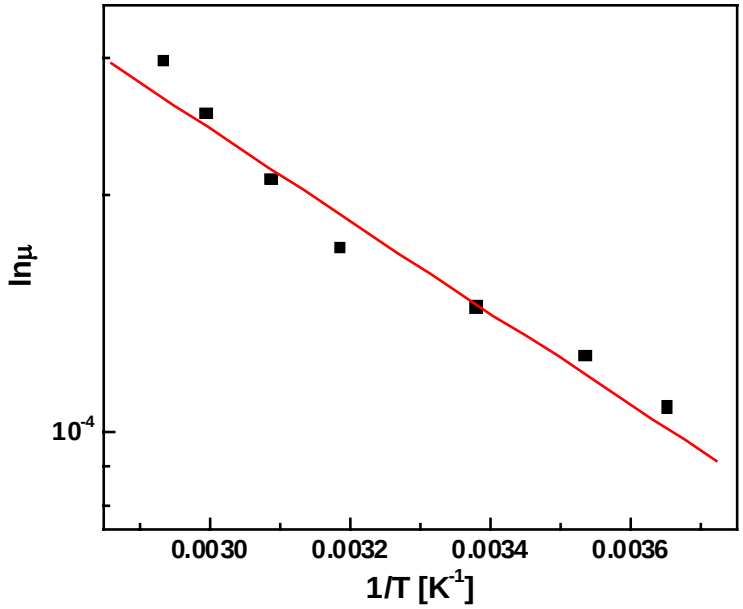

Fig. 5.24 Charge carrier mobility on temperature dependence for Si/SiO_2/PPy/Al sample.

The positive charge carrier mobility can be obtained from the intercept *B* of the straight segment of the ln j/U vs. $U^{1/2}$ curve. From Eq. 5.4 one can estimate the intercept *B* and the slope *A* of the linear segment as below:

$$A = \frac{\beta}{d^{1/2} kT} \qquad \text{Eq. 5.5}$$

$$B = \ln\left(\frac{qN_e\mu}{d}\right) - \frac{E}{kT} \qquad \text{Eq. 5.6}$$

From the slope *A* of this linear segment in ln (J/U) vs. $U^{1/2}$ plot, based on Eq. 5.5 one can estimate constant β average value 0.01 eV $V^{-1/2}$ $cm^{1/2}$. The potential energy barrier, *E*, at the metal/polymer interface can be estimated from the ln j vs. T^{-1} plot, where we have

$$\left[\frac{\partial \ln j}{\partial T^{-1}}\right]_{U=const} = \frac{\beta d^{-1/2} U^{1/2} - E}{k} \qquad \text{Eq. 5.7}$$

Then we can estimate *E* for positive charge carriers in the PPy/Al interface as 0.052 eV. Assuming N_e = 2.5 × 10^{19} cm^{-3} [274], the positive charge carrier mobility for different temperatures was estimated. In Fig. 5.24 we present the ln μ vs. T^{-1} curve. At room temperature the mobility for positive charge carriers is 1.4 × 10^{-4} $cm^2 \cdot V^{-1}/s$, two order of magnitude higher than the values reported in the literature for the electrodeposited PPy films [275] and lower than the highest mobility value reported in the literature for PPy (ab. 10^{-1} $cm^2 \cdot V^{-1}/s$), which was observed in p-toluene sulfonate doped PPy [276].

5.5 Characterization of Polypyrrole Films on Modified Substrate by Electrochemical Polymerization

5.5.1 Electrochemical Polymerization of Polypyrrole Films on Modified Substrates

5.5.1.1 Oxidation Potential

Electrochemical experiments were carried out in a three-compartment three–electrode glass cell with Ag/Ag^+ non-aqueous reference electrode. The working electrode and counter-electrodes Pt were cleaned ultrasonically. The oxidation potential of the synthesized adhesion promoters was measured by cyclic voltammetry. Cyclic voltammetry (CV) experiments were conducted at room temperature on a EG and G Princeton Applied Research model

potentistat/galvanostat. Oxidation potentials of these adhesion promoters are shown in Fig. 5.25.

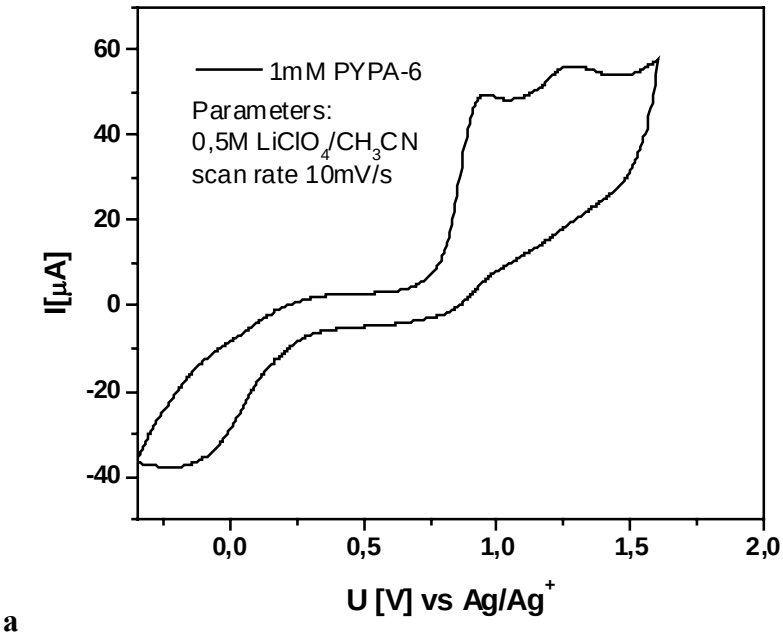

a

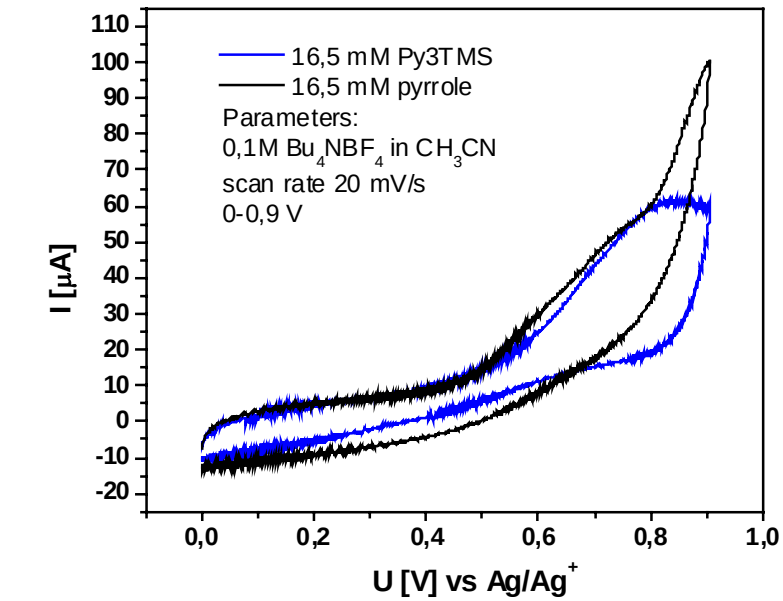

b

Fig. 5.25 Cyclc voltammograms for (a) PYPA-6; (b) 3-PyTMS

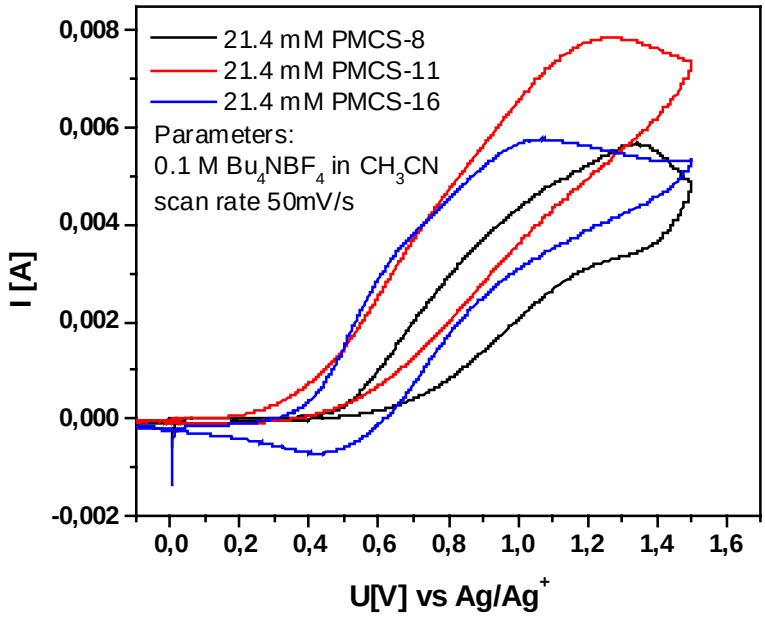

c

Fig. 5.25 Cyclc voltammograms for (c) PMCS

The oxidation potential of 1-substituted pyrrole derivatives (Fig. 5.25c) is higher than pyrrole and we observe that as the chain length increases the oxidation potential decreases. This high potential can be explained in terms of the steric and electronic factors, which make the oxidation of 1-substituted pyrroles a bit difficult. And the oxidation potential of 3-substituted pyrrole derivatives (Fig. 5.25a,b) is slightly lower than that of pyrrole due to the effect of the 3-substituted alkyl group. The obtained values are in accordance with the known and widely investigated 1-substituted and 3-substituted pyrroles. These 1- or 3-substituted pyrrole derivatives have a possibility to copolymerize with pyrrole or other pyrrole derivative due to their close oxidation potentials. On potential benefit of the positive shift in Epa (oxidation potential) it is that the films formed from 1-substituted pyrrole derivatives will be less reactive to atmospheric oxidation. This implies improved handling, storage and lifetime characteristics for chemical sensors fabricated using such films.

To investigate the adsorption of pyrrole derivatives taking place on the Ta, and Ti surfaces, EIS measurements were used. Through the EIS measurement, the double layer resistance and capacitance could be determined after fitting the equivalent model. Fig. 5.26 showed that the resistance increase and capacitance decrease after the electrode modified by PYPA. Such a behavior can be attributed to the presence of insulating alkyl chains on the electrode, which can block the electrode. We may also observe that the resistance did not increase much. This indicated that electron transfer to solution species at these modified electrode is not completely blocked; it may be have the presence of defects in the adsorbed layer.

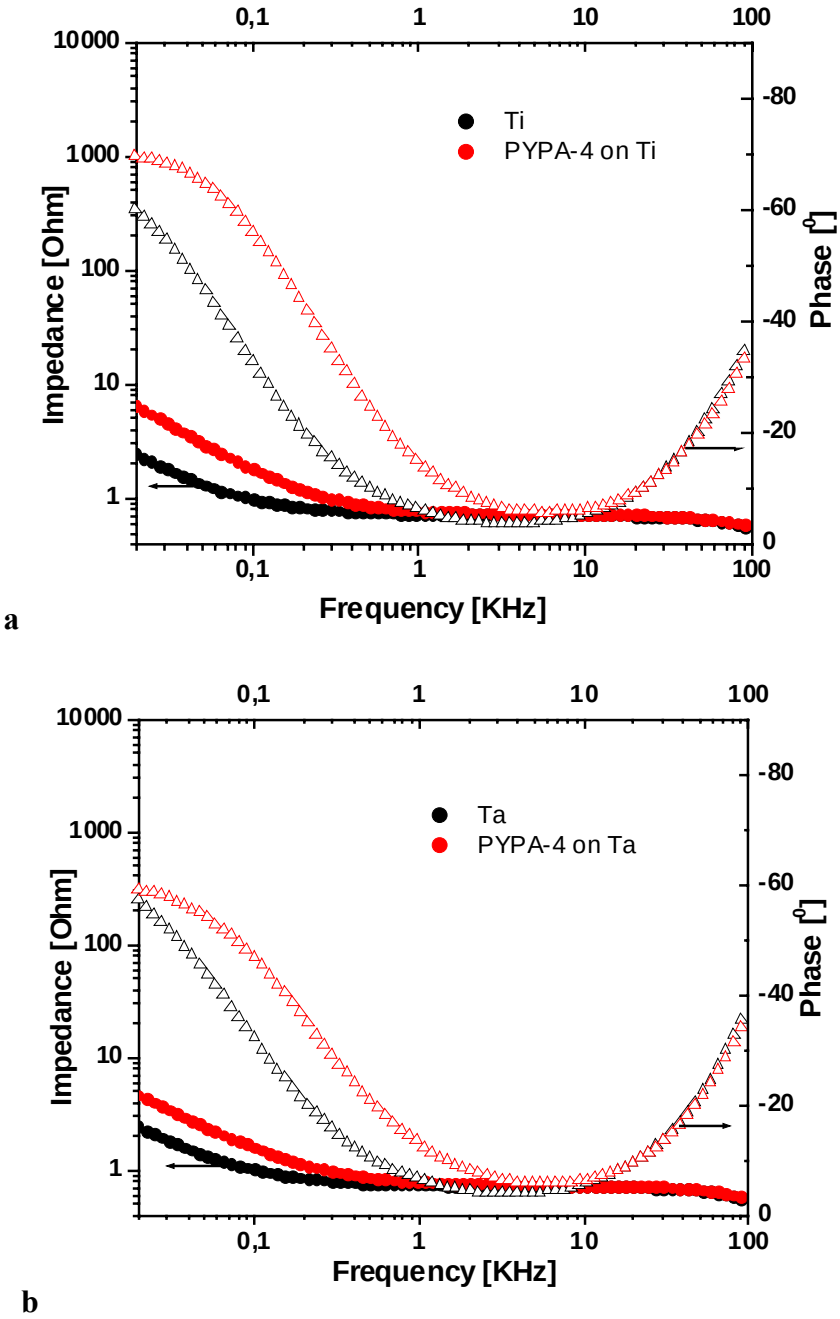

Fig. 5.26 (a). EIS of bare Ti and modified Ti; (b). EIS of bare Ta and modified Ta.

To understand the function of pyrrole molecules on the Ti surface during the electropolymerization of polypyrrole, the oxidation potential of the PMCS-modified Ti electrode were measured by CV. Fig. 5.27 demonstrates that the PMCS-modified Ti electrode lead to dramatic changes for the first cycle in CV. The peak in the first cycle could be attributed to the oxidation potential of the pyrrole head group on the modified Ti electrode. The first positive potential excursion of the surface-bound pyrrole monolayers yielded a characteristic curve that was not reproduced in subsequent scans. This has also been reported

by other group [163]. This oxidation potential corresponded to the expected for the oxidation of the substituted pyrroles to the pyrrole radical cation.

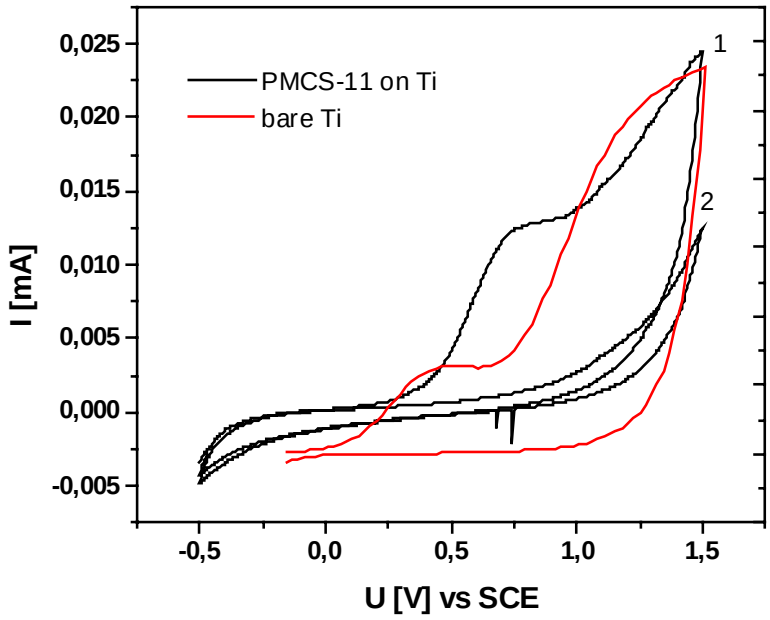

Fig. 5.27 Cyclic voltammograms of PMCS-modified Ti and bare Ti in 0.1 M $LiClO_4$/ACN at 10 mV/s.

5.5.1.2 Electrochemical Polymerization

The deposition of adsorbed layers of synthesized adhesion promoters on electrodes was performed by immersing the electrodes in organic solutions of the appropriate adhesion promoters as described in the chapter 4.

The electrochemical polymerization of the adhesion promoters-modified substrates was carried out from electrolyte solution (0.1 M $LiClO_4$ in acetonitrile) containing 0.1 M pyrrole, which has been redistilled before use. After electrochemical polymerization, the films grown on the adhesion promoters-modified electrodes were rinsed with acetonitrile and ethanol, sonicated in ethanol for 3 min, and blown dry with nitrogen. The films grown on bare electrodes were not sonicated.

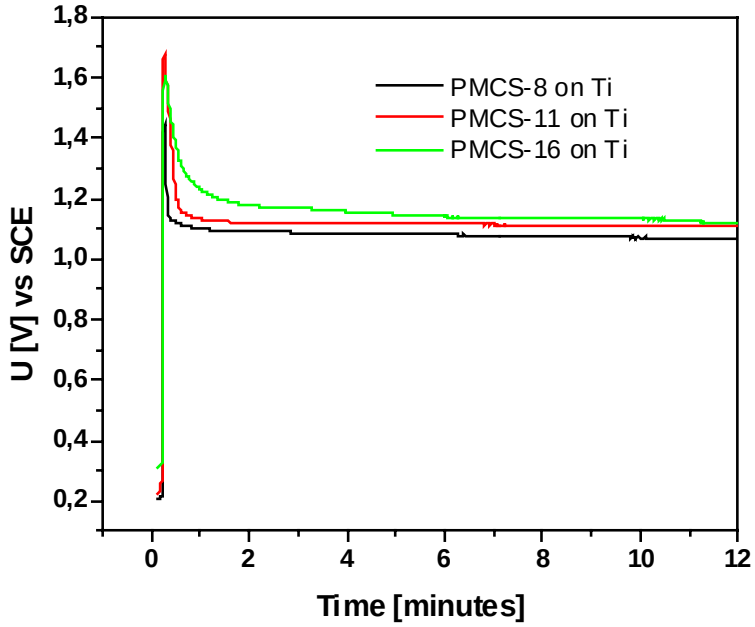

Fig. 5.28 Chronopotentiometry of electrodeposition of polypyrrole on PMCS-modified Ti in 0.1 M $LiClO_4$/ACN at current density 1 mA/cm^2

Chronopotentiometric polymerization of pyrrole on PMCS-modified Ti electrode was performed in 0.1 M pyrrole in 0.1 M $LiClO_4$/ACN at current density 1 mA/cm^2 for 12 min. The chronopotentiometry data for the electropolymerization of pyrrole on the three Ti electrodes modified with different chain length PMCS were shown in Fig. 5.28. On the three PMCS-modified Ti electrodes, the potential almost immediately rose after the current was applied due to pyrrole oxidation, then, the potential decreased fast to a constant value. These values were the oxidation potential of polypyrrole electrochemicallly deposited on modified electrode. We can clearly see that the longer the alkyl chain of PMCS, the higher the potential for electropolymerization. This result was consistent with the ellipsometry data, which showed that PMCS with long alkyl chain formed more compact monolayers on the oxide substrates and therefore, exhibited higher blocking properties.

Potentiostatic polymerization of polypyrrole film on unmodified electrode and PYPA-8 modified electrode from 0.1 M pyrrole in 0.1 M $LiClO_4$/ACN (versus SCE, scan rate 10 mV/s) was carried out to give thick black films.

In order to investigate the redox-process of the polypyrrole films, a multi-sweep voltammogram of polypyrrole is presented in Fig. 5.30. The cyclic voltammograms showed broad oxidation and reduction peaks of polypyrrole. The polypyrrole grafted on Ti electrode behaved similarly. The polypyrrole films formed on the adhesion promoter modified electrode can be reduced and the reoxidized reversibly. The doping and dedoping processes can be

repeated for several cycles without observable changes in the cycle voltammogram curves for these polypyrrole films. These results suggested that the electroactivity of polypyrrole films is stable during the experiments and the anions could move in and out of the polypyrrole films.

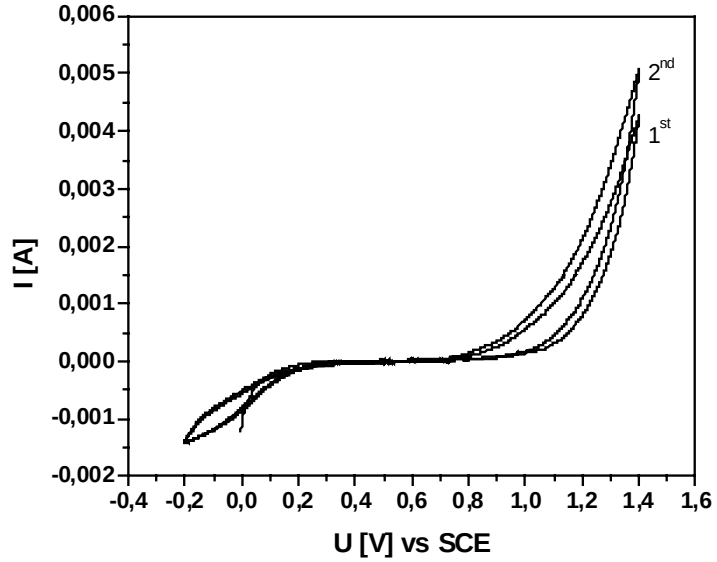

Fig. 5.29 CV of polymerization of polypyrrole on PYPA-modified electrode at 0.1 M $LiClO_4$/ACN, scan rate 10 mV/s

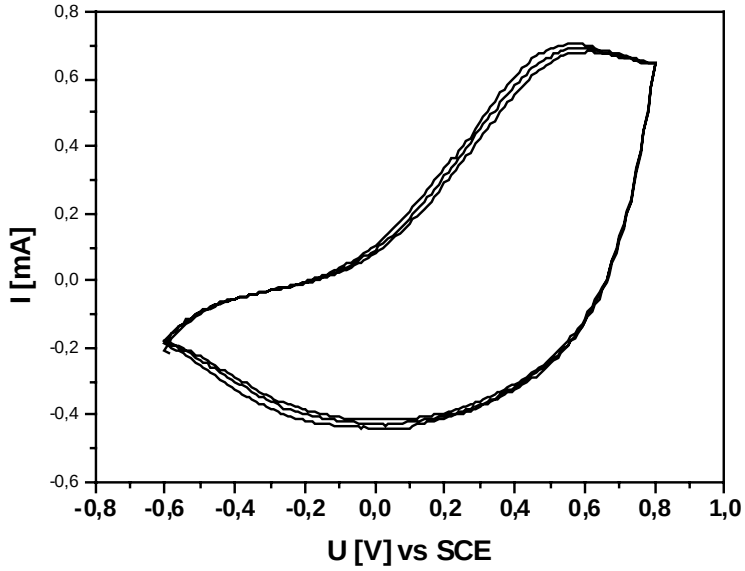

Fig. 5.30 Doping and dedoping curves of the polypyrrole films grown onto PYPA-modified Ta electrode in 0.1M $LiClO_4$/ACN, scan rate 10 mV/s

5.5.2 Characterization of Polypyrrole Films

The polymer films were prepared by chronopotentiometry and were examined for their semi-conducting behavior using EIS measurements. The EIS was employed to determine the

resistance and capacitance of polypyrrole as a function of the applied potential. Impedance measurements were carried out in a monomer free solution with IM5d impedance measuring instrument of Zahner Electric. An AC amplitude of mV was applied in the frequency range of 100 KHz to 0.1 Hz using 10 points per decade. For each film, the impedance spectra were obtained between the potential range 0.4 V to –1.4 V in steps of 0.1 V. The films were allowed to equilibrate for 10 minutes at each potential being measured.

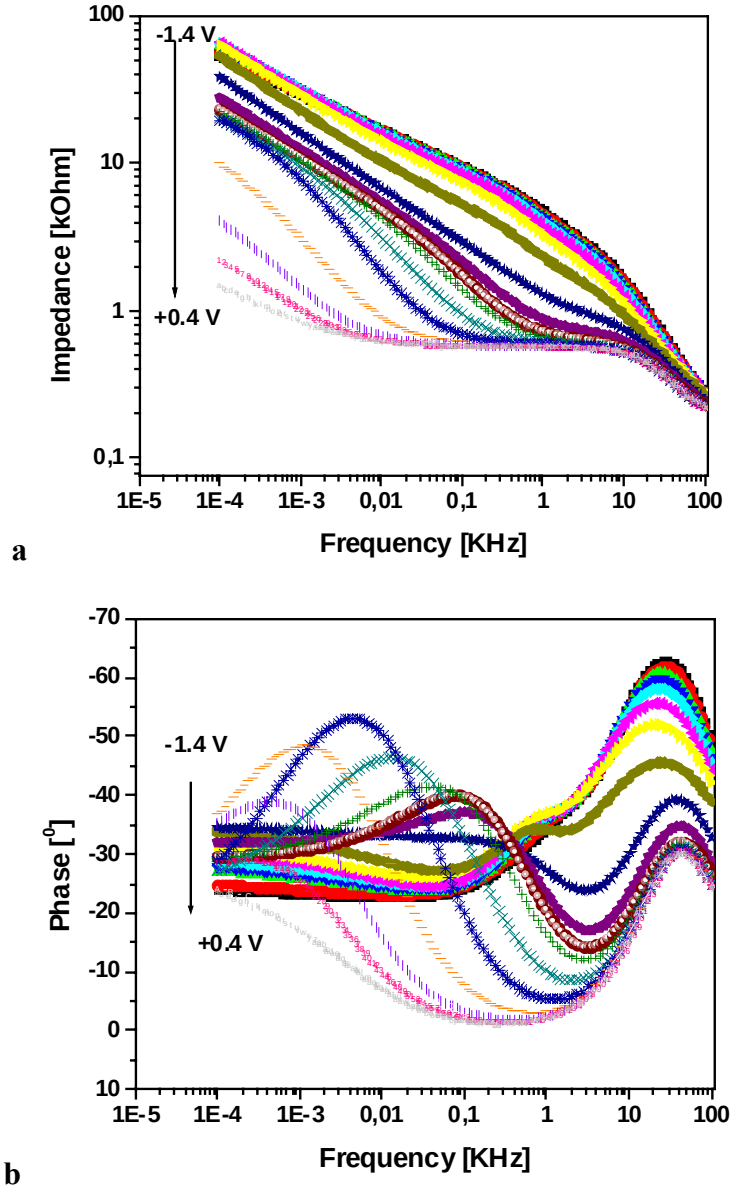

Fig. 5.31 Bode plots of polypyrrole on PMCS-8 modified Ti electrode in 0.1M $LiClO_4$ in acetonitrile, at ifferent potentials. a. Modulus of impedance; b. Phase angle

The electroactivity of polypyrrole films on Ti was also demonstrated by EIS measurements. The impedance data were obtained at potentials between 0.4 V to –1.4 V in 0.1 M $LiClO_4$ in acetonitrile. The step potential was 0.1 V and films were allowed to equilibrate for 10 min. at

each potential before being measured. Fig.5.31 showed the impedance plots for a polypyrrole films on the modified electrode in organic solution.

The experimental data can be described using the equivalent circuit model shown in Fig. 5.32a. The Bode plot can be divided into three frequency parts, which are typical for the partial processes at the electrode in electrolyte solution (Fig. 5.33b) [277]. The high frequency range (part I) of the model can be determined to the electrolyte resistance R_E and an artifical capacitance C_x, which is caused by the cell design. The medium-frequency range (part II) can be determined to the resistance of the polymer film R_{pm}. Resistance R_{pm} and capacitance C_{pm} are related to the redox process of the polymer film. The low-frequency range (part III) can be attributed to the electrochemical reaction taken place at the film/electrode interface.

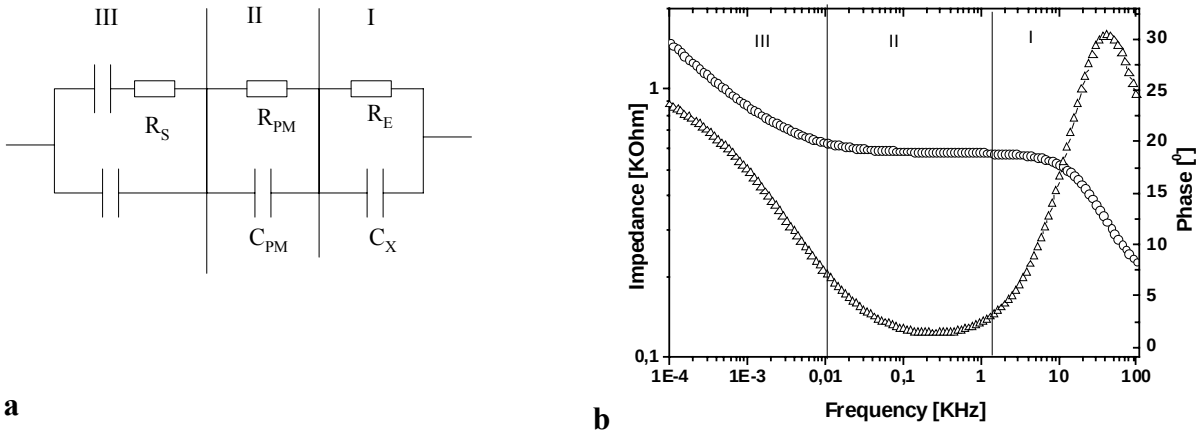

Fig. 5. 32 (a). Equivalent circuit; (b). Bode plot of PPy film on PMCS-8 modified Ti electrode at 0.4V

Using this circuit model, the capacitance and the resistance in the region of 0.4V to –1.4V can be fitted. Fig.5.33 showed the results of impedance measurements (in the form of Mott-Schottky plot for representative structure). The value for the flat band potential E_{fb} was determined by extrapolation to $c^{-2} = 0$. In this measurement, the flat band potential is –0.62 V vs SCE. The negative slop for the Mott-Schottky plot corresponds to p-type conductivity of the polypyrrole films. Therefore, Fig. 5.33 confirmed that the polypyrrole film was a p-type semiconductor, which is in a good agreement with the literature [230].

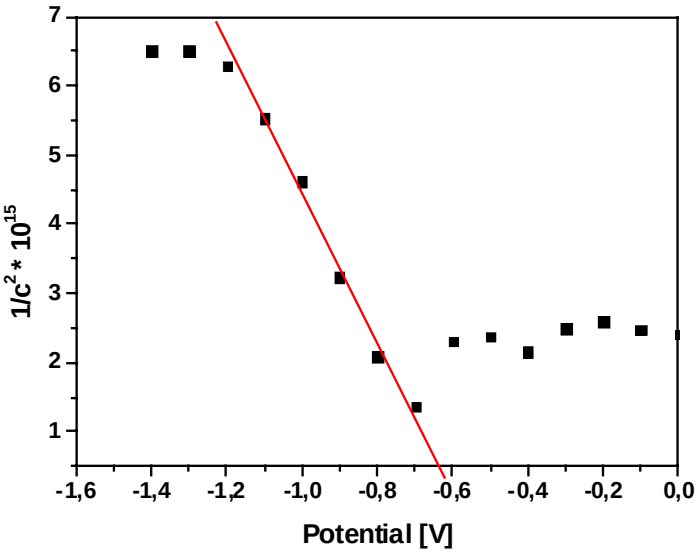

Fig. 5.33 Mott-Shottky plot of PPy film on PMCS-8 modified Ti electrode

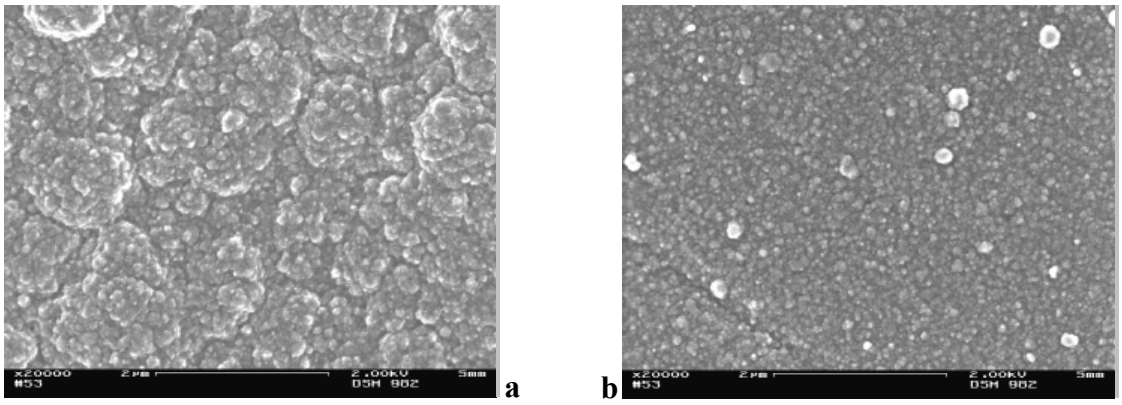

Fig. 5.34 SEM of polypyrrole on (a) bare Ta and (b) Ta electrode modified with PYPA-4. Deposition from 0.1 M pyrrole in 0.1 M $LiClO_4$ in acetonitrile at 10 mV/s scan rate versus SCE.

To investigate these morphological differences, Fig. 5.34 presented polypyrrole films deposited on unmodified and adhesion promoter-modified Ta electrodes (0.1 M $LiClO_4$ in acetonitrile at scan rate 10 mV/s versus SCE). Films deposited on bare Ta electrodes display the morphlogical appearance of polypyrrole [278]. The films deposited on modified electrodes are smoother and less porous, consisting of a dense plane of 5-10 μm features. Moreover, polypyrrole on adhesion promoter modified electrode remained strongly bound to the substrate, contrary to bare and unmodified surfaces as shown by photographs for polymer films submitted to qualitative peel test (Fig. 5.35).

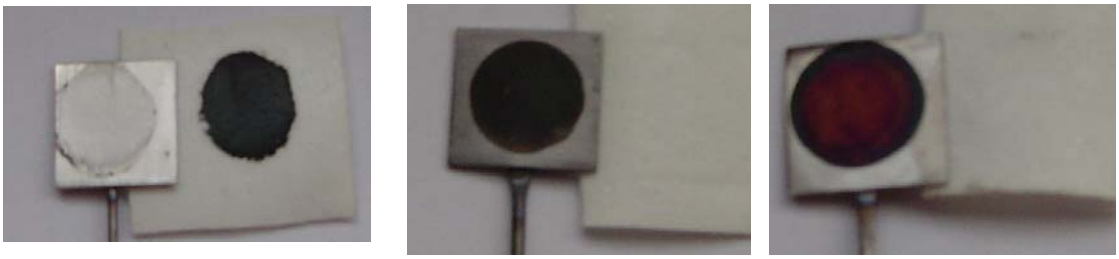

Fig. 5.35 Photographs of polypyrrole films grown in acetonitrile from bare Ti (a) and Ti substrates modified by PMCS (b) and PYPA (c) and submitted to a peel test using 3M adhesive tape.

Chapter 6 Application of Polypyrrole Films

6.1 Polypyrrole Films Used as Humidity Sensors

A sensor is referred to a device, which provides direct information about the chemical composition of its environment [279, 280]. It consists of a physical transducer and a selective layer. In any sensor the sensing process can be divided into two parts; recognition, which results in selectivity, and amplification, which increases the power of the usually weak signals to the level at which it can be conveniently manipulated by electronics. Selectivity is the "HEART" of the design in all the sensors. It is invariably provided by a material in which some selective interaction of species of interest takes place as electrical current or potential or conductivity, intensity of light, mass, temperature, etc.

A number of conventional organic and inorganic materials have been used as sensing materials for humidity. For example, a number of polymer-based humidity sensors have been examined by Sakai et al and Sata [281-284]. Metal oxides such as porous thin films of alumina have been used for humidity sensors since the 1940s [285]. In recent years, sensors based on conducting polymers have been successfully demonstrated for a range of polymer types. Heteroatomic polymers can act as gas and humidity sensors [286, 287]. In particular, humidity and gas sensors using polypyrrole as sensing material have been described [288-293]. After exposure to organic gas or vapor, the conductivity of conducting polymers can reversibly return to the original value. The reversibility is a main feature for most sensing applications, when conducting polymers are exposed to humidity or bulk water the reactions between water molecules and the polymers lead to an irreversible increase in resistivity (a decrease in conductivity). Unlike gas or organic vapors, water molecules appear to be strongly bound to the PPy backbone and / or react with the associated doping. At present, the reaction mechanism between PPy and water molecules is not well understood. For most applications, the effect of humidity/water on the conductivity of conducting polymers has been seen as an advantage [294]. However, the magnitude of the response to water can be an advantage for those applications in which the arrival of moisture is the information required. The sensors can be applied in portable equipment for safety and health purposes, for instance for (house) painters.

Depending on the operating principles, the humidity sensors can be classified into three categories based on

- The change in electrical resistivity;
- The change in capacitance;
- The gravimetric change on absorbing water vapour (eg. quartz crystal oscillator).

6.1.1 Soluble Polypyrrole Used as Humidity Sensors

Here our sensing materials were based on soluble 3-substituted polypyrroles with phosphonic acid group. The polymer films were prepared by spin-coating of these synthesized 3-substituted polypyrroles on a ceramic substrate having two Al electrodes on them. The thickness of the polymer films is about 200 nm. This sample was measured DC/AC kinetics under wet and dry gas influence: The DC current or AC capacitance (Cs or Cp), resistance (Rs or Rp) or conductivity (G) signals were detected with constant voltage level. The measurement was controlled by PC and during the measurement by switching the wafer, one could change the gas flow from dry to wet state or oppositely from wet to dry state. The system RH (relative humidity) changing response time is less than 2 sec. Thus, the influence by the system description is negligible. With applying the extended voltage on samples (U < 40 V), one could measure the kinetics influenced by the additional electrical field.

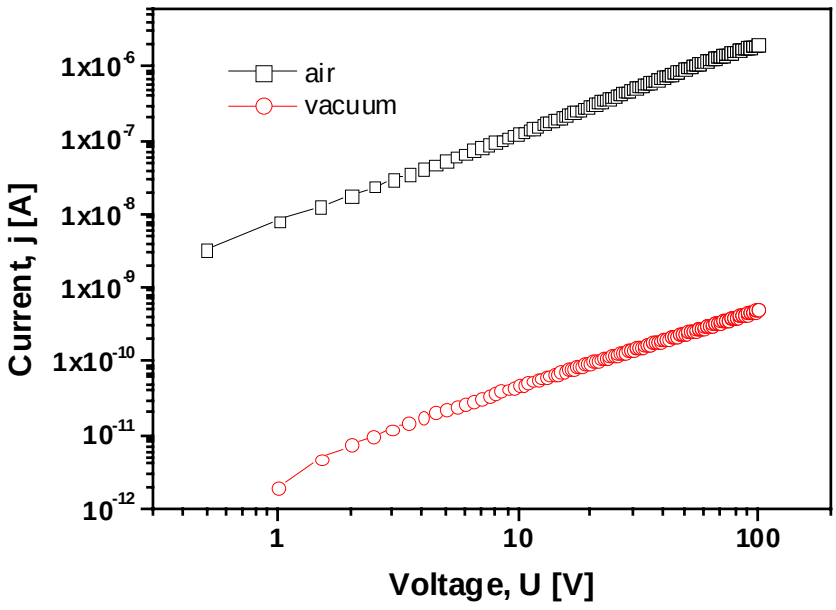

Fig. 6.1 Changes of DC current with voltage in vacuum and on air (sample: polyPYPA-6)

The change of DC electric current with applying voltage in vacuum and on air was shown in Fig. 6.1. It was clearly that the current of the sample measured on air was three orders of

magnitude higher than that of the sample kept in vacuum. This indicated that 3-substituted phosphonic acid polypyrrole was sensitive to moisture.

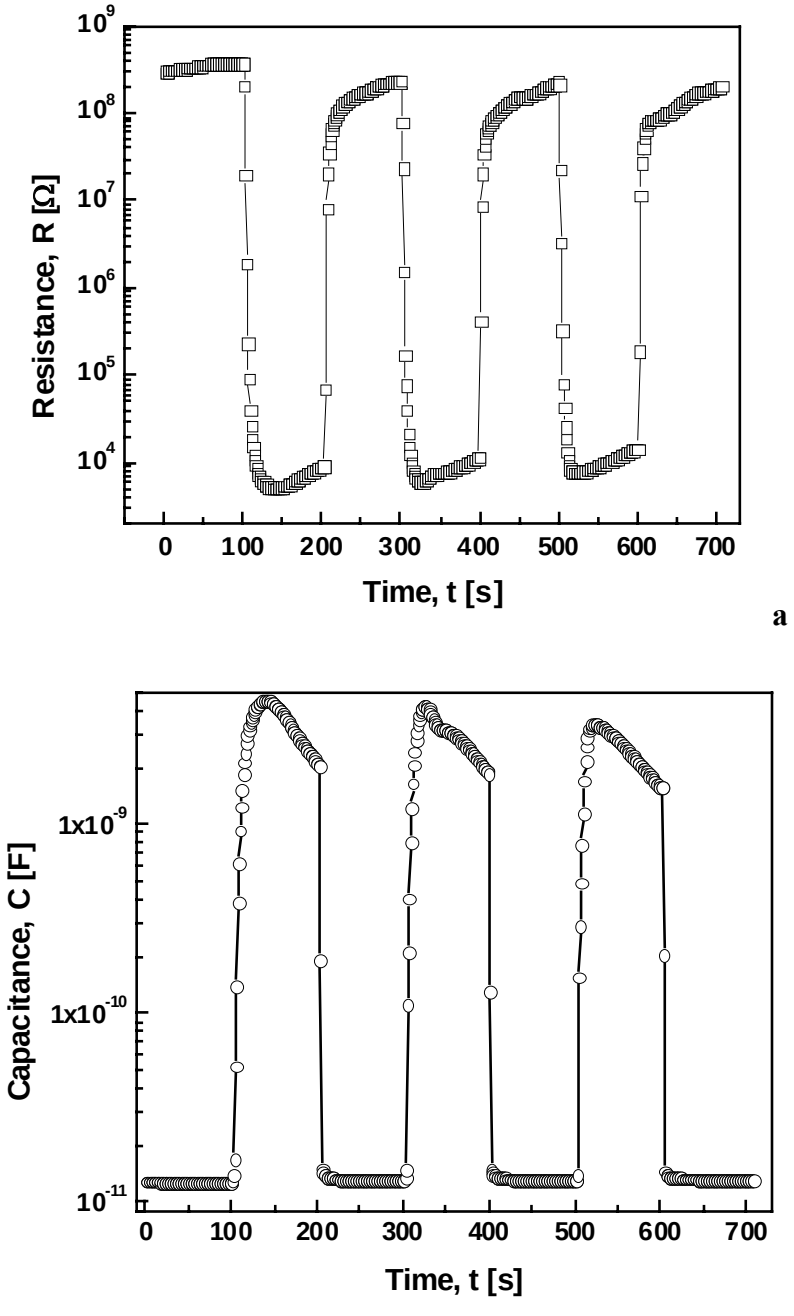

Fig. 6.2 Changes of the resistance (a) and capacitance (b) with the RH change from 2.5% to 96%.

The changes of the resistance and capacitance for relative humidity changes from 2.5 to 96 % (fast changing during about 2 sec realized by the switching between dry and wet flowing nitrogen) are given in Fig. 6.2. The change of the resistance was more than four orders of magnitude (thickness of the film was ca. 200 nm); for thinner layers even larger changes could be detected. Similar changes were also observed in DC conductivity. Figure 6.2b showed that capacitance changes were more than two orders of magnitudes. It could be

pointed out that both resistance and capacitance changes were stable and fully reproducible. It proved that it is possible to fabricate some sensor devices based on PPy materials for humidity change determination.

The electrical responses of the polymer have contributions from two distinct and additive factors. The first (electrical effect) results from in the interaction of H2O with the conjugated polymer backbone causing a change in the charge carrier concentration or charge carrier mobility with a change in the resistance of the film. The second results from a solvent-type interaction causing a resersible swelling of the polymer and resulting in a change in resistance may be due to a reduction of the charge hopping between polymer chains. The swelling –type interation would be influenced by the nature of the sidechains with H2O able to interact via van der Waals forces/H-bonding and be adsorbed into the polymer materials. A major reason is that the mode of response for polypyrrole is reported to be predomaintly due to a proton transfer mechanism. When the water physisorption on the polymer film surface, under an externally applied electric field, polarization of electronic change of the adsorbed water molecules which posses a high dielectrical constant formed dipoles and reorient freely resulting in additional free hole charge carriers which cause an increase in conductivity and thus a decrease in resistivity.

6.1.2 Polypyrrole Films on Modified Substrate Used as Humidity Sensors

We also measured the polypyrrole films produced by chemical deposition of polypyrrole on the silane-modified substrates. The samples were prepared as described in chapter 5.4.5. Fig. 6.3 showed the j-V plot in different environment.

When the sample was exposed to air, the current was higher compared with that of measured in vacuum or in nitrogen. This means that the conductivity is strongly influenced by the moisture. Under the influence of humidity one can expect dissociation of the molecule and formation of two types of species: ion-pairs and free charge carriers after full dissociation in external electric field. The formation of dipolar species results in the broadening of the transport hopping state distribution. Thus, the charge carrier mobility decreases and electric permittivity increases. On the other hand, full dissociation results in the formation of free charge carriers, which can move in the transport polymer matrix. Because electrical conductivity is the product of the unit charge, charge carrier mobility, μ, and free charge carrier concentration, n, the final change of the conductivity under the humidity exposure depends on the equilibrium of the changes $\Delta\mu$ and Δn. In our case the contribution to the

conductivity of the increase in free charge carrier concentration is higher than the decrease in charge mobility; thus, both AC and DC conductivity increase. Such kind of material used as humidity sensor based on FET was described later.

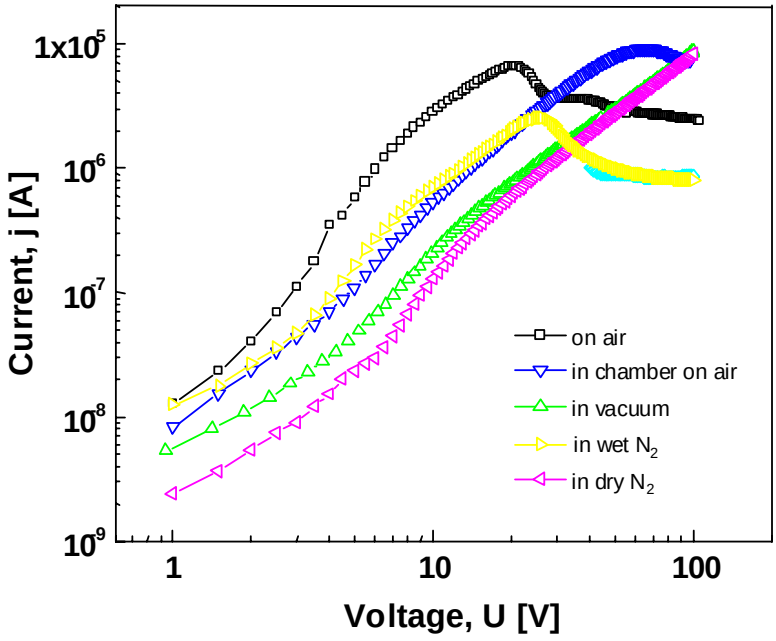

Fig. 6.3 The current-voltage characteristics for Si/SiO_2/PPy/Al sample (thickness = 87 nm) in different measurement environments.

6.2 Polypyrrole Films Used as FET

Among the various application of conducting polymers, one of the most promising applications is organic field-effect transistors (OFETs) and integrated circuits [295]. Conjugated polymers have a disadvantage as low carrier mobility due to the presence of molecular disorder or impurities, which act as traps. It was found that the high mobilities are related to self-organization of the polymer chain in the solid state [296]. Several chemical field-effect-transistors have been described using the principle of field effect [31].

The Source-Drain j-U characteristics of FETs were measured by applying the extended constant gate voltage (U_g) on the sample, detail arrangement was shown in Fig. 6.4.

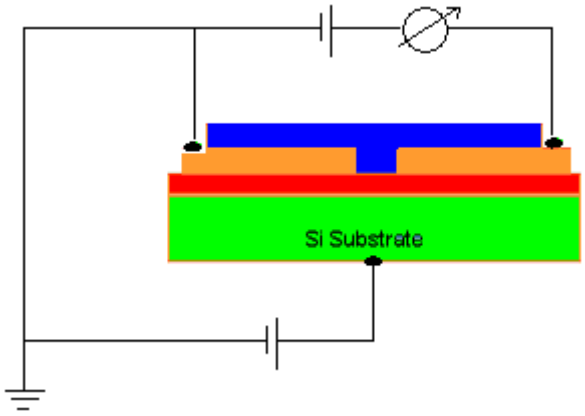

Fig. 6.4 Measurement arrangement of FET structure

OFETs devices based on PPy film deposited by surface chemical polymerization were prepared. The typical film thickness about 100 nm was controlled by polymerization condition. The advantage of such technique was the good adhesion of PPy film on the substrates due to the adhesion promoter. Fig. 6.5 gave the source-drain j-V characteristics for different gate voltages.

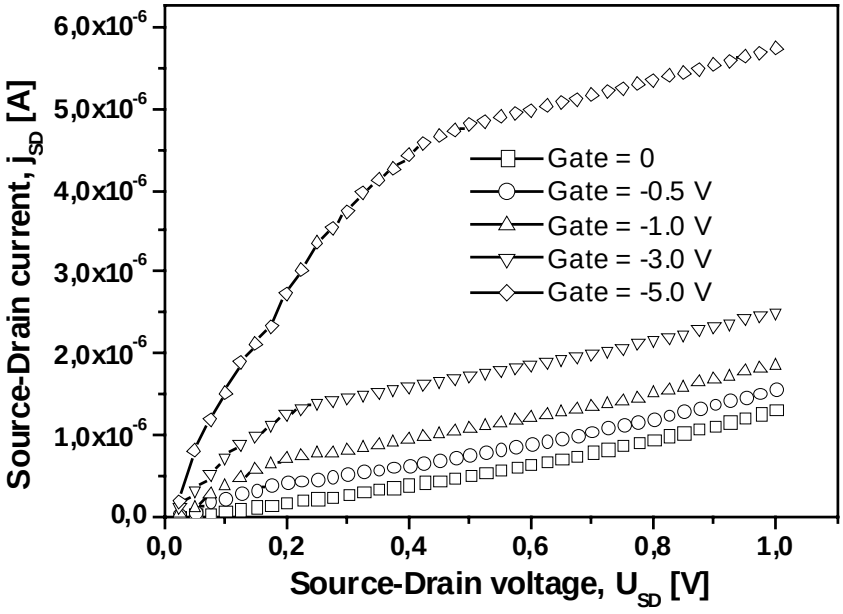

Fig. 6.5 Source-drain j-U characteristics under different gate voltages measured in vacuum at room temperature.

It was difficult to calculate the charge carrier mobility based on the saturated source-drain current because of the unsaturated current shape. Thus, the linear model was used for the field-effect charge carrier mobility calculation. Based on Eq. 6.1:

$$j_{sd} = \frac{Z}{L}\mu C_i\left[(U_g - U_t)U_d - \frac{U_d^2}{2}\right] \qquad \text{Eq. 6.1}$$

where Z = 5 mm, L = 20 μm, $C_i = 2 \times 10^{-4}$ F/m^2, the field-effect charge carrier mobility μ can be calculated as $\mu = 6 \times 10^{-3}$ cm^2/ V s. The unsaturated high voltage part can be explained by Channel length modulation, which is caused by the increase of the depletion layer width at the drain as the drain voltage is increased. This leads to a shorter channel length and an increased drain current. The channel-length-modulation effect typically increases in small devices with low-doped substrates. An extreme case of channel length modulation is punch through where the channel length reduces to zero. Proper scaling can reduce channel length modulation, namely by increasing the doping density as the gate length is reduced.

Chapter 7 Conclusion and Outlook

7.1 Conclusion

For grafting adhesive polypyrrole films on substrates, adhesion promoters were used to connect polypyrrole films and substrates. The 3-substituted pyrrole and 1-substituted pyrrole derivatives with two functionalized groups were designed as adhesion promoters between PPy film deposited chemically or electrochemically on oxide or metal substrates, with the pyrrole moieties incorporated into the PPy film and another anchoring group bonded to the substrate. The anchoring group was designed according to the characterization of the substrate surface. For the acidic SiO_2 surface, organosilanes (trichlorosilane, monochlorosilane, trimethoxysilane) were used. For amphiphilic or basic characteristic surface, such as Ti/TiO_2, Ta/Ta_2O_5, Al/Al_2O_3, and Fe/Fe_2O_3, the phosphonic acid group was used. The spacer groups between terminal group and head group with different alkyl chain length from 4-carbons to 16-carbons in the monomer were investigated.

ω-(pyrrol-3-yl alkyl) phosphonic acids, 11-(pyrrol-3-yl undecyl) trimethoxysilanes and ω-(pyrrol-1-yl alkyl) organosilanes were successfully synthesized and characterized by IR, NMR, elemental analysis. ω-(pyrrol-3-yl alkyl) phosphonic acids and ω-(pyrrol-1-yl alkyl) organosilanes are commonly new compounds. They have not been reported in any literature. From the synthetic procedures and yields, the synthesis of 3-substituted pyrrole derivatives was more difficult and complicated compared to the synthesis of 1-substituted pyrrole derivatives. And the synthesis of the shorter chain length pyrrole derivatives is not easy as compared to the longer chains due to the easy polymerization of the reactive system.

The synthesized compounds were studied for their adsorption behavior on the oxide substrate using contact angle measurement, ellipsometry, SPR, grazing incident FTIR, UV-VIS spectroscopy, and angle resolved XPS etc.

Contact angle measurement and ellipsometry data showed that high concentrations in apolar hydrocarbon solvent (bicyclohexyl) and long reaction times (tens hours/several days) are sufficient to form tightly packed monolayer of ω-(pyrrol-1-yl alkyl) monochlorosilanes (PMCS) on substrates. The thickness of these monolayers is from 0.8 nm to 2.6 nm depending on alkyl chain length. The longer alkyl chain length resulted in well-packed monolayers. Compared with PMCS, ω-(pyrrol-1-yl alkyl) trichlorosilanes (PUTS) can be grafted on the oxide substrate in low concentration (0.03%v) and shorter reaction times (5 min) to yield

dense monolayers, but their oligomerization during adsorption should be controlled. For the same chain length, a more compact monolayer was obtained from PUTS-11 compared to PMCS-11. Considering the easy oligomerization of PUTS, thus, PMCS appears more favorable for the grafting of monolayer on SiO_2 surface with the reaction requirement.

Adsorption kinetics were studied by SPR and showed that the adsorption took place within a few seconds, then it continuously increased and reached a plateau. Grazing incident FTIR showed the presence and shifting of symmetric and asymmetric CH_2-strectching vibration, revealing the presence and the order of the monolayer. A long adsorption time presented well-ordered monolayer of PMCS. The orientation of the monolayer was determined by XPS. Angle-resolved XPS indicated that the silane group of PMCS and PUTS are preferentially adsorbed on the oxide surface and the pyrrole groups are away from the surface.

The same study was used to investigate the adsorption behavior of 11-(pyrrol-3-yl undecyl) trimethoxysilane (3-PyTMS). The two functional groups, trimethoxysilane and the NH group from pyrrole, have the possibility to react with the OH groups from the oxide substrate surface. XPS measurement revealed that trimethoxysilane is attached to the oxide surface and pyrrole group on top, and the adsorbed layer is a multilayer due to the possible formation of H-bond between NH from pyrrole and oxygen atom from trimethoxysilane, or the formation of vertical polymerization. The measured thickness by XPS is about 3.12 nm, it is bigger than the calculated thickness of 2.26 nm.

For the amphiphilic or basic surface, such as Ti/TiO_2, Ta/Ta_2O_5, Al/Al_2O_3, and Fe/Fe_2O_3, phosphonic acid group was used as anchoring group. Contact angle data showed that more compact adsorbed layers on the metal substrates were obtained from the longer alkyl chain derivatives (PYPA). Angle-resolved XPS revealed that the phosphonic acid group adsorbed on the metal surface and pyrrole group is away from the surface. XPS data also showed that in the case of 6-(pyrrol-3-yl hexyl) phosphonic acid, a uniform, well-oriented adsorbed layer was formed on the Ti and Al surfaces compared to that on the Ta surface.

The orientation of these synthesized monomers was assumed to be suited as adhesion promoter. Surface deposition of polypyrrole on the adhesion promoter modified (silane-modified and phosphonic acid-modified) substrates by chemical and electrochemical polymerization were investigated. PPy films formed on the modified surfaces by surface chemical polymerization showed a better adhesion compared to those on the unmodified surfaces. UV-VIS and Raman data revealed that the films are in their oxidizing state, but low

doping level. The morphology of PPy films was influenced by the alkyl chain length of the adhesion promoter and the deposition condition, such as choice of oxidant and solvent. PPy films deposited on modified substrate with longer alkyl chains adhesion promoter have a smoother morphology than that of films on adhesion promoter with shorter alkyl chains. The thickness of the resulting PPy films were controlled by the polymerization conditions, such as choice of solvent, deposition time, pyrrole to oxidant ratio and monomer concentration. PPy films with thickness in the range of 10-400 nm adhered firmly on the surface. The electrical properties were studied by current-voltage (j-V) measurement. The current-voltage (j-V) characteristics of the polypyrrole film revealed that the charge transport is mainly governed by the thermionic emission in the thinner films. Temperature dependence of j-V characteristics of Si/SiO_2/Ppy/PMCS-16/Al films revealed that the current increases with temperature, the film shows a typical semiconductor behavior. At room temperature the mobility for positive charge carriers is 1.4×10^{-4} $cm^2 \cdot V^{-1}/s$, two order of magnitude higher than the values reported in the literature for the electrodeposited PPy films [275] and lower than the highest mobility value reported in the literature for PPy (ab. 10^{-1} $cm^2 \cdot V^{-1}/s$), which was observed in p-toluene sulfonate doped PPy [276].

The use of these adhesion promoters modified electrode for electrochemical polymerization resulted in adhesive polypyrrole films. The presence of adhesion promoter enhances the morphological packing of polypyrrole, affording a smooth, compact film. EIS measurement and Mott-Schottky plot indicated that polypyrrole is a p-type semiconductor.

Also the 3-substituted pyrrole phosphonic acids were found to be homo-and co-polymerizable (with pyrrole) under chemical methods. $Na_2S_2O_8$ was used as oxidant and MeOH as solvent. IR, UV-VIS, and TGA, DSC investigated these homopolymers and copolymers. IR and UV-VIS data showed that these polymers are all in low doping level. TGA and IR data revealed that copolymers are real copolymers instead of mixture of two homopolymers. TGA also showed that homopolymers are less stable than polypyrrole due to the 3-substituent. The most interesting thing about the copolymers and homopolymers is that they show a glass transition temperature.

The 3-substituted homopolypyrrole films obtained by spin coating were tried to use as humidity sensors. It is observed that the resistivity of the 3-substituted homopolypyrrole sensors increases and capacitance decreases during exposure to humid air. The polypyrrole films obtained by surface chemical polymerization were also used as FET. The field-effect charge carrier mobility μ can be calculated as $\mu = 6 \times 10^{-3}$ $cm^2/ V s$.

7.2 Outlook

Polypyrrole films proved to be used as humidity sensors. Recently, there has considerable interest in using polypyrrole to manufacture sensing devices for organic volatile compounds. Aroma sensors can become essential instruments for quality control of beverages and food products and for environmental monitoring, especially if simple and inexpensive devices that provide accurate real time discrimination of chemical scents can be developed. The sensitiveness of conducting polymers to environmental changes usually lack specificity. The corrresponding samples tend to exhibit a broad reponse band for different gases and vapors and this precludes their use as independent sensors. The fast response of thin films to adsorption and desorption of volatile compounds will be a biggest challenge in the future.

One of the most interesting of research in conducting polymers lies in the development of biosensing devices (usually called biosensors or receptrodes). Titanium has been considered as the metallic biomaterials of choice, a field where is a need to control surface modifications of the oxide layer. Another interesting thing is in the field of bone implants. The interaction between the metal surface of the biomaterial and the newly formed bone tissue is known to be critical for the success of the implant setting.

After the first reported works by Mengoli et al. [297] then DeBerry [298] on the corrosion protection of metal by inherently conducting polymers, there have been attempts both to propose a comprehensive mechanism as well as to optimize the protection efficiency of these films against corrosion. Conducting polymers play the role of barriers, which may hinder the transpot of cathodic reactants, e.g. dissolved oxygen in neutral media, towards the metal or the removal of the corrosion products from the metal. On the other hand, inorganic films and in particular noble metals, can be used as protective coatings to cover less noble metals, which possess a passivity domian, and therefore, initiate anodic galvanic protection. So investigating of the corrosion affored by polypyrrole films, finding optimum protection conditions and understanding the reasons for the loss of protection are an interesting topic.

References

[1] R. L. Greene, G. B. Street, L. J. Sutude, *Phys. Rev. Lett*. 34 (1975) 577.

[2] H. Shirakawa, E. J. Louis, A. G. MacDiarmid, C. K. Chiang, A. J. Heeger, *J. Chem. Soc. Chem. Commun.* (1977) 578.

[3] T. A. Skotheim, *Handbook of Conducting Polymers*, Vol. 1 &2, Marcel Dekker, New York, 1986.

[4] K. S. V. Srinivasan, *Macromolecules*, New Frontiers, Vol. 1 &2, Allied Publishers, India, 1998.

[5] T. S. Moss, *Handbook of Semiconductors*, Vol. 1, Elsevier, Amsterdam, 1992.

[6] R. S. Kohlman, J. Joo, A. J. Epstein, J. E. Mark, editor. *Physical properties of polymers handbook*, New York: American Institute of Physics, 1996 (453pp. And references therein).

[7] J. H. Burroughes, C. A. Jones, R. H. Friend, *Nature*, 335 (1988) 137.

[8] R. H. Baughman, L. W. Shacklette, R. L. Elsenbaumer, E. J. Plichta, C. Becht, In: P. I. Lazarev, editor. *Molecular electronics*, Dordrecht: Kluwer Academic, 1991.

[9] T. F. Otero, Rodriguez. In: M. Aldissi, editor. *Intrinsically conducting polymers: an emerging technology*, Dordrecht: Kluwer Academic, 1993.

[10] V. Saxena, B. D. Malhotra, *Current Appl. Phys*.3 (2003) 293.

[11] J. Gao, A. J. Heeger, J. Y. Lee, C. Y. Kim, *Synth. Met*. 82 (1996) 221.

[12] S. Radhakrishnan, P. Somani, *Mater. Lett*. 37 (1998) 192.

[13] J. A. Pomposo, J. Rodriguez, H. Grande, *Synth. Met*. 104 (1999) 107.

[14] J. Miasik, A. Hopper, B. C. Tofield, *J. Chem. Soc. Faraday Trans. I* 82 (1986) 1117.

[15] L. S. Hwang, J. M. Ko, H. W. Rhee, C. Y. Kim, *Synth. Met*. 55-57 (1993) 3671.

[16] G. E. Collins, L. J. Buckley, *Synth. Met.* 78 (1996) 93.

[17] R. M. L. Van de Leur, A. Van der Waal, *Synth. Met*. 102 (1999) 1330.

[18] J. E. G. De Souza, B. B. Neto, F. L. Dos Santos, C. P. De Melo, M. S. Santos, T. B. Ludemir, *Synth. Met.* 102 (1999) 1296.

[19] H. Nguyen Thi Le, B. Garcia, C. Deslouis, Q. Le Xuan, *Electrochimica Acta* 46 (2001) 4259.

[20] G. S. Akundy, J. O. Iroh, *Polymer* 42 (2001) 9665.

[21] C. A. Ferreira, S Aeiyach, A. Coulaud, P. C. Lacaze, *J. Appl. Electrochem*. 29(1999) 259.

[22] K. Kaneto, S. Takeda, K. Yoshino, *Jpn. J. Appl. Phys.* 24 (1985) L 553.

[23] S. Miyauchi, Y. Goto, I. Tsubata, Y. Sorimachi, *Synth. Met*. 41-43 (1991) 1051.

[24] Y. Lvov, G. S. Decher, *Macromolecules*, 26 (1993) 5396.

[25] G. Decher, J. Hong, J. Schmitt, *Thin Solid Films,* 210-211 (1992) 831.

[26] W. Chen, T. J. McCarthy, *Macromolecules*, 30 (1997) 78.

[27] M.K. Ram, M. Salerno, M. Adami, P. Faraci, C. Nicolini, *Langmuir*, 15 (1999) 1252.

[28] A. C. Fou, M. F. Rubner, *Macromolecules*, 28 (1995) 7115.

[29] J.H. Cheung, W.B. Stockton, M. F. Rubner, *Macromolecules*, 30 (1997) 2712.

[30] W. B. Stockton, M. F. Rubner, *Macromolecules*, 30 (1997) 2717.

[31] H. Hong, D. Davidov, Y. Avany, H. Chayet, E. Z. Faraggi, R. Neumann, *Adv. Mater.* 7 (1995) 846.

[32] A. C. Fou, F. M. Onitsuka, D. Howie, M. F. Rubner, *Polym. Mater. Sci. Engng.* 72 (1995) 160.

[33] Z. G. Qi, N. G. Rees, P. G. Pickup, *Chem. Mater.* 8 (1996) 701.

[34] A. Deronzier, J. C. Moutet, Coord. *Chem. Rev*. 147 (1996) 339.

[35] R. Singh, A. K. Narnla, R. P. Tandon, A. Mansingh, S. Chandra, *J. Appl. Phys.* 79 (1996) 1476.

[36] J. Y. Quyang, Y. F. Li, *Synth.Met.* 75 (1995) 1.

[37] E. L. Kupila, J. Kanare, *Synth. Met*. 74 (1995) 241.

[38] B. Sun, D. P. Schweinsberg, *Synth. Met*. 68 (1994) 49.

[39] C. N. Sayre, D. M. Collard, *Langmuir*, 13 (1997) 714.

[40] R. J. Willcut, R. L. McCarley, *J. Am. Chem. Soc*. 116 (1994) 10823.

[41] J. Kowalik, L. Tolbert, Y. Ding, L. A. Bottomley, *Synth. Met*. 55-57 (1993) 1171.

[42] E. Sabatani, Y. Gafni, I. Rubinstein, *J. Phys. Chem.* 99 (1995) 12305.

[43] Z. Mekhalif, J. Delhalle, P. Lang, F. Garnier, J.-J. Pireaux, *Synth. Met*. 96 (1998) 165.

[44] L. F. Rozsnyai, M. S. Wrighton, *Chem. Mater*. 8 (1996) 309.

[45] A. Simon, A. J. Ricco, M. S. Wrighton, *J. Am. Chem. Soc*. 104 (1982) 2031.

[46] C.-G. Wu, C.-Y. Chen, *J. Mater. Chem*. 7 (1997) 1409.

[47] A. Guiseppi-Elie, A. M. Wilson, J. M. Tour, T. W. Brockmann, P. Zhang, D. L. Allara, *Langmuir,* 11 (1995) 1768.

[48] F. Faverolle, A. J. Attias, B. Bloch, P. Audebert, C. P. Andrieux, *Chem. Mater.* 10 (1998) 740.

[49] D. Cossement, F. Plumier, J. Delhalle, L. Hevesi, Z. Mekhalif, *Synth. Met*. 138 (2003) 529.

[50] T. Yong, *Miscellaneous Works*; G. Peacock, ED.; Murray: London, 1855, Vol. 1, p. 418.

[51] T. Yong, *Philos. Trans. R. Soc. London*, 95 (1805) 65.

[52] R. M. A. Azzam, N. M. Bashara, *Ellipsometry and Polarized Light; North-Holland Publishing Company: Amsterdam,* 1977

[53] F. L. McCrackin, E. Passaglia, R. R. Stromberg, H. L. Steinberg, *J. Res. Natl. Bur. Stand, Sect A.* 67 (1967) 363.

[54] M. Iwamoto, M. Suzuki, T. Hino, *Shin. Ku*. 28 (1986) 693.

[55] J. O. Birzer, H. J. Schulzer, *J. Colloid. Polym. Sci.* 264 (1986) 642.

[56] G. L. Gaines, Jr. *Insoluble Monolayers at Liquid-Gas Interface* ; Interscience : New York, 1966.

[57] S. R. Wasserman, G. M. Whitesides, I. M. Tidswell, B. M. Ocko, P. S. Pershan, J. D. Axe, *J. Am. Chem. Soc.* 111 (1989) 5852.

[58] N. Rozlosnik, M. C. Gerstenberg, N. B. Larsen, *Langmuir*, 19 (2003) 1182.

[59] W. Knoll, *Annu. Rev. Phys. Chem*. 49 (1998) 569.

[60] C. E. Miller, W. H. Meyer, W. Knoll, G. Wegner, Ber. Bunsen-Ges, *Phys. Chem.* 96 (1992) 869.

[61] K. A. Peterlinz, R. Georgiadis, *Langmuir*, 12 (1996) 4731.

[62] B. P. Nelson, T. E. Grimsrud, M. R. Liles, R. M. Goodman, R. M. Corn, *Anal. Chem*. 71 (2001) 1.

[63] W. Knoll, Annu. *Rev. Phys. Chem*. 49 (1998) 569.

[64] I. Pockrand, *Surf. Sci.* 72 (1978) 577.

[65] A. Ishitani, H. Ishida, F. Soeda, Y. Nagaswa, *Anal. Chem.* 54 (1982) 682.

[66] A. Ulman: *An introduction to ultrathin organic films: From Langmuir-Blodgett to Self-Assembly*, Academic Press Inc., San Diego, 1991.

[67] A. Einstein, *Ann. Phys*. 17 (1905) 132.

[68] N. Tillman, A. Ulman, J. Elman, *Langmuir*, 5 (1989) 1020.

[69] N. Tillman, A. Ulman, J. Elman, *Langmuir*, 6 (1990) 1512.

[70] T. Iyoda, M. Ando, T. Kaneko, A. Ohtani, T. Shimidzu, K. Houda, *Tetrahedran Lett*. 1986, 27, 5633.

[71] T. Iyoda, M. Ando, T. Kaneko, A. Ohtani, T. Shimidzu, K. Houda, *Langmuir*, 1986, 3, 1169.

[72] T. Shimidzu, T. Iyoda, M. Ando, A. Ohtani, T. Kaneko, K. Houda, *Thin Solid Films,* 160 (1988) 67.

[73] M. Ando, Y. Watanabe, T. Iyoda, K. Houda, T. Shimidzu, *Thin solid Films*, 179 (1989) 225.

[74] K, Hong, R. B. Rosner, *Chem. Mater*. 2 (9190) 82.

[75] R. B. Dabke, A. Dhanabalan, S. Mahor, S. S. Talwar, R. Lal, A. Q. Contractor, *Thin solid Films*, 335 (1998) 203.

[76] A. Marletta, D. Goncalves, O. N. Oliveira Jr., R. M. Faria, F. E. G. Guimaraes, *Synth. Met*. 119 (2001) 207.

[77] J. F. Penneau, M. Lapkowski, E. M Genies, *New J. Chem*. 13, (1989) 449.

[78] M. K. Ram, E. Maccioni, C. Nicolini, *Thin Solid Films*, 303 (1997) 27.

[79] J. H. Cheung, E. Punkka, M. Rikukawa, M. B. Rosner, A. J. Rorappa, M. F. Rubner, *Thin Solid Films*, 210 (1992) 246.

[80] D. Li, B. I. Swanson, J. M. Robinson, M. A. Hoffbauer, *J. Am. Chem. Soc*. 115 (1993) 6975.

[81] R. G. Nuzzo, D. L. Allara, *J. Am. Chem. Soc*. 105 (1983) 4481.

[82] R. G. Nuzzo, F. A. Fusco, D. L. Allara, *J. Am. Chem. Soc*. 109 (1987) 2358.

[83] R. Maoz, L. Netzer, J. Gun, J. Sagiv, *J. Chim. Phys. (Paris),* 85 (1988) 1059.

[84] L. Netzer, J. Sagiv, *J. Am. Chem. Soc.* 105 (1983) 674.

[85] N. Tillman, A. Ulman, T. L. Penner, *Langmuir*, 5 (1989) 101.

[86] H. O. Finklea, L. R. Robinson, A. Blackburn, B. Richter, D. Allara, T. Bright, Langmuir, 2 (1986) 239.

[87] D.L. Allara, A. N. Parikh, F. Rondelez, *Langmui*r, 11 (1995) 2357.

[88] C. Jung, O. Dannenberger, Y. Xu, M. Buck, M. Grunze, *Langmuir*, 14 (1998) 1103.

[89] M. R. Linford, C. E. D. Chidsey, *J. Am. Chem. Soc*. 115 (1993) 12631.

[90] A. R. Pike, S. N. Patole, N. C. Murray, T. Ilyas, B. A. Connolly, B. R. Horrocks, A. Houlton, *Adv. Mater*. 15 (2003) 254.

[91] W. Gao, L. Dickinson, C. Grozinger, F. G. Morin, *Langmuir*, 12 (1996) 6429.

[92] I. Maege, E. Jaehne, A. Henke, H.-J. P. Adler, C. Bram, M. Stratmann, *Macromol.Symp*. 126 (1997) 7.

[93] D. Brovelli, G. Haehner, L. Ruiz, R. Hofer, G. Kraus, A. Waldner, J. Schloesser, P. Oroszlan, M. Ehrat, N. D. Spencer, *Langmuir*, 15 (1999) 4325.

[94] G. Busch, E. Jaehne, X. Cai, S. Oberoi, H.-J. P. Adler, *Synth. Met*.137 (2003) 871.

[95] E. B. Troughton, C. D. Bain, G. M. Whitesides, R. G. Nuzzo, D. L. Allara, M. D. Porter, *langmui*r, 4 (1984) 365.

[96] D. L. Allara R. G. Nuzzo, *Langmuir*, 1 (1985) 52.

[97] N. E. Schlotter, M. D. Porter, T. B. Bright, D. L. Allara, *Chem. Phys. Lett*. 132 (1986) 93.

[98] D. L. Allara, *Atomic and Nanometer-scale modifications of materials fundamentals and applications* 1993, 275.

[99] P. E. Laibinis, C. D. Bain, G. M. Whitesides, *J. Phys. Chem*. 95 (1991) 7017

[100] P. E. Laibinis, G. M. Whitesides, D. L. Allara, Y.-T- Tao, A. N. Parikh, R. G. Nuzzo, *J. Am. Chem. Soc*. 113 (1991) 7152.

[101] P. E. Laibinis, G. M. Whitesides, *J. Am. Chem. Soc*. 114 (1992) 1990.

[102] J. Sagiv, *J. Am. Chen. Soc*. 102 (1980) 92.

[103] J. Breme, V. Biehl, A. Hoffman, *Adv. Eng. Mater*. 2 (2000) 270.

[104] J. S. Quinton, P. C. Dastdoor, *Surf. Interface Anal*. 28 (1999) 12.

[105] S. Mishra, J.J. Weimer; J. Adhes. *Sci. Technol*. 11 (1997) 337.

[106] D. Cossement, Y. Delrue, Z. Mekhalif, J. Delhalle; L. Hevesi, *Surf. Interface Anal.* 30 (2000) 56.

[107] E. De Giglio, M. R. Guascito, L. Sabbatini, G. Zambonin, *Biomaterials* 22 (2001) 2609.

[108] A. H. Carim, M. M. Dovek, C. F. Quate, C. Vorst, *Science*, 237 (1987) 630.

[109] I. Mage, E. Jaehne, H. -J. P. Adler, A. Henke, and C. Jung, C. Bram, *Prog. In. Org. Coatings*, 34 (1998) 1.

[110] M. Agular, N. Satre, *Inorg. Chem*. 10 (1989) 93.

[111] M. D. Francis, R. G. Rusell, *Science*, 165 (1969) 1264.

[112] G. Cao, G. Hong, Acc. *Chem. Res*. 25 (1990) 420.

[113] J. Breme, V. Biehl, A. Hoffmann, *Adv. Eng. Mater*. 2 (2000) 270.

[114] W. Laureyn, D. Nelis, P. Van Gerwen, K. Baert, L. Hermans, R. Magnee, J. J. Pireaux, G. Maes, *Sensors Actuators B*, 68 (2000) 360.

[115] J. P. Folkeers, G. Whitesides, S. Bucholz, *Langmu*ir, 11 (1995) 813.

[116] G. L. Duveneck, M. Pawlak, D. Neuschaefer, E. Baer, U. Pieles, M. Ehrat, *Sens. Actuators B,* 38-39 (1997) 88 .

[117] C. D. Bain, E. B. Troughton, Y.-T. Tao, J. Evall, G. M. Whitesides, R. G. Nuzzo, *J. Am. Chem. Soc*. 111 (1989) 321.

[118] X.-M. Zhao, J. L. Wilbur, G. M. Whitesides, *Langmuir*, 12 (1996) 3257.

[119] E. P. Plueddemann, *Silane Coupling Agents*. Plenum Press: New York, 1991

[120] D. G. Kurth, T. Bein, *Langmuir*, 11 (1995) 3061.

[121] D. L. Angst, G. W. Simmons, *Langmuir*, 7 (1991) 2236.

[122] H. Brunner, T. Vallant, U. Mayer, H. Hoffmann, *Surf. Sci*. 368 (1996) 279.

[123] R. Helmy, A. Y. Fadeev, *Langmuir*, 18 (2002) 8924.

[124] I. Rubinstein, J. Rishpon, E. Sabatini, A. Redondo, S. Gottesfeld, *J. Am. Chem. Soc*. 112 (1987) 6135.

[125] J. Kowalik, L. Tolbert, Y. Ding, L. Bottomley, K. Vogt, P. Kohl, *Synth. Met*. 55 (1993) 1171.

[126] R. J. Willcut, R. L. McCarley, *J. Am. Chem. Soc*. 116 (1994) 10823.

[127] R. J. Willcut, R. L. McCarley, *Langmuir*, 11 (1995) 296.

[128] R. J. Willcut, R. L. McCarley, *Anal. Chim. Acta*. 307 (1995) 269.

[129] R. J. Willcut, R. L. McCarley, *Adv. Mater*. 7 (1995) 759.

[130] D. M. Collard, C. N. Sayer, *J. Electroanal. Chem*. 375 (1994) 367.

[131] D. M. Collard, C. N. Sayer, *Synth. Met*. 69 (1995) 459.

[132] C. N. Sayer, D. M. Collard, *Langmuir*, 11 (1995) 302.

[133] M. Nishizawa, Y. Miwa, T. Matsue, I. Uchida, *J. Electrochem. Soc*. 140 (1993) 1650.

[134] Z. Mekhalif, P. Lang, F. Garnier, *J. Electroanal. Chem*. 399 (1995) 61.

[135] R.-K. Lo, J. E. Ritchie, J.-P. Zhou, J. Zhao, J. T. McDevitt, F. Xu, C. A. Mirkin, *J. Am. Chem. Soc*. 118 (1996) 11295.

[136] A. Simon, A. J. Ricco, M. S. Wrighton, *J. Am. Chem. Soc*. 104 (1982) 2031.

[137] C.-G. Wu, C.-Y. Chen, *J. Mater. Chem*. 7 (1997) 1409.

[138] A. Guiseppi-Elie, A. M. Wilson, J. M. Tour, T. W. Brockmann, P. Zhang, D. L. Allara, *Langmuir*, 11 (1995) 1768.

[139] F. Faverolle, A. J. Attias, B. Bloch, P. Audebert, C. P. Andrieux, *Chem. Mater*. 10 (1998) 740.

[140] Z. Huang, P.-C. Wang, A. G. MacDiarmid, Y. Xia, G. Whitesides, *Langmuir*, 13 (1997) 6480.

[141] H. O. Finklea, *Self-assembled monolayers on Eletcrodes* , in Encyclopedia of Analytic Chemistry, Edited by R. A. Meyers, © John Wiley & Sons Ltd, Chichester, 1999.

[142] D. J. Cram, B. Rickborn, G. R. Knox, *J. Amer. Chem. Soc.* 82 (1960) 6412.

[143] D. J. Cram, B. Rickborn, C. A. Kingsbury, P. Haberfield, *ibid.,* 83 (1961) 3678.

[144] C. F. Hobbs, C. K. Mcmillin, P. Papdopoulos, C. A. VanderWerf, *J. Amer. Chem. Soc.,* 84 (1962) 43-51.

[145] H. Heaney, S. V. Ley, *J. Chem. Soc., Perkin I*, 1 (1973) 499-500.

[146] C. F. Candy, R. A. Jones, *J. Org. Chem*. 36 (1971) 3993.

[147] N. Wang, K. Teo, H. J. Anderson, *Can. J. Chem.* 55 (1977) 4112.

[148] V. Bocchi, G. Casnati, A. Dossena, F. Villani, *Synthesis*, 1976, 414.

[149] W. C. Guida, D. J. Mathie, *J. Org. Chem*. 45 (1980) 3172-3176.

[150] D. Cossement, C. Pierard, J. Delhalle, J.-J. Pireaux, L. Hevesi, Z. Mekhalif, *Surf. Interface Anal*. 31 (2001) 18-22.

[151] G. Inzeelt, V. Kertesz, A. Nyaback, *J. Solid State Electrochem*. 3 (1999) 251-257.

[152] A. R. Pike, S. N. Patole, N. C. Murray, *Adv. Mater*. 15 (2003) 254-257.

[153] J. L. Speier, *Adv. Organomet. Chem*. 17 (1979) 407.

[154] T. Hiyama, T. Kusumoto, *Comprehensive Organic Synthesis*, 8 (1991) 763.

[155] I. Ojima, *In the chemistry of organic silicon compounds*, S. Patoi, Z. Rappoport (Eds.), John Wiley: Chichester, 1989, 1479.

[156] T. Hiyama, T. Kusumoto, *Comprehensive organic synthesis*, 8 (1991) 7.

[157] S. R. Wasserman, Y.-T. Tao, G. M. Whitesides, *Langmu*ir, 5 (1989) 1074.

[158] I. Markovich, D. Mandler, *J. Electroanal. Chem*. 484 (2000) 194-202.

[159] A. Y. Fadeev, T. J. McCarthy, *Langmuir*, 15 (1999) 3759.

[160] A. Y. Fadeev, T. J. McCarthy, *Langmuir,* 16 (2000) 7268.

[161] A. Ulman: *An introduction to ultrathin organic films: From Langmuir-Blodgett to Self-Assembly,* Academic Press Inc., San Diego, 1991.

[162] R. A. Jones, G. P. Bean, *The chemistry of pyrrole*, EDS. Academic Press: London, 1977, P 210, 460-463.

[163] a. E. Smela, G. Zuccarello, H. Kariis, B. Liedberg, *Langmuir*, 14 (1998) 2970; b. E. Smela, H. Kariis, Z. Yang, M. Mecklenburg, B. Liedberg, *Langmuir*, 14 (1998) 2984.

[164] E. Pretsch, T. Clerc, J. Seibl, W. Simon, Tables of spectral data for the structure determination of organic compounds, Springer Verlag: Berlin, 1983, PP U10, U15, U50, U70, U135.

[165] A. V. Kiselev, A. Y. Korolev, R. S. Petrova, K. D. Shcherbakova, *Colloid J.* 22 (1960) 671.

[166] L. Boksanyi, O. Liardon, E. sz. Kovats, *Adv. Colliod Interface Sci.* 6 (1976) 95.

[167] D. W. Sindorf, G. E. Maciel, *J. Phys. Chem*. 86 (1982) 5208.

[168] K. Szabo, N. L. Ha, P. Schneider, P. Zeltner, E. sz. Kovats, *Helv. Chim. Acta* 67 (1984) 2128.

[169] J. N. Kinkel, K. K. Unger, *J. Chromatogr*. 316 (1984) 193

[170] M. D. Porter, T. B. Bright, D. L. Allara, C. E. D. Chidsey, *J. Am. Chem. Soc.*, 109 (1987) 3559.

[171] A. N. Parikh, B. Leidberg, S. V. Atre, M. Ho, D. L. Allara, *J. Phys. Chem*. 99 (1995) 9996.

[172] K. Kojio, S. Ge, A. Takahara, T. Kajiyama, *Langmiur*, 14 (1998) 971.

[173] D. W. Britt, V. Hlady, *Langmiur*, 15 (1999) 1770.

[174] R. G. Snyder, H. L. Straus, C. A. Elliger, *J. Phys. Chem*., 86 (1982) 5145.

[175] C. E. Loader, H. J. Anderson, *Can. J. Chem*. 59 (1981) 2673.

[176] H. J. Anderson, C. E. Loader, *Synthesis*, 1985, 353.

[177] J. Desales, R. Greenhouse, J. M. Muchowski, *J. Org. Chem*. 47 (1982) 3668.

[178] C. F. Candy, R. A. Jones, P. H. Wright, *J. Chem. Soc. C* , 1970, 2563.

[179] D. J. Chadwick, S. T. Hodgson, *J. Chem. Soc., Perkin Trans 1*, 1983, 93.

[180] M. Kakushima, P. Hamel, R. Frenett, J. Rokach, *J. Org. Chem*. 48 (1983) 3214.

[181] J. Rokach, P. Hamel, M. Kakushima, G. M. Smith, *Tetradron Lett*. 22 (1981) 4901.

[182] R. X. Xu, H. J. Anderson, N. J. Gogan, C. E. Loader, R. McDonald, *Ibid*, 22 (1981) 4899.

[183] J. M. Muchowski, D. R. Solas, *Tetrahedron Lett*. 24 (1983) 3455.

[184] B. L. Bray, P. H. Mathies, R. Naef, D. R. Solas, T. T. Tidwell, D. R. Artis, J. M. Muchowski, *J. Org. Chem*. 55 (1990) 6317.

[185] A. Ho-Hoang, F. Fache, G. Boiteux, M. Lemaire, *Synth.Met*. 62 (1994) 277.

[186] B. P. J. De Lacy Costello, P. Evans, N. Guernion, N. M. Ratcliffe, P. S. Sivanand, G. C. Teare, *Synth. Met*. 114 (2000) 181.

[187] H, J. Anderson, C. E. Loader, *Synthesis*, 4 (1985) 353.

[188] C. D'Silva, R. Iqbal, *Synthesis*, 4 (1996) 457.

[189] A. Zelikin, V.R. Shastri and R.Langer, *J.Org. Chem*. 64 (1999) 3379.

[190] R. Greenhouse, C. Ramirez, and J. M. Muchowski, *J. Org. Chem*. 50 (1985) 2961.

[191] G. M. Kosolapof, L.Maier in *Organic Phosphorus Compounds*, Wiley; New York, 7 (1976) 9.

[192] N. Gauvry, J. Mortier, *Synthesis*, 4 (2001) 553.

[193] R. Robinowitz, *J. Org. Chem*. 28 (1963) 2975.

[194] C.E. Mckenna, M. T. Higa, N. H. Cheung, M.-C. Mckenna, *Tetrahedron Lett*. 18 (1977) 155.

[195] C. E. Mckenna, J. Schmidhauser, *J. Chem. Soc. Chem. Commun*. 1979, 739.

[196] A. J. Rudinskays, T. L. Hullar, R. L. Salvader, *J. Org. Chem*. 42 (1977) 2771.

[197] C. J. Salomon, E. Breuer, *Tetrahedron Lett*. 36 (1995) 6759.

[198] G. M. Blackburn, D. Ingleson, *J. Chem. Soc. Chem. Commun*. 1978, 870.

[199] T. Morita, Y. Okamoto, H. Sakurai, *Tetrahedron Lett*. 19 (1978) 2523.

[200] W. M. Sigmund, G. Weeraskera, C. Marestin, S. Styron, H. Zhou, M. Z. Elsabee, J. Ruehe, G. Wegner, R. S. Duran, *Langmuir*, 15 (1999) 6423.

[201] P. J. Langley, F. J. Davis and G. R. Mitchell, *J. Chem. Soc., Perkin Trans.* 2 (1997) 2229.

[202] S. Oberio Master thesis, TU-Dresden, 2002.

[203] C. D. Bain, E. B. Troughton, Y.-T. Tao, J. Evall, G. M. Whitesides, R. G. Nuzzo, *J. Am. Chem. Soc*. 111 (1989) 321 .

[204] W. Gao, L. Dickinson, C. Grozinger, F. G. Morin, L. Reven, *Langmuir*, 12 (1996), 6429; b. R. D. Ramsier, P. N. Henriksen, A. N. Gent, *Sur. Sci*. 203 (1988) 72.

[205] I. Doudevski, D. K. Schwartz, Applied Surface Science 175-176 (2001) 17.

[206] E. Jaehne, D. Ferse, G. Busch, H.-J. P. Adler, A. Singh, Indra K. Varma, Des. Mon. *Polymers*, 5 (2002) 427.

[207] G. Beamson, D. Briggs, *HRXPS of organic polymers*. The Scienta ESCA A300 Database. John Wiley: Chichester, 1992.

[208] B. L. Bray, P. H. Mathies, R. Naef, D. R. Solas, T. T. Tidwell, D. R. Artis, J. M. Muchowski, *J. Org. Chem*. 55 (1990) 6317-6328.

[209] A. P. Kozikowski, X.-M. Cheng, *J. Org. Chem.* 49 (1984) 3239-3240.

[210] C. K. Chiang, Y. W. Park, A. J. Heeger, H. Shirakawa, E. J. Louis, A. G. MarDiarmid, *Phys. Rev. Lett*. 39 (1977) 1098.

[211] A. F. Diaz, K. K. Kanazawa, G. P. Gardini, *J. Chem. Soc., Chem. Commun*. 1979, 635.

[212] A. F. Diaz, *Chem. Sci*. 17 (1981) 142.

[213] G. Tourillon, F. Garnier, *J. Electroanal. Chem*. 135 (1982) 173.

[214] J. Bargon, S. Mohamand, R. J. Waltman, *IBM J. Res. Develop*. 27 (1983) 330.

[215] M. Delamer, P. C. Lacaze, J. Y. Dumousseau, J. E. Dubois, *Electrochim. Acta*, 27 (1982) 61.

[216] A. F. Diaz, J. A. Logan, *Electroanal. Chem.* 111 (1980) 111.

[217] E. M. Genies, C. Tsintavis, A. A. Syed, *Mol. Cryst. Liq. Cryst*., 121 (1985) 181.

[218] W. Sauerer, *Kunststoffe Werkstoffe-Verarbeitung-Anwendung*, 81 (1989) 8.

[219] M. Yamaura, T. Hagiwara, M. Hirasaka, T. Demura, K. Iwata, *Synth. Met*. 28 (1989) 157.

[220] F. Vögtle, *Supramolekulare Chemie,* 1992, Teubner Verlag, Stuttgart.

[221] A. J. Heeger, S. Kivelson, J. R. Schrieffer, W. P. Su, *Rev. Mod. Phys*. 60 (1988) 781.

[222] G. P. Gardini, *Adv. Heterocycl. Chem*. 15 (1973) 67.

[223] A. Angeli, *Gazz. Chim. Ital.* 42 (1916) 279.

[224] V. Varacco, V. Bocchi, *C. R. Acad. Sci. Ser. C.,* 267 (1968) 433.

[225] E. Simon, E. Sable, H. Handel, M. L'Her, *Electrochim Acta*, 45 (1999) 855-863.

[226] J. Joo, J. K. Lee, S. Y. Lee, K. S. Jang, E. J. Oh, A. J. Epstein, *Macromolecules*, 33 (2000) 5131.

[227] H. S. Nalwa: *Handbook of surfaces and interfaces of materials*, Ed. H. S. Nalwa, Academic Press, 2001.

[228] H. Korri-Youssoufi, F. Garnier, P. Srivastave, P. Godillot, A. Yassar, *J. Am. Chem. Soc*. 119 (1997) 7388.

[229] M. Zhou, J. Heinze, *Electrochim. Acta*, 44 (1999) 1733.

[230] P. Chandrasekhar (Eds.), *Conducting Polymers, Fundamentals and Applications*, A Pratical Approach; Kluwer Academic Publishers, Boston/Dordrecht/London, 1999.

[231] S. Machida, S. Miyata, A. Techagumpuch, *Synth. Met*. 31 (1989) 311.

[232] Y. E. Whang, J. H. Han, H. S. Nalwa, T. Watanabe, S. Miyata, *Synth. Met*. 41-43 (1991) 3043.

[233] E. M. Genies, G. Bidan, A. Diaz, *J. Electrochem. Soc*. 149 (1983) 101.

[234] C. K. Chiang, C. K. Fincher, Y. W. Park, A. J. Heeger, H. Shirakawa, E. J. Louis, S. C. Gau, A. G. MacDiarmid, *Phys. Rev. Lett.* 39 (1977) 1089.

[235] W. M. Genies, G. Bidan, A. Diaz, *J. Electroanal. Chem*. 149 (1983) 101.

[236] J. Chen, A. J. Heeger, *Synth. Met*. 24 (1988) 311.

[237] A. F. Diaz, J. Bargon, „ *Electrochemical Synthesis of Conducting Polymers*", chapter 3 (p.81) in Skotheim, T. A. (Ed.), Handbook of Conducting Polymers, Vol. 1, Marcel Dekker, Inc., New York, USA (1986).

[238] H. Nguyen Thi Le, B. Garcia, C. Deslouis, Q. Le Xuan, *Electrochim. Acta,* 46 (2001) 4259.

[239] H. Hammache, L. Makhloufi, B. Saidani, *Corrosion Sci.* 45 (2003) 2031.

[240] J. O. Iroh, W. Su, *J. Appl. Polym. Sci*. 71 (1999) 2075.

[241] G. S. Akundy, J. O. Iroh, *Polymers*, 43 (2001) 9665.

[242] G. B. Street, „*Polypyrrole from Powders to Plastics*", chapter 8 (p.265) in Skotheim, T. A. (Ed.), Handbook of Conducting Polymers, Vol. 1, Marcel Dekker, Inc., New York, USA (1986).

[243] G. Tourillon, F. Garnier, *J. Electroanal. Chem*. 161 (1984) 51.

[244] G. Tourillon, F. Garnier, *J. Electroanal. Chem*. 135 (1982) 173.

[245] G. B. Street, T. C. Clarke, *IBM J. Res. Dev*. 25 (1981) 51.

[246] H. D. Tabba, K. M. Smith, *J. Org. Chem*. 49 (1984) 1870.

[247] M. Kijima, H. Hasegawa, H. Ahirakawa, *J. Polym. Sci. A Polym. Chem*. 36 (1998) 2691.

[248] I. Cuadrado, C. M. Casado, F. Lobete, B. Alonso, B. Gonzalez, J. Losada, U. Amador, *Organometallics,* 18 (1999) 4960.

[249] I. Berlot, Y. Chevalier, P. Labbe, J. C. Moutet, *Langmuir*, 17 (2001) 2639.

[250] S. Chao, M. S. Wrighton, *J. Am. Chem. Soc*. 109 (1987) 2197.

[251] A. Merz, A. Maimerl, A. J. Owen, *Synth. Met*. 25 (1988) 89.

[252] A. F. Diaz, J. I. Castillo, K. K. Kanazawa, J. A. Logan, M. Salmon, O. Fajardo, *J. Electroanal. Chem*. 133 (1982) 233.

[253] G. Zotti, G. Schiavon, A. Berlin, G. Pagani, *Synth. Met*. 40 (1991) 299.

[254] A. O. Patil, Y. Ikenoue, N.Basescu, N. Colaneri, J. Chen. F. Wudl, A. J. Heeger, *Synth. Met*. 20 (1987) 151.

[255] A. O. Patil, Y. Ikenoue, F. Wudl, A. J. Heeger, *J. Am. Chem. Soc*. 109 (1987) 1858.

[256] C. P. andrieux, P. Hapiot, *Chem. Mater.* 9 (1997) 723.

[257] J. Paloheimo, E. Punkka, H. Stubb, P. Kuivalainen, „Polymer field effect transistors for transport property studies“, Proc. Of NATO ASI conference on „*Lower Dimensional Systems and Molecular Electronics*“, Spetses, Greece 12-23 June 1989, Metzger, R. M. (Ed.), PlenumPress, New York, USA (1990).

[258] Skothiem (Ed.), *Handbook of conducting polymers*, Marcel Dekker, Inc., 1986.

[259] E. Krivain, V. Csaba, *J. Solid State Electrochem.* 5 (2001) 507.

[260] W. M. D. Arirgan, D. S. Gray, *Analytica Chimca Acta*, 402 (1999) 157-167.

[261] R. Valaski, S. Ayoub, L. Micaroni, I. A. Hümmelgen, *Thin Solid Films,* 415 (2002) 206.

[262] C. Yuan, P. Li, J. Shan, H. Zhang, *Supramol. Sci.* 5 (1998) 751.

[263] D. Schmeißer, A. Bartl. L. Dunsch, H. Naarmann, W. Göpel, *Synth. Met*. 93 (1998) 43.

[264] S. Rapi, V. Bocchi, G. P. Gardini, *Synth. Met.* 24 (1988) 217.

[265] B. P. J. de Lacy Costello, P. Evans, N. Guernion, N. M. Ratcliffe, P. S. Sivanand, G. C. Teare, *Synth. Met.* 114 (2000) 181.

[266] I. Balberg, *Phys. Rev. Lett.* 59 (1987) 1305.

[267] M. Kijima, H. Hasegawa, H. Shirakawa, *J. Polym. Sci. A: Polym. Chem.* 36 (1998) 2691.

[268] Y. Furukawa, S. Tazawa, Y. Fujii, I. Harada, *Synth. Met.* 24 (1988) 329.

[269] C.-G. Wu, C,-Y. Chen, *J. Mater. Chem.* 7 (1997) 1409.

[270] S. Machida, S. Miyata, A. Techagumpuch, *Synth. Met.* 31 (1989) 311

[271] G. P. McCarthy, S. P. Armes, S. J. Greaves, J. F. Watts, *Langmuir,* 13 (1997) 3686.

[272] J. M. Ribo, M. C. Anglada, J. M. Hernandez, X. Zhang, N. Ferrer-Anglada, A. haibi, B. Movaghar, *Synth. Met*. 97 (1998) 229.

[273] J. Simmons, *Phys. Rev. Lett.* 25 (1965) 967.

[274] D. Ma, I.A. Hummelegen, *J. Phys. D: Appl. Phys*. 33 (2000) 1376.

[275] R. Valaski, S. Ayoub, L. Micaroni, I.A. Hummelegen, *Thin Solid Films,* 415 (2002) 206.

[276] K. kaneto, *Thin Solid Films,* 393 (2001) 249.

[277] P. T. Nguyen, U. Rammelt, W. Plieth, *J. Solid State Electrochem.,* 7 (2003) 497.

[278] F. Beck, M. Oberst, Makromol. Chem., *Macromol. Symp.* 8 (1987) 97

[279] C. Nylander, *J. Phys. E.*18 (1985) 736.

[280] J. Janta, A. Bezegh, *Anal. Chem.* 60 (1988) 63R.

[281] Y. Sakai, Y. Sadaoka, K. Ikeuchi, *Sensors and Actuators,* 9 (1986) 125.

[282] Y. Sakai, Y. Sadaoka, K. Ikeuchi, *Sensors and Actuators,* 13 (1988) 243.

[283] M. Matsuguch, T. Kuroiwa, T. Miyagishi, S. Suzuki, T. Ogura, Y. Sakai, *Sensors and Actuators B,* 52 (1998) 53.

[284] T. Sata, *Sensors and Actuators B*, 13 (1995) 63.

[285] F. Traversa, A. C. Jason, *Nature,* 171 (1953) 177.

[286] A. Guiseppi-Elie, G. G. Wallace, T. Matsue, in "*Handbook of Conducting Polymers 2nd edition*" Marcel Dekker, NY, 1998, p963.

[287] G. Bidan, *Sensors and Actuators B*, 6 (1992) 45.

[288] J. Miasik, A. Hopper, B. C. Tofield, *J. Chem. Soc. Faraday Trans. I*, 82 (1986) 1117.

[289] T. Hanawa, S. Kuwabata, H. Hashimoto, H. Yoneyama, *Synth. Met.* 30 (1989) 173.

[290] S. Dong, Z. Sun, Z. Lu, *J. Chem. Soc. Chem. Commun.* 1988, 993.

[291] L. S. Hwang, J. M. Ko, H. W. Rhee, C Y. Kim, *Synth. Met.* 55-57 (1993) 3671.

[292] R. M. L. Van de Leur, A. Van der Waal, *Synth. Met.* 102 (1999) 1330.

[293] G. E. Collins, L. J. Buckley, *Synth. Met.* 78 (1996) 93.

[294] A. Assadi, G. Svensson, M. Wilander, O. Inganäs, *Appl. Phys. Lett.* 53 (1998) 19.

[295] M. Matters, D. M. De Leeuw, M. J. C. M. Vissenberg, C.M. Hart, P. T. Herwig, T. Geuns, C. M. J. Mutsaers, C. J. Drurg, *Optical Materials*, 12 (1999) 189.

[296] H. Sirringhaus, P. T. Brown, R. H. Friend, M. M. Nielsen, K. Bechgaard, B. M. W. Langeveld-Voss, A. J. H. Spiering, R. A. J. Janssen, E. M. Meijer, *Synth. Met.* 111 & 112 (2000) 129.

[297] G. Mengoli, M. Munari, P. Bianco, M. M. Musiani, *J. Appl. Polym. Sci.* 26 (1981) 4247.

[298] D. W. DeBerry, *J. Electrochem. Soc.* 132 (1985) 1022.

Materials

Acetonitrile (99%, Fluka)

Bicyclohexyl (99%, Aldrich)

4-Bromobutyl chloride (97%, ABCR)

6-Bromohexanoyl chloride (97%, ABCR)

8-Bromoctanoic acid (97%, ACROS)

11-Bromoundecanoic acid (97%, ACROS)

6-Bromo-1-hexene (97%, Fluka)

8-Bromo-1-octene (97%, Aldrich)

11-Bromo-1-undecene (96%, ABCR)

N-Bromosuccinimide (Merck)

Bromotrimethylsilane (98%, ACROS)

Butyllithium solution (Fluka)

Chlorodimethylsilane (98%, Aldrich)

DMSO (p.a., Fluka)

Lithium perchlorate (995, ACROS)

Platinum (0)-1,3-divinyl-1,1,3,3-tetramethyl disiloxane complex, solution in xylenes (Fluka)

Potassium (Riedel-de Haën,cylindrical pieces)

1-(phenyl sulfonyl) pyrrole

Pyrrole (98%, Aldrich) was purified before use by vacuum distillation

Tantalum (99%, Aldrich) was mechanically polished by fine diamond paper

Titanium (99%, Aldrich) was mechanically polished by fine diamond paper

THF (p.a., Fluka, absolute)

Tetrabutyl ammonium fluoride on silica gel (Fluka)

Trichlorosilane (99%, Aldrich)

Triethyl phosphite (Fluka)

1-(Triisopropylsilyl) pyrrole (95%, Aldrich)

Trimethoxysilane (95%, Aldrich)

Other reagents and solvents were obtained from Aldrich Chemical Co. and used as received.

List of Abbreviations

ACN	Acetonitrile
AFM	Atomic force microscopy
CV	Cyclic voltammetry
DMSO	Dimethyl sulphoxide
DSC	Differential Scanning Calorimetry
EIS	Electrochemical impedance spectroscopy
Eq.	Equation
FET	Field effect transistor
HOMO	The highest occupied molecular orbitals
IR	Infra red
LB	Langmuir-Blodgett
LUMO	The lowest unoccupied molecular orbitals
NBS	N-bromosuccinimide
NMR	Nuclear magnetic resonance
PANi	Polyaniline
PMCS	ω-(Pyrrol-1-yl alkyl) dimethylchlorosilanes
PMCS-6	6-(Pyrrol-1-yl hexyl) dimethylchlorosilane
PMCS-8	8-(Pyrrol-1-yl octyl) dimethylchlorosilane
PMCS-11	11-(Pyrrol-1-yl undecyl) dimethylchlorosilane
PMCS-16	16-(Pyrrol-1-yl hexdecyl) dimethylchlorosilane
PP	Polyphenylen
PPy	Polypyrrole
PT	Polythiophene
PUTS	ω-(Pyrrol-1-yl alkyl) trichlorosilane

PUTS-6	6-(Pyrrol-1yl hexyl) trichlorosilane
PUTS-11	11-(Pyrrol-1-yl undecyl) trichlorosilane
PYPA	ω-(Pyrrol-3-yl alkyl) phosphonic acids
PYPA-4	4-(Pyrrol-3-yl butyl) phosphonic acid
PYPA-6	6-(Pyrrol-3-yl hexyl) phosphonic acid
PYPA-8	8-(Pyrrol-3-yl octyl) phosphonic acid
PYPA-11	11-(Pyrrol-3-yl undecyl) phosphonic acid
PYPE-4	4-(Pyrrol-3-yl butyl) phosphonic acid ester
PYPE-6	6-(Pyrrol-3-yl hexyl) phosphonic acid ester
PYPE-8	8-(Pyrrol-3-yl octyl) phosphonic acid ester
PYPA-11	11-(Pyrrol-3-yl undecyl) phosphonic acid ester
3-PyTMS	11-(Pyrrol-3-yl undecyl) trimethoxysilane
RH	Relative humidity
RT	Room temperature
SAMs	Self-Assembly monolayers
SEM	Scanning electron microscopy
SPR	Surface Plasmon Resonance
TGA	Thermogravimetric analysis
THF	Tetrahydrofuran
TIPS-pyrrole	1-Triisopropylsilyl pyrrole
XPS	X-ray photoelectron spectoscopy

Thickness of polymer layers made from surface polymerization (by AFM)

Adhesion promoters	**Pomerization time (h)**	**Oxidant**	**M_{py}/ $M_{oxd.}$**	**Surface**	**Thickness (nm)**
PMCS-6	1	$Na_2S_2O_8$	0.24	Very rough	150
PMCS-8	1	"	0.24	rough	50
PMCS-8	1.5	"		rough	80
"	20	"	0.17	"	80.91a
"	24	$FeClO_4$	0.17	"	125b
PMCS-11	1h	$Na_2S_2O_8$	0.25	smooth	45
"	1.5	"	0.25	smooth	55
""	2	"	0.25	"	160
"	3	"	0.25	"	200
"	4	"	0.25	"	240
"	5	"	0.25	"	220
"	6	"	0.25	"	225
"	2	"	0.17	"	50
"	2	"	0.19	"	150
"	2	"	0.21	"	50
"	2	"	0.23	"	130
"	2	"	0.24	"	110
"	2	"	0.25	"	150
"	20	"	0.17	"	16.56a
"	24	$FeClO_4$	0.17	"	158.3b
PMCS-16	1	$Na_2S_2O_8$	0.24	smooth	50
"	1.5	"	0.24	smooth	60
"	2	"	0.24	"	155
"	3	"	0.24	"	220
"	4	"	0.24	rough	250
"	20	"	0.17	"	63.35a
"	24	$FeClO_4$	0.17	"	166b
"		$FeClO_4$	0.17	"	34.14a
"	24	$(MoO)_{12}PO_4.xH_2O$	0.17	"	35.28a

Solvent: $MeOH/H_2O$ (2/1); substrate: Si/ SiO_2, SiO_2 layer thickness 100nm; adsorption time: 48 h.

Thickness of **a** was measured by ellipsometry (thin SiO_2 (3 nm) substrate).

Thickness of **b** was measured by AFM (thick SiO_2 (200nm) substrate).

Publications and Posters

1. X.Cai, E. Jaehne, H.-J. Adler, "Pyrrole-substituted alkyl silanes as new adhesion promoter on oxide substrates", Macromolecular Symposia "Reactive Polymer", Macromol. Symp. 210 (2004) 131.
2. B. Adolphi, E. Jähne, X. Cai, G. Busch, „Characterization of the adsorption of ω-(thiophen-3-yl alkyl) phosphonic acids on metal oxides with AR-XPS", Anal. Bioanal: Chem. 379 (2004) 646:
3. G. Busch, E. Jaehne, X. Cai, S. Oberoi, H.-J. Adler, Ultrathin layers for adhesion promotion", Synth. Met., 137 (2003) 871.
4. G. Busch, E. Jaehne; X. Cai, H.-J. Adler; „Surface properties of metal oxides-from macro-to-nanoscale", European Cells and Materials, 6 (2003) 64:
5. X. Cai, E. Jähne, H.-J.P. Adler, " Synthesis and characterization of new adhesion promoter for grfting conducting polymer on oxide substrate", XXVII FATIPEC Congress, April, 2004, France.
6. X. Cai, S. Oberoi, E. Jähne, H.-J. P. Adler, „ Synthesis of new adhesion promoters for deposition of conducting polymers", XXVI FATIPEC Congress, September, 2002, Dresden.
7. X. Cai, G. Busch, E. Jähne, H.-J. P. Adler, „ Synthesis and characterization of new adhesion promoters made from 3-substituted pyrrole derivatives", 6th Austrian Polymer Meeting and XXIst International H. F. Mark- Symposium, September, 2003, Wien.
8. X. Cai E. Jähne, H.-J. P. Adler, „ Pyrrole-substituted alkyl silanes as new adhesion promoter on oxide substrate", 2nd International Symposium on " Reactive Polymers in Inhomogeneous Systems, in Melts and at Interfaces", September, 2003, Dresden.
9. X. Cai, E. Jähne, H.-J. P. Adler, „ Synthesis and application of ω-(pyrrol-1-yl alkyl) silanes", V International Polymer Seminar Gliwice 2003, July, 2003, Gliwice, Poland.
10. C. M. Intelmann, M. Schneider, W. Plieth, X. Cai, E. Jähne, H.-J. P. Adler, „ Polypyrrole composite substrate", 2nd International Symposium on " Reactive Polymers in Inhomogeneous Systems, in Melts and at Interfaces", September, 2003, Dresden.
11. G. Wang, S. Nespurek, X. Cai, E. Jähne, H.-J. P. Adler, W. Plieth, „ Electronic properties of organic materials: towards field-effect transistor (OFET) sensors",2nd International

Symposium on " Reactive Polymers in Inhomogeneous Systems, in Melts and at Interfaces", September, 2003, Dresden.

12. G. Wang, S. Nespurek, X. Cai, E. Jähne, H.-J. P. Adler, „Electronic properties of a new adhesion promoter and its application in organic field-effect transistor by surface polymerization", International Workshop an: Advances in Molecular Electronic: from Molecular Materials to Single-molecule Devices, February, 2004, Dresden.
13. G. Busch, E. Jähne, X. Cai, S. Oberoi, H.-J. Adler, "Ultrathin Films for Adhesion Promotion", ICSM 2002, Shanghai.

Presentations

1. X.Cai, E. Jaehne, H.-J. Adler "Preparation of polypyrrole films on modified substrates", Presented in European graduate school (EGC) " Advanced polymeric materials" workshop 2004, Gliwice
2. X.Cai, E. Jaehne, H.-J. Adler "Synthesis and application of pyrrole derivatives", Presented in Graduiertenkolleg: Structure-Eigenschaftes-Beziehungen bei Heterocyclen workshop 2003, Dresden:
3. X.Cai, E. Jaehne, H.-J. Adler "Synthesis and application of adhesion promoting layers made from pyrrole and thiophene derivatives", Presented in European graduate school (EGC) " Advanced polymeric materials" workshop 2002, Prague.

Acknowledgements

I would like to express my sincere gratitude to Prof. Dr. Hans-Jürgen Adler for encouraging me to perform this work and in providing me the support and facilities at the Institute.

Words are inadequate to thank Dr. Evelin Jähne for her guidance who has been the source of inspiring guidance constant encouragement, valuable suggestions and cooperation. No matter in the work or in the normal life, she gave me a lot of help.

I cannot forget all my colleagues in our group, Mr. Dirk Ferse, Mr. Gernot Busch, Ms. Sonia Oberoi, Ms. Nataliya Kiriy and Ms. Mandy Gnauck for their patience and active cooperation.

I would express my deepest thanks to Dr. P. T. Nguyen and Mr. L. M. Duc and Dr. Rammelt from the Institute of Physical Chemistry and Electrochemistry for providing me all the possible facilities for my measurements. They provided me with all the help and support in my measurements. I also would like to thank Mr. M. Intelmann from the same institute for cooperation.

I would also acknowledge Ms. M. Dziewiencki for IR and contact angle measurements, Ms. I. Poitz for thermal analysis, Ms. A. Rudolph for the NMR measurements, Dr.-Ing Karin Kamloth for CV measurement and some valuable discussion, Ms. Kern for SEM measurement, and Dr. B. Adolphi for XPS measurement. I also would like to thank Ms. U. Schulze and Ms. J. Hunger for their help.

My deepest thanks are also to Dr. S.-L. Gao (for AFM measurement) and Dr. M. Wang (for ellipsometry measurement) from the Institute of Polymer Research who helped in my surface characterization measurements.

I am very much grateful to EGK720 for providing the financial assistance to me.

Last, but not the least I would thank my husband Wenge and my daughter whose inspiration and constant encouragement were a source of sustenance in carrying out the work.

Especially, I would like to acknowledge European Graduate Colleage 720 “Advanced polymeric Materials” for financial support.

Versicherung

Hiermit versichere ich, dass ich die vorliegende Arbeit ohne unzulässige Hilfe Dritter und ohne Benutzung anderer als der angegebenen Hilfsmittel angefertigt habe; die aus fremden Quellen direkt oder indirekt übernommenen Gedanken sind als solche kenntlich gemacht. Die Arbeit wurde bisher weder im Inland noch im Ausland in gleicher order ähnlicher Form einer anderen Prüfungsbehörde vorgelegt.

Cai, Xuediao

Erklärung

Die vorliegende Arbeit wurde unter der wissenschaftlichen Betreuung von Prof. Hans-Jürgen Adler in der Zeit von Sept. 2001 bis Dez. 2004 im Institute für Makromolekulare Chemie und Textilchemie der Technischen Universität Dresden angefertigt. Es haben keine frühen erfolglosen Promotionsverfahren stattgefunden.

Ich erkenne die Promotionsordnung der Fakultät Mathematik and Naturwissenschaften der Technischen Universität Dresden vom 16. 04. 2003 in vollem Umfang an.

Dresden, den 01. Dezember 2004

Cai, Xuediao